Reactive Nitrogen in the Tropical Troposphere

William Manning

MSc by Research

University of York

Chemistry

February, 2013

Abstract

The aim of this project was to calibrate a thermal-decomposition chemiluminescence (TD-Chem) instrument, capable of measuring the composition of the reactive nitrogen pool at the Cape Verde Atmospheric Observatory (CVAO) in the remote tropical troposphere. This data will be used in global atmospheric models in an attempt to better understand the sources of NO_x in the remote troposphere and how these could affect background ozone (O_3) levels.

Existing nitrogen oxides (NO_x = NO + NO_2) data from the CVAO was analysed for the measurement period of October 2006 to December 2011. The aim of this analysis was to identify the cause of the NO_2 diurnal, which exhibits a maximum mixing ratio at solar noon, in contrast to the minimum expected due to NO_2 photolysis in a clean environment. This anomaly was referred to as ΔNO_2. It was found that between 4.12.2007 and 28.2.2009, ΔNO_2 was significantly higher and caused an average increase in ΔNO_2 of 5.09 ± 0.94 pptv to the entire dataset. This period corresponded with the orientation of the inlet, resulting in the heating of the sample and potentially significant levels of thermal dissociation of peroxyacetyl nitrate (PAN) to produce the NO_2 observed. Future speciated measurements of the reactive nitrogen pool will help address the ΔNO_2 anomaly fully.

Calibrations of the inlet in the TD-Chem instrument were carried out using PAN, n-propyl nitrate (NPN) and nitric acid (HNO_3) standards to represent peroxyacyl nitrate (PNs), alkyl nitrate (ANs) and HNO_3 reservoirs. Quantification of the standards was achieved using a molybdenum oven and a gold oven in conjunction with a small flow of carbon monoxide, both heated to 300℃. Both methods are known to cause ~ 100 % conversion of NO_y compounds to NO, to allow detection via chemiluminescence (NO_y = NO_x + PNs, ANs, HNO_3, aerosol nitrate, halogen nitrates etc.). Both ovens agreed on the concentration of the standards to > 99 %. Temperature ramp experiments quantified the temperature range at which each standard thermally dissociated to form NO_2 and a companion radical in each of the quartz ovens used in the TD-Chem instrument. All experiments show thermal dissociation kinetics consistent with current understanding and kinetic theory. Deviations that do occur are either known and can be quantified, have been experimentally deduced, or a work schedule is in place in order to quantify them in the near future. Completion of the instrument calibration and subsequent installation of the TD-Chem instrument at the CVAO is projected to be in the summer of 2013.

Contents

		Page Number
	List of Figures	1
	List of Tables	4
	Preface	5
	Acknowledgements	7
	Author Declaraton	8
1.	**The Atmospheric System**	9
1.1.	Atmospheric Structure and Composition	10
1.2.	The Boundary Layer	14
1.3.	Tropospheric Chemistry	16
	References	23
2.	**Reactive Nitrogen**	25
2.1.	The Nitrogen Cycle	26
2.2.	Reactive Nitrogen	28
2.2.1.	Nitrous Oxide, N_2O	29
2.2.2.	Peroxyacyl Nitrates, PNs	30
2.2.3.	Alkyl Nitrates, ANs	34
2.2.4.	Nitric Acid, HNO_3	41
2.2.5.	NO_3 Aerosol	44
2.2.6.	Halogen Nitrates	45
2.2.7.	Nocturnal Chemistry, NO_3 and N_2O_5	46
	References	48
3.	**NO_x Measurements**	62
3.1.	Measurement Techniques	63
3.1.1.	Differential Optical Absorption Spectrometry (DOAS)	63
3.1.2.	Cavity Ring-Down Spectrometry (CRDS)	64

3.1.3. Laser Induced Fluorescence (LIF) 65
3.1.4. Chemiluminescence 65
3.1.5. O_3 Measurements 67
3.2. CVAO NO_x Instrument 68
3.2.1. NO_x Inlet 68
3.2.2. Measurements 73
3.3. ACTRIS 79
3.4. Summary 84

References 85

4. Cape Verde Atmospheric Observatory (CVAO) 87
4.1. Remote, Tropical Marine Boundary Layer 88
4.2. Cape Verde Atmospheric Observatory (CVAO) 89
4.2.1. CVAO 89
4.2.2. Air Mass Classification 91
4.2.3. CVAO, NO_x and O_3 92
4.2.4. NO_2 Diurnal, ΔNO_2 114
4.3. Summary 125

References 126

5. NO_y Measurements 131
5.1. NO_x, NO_y and Models 132
5.2. NO_y Inlet 134
5.2.1. NO_y Inlet 134
5.2.2. Measurements 139
5.3. NO_y Inlet Calibration 143
5.3.1. Standards 143
5.3.2. Experimental Methods 146
5.3.2.a. Standard Calibration 146
5.3.2.b. Temperature Ramps 150
5.4. Results 151
5.4.1. Peroxyacetyl Nitrate, PAN 151
5.4.2. n-Propyl Nitrate, NPN 153
5.4.3. Nitric Acid, HNO_3 156

5.5. Discussion 163
5.6. Conclusion 166

References 167

Appendices 169

Bibliography 173

List of Figures

		Page Number
1.1	Temperature profile and layered structure of the Earth's atmosphere.	10
1.2	Global radiative forcings.	13
1.3	typical diurnal cycle of the continental boundary layer.	14
1.4	Cross-sectional view of the Intertropical Convergence Zone (ITCZ).	15
1.5	Brewer-Dobson circulation and stratosphere-troposphere exchange (STE).	19
1.6	Relationship between net O_3 production and NO concentration.	21
2.1	The Nitrogen Cycle.	27
3.1	CVAO NO_x instrument.	69
3.2	CVAO NO_x inlet.	70
3.3	CVAO ozonizer box.	71
3.4	CVAO snooper box.	72
3.5	CVAO NO_x measurement cycle.	73
3.6	Signal output during conversion efficiency calculation.	75
3.7	CVAO precision frequency distribution plot.	76
3.8	ACTRIS blind standard results.	79
3.9	ACTRIS precision frequency distribution plot.	81
3.10	ACTRIS NO mixing ratio ramping experiment.	82
3.11	ACTRIS NO titration ramping experiment.	83
3.12	ACTRIS overnight and early morning ambient signal.	83
4.1	Map of the Cape Verde Islands and location of the CVAO.	89
4.2	The Cape Verde Atmospheric Observatory (CVAO).	90
4.3	Wind direction and speed rosette measured at the CVAO.	90
4.4	CVAO air masses and typical 10-day NAME back trajectories.	91
4.5	NO, NO_2, NO:NO_2 and O_3 data measured at the CVAO between October 2006 and December 2010.	93
4.6	Temperature and solar flux diurnal cycles at the CVAO.	105
4.7	Annual cycle of NO, NO_2 and O_3 average monthly mixing ratios measured at the CVAO.	105
4.8	Seasonality of air masses sampled at the CVAO.	107
4.9	NO_x frequency distribution plots for each wind mass measured at the CVAO	108
4.10	Diurnal cycle of NO, NO_2 and O_3 average monthly mixing ratios measured at the CVAO.	111
4.11	Measured ΔO_3 values and daytime NO showing dependency of O_3 dynamics on NO at the CVAO.	112

4.12 Modelled ΔO_3 values constrained by NO mixing ratios ranging from 1-40 pptv. 113

4.13 NO diurnal cycle averaged by year. 115

4.14 NO_2 diurnal cycle averaged by year. 115

4.15 Average ΔNO_2 values and standard deviation averaged by year. 116

4.16 NO diurnal cycle averaged by season. 116

4.17 NO_2 diurnal cycle averaged by season. 117

4.18 Average ΔNO_2 values and standard deviation averaged by season. 117

4.19 NO diurnal cycle averaged by air mass. 118

4.20 NO_2 diurnal cycle averaged by air mass. 118

4.21 NO diurnal cycle averaged by maintenance period. 119

4.22 NO_2 diurnal cycle averaged by maintenance period. 120

4.23 Average ΔNO_2 values and standard deviation averaged by maintenance period. 120

4.24 NO_2 diurnal for all data and all data except maintenance period 2 plotted alongside solar flux. 121

4.25 Hourly NO and solar flux values averaged for each maintenance period. 121

4.26 Hourly NO_2 and solar flux values averaged for each maintenance period. 122

4.27 Absorption cross sections of NO_2 and all potentially interfering species at 298 K. 124

5.1 Comparison of NO mixing ratios observed at the CVAO and predicted by GEOS-Chem. 123

5.2 Comparison of NO_2 mixing ratios observed at the CVAO and predicted by GEOS-Chem. 123

5.3 Improved NO_y composition data following the installation of the NO_y inlet in comparison to current measurements at the CVAO. 123

5.4 Modelled temperature dissociation ranges for a variety of NO_y species. 124

5.5 CVAO NO_y instrument. 125

5.6 CVAO NO_y inlet. 136

5.7 CVAO NO_y controller. 137

5.8 CVAO updated NO_x inlet. 138

5.9 CVAO NO_y measurement cycle. 139

5.10 Modelled NO_2 yield following temperature ramp of an equal mixture of PAN, NPN and HNO_3 totalling a mixing ratio of 1 ppbv. 141

5.11 Schematic of plumbing used for PAN synthesis in acetone excess and analysis. 143

5.12 Schematic of plumbing used for the NPN standard. 144

5.13 Schematic of plumbing used for HNO_3 synthesis and analysis. 145

5.14 HNO_3 permeation tube weighing's plotted against time. 145

5.15 PAN standard calibration using the gold NO_y converter. 147

5.16 PAN standard calibration using the molybdenum NO_y converter. 147

5.17 NPN standard calibration using the gold NO_y converter. 148

5.18 NPN standard calibration using the molybdenum NO_y converter. 148

5.19 HNO_3 standard calibration using the gold NO_y converter. 149

5.20 HNO_3 standard calibration using the molybdenum NO_y converter. 149

5.21 PAN temperature ramp in the Q3 oven. 152

5.22 PAN temperature ramp in the Q6 oven. 152

5.23 Schematic of novel plumbing system to be used for PAN synthesis in NO excess. 153

5.24 NPN temperature ramp in the Q1 oven. 154

5.25 NPN temperature ramps in the Q3 oven. 154

5.26 NPN temperature ramps in the Q6 oven 156

5.27 HNO_3 temperature ramps in the Q3 oven. 157

5.28 HNO_3 temperature ramps in the Q6 oven. 158

5.29 HNO_3 temperature ramp in the Q6 oven with the acetone permeation tube removed from the permeation oven. 159

5.30 HNO_3 temperature ramp in the Q6 oven with a stainless steel cooling region downstream of the Q6 oven. 160

5.31 Zero air temperature ramp in the Q6 oven with the permeation oven in series but empty. 161

5.32 Zero air temperature ramp in the Q6 oven with the permeation oven bypassed. 161

5.33 HNO_3 temperature ramp in the Q6 oven with a new blank permeation tube filled with high purity HNO_3. 162

5.34 Correlation between NO and NO_2 during temperature ramp experiments. 163

5.35 Average thermal dissociation ranges and standard for all of the standards in each oven tested. 165

List of Tables

		Page Number
1.1	Principal gases of dry air.	12
2.1	Estimates of the global tropospheric NO_x budget.	26
2.2	Important reaction pathways for nitrogen cycling.	27
3.1	Parameter settings during instrument operation.	68
3.2	Description of parts in the CVAO NO_x inlet.	70
3.3	Description of parts in the CVAO ozonizer box.	71
3.4	Description of parts in the CVAO snooper box.	72
3.5	Details of all the institutions involved in the NO_x comparison as part of the ACTRIS programme and the technique used for measurements.	80
3.6	Uncertainty and precision measurements of the CVAO and laboratory NO_x chemiluminescence instruments.	84
4.1	Monthly day and night time average O_3 mixing ratios measured at the CVAO.	102
4.2	Monthly day and night time average NO mixing ratios measured at the CVAO.	103
4.3	Monthly day and night time average NO_2 mixing ratios measured at the CVAO.	104
4.4	O_3 destruction regimes measured in remote boundary layer environments.	114
4.5	Dates of maintenance periods and changes to inlet design and setup.	119
5.1	Description of parts in the CVAO NO_y inlet.	136
5.2	Description of parts in the CVAO NO_y controller.	137
5.3	Description of parts in the CVAO updated NO_x inlet.	138
5.4	Rate constant parameters used in the kinetic model.	141
5.5	Temperature difference between the observed NO_x and modelled NO_2 for each standard in each of the quartz ovens tested.	162

Preface

Nitrogen oxides (NO_x = NO + NO_2) in the atmosphere affect the concentration of the hydroxyl radical (OH), the main atmospheric oxidising agent, and control the photochemical formation of ozone (O_3). This is important because the changing levels of O_3 in the troposphere impairs the ability of countries downwind to achieve air quality standards, put in place to offset the adverse impacts of O_3 on human health, crops and wildlife at high concentrations. By controlling O_3 availability and OH concentrations, through the reaction of hydroperoxy radicals (HO_2) with nitric oxide (NO), nitrogen oxides influence the atmospheres oxidising capacity and as a result, the rate of removal of species such as methane (CH_4), carbon monoxide (CO) and other volatile organic carbon species (VOCs). Hence although they are not climate gases in the classical sense, nitrogen oxides significantly influence global climate through the perturbation of CH_4 and O_3 concentrations, both important greenhouse gases. This process is of particular importance in the remote tropical troposphere because the mixing ratios of nitrogen oxides are close to the critical mixing ratio, whereby the typical O_3 destruction regime changes to one of photochemical O_3 production and due to the high levels of solar radiation and water vapour (and thus OH concentration), the majority of CH_4 oxidation occurs here.

Anthropogenic emissions dominate NO_x sources in the northern hemisphere. The oxidation of NO_x in the continental boundary layer to peroxyacyl nitrates (PNs), alkyl nitrates (ANs) and nitric acid (HNO_3), occurs in less than a day and consequently, NO_x levels in remote regions are typically very low. As described above, the production or loss of O_3 is critically dependent on the NO_x mixing ratio in the range of 5-100 pptv and as a result, only a small fraction of NO_x emissions must be transported to remote regions in order for significant O_3 production to occur. It has been suggested that this is made possible due to the more stable nitrogen oxides, which following transport to remote regions, decompose to form NO_x. Although the chemistry involved in these processes is thought to be well understood, experimental verification is lacking on both spatial and temporal scales due to the difficulties involved in measuring these longer-lived species in remote environments. This is highlighted by global atmospheric models which consistently underestimate NO_x mixing ratios and therefore their impact, in the remote tropical marine boundary layer.

The aim of this project is to calibrate a thermal-decomposition chemiluminescence (TD-Chem) instrument and install this system at the Cape Verde Atmospheric Observatory (CVAO). This instrument will be capable of measuring the

composition of the reactive nitrogen pool in more detail in the remote tropical troposphere providing an exciting and novel data series. This data will then be used in global atmospheric models in an attempt to better understand the sources of NO_x in the remote troposphere and how these could affect background O_3 levels.

Acknowledgements

I owe many thanks, to many people, for helping me complete my Masters, having gone up and across in the world of science. From the University, I would like to thank my supervisors Prof. Lucy Carpenter and Dr. James Lee for all of their help and support throughout my time at York. Thank you also to my internal and external examiners, Dr. Piero Di Carlo and Dr. Jacqui Hamilton for passing me. Finally, thank you to everyone else in the Atmospheric Chemistry Group, for being a part of my office, laboratory and field work life, as well as the football team.

Away from work, I would like to thank all of my family and friends for feigning interest when asking “what have you been up to recently?”. To my wife, Emma, I offer a big thank you for not asking the same question, yet having the patience to hear the same answer. Finally thanks to Lionel for not feigning interest at all.

Author Declaration

I hereby certify that I am the sole author of this thesis and that no part of this thesis has been published or submitted for publication.

I certify that, to the best of my knowledge, my thesis does not infringe upon anyone's copyright nor violate any proprietary rights and that any ideas, techniques, quotations, or any other material from the work of other people included in my thesis, published or otherwise, are fully acknowledged in accordance with the standard referencing practices.

I declare that this is a true copy of my thesis, including any final revisions, as approved by my thesis committee.

Chapter 1

THE ATMOSPHERIC SYSTEM

1. 1. Atmospheric Structure and Composition

Earths' atmospheric system is composed of distinct layers as a result of temperature variation with altitude (figure 1.1). This change in temperature with altitude is called the lapse rate, whereby a positive lapse rate denotes temperature decreasing with altitude. Each layer in the atmosphere is separated by a change in lapse rate, or temperature inversion, the position of which varies temporally and spatially in both the horizontal and vertical and forms a physical barrier to vertical chemical transport.

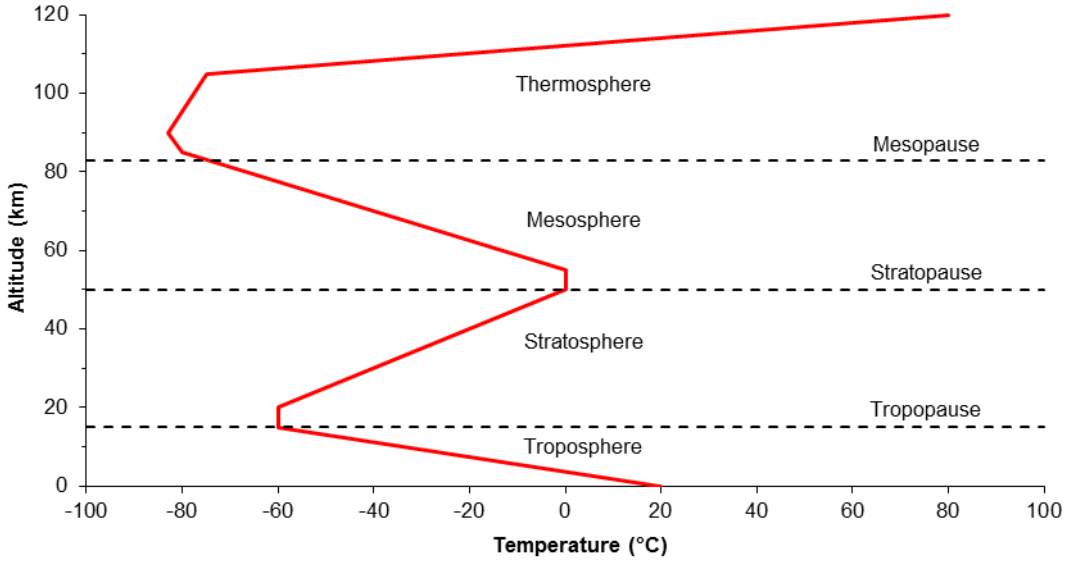

Figure 1.1. Temperature profile and layered structure of the Earth's atmosphere.

The stratosphere, meaning 'layered', gets its name due to the stratified air mass within this region. This occurs due to the increasing temperature with altitude, resulting in cold dense air and warm buoyant air at the tropopause and stratopause boundaries respectively. Within the lower stratosphere, O_3 concentrations peak between 25-30 km, having significant implications for a number of atmospheric processes. Here, O_3 is involved in a series of photochemical reactions referred to as the Chapman Cycle (reactions 1.1-1.4), which generates a steady state concentration of O_3 in the stratosphere, balanced between photochemical production and removal via reaction with molecular oxygen.

$$O_2 + h\upsilon \rightarrow 2O \quad (1.1)$$

$$O + O_2 + M \rightarrow O_3 \quad (1.2)$$

$$O + O_3 \rightarrow 2O_2 \quad (1.3)$$

$$O_3 + h\upsilon \rightarrow O(^1D) + O_2 \quad (1.4)$$

O_3 strongly absorbs solar radiation at wavelengths (λ) between 200-310 nm, dissociating to form electronically excited oxygen. Following oxygen photodissociation (1.1) and light absorption by O_3 up to the threshold value equivalent of 310 nm (1.4), excess energy is released as heat. These reactions combined are responsible for the increasing temperature with altitude in the stratosphere (figure 1.1) and play a vital role in protecting life on Earth by absorbing harmful ultraviolet (UV) radiation ($\lambda <$ 290 nm). As a result of this absorption, only lower energy radiation penetrates to the troposphere ($\lambda >$ 290 nm) limiting those molecules that are involved in tropospheric photochemistry. This radiation is termed actinic radiation. This has important implications as photochemical reactions are one of the main processes that initiate removal mechanisms in the atmosphere.

The rate coefficient for the photolysis of a molecule, J (s^{-1}) is given in equation 1.5.

$$J = \int \sigma(\lambda\, T)\, \varphi(\lambda\, T)\, F(\lambda)\, d\lambda \quad (1.5)$$

Where, $\sigma(\lambda,T)$ is the absorption cross section and $\varphi(\lambda,T)$ is the quantum yield. Both of these parameters are dependent on wavelength (λ) and temperature (T) and are molecule specific. The product of the absorption cross section and quantum yield is then multiplied the actinic flux, $F(\lambda)$, which is a measure of the radiative flux from all directions on a volume of air and given the units, photons cm^{-2} nm^{-1}. The whole expression is then integrated over all wavelengths, $d\lambda$, to give the photolytic rate coefficient, J.

Due to the gravitational pull of the Earth, approximately 80 % of the total atmosphere is located in the troposphere including essentially all of the water vapour, clouds and precipitation, which provide important mechanisms for the scavenging of pollutants from the atmosphere. The troposphere, ‘tropos’ meaning ‘turning’, is so called due to the strong convective currents that occur in this region of the atmosphere. Absorption of radiation at the Earths’ surface results in warm, buoyant air existing below cold, dense air. This creates a strong vertical mixing, allowing surface emissions to rise to the tropopause in just a few days. Species that are sufficiently both chemically and physically inert (such as some anthropogenic

emissions) are also able to traverse the tropopause boundary layer into the stratosphere. Once in the stratosphere, little vertical mixing and reduced water vapour means that scavenging processes in this region are much slower and due to the higher energy radiation above the O_3 layer, species are subject to photodissociation to form reactive products that can disrupt the chemistry of the stratosphere.

The troposphere can be further divided into two sections, the free troposphere which adjoins to the tropopause, a capping inversion which varies from 8 - 18 km in altitude, and the boundary layer, which is situated immediately above the Earth's surface. The atmospheric boundary layer has been defined as "the layer of air directly above the Earth's surface in which the effects of the surface (friction, heating and cooling) are felt directly" (Garratt, 1992). It is characterised by highly turbulent mixing and is the region of the atmosphere into which most anthropogenic (man-made), biogenic (biologically produced) and natural chemical emissions occur and therefore, physical and chemical processes that occur in this region directly affect the quality of the air that we breathe. Consequently, research has aimed at understanding the sources, sinks and processes of the chemical components in this environment.

Nitrogen (78 %) and oxygen (21 %) dominate the atmospheric composition and are ubiquitously distributed (table 1) (Wayne, 2000). However, trace gases that exist in concentrations on the scale of parts per billion (ppbv) or parts per trillion (pptv) by volume, show much greater variation in their distribution and have significant impacts on both air quality and the Earth's climate and radiative balance.

Table 1.1. Principal gases of dry air (Wayne, 2000)

Constituent	Percent by Volume	Concentrations in Parts Per Million (ppmv)
Nitrogen (N_2)	78.084	780,840.0
Oxygen (O_2)	20.946	209,460.0
Argon (Ar)	0.934	9,340.0
Carbon Dioxide (CO_2)	0.036	360.0
Neon (Ne)	0.00182	18.2
Helium (He)	0.000524	5.24
Methane (CH_4)	0.00015	1.5
Krypton (Kr)	0.000114	1.14
Hydrogen (H_2)	0.00005	0.5

Anthropogenic activities following the industrial revolution, such as the burning of fossil fuels, deforestation and the development of synthetic chemicals have led to significant alterations in the composition of the natural atmosphere. This is highlighted by figure 1.2, produced by the Intergovernmental Panel on Climate Change (IPCC) (2007), and summarises large effect these activities are having on global radiative forcing alone.

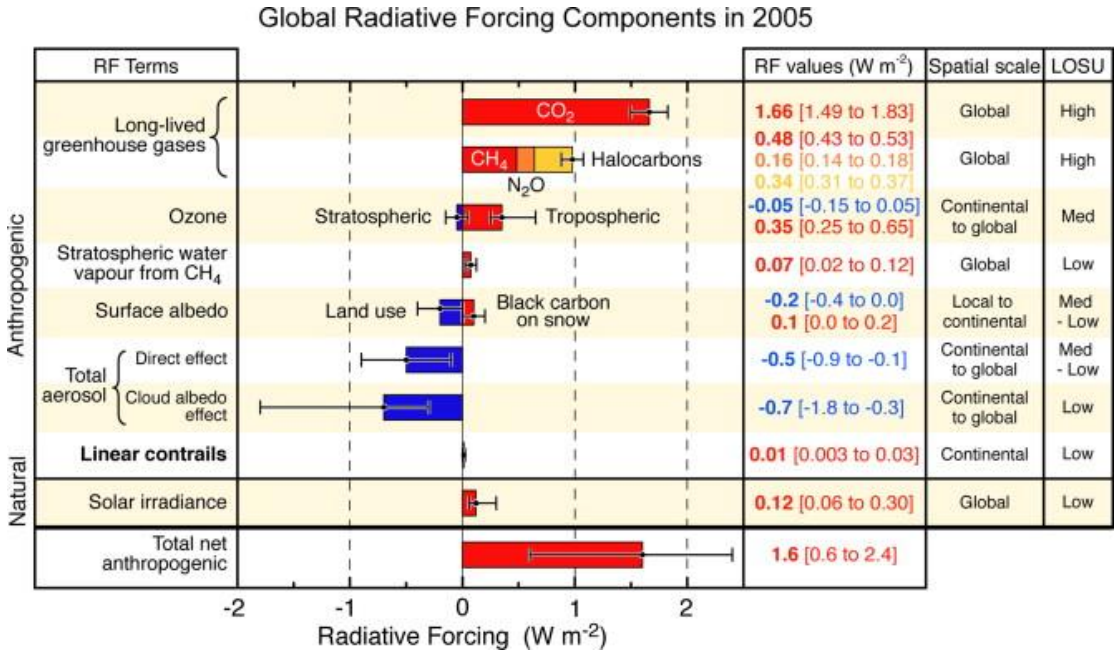

Figure 1.2. Global radiative forcings in 2005 relative to the start of the industrial era (about 1750), including the spatial scale of the forcing and the level of scientific understanding (LOSU) (IPCC, 2007).

1.2 The Boundary Layer

The continental boundary layer, typically 0.5-2 km in altitude (Wayne, 2000), has a well-defined diurnal cycle as shown in figure 1.3. Following sunrise, solar radiation heats the Earth's surface which in turn warms the boundary layer air mass. As this air mass becomes less dense, it ascends creating turbulence. This turbulent layer is also known as the mixed layer, the depth of which peaks late in the afternoon. This increase in the mixed layer is due to entrainment of the air mass situated above it. This air originates from a stable layer that remains on top of the mixed layer known as the entrainment zone. At sunset, the convective cells within the mixed layer begin to degrade to form what is known as the residual layer. The lowest part of this residual layer is further stabilised by radiative cooling and is characterised by weak, infrequent turbulence.

In comparison with the continental boundary layer, the dynamics of the marine boundary layer are much reduced as sea surface temperatures do not vary as much during the diurnal cycle, thereby restricting the formation of turbulence. Due to this inherent stability, any variation is more a result of large scale processes.

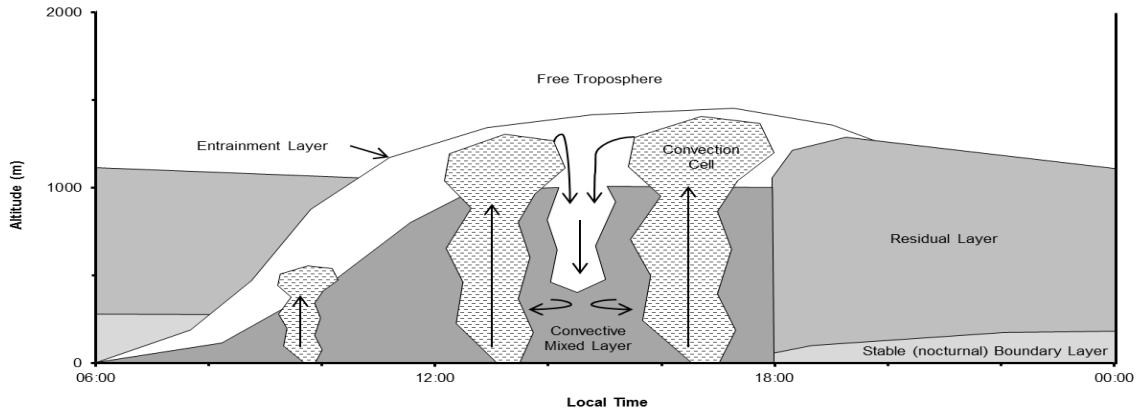

Figure 1.3. The typical diurnal cycle of the continental boundary layer (Adapted from Finlayson-Pitts and Pitts, 2000).

As a result of vertical convective mixing, atmospheric constituents frequently come into contact with the Earth's surface allowing deposition to provide a mechanism of removal. The principle movement of air masses and therefore pollutants in the boundary layer is vertically within thermals as oppose to the comparatively weak horizontal transport determined by surface winds, meaning that emissions are spatially confined. However, depending on the magnitude of the

turbulence in the mixed layer, pollutants within the boundary layer that are not removed from the system can be transported and incorporated into the free troposphere on the timescale of days. Within the free troposphere, atmospheric circulation is predominantly horizontal and allows long range transport around the world in the longitudinal direction on the timescale of weeks and meridional transport on the time scale of months for a latitudinal change of approximately 45°. Inter-hemispheric transport requires approximately 1 year due to the Intertropical Convergence Zone (ITCZ). As shown in figure 1.4, this is a low pressure system typically found around the equator, though it does show seasonal variation of up to 25° latitude due to variations in the Earths' surface. It is a result of solar heating causing vertical convection and the creation of a low pressure region. Subsequently, subtropical air is drawn in and the convergence of both the north- and south- east trade winds reinforces this strong vertical convection, thereby inhibiting horizontal transport and inter-hemispheric mixing.

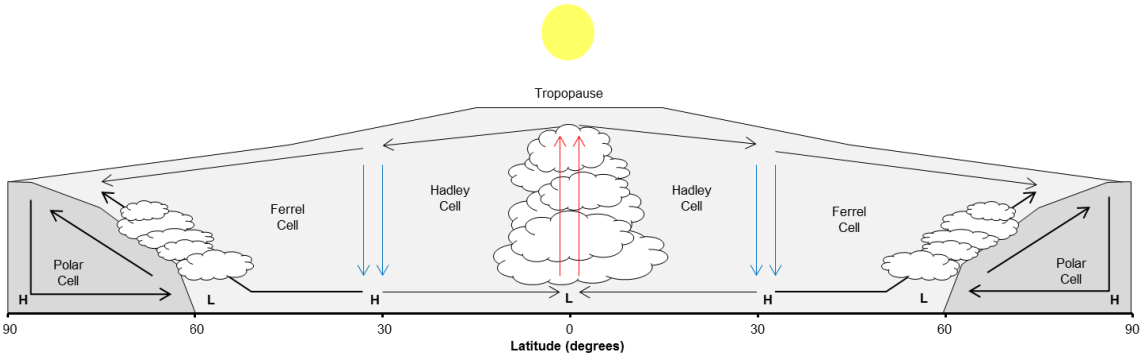

Figure 1.4. Cross-sectional view of the Intertropical Convergence Zone (ITCZ). Arrows indicate direction of wind flow. H = area of high pressure, L = area of low pressure.

1.3. Tropospheric Chemistry

As discussed above, stratospheric O_3 has significant influence over many atmospheric processes and is vital for life on Earth due to absorption of harmful UV radiation. It also plays an important role in the troposphere as a source of OH as a result of photodissociation (reactions 1.6 and 1.7).

$$O_3 + h\upsilon \rightarrow O(^1D) + O_2 \quad 1.6$$

$$O(^1D) + H_2O \rightarrow 2OH \quad 1.7$$

Approximately 90 % of the $O(^1D)$ formed in reaction 1.6 is quenched back to ground state $O(^3P)$ via reaction with an unreactive species, or 'bathgas' denoted as 'M' before recombining with molecular oxygen to reform O_3. In air, M is normally accepted to be N_2 or O_2. The remaining 10 % reacts with water vapour to produce two OH radicals for every O_3 molecule via reaction 1.7. Despite typically only ever being present at concentrations of approximately 10^6 molecules cm^{-3} (Prinn et al., 1995), owing to its' high reactivity OH is considered to be the most important tropospheric species. It is responsible for initiating most atmospheric oxidative processes and controlling the lifetimes and rates of removal of many trace gases and pollutants, such as CH_4 and CO. This process is of particular importance in the remote tropical marine boundary layer, where due to the high levels of solar radiation and water vapour and therefore OH radicals, up to 80 % of the global CH_4 oxidation occurs.

Pollutants that are both physically inert and resistant to removal via OH oxidation or photodissociation are able to be transported across the tropopause boundary into the stratosphere. Nitrogen dioxide (N_2O) and chlorofluorocarbons (CFCs) are examples of such species. As described previously, at higher altitudes higher energy solar radiation exists prior to O_3 absorption and can lead to the photodissociation of these compounds resulting in the production of radical species that can destroy O_3 and can lead to a thinning of the stratospheric O_3 layer. This process is highlighted in reaction scheme 1.8 using the CFC, trichlorofluoromethane ($CFCl_3$).

$$CFCl_3 + h\upsilon \rightarrow CFCl_2 + Cl \quad (1.8a)$$
$$Cl + O_3 \rightarrow ClO + O_2 \quad (1.8b)$$
$$ClO + O \rightarrow Cl + O_2 \quad (1.8c)$$

$$\textit{Net:}\ O_3 + O \rightarrow 2O_2 \quad (1.8)$$

Following the discovery of the Antarctic O_3 hole in 1985 (Farman et al, 1985), international effort along with the Montreal Protocol and its' subsequent revisions called for a complete ban on CFC production and consumption by 1996 (Ozone Secretariat United Nations Environment Programme, 2006). Further studies of the impact of this legislation and CFC trends suggest that concentrations have begun to decrease indicating successful implementation of the ban leading to a cessation of emissions (Prinn et al., 1995).

Despite the importance of O_3 as a precursor to OH and therefore the removal of pollutants, in the troposphere, O_3 itself is a pollutant and a powerful oxidative stressor. At high enough concentrations it can cause damage to crops, livestock and public health by degrading air quality. It is also a greenhouse gas (figure 1.2) and has been associated with increased death rates by contributing to the formation of photochemical smog (Finlayson-Pitts and Pitts, 2000).

The tropospheric loss mechanism of O_3 is via OH initiated oxidation of carbon monoxide, CH_4 and other volatile organic carbons (VOCs). This is demonstrated by the reactions with CO and CH_4 in reaction schemes 1.9 and 1.10 respectively.

$$CO + OH \rightarrow H + CO_2 \quad (1.9a)$$
$$H + O_2 + M \rightarrow HO_2 + M \quad (1.9b)$$
$$HO_2 + HO_2 \rightarrow H_2O_2 + O_2 \quad (1.9c)$$

$$\textit{Net:}\ CO + OH + HO_2 \rightarrow CO_2 + H_2O_2 \quad (1.9)$$

$$CH_4 + OH \rightarrow CH_3 + H_2O \quad (1.10a)$$
$$CH_3 + O_2 + M \rightarrow CH_3O_2 + M \quad (1.10b)$$
$$CH_3O_2 + HO_2 \rightarrow CH_3OOH + O_2 \quad (1.10c)$$

$$\textit{Net:}\ CH_4 + OH + HO_2 \rightarrow CH_3OOH + H_2O \quad (1.10)$$

As the OH radical involved in reactions 1.9 and 1.10 is produced via O_3 photolysis, as described previously through reactions 1.6 and 1.7, and the products CH_3OOH and H_2O_2 are water soluble peroxides that can be removed efficiently from the system through precipitation and deposition processes, these reactions represent an O_3 loss mechanism.

Tropospheric O_3 was initially thought to be of stratospheric origin, and although this is true, it is now recognised as being only a minor source. In comparison to 'O_3 rich' stratospheric air (typically 10ppmv), tropospheric air is relatively 'O_3 deplete' (0.04ppmv) (Lelieveld and Dentener, 2000). Vertical convection of tropospheric air in the tropics (~0° latitude) via the extratropical pump is slow and as a result, much of the uplifted air is transported towards the mid-latitudes without reaching the stratosphere. During the vertical transport of O_3 depleted tropospheric air into the stratosphere, O_3 is produced via O_2 photolysis (reactions 1.1-1.4). This is most efficient at tropical latitudes and is followed by O_3 transport poleward by the Brewer-Dobson circulation (Brewer, 1949; Dobson, 1956) (figure 1.5). O_3 accumulates in this circulating air mass during transport before enriching the troposphere with O_3 through stratosphere-troposphere exchange (STE). This exchange can occur via two main pathways; the simple descending of an air mass as it cools during transport or movement across layers of constant potential temperature that cross the tropopause. Potential temperature is the temperature an air parcel would have if it were compressed or expanded under adiabatic conditions to a reference pressure, without the exchange of heat with the environment (Finlayson-Pitts and Pitts, 2000). Movement of an air parcel across areas of constant potential temperature requires no change in heat and is therefore a rapid process.

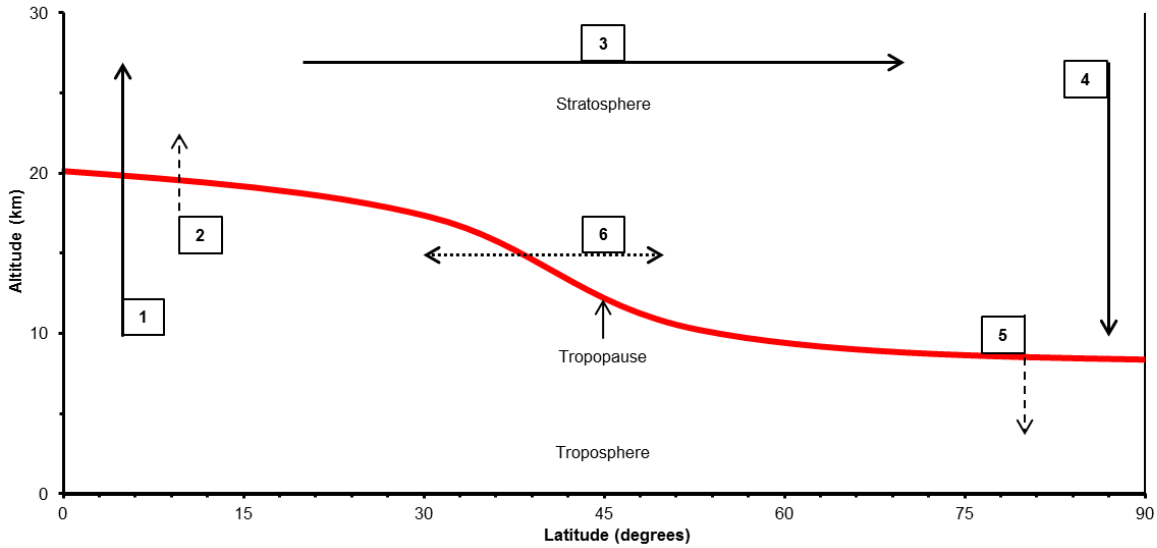

Figure 1.5. Schematic representation of the Brewer-Dobson circulation and stratosphere-troposphere exchange (STE). 1 = air is warmed at the tropics and rises. 2 = O_3 deplete air crosses the tropopause into the stratosphere. 3 = Circulation transports air mass polewards as O_2 is converted to O_3. 4 = Air cools and sinks at high latitudes. 5 = O_3 rich air crosses the tropopause into the troposphere. 6 = Air parcel of constant potential temperature crossing the tropopause.

The major source of tropospheric O_3 however, involves the photochemistry and oxidation of CO and VOCs as described above (1.9 and 1.10), in the presence of nitric oxide (NO) and nitrogen dioxide (NO_2), collectively termed NO_x. Due to the ease with which NO and NO_2 easily interconvert, they act as catalysts for many important atmospheric reactions including the null cycle (NO_x cycle) as shown in reactions 1.11-1.13.

$$NO + O_3 \rightarrow NO_2 + O_2 \qquad 1.11$$

$$NO_2 + h\upsilon \rightarrow NO + O(^3P) \qquad 1.12$$

$$O(^3P) + O_2 + M \rightarrow O_3 + M \qquad 1.13$$

This cycle reaches a photostationary steady state (PSS) within a couple of minutes (Crawford, 1996) with the NO to NO_2 ratio, also known as the Leighton relationship, being controlled by O_3 concentration, temperature and light. This relationship is defined in equation 1.14, where $j(NO_2)$ is the photolysis rate of reaction 1.12 and $k_{1.11}$ is the reaction rate of 1.11.

$$\frac{[NO_2]}{[NO]} = \frac{k_{1.11}[O_3]}{j(NO_2)} \qquad 1.14$$

However, this cycle only holds if O_3 is the only oxidant causing the conversion of NO to NO_2. Peroxy radicals (RO_2 and HO_2) formed during the oxidation of CO and VOC by OH (1.9b and 1.10b) can also oxidise NO to NO_2 thereby perturbing the PSS and creating the catalytic production of O_3 by preserving active radicals. The alternative reaction pathways for 1.9 and 1.10 in the presence of NO_x are illustrated in reaction schemes 1.15 and 1.16 respectively.

$CO + OH$	$\rightarrow$	$H + CO_2$	1.15a
$H + O_2 + M$	$\rightarrow$	$HO_2 + M$	1.15b
$HO_2 + NO$	$\rightarrow$	$OH + NO_2$	1.15c
$NO_2 + h\upsilon$	$\rightarrow$	$O(^3P) + NO$	1.15d
$O(^3P) + O_2 + M$	$\rightarrow$	$O_3 + M$	1.15e
Net: $CO + 2O_2 + h\upsilon$	$\rightarrow$	$CO_2 + O_3$	1.15

$CH_4 + OH$	$\rightarrow$	$CH_3 + H_2O$	1.16a
$CH_3 + O_2 + M$	$\rightarrow$	$CH_3O_2 + M$	1.16b
$CH_3O_2 + NO$	$\rightarrow$	$CH_3O + NO_2$	1.16c
$CH_3O + O_2$	$\rightarrow$	$CH_2O + HO_2$	1.16d
$HO_2 + NO$	$\rightarrow$	$OH + NO_2$	1.16e
$2\,[NO_2 + h\upsilon$	$\rightarrow$	$NO + O]$	1.16f
$2\,[O + O_2 + M$	$\rightarrow$	$O_3 + M]$	1.16g
Net: $CH_4 + 4O_2 + h\upsilon$	$\rightarrow$	$CH_2O + 2O_3 + H_2O$	1.16

The oxidation of VOCs in the presence of NO_x represent the only known production pathway of O_3 in the troposphere, highlighting the importance of NO_x in the O_3 budget. This importance is demonstrated by figure 1.6, which shows the net change of O_3 with changes in the NO_x mixing ratio. Here, a negative P_{O3} represents net O_3 loss.

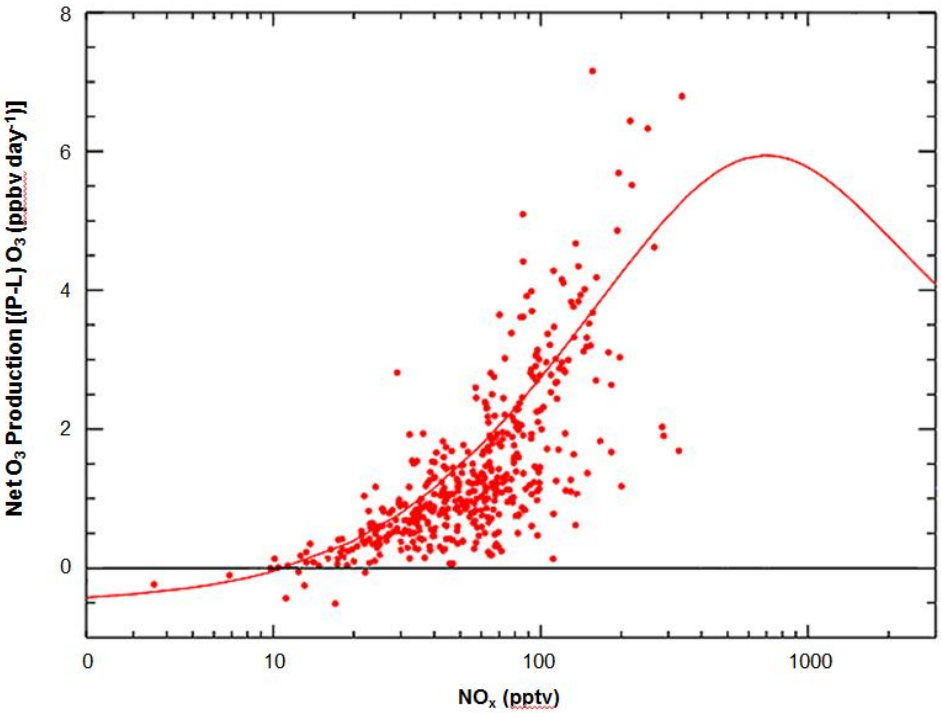

Figure 1.6. Relationship between net O_3 production and NO concentration (adapted from Jaeglé et al, 1998).

The NO_x concentration at which point there is a transition from an O_3 production to an O_3 destruction regime (x-intercept), is known as the compensation point (figure 1.6). This is largely dependent on the rates of two competing reactions (1.17 and 1.18).

$$HO_2 + O_3 \rightarrow OH + 2O_2 \qquad 1.17$$

$$HO_2 + NO \rightarrow OH + NO_2 \qquad 1.18$$

For net O_3 destruction, the conversion of HO_2 to OH must proceed through the reaction with O_3 (1.17), whereas for net O_3 production, the reaction between HO_2 and NO (1.18) must dominate, i.e. when the NO concentration is high.

Kinetic analysis of this system found that the reaction rate of 1.18 is 4000 times the rate of 1.17 (Crutzen, 1986), suggesting that net O_3 production should occur when the NO to O_3 ratio increases to greater than 1:4000. However the compensation point at two coastal sites, Cape Grim, Tasmania and Mace Head, Ireland, was found to be significantly higher than that predicted based solely on the kinetics of the reactions. This was attributed to the high humidity found in the marine boundary layer resulting in greater OH production and therefore O_3 destruction (Carpenter et al., 1997). In areas of very low NO_x concentrations, such as those

found in remote, marine environments, the dominant reactions of radicals are self-reactions to form water soluble peroxides (1.19-1.22).

$$HO_2 + OH \rightarrow H_2O + O_2 \quad 1.19$$

$$HO_2 + HO_2 \rightarrow H_2O_2 + O_2 \quad 1.20$$

$$HO_2 + RO_2 \rightarrow \text{products} \quad 1.21$$

$$RO_2 + RO_2 \rightarrow \text{products} \quad 1.22$$

These products are then removed from the system and therefore represent radical terminating reactions. As the rate of these self-reactions depends on the square of the radical concentration, these loss processes increase in areas of high radical concentrations (Thornton et al, 2002). This loss of radicals means NO concentrations must increase so that the HO_2 reacts predominantly via reaction 1.18 in order to allow O_3 production.

At high NO_x concentrations, the system becomes NO_x saturated (or VOC limited) and NO_x becomes a sink for radicals rather than recycling them, due to the formation of HNO_3 and alkyl nitrates (1.23 and 1.24), thereby removing active radicals from the system.

$$OH + NO_2 \rightarrow HNO_3 \quad 1.23$$

$$RO_2 + NO \rightarrow RONO_2 \quad 1.24$$

References

Alapati, K., Raman, S., 1989. A study of the seasonal migration of ITCZ and the quasi-periodic oscillations in a simple monsoon system using an energy balance model. *Meteorology and Amospheric Physics*. 41, 191-211.

Brewer, A., 1949. Evidence for a world circulation provided by the measurements of helium and water vapour distribution in the stratosphere. *Quarterly Journal of the Royal Meteorological Society*. 75, 351-363.

Crawford, J., Davis, D., Chen, G., Bradshaw, J., Sandholm, S., Gregory, G., Sachse, G., Anderson, B., Collins, J., Blake, D., Singh, H., Heikes, B., Talbot, R., Rodriguez, J., 1996. Photostationary state analysis of the NO2-NO system based on airborne observations from the western and central North Pacific. *Journal of Geophysical Research-Atmospheres*. 101, 2053-2072.

Crutzen, P. J., 1986. The role of the tropics in atmospheric chemistry, in Geophysiology of Amazonia. John Wiley, New York.

Dobson, G. M. B., 1956. Origin and distribution of the plolyatomic molecules in the atmosphere. *Proceedings of the Royal Society of London. Series A, Mathematical and Physical Sciences*. 236, 187-193.

Farman, J., Gardiner, B., Shanklin, J., 1985. Large losses of total ozone in Antarctica reveal seasonal ClOx/NOx interaction. Nature. 315, 207-210.

Finlayson-Pitts, B. J., Pitts, J. N., 2000. Chemistry of the Upper and Lower Atmosphere (1st Edition). Academic Press.

Garratt, J. R., 1992. The Atmospheric Boundary Layer. Cambridge University Press.

IPCC Core Writing Team, Pachauri, R., Reisinger, A., 2007. Intergovernmental Panel for Climate Change (IPCC) Fourth Assessment Report: Climate Change 2007. Technical report.

Jaegle, L., Jacob, D., Wang, Y., Weinheimer, A., Ridley, B., Campos, T., Sachse, G., Hagen, D., 1998. Sources and chemistry of NOx in the upper troposphere over the United States. *Geophysical Research Letters*. 25, 1705-1708.

Lelieveld, J., Dentener, F., 2000. What controls tropospheric ozone? *Journal of Geophysical Research-Atmospheres*. 105, 3531-3551.

Secretariat United Nations Environment Programme (Ed.), 2006. Handbook for the Montreal Protocol on substances that deplete the ozone layer, (7th Edition).

Prinn, R., Weiss, R., Miller, B., Huang, J., Alyea, F., Cunnold, D., Fraser, P., Hartley, D., Simmonds, P., 1995. Atmospheric trends and lifetimes of CH3CCl3 and global OH concentrations. *Science*. 269, 187-192.

Thornton, J. A., Wooldridge, P. J., Cohen, R. C., Martinez, M., Harder, H., Brune, W. H., Williams, E. J., Roberts, J. M., Fehsenfeld, F. C., Hall, S. R., Shetter, R. E., Wert, B. P., Fried, A., 2002. Ozone production rates as a function of NOx abundances and HOx production rates in the Nashville urban plume. *Journal of Geophysical Research*. 107, 4146-4163.

Wayne, R. P., 2000. Chemistry of Atmospheres (3rd Edition). Oxford University Press.

Chapter 2

REACTIVE NITROGEN

2.1. *The Nitrogen Cycle*

Molecular nitrogen is the most abundant constituent in the global atmosphere (table 1.1) but due to its stability, it does not take part in tropospheric chemistry. However at temperatures greater than 2000 °C, atmospheric nitrogen and oxygen can react to form NO. These conditions arise primarily through lightning and combustion (burning of fossil fuels or biomass). As discussed previously in section 1.3, due to the ease with which NO and NO_2 interconvert as a result of O_3 oxidation and photolysis, these compounds enter into a photostationary steady state. This cycle is shown in reactions 1.11-1.13 and is termed, the NO_x cycle. Estimated NO_x emissions from the major sources are listed in table 2.1. Whilst the burning of fossil fuels is the major global source of NO_x, soils and lightning dominate natural emissions. The emissions of these sources however are difficult to quantify due to their high spatial and temporal variability (Williams and Fehensfeld, 1991; Montanyà et al., 2007).

Table 2.1. Estimates of the global tropospheric NO_x budget from Forster et al. (2007), showing both natural and anthropogenic NO_x sources.

Source	Emission of NO_x Tg N yr^{-1}	Percentage of Total %
Fossil fuel	33.0	63.6
Aircraft	0.7	1.3
Biomass burning	7.1	13.7
Soils	5.6	10.8
Lightning	5.0	9.6
Stratosphere	< 0.5	1.0
Total	**51.9**	

Figure 2.1 shows the Earths nitrogen cycle with important processes listed in table 2.2. Denitrification is the reduction of the nitrate ion (NO_3^-) by bacteria during anaerobic respiration and can lead to the release of NO, nitrous oxide (N_2O) or atmospheric nitrogen (N_2). Nitrification is the reverse process, whereby nitrifying bacteria first convert ammonium ions (NH_4^+) to nitrite (NO_2^-) and then into NO_3^-. The conversion of decomposing organic matter to NH_4^+ is called ammonification,

The major atmospheric loss mechanisms of nitrogen containing compounds are wet and dry deposition of nitric acid (HNO_3) as a result of its high solubility or through biological uptake to allow incorporation of organic nitrogen into important

compounds within the organism, such as amino acids or chlorophyll. Biological removal processes include; NO_2 stomatal uptake by plants, uptake of nitrate (NO_3^-) and ammonium ions (NH_4^+) via assimilation (Postgate, 1982) (table 2.2) or fixation of atmospheric nitrogen (N_2) by bacteria that contain the nitrogenase enzyme and typically inhabit soils and root nodules of leguminous plants.

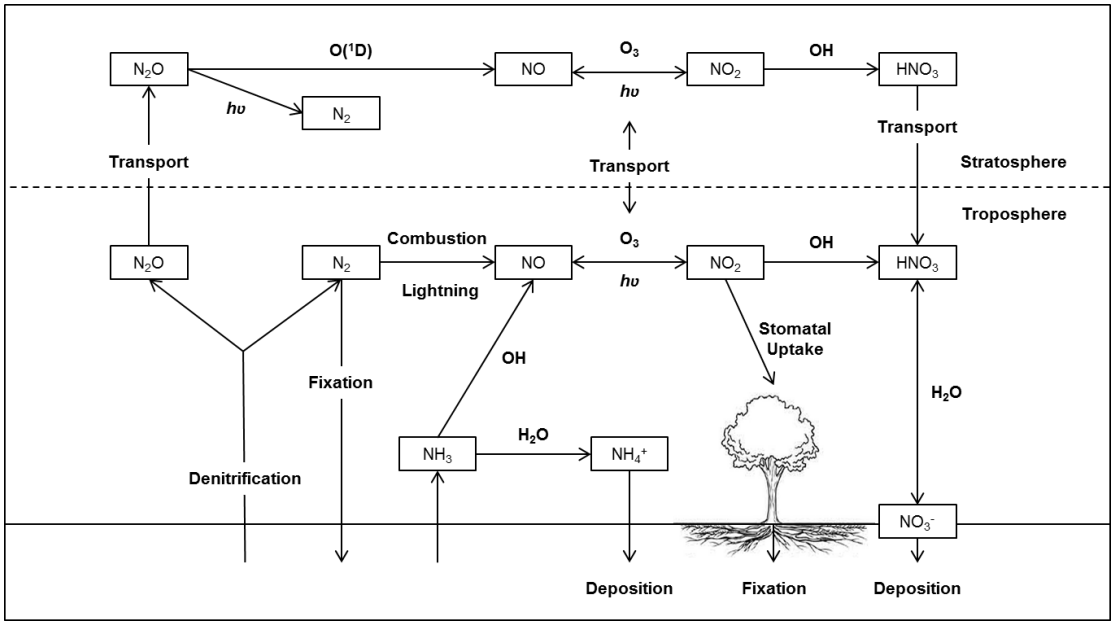

Figure 2.1. The Nitrogen Cycle.

Table 2.2. Important reaction pathways for nitrogen cycling.

Process	Reactions
Denitrification:	$NO_3^- \rightarrow NO_2^- \rightarrow NO \rightarrow N_2O \rightarrow N_2$
Nitrification:	$NH_4^+ \rightarrow NO_2^- \rightarrow NO_3^-$
Ammonification:	Organic N $\rightarrow NH_3 \rightarrow NH_4^+$
Assimilation:	NH_4^+ or NO_3^- $\rightarrow$ Organic N
Fixation:	$N_2 \rightarrow NH_3$ or NO

2.2. Reactive Nitrogen

As described in Chapter 1, variation in NO_x concentrations plays a pivotal role in determining whether a system exhibits O_3 production or destruction (O_3 compensation point). The nonlinearity in this relationship (Liu et al., 1987) means that O_3 production efficiency (the number of O_3 molecules produced per molecule of NO_x) is greater at lower NO_x concentrations and therefore, minimal transport of NO_x emissions to the remote troposphere is required in order to create significant O_3 production (Jacob et al., 1993).

This transport is restricted however as the oxidation of NO_x occurs in less than a day and its distribution is therefore restricted to the source region. The atmospheric pool of oxidised nitrogen products, also known as reactive nitrogen, is abbreviated as NO_y. This is defined as "the sum of NO_x and all oxidised nitrogen species that represent sources or sinks of NO_x through processes that occur on relatively short timescales" (Wayne, 2000). This includes NO_x, peroxy nitrates (RO_2NO_2, PNs), alkyl nitrates ($RONO_2$, ANs), HNO_3, HONO, HO_2NO_2, halogen nitrates, nitrate aerosol, NO_3 and N_2O_5. The term NO_z is also used to separate NO_x and NO_y species ($NO_z = NO_y - NO_x$).

The lifetimes of NO_z compounds are determined by characteristics such as their thermal stability, solubility, photolysis rates, reaction with OH and deposition velocities. It has been suggested that those species with longer lifetimes such as PNs act as a reservoir for NO_x, allowing long-range transport and chemical connectivity between polluted and remote environments, resulting in perturbations to the local O_3 regime (Crutzen, 1979). In this section, these individual components of NO_z will be discussed in detail.

2.2.1. Nitrous Oxide, N_2O

Although N_2O is a NO_x source in the stratosphere, it is generally excluded from the NO_y definition due to its inherent chemical and physical stability in the troposphere. However due to its importance in atmospheric processes, it warrants a description here. As described in section 2.1, N_2O can be produced naturally through the process of denitrification. Anthropogenic emissions include manufacturing processes and the burning of fossil fuels, but the dominant source is a result of increased nitrogen loading on terrestrial systems due to intensive agriculture practices, such as the use of fertiliser as well as land use change, which act to enhance soil emissions (Forster et al., 2007). These soil emissions are also regulated by temperature and moisture (Parton et al., 1998). As N_2O is a greenhouse gas with a global warming potential (GWP) 310 times that of CO_2, climate change could have important implications for the role of N_2O in the future.

Due to its stability within the troposphere, it can also be transported into the stratosphere where the increase in solar energy causes N_2O photolysis resulting in the production of NO as shown in reaction 2.1. This source of NO_x in the stratosphere can then contribute to the destruction of the O_3 layer (reaction 2.2).

$$N_2O + O \rightarrow NO + O_2 \qquad 2.1$$

$$NO + O_3 \rightarrow NO_2 + O_2 \qquad 2.2a$$
$$NO_2 + O(^3P) \rightarrow NO + O_2 \qquad 2.2b$$

$$\textit{Net: } O_3 + O(^3P) \rightarrow 2O_2 \qquad 2.2$$

However, despite its role as a GHG and being recently labelled as the dominant ozone-depleting substance in the atmosphere (Ravishankara et al., 2009), it remains unregulated by the Montreal Protocol and is therefore set to remain the most damaging compound for stratospheric O_3 and a potential threat to the Earth's climate into the future.

2.2.2. Peroxyacyl Nitrates, PNs

Peroxy nitrates (molecules of the form RO_2NO_2, or PNs) represent a dominant fraction of the reactive nitrogen pool, often constituting between 10-80 % (Singh and Hanst, 1981; Roberts, 1990; Cleary et al., 2004). PNs can be further divided into two groups depending on the nature of the peroxy radical. Peroxy acyl nitrates (PANs) are formed where RO_2 is of the structure R'C(O)OO, whereas non-acyl peroxy nitrates form when RO_2 does not terminate in a peroxycaroboxylic group or is HO_2 (Wooldridge et al., 2010).

Production of PANs in the atmosphere occurs via OH initiated oxidation (2.3) or photolysis (2.4) of aldehydes, ketones and other oxygenated VOCs (oVOCs). This generates peroxy radicals (RO_2 or HO_2), which then react with NO_2 as shown in the forward reaction of 2.5.

$$\text{oVOC} + \text{OH} + \text{O}_2 \rightarrow \text{RC(O)O}_2 \qquad 2.3$$

$$\text{oVOC} + h\nu + \text{O}_2 \rightarrow \text{RC(O)O}_2 \qquad 2.4$$

$$\text{RC(O)O}_2 + \text{NO}_2 \leftrightarrow \text{RC(O)OONO}_2 \qquad 2.5$$

PNs exist in equilibrium and exhibit a strong temperature dependence (2.5). For example, PANs have thermal stabilities characteristic of the $RC(O)OO\text{-}NO_2$ bond, which is independent of the nature of the R-group (Roberts and Bertman, 1992) and leads to atmospheric lifetimes of minutes in the boundary layer (T > 287 K) and months in the free troposphere (T < 263 K). Mixing ratios for PANs range from < 2 pptv in the remote marine boundary layer up to several ppbv in urban areas, whereas non-acyl peroxy nitrates, which have much shorter lifetimes, only show significant concentrations in colder regions of the atmosphere (Murphy et al., 2004; Browne et al., 2010).

The relative abundance of PN species are a reflection of their sources. Accordingly peroxyacetyl nitrate (PAN, $CH_3C(O)OONO_2$), which has multiple oVOC sources, both biogenic (acetaldehyde, ethanol, isoprene and some monoterpenes) and anthropogenic (ethane, acetaldehyde, acetone, toluene and higher alkanes), typically comprises 80 % of the PN reservoir (Roberts et al., 2007).

The diversity of possible PAN precursors has been demonstrated via the significance of isoprene oxidation products; methyl glyoxal (MGLY), methyl vinyl ketone (MVK) and methacrolein (MACR). Cleary et al (2007) found that in areas of high isoprene emissions, the acyl peroxy radical concentration required to produce typical PAN concentrations was three times higher than that produced by

acetaldehyde alone, consistent with previous findings suggesting isoprene photochemistry was the source (Roberts et al., 2006). This was confirmed by LaFranchi et al (2009) who found that in a forest environment (strong biogenic influence), MGLY, MVK, MACR and biacetyl represented up to 63 % of the total source of acyl peroxy radicals at 20°C, with MACR explaining 35 % on average. At lower temperatures (reduced biogenic emissions), acetaldehyde accounted for ~60% of the acyl peroxy radical source. Similarly, in urban environments with low isoprene emissions, PAN concentrations are consistent with that of acetaldehyde as the sole source (Roberts et al., 2001).

Although PAN dominates the PNs reservoir, many other homologues exist, though in lower abundance, including; peroxypropionyl nitrate (PPN, $C_2H_5C(O)OONO_2$), peroxymethacryloyl nitrate (MPAN, $CH_2=C(CH_3)C(O)OONO_2$), peroxyisobutyryl nitrate (PiBN, $(CH_3)_2CHC(O)OONO_2$), peroxyacryloyl nitrate (APAN, $CH_2=CHC(O)OONO_2$), peroxybutyryl nitrate (PnBN, $CH_3(CH_2)_2C(O)OONO_2$) and peroxybenzoyl nitrate (PBzN, $C_6H_5C(O)OONO_2$), with many more predicted (Cleary et al., 2007).

In contrast to PAN, PPN and MPAN, which are typically one order of magnitude lower in concentration (Roberts et al., 2007), are derived solely from the oxidation of anthropogenic emissions of n-alkanes and MACR respectively. As a result of this correlation between PN species and their precursors, the PNs composition can be used as a tracer to determine the relative contributions of anthropogenic and biogenic hydrocarbons to O_3 production (Williams et al., 1997; Roberts et al., 1998, 2001).

PNs are considered to be one of the most important NO_x reservoirs due to their role in long-range transport of emissions, with PAN alone being responsible for 5-10 % of all NO_x being vented from the boundary layer to the free troposphere (Moxim et al., 1996; Hudman et al., 2004). The thermal equilibrium described above in which PANs exist (2.5), led to the hypothesis that following formation in polluted source regions near the earth's surface, vertical transport into the free troposphere could lead to their preservation at low temperatures. Under free tropospheric conditions the residence time of these emissions would then be increased, allowing long-range horizontal transport. Subsequent warming of the air mass, as it is transported towards the tropics via the trade winds or due to sinking of the air mass into the boundary layer, would shift this equilibrium allowing the reformation of NO_x in areas downwind of their original emission source. This process could potentially result in the perturbation of the local O_3 regime and lead to areas of significant O_3 production in the clean, remote troposphere (Crutzen, 1979; Singh and Hanst, 1981).

This process is today, still considered to be the most important mechanism for NO_x transport in the atmosphere and is currently being strongly investigated in connection with the rapid economic and industrial growth of Asia and subsequent intercontinental transport of O_3 and its precursors into North America (Parrish et al., 2009; Walker et al., 2010; Hsu et al., 2102). Although quantitative estimates of the specific ozone sources involved in this transport are lacking, recent model analysis predicts that with the exclusion of Asian anthropogenic emissions, 53 % of O_3 exceedances of 75 ppbv in North America would not occur (Lin et al., 2012). This 75 ppbv threshold represents the national standard for ambient air quality in the United States of America.

The thermal equilibrium that controls the abundance of PANs means that the rates of reaction with OH and photolysis are too slow to be significant loss processes for PANs under boundary layer conditions (Talukdar et al., 1995). For example, of PAN, PPN and MPAN, only MPAN has a significant loss rate as a result of OH oxidation due to its alkene source (Orlando and Tyndall, 2002). Consequently in the boundary layer, reactions between peroxyacyl radicals with NO (2.6), HO_2 (2.7) and RO_2 (2.8) represent the dominant loss pathway of PANs. The rates of these reactions are considered to be independent of the R-group (Roberts and Bertman, 1992).

$RC(O)O_2 + NO$	→	Products	2.6
$RC(O)O_2 + HO_2$	→	Products	2.7
$RC(O)O_2 + RO_2$	→	Products	2.8

Dry deposition is another process by which PANs may be lost from the system. Whereas early studies had assumed that atmosphere-biosphere cycling of reactive nitrogen compounds such as PAN and HNO_3 would cause exclusively negative impacts on ecosystem health due to phytotoxicity and the acidification of soils and waterways respectively, recent studies have postulated that active foliar uptake of atmospheric reactive nitrogen by biota could be a major source of global nitrogen input to the ecosystems (Sparks et al., 2003; Sparks et al., 2009). Estimates suggest that up to 20 % of regional dry deposition of nitrogen can be a result of foliar uptake of PAN in some areas and could therefore result in increased ecosystem productivity (Teklemariam and Sparks, 2004).

Modelling studies trying to recreate the biologically induced dry deposition velocities (V_d) of PAN in a forest environment consistently underestimate those observed (Wolfe et al., 2011; Wu et al., 2012). Although stomatal V_d has been reasonably well characterised, the use of biological processes to constrain stomatal

uptake such as leaf area index and CO_2 assimilation improved model simulations (Wu et al., 2012). However both models used by Wu et al (2012) consistently underestimated V_d by 20-50 % during both day and night. Thermal decomposition of PAN was also shown to be a minor loss pathway due to the lack of relationship between total surface conductance and temperature (Wu et al., 2012). It is therefore suggested that current model underestimation is due to oversimplification of nonstomatal processes (processes that dominate at night) and that key meterological parameters, specifically friction velocity and surface wetness, and biological conditions should be included in deposition models (Wolfe et al., 2011; Wu et al., 2012).

Although this possible atmosphere-biosphere interaction which has thus far received little attention, provides a potentially important mechanism in the modelling of both atmospheric reactive nitrogen budgets and O_3 regimes and terrestrial ecosystem productivites, both of which will also affect climate, it remains a confused picture. This is highlighted by studies measuring ΣPNs and speciated measurements of PAN, PPN and MPAN at a coniferous forest site in California, USA (Farmer et al., 2006; Wolfe et al., 2009; Min et al., 2012). Initial eddy covariance studies suggested that the total flux of PNs was from the canopy into the overlying atmosphere (Farmer et al., 2006). Although a later study at the same site also found the same for ΣPNs, individual measurements of PAN, PPN and MPAN showed that these compounds were being deposited at different rates (Wolfe et al., 2009). Min et al (2012) have since found that these three species deposit approximately 30-60 % faster than ΣPNs. This discrepancy and apparent temporal variation was attributed to the formation of other, yet unidentified PANs within the canopy, with the diurnal cycle and temperature variation thought to be due to cycles in the biogenic production of different VOC precursors (Min et al., 2012).

Furthermore, similar to OH and photolysis initiated loss mechanisms, the rate of biological uptake of PANs cannot compete with the rate of chemical loss due to thermal decomposition at daytime temperatures and will therefore become more important in colder regions or at night (Turnipseed et al., 2006). Additionally, these spatial and temporal variations in the deposition of PANs will also differ to those of HNO_3 that are thought to be controlled predominantly by turbulent transport to surfaces (Min et al., 2012). Research is therefore required in order to better understand these processes and as a result, better quantify the loss processes of one of the most dominant reactive nitrogen reservoirs in the atmosphere.

2.2.3. Alkyl Nitrates, ANs

Alkyl nitrates (ANs) are of the form $RONO_2$ and the composition of this fraction is known to be complex. They can be classified as mono- or multi- functional, branched or linear (Bertman et al., 1995 ; Fischer et al., 2000).

Early studies were often confounded by the difficulties in measuring the different components of NO_y and many experiments that measured comprehensive suites of NO_y species, found that the sum of individual measurements (NO_{yi}) was less than that of the total NO_y, with the greatest discrepancies found in photochemically processed air masses (Russo et al., 2010). This disagreement came to be known as the 'missing NO_y' (Fahey et al., 1986). In recent years, ANs have become the subject of intense investigation following a study by Day et al (2003) which suggested that ANs are responsible for most, if not all of the 'missing NO_y'. Using thermal dissociation laser induced fluorescence (TD-LIF), Day et al measured NO_2, ΣPNs, ΣANs and HNO_3 within an urban plume at three continental sites as it was processed during transport. Over an annual cycle in both urban and rural environments, ΣANs were found to comprise 10-20% of total NO_y, an order of magnitude higher than previous reports (Flocke et al., 1998).

Tropospheric ANs are secondary products of OH initiated hydrocarbon oxidation in the presence of NO_x, as shown in reactions 2.9-11. They are also the primary NO_y emissions from both the oceans (Atlas et al., 1993) and biomass burning (Simpson et al., 2002)

$RH + OH$	$\rightarrow$	$R + H_2O$	2.9
$R + O_2$	$\rightarrow$	RO_2	2.10
$RO_2 + NO$	$\rightarrow$	$RO + NO_2$	2.11a
	$\rightarrow$	$RONO_2$	2.11b

Depending on the R group the branching ratio of AN formation (2.11b) ranges between 1-10's of percent, with high molecular weight and low temperatures favouring AN formation (Atkinson et al., 1983). Although this is evidently the minor branch of the reaction between peroxy radicals (RO_2) and NO, the formation of ANs is believed to be one of the major pathways for converting NO_x from radical form to inactive reservoirs at, or near, the Earth's surface by terminating the NO_x cycle, thereby preventing subsequent O_3 production (Ranschaert et al., 2000; Horowitz et al., 2007). As O_3 and ANs share the OH radical as a common precursor in their formation pathways, Day et al (2003) suggest that they should be correlated by the

gradient of the correlation based on the branching ratios of reactions 2.11a and 2.11b as described by equation 2.12.

$$\propto = \frac{k_{2.3b}}{(k_{2.3a} + k_{2.3b})} \qquad 2.12$$

Where α is the branching ratio and *k* is the rate constant for the respective reaction pathways of reaction 2.11. As branching ratios increase with hydrocarbon carbon chain length within homologous series, the hydrocarbon that is the precursor of the RO_2 can be inferred from the correlation between O_3 with ΣANs and therefore also provide a direct test of the hydrocarbon component of models describing O_3 production (Day et al., 2009). However, processing of the air mass during transport such as losses due to deposition will alter the observed correlation making estimates of the hydrocarbon precursors erroneous, especially during long distance transport unless the loss mechanisms are quantified.

As stated, the oceans are another source of ANs and could therefore have a large impact on the remote, marine boundary layer. Peak concentrations of up to 80 pM have been found in the tropics, associated with the equatorial upwelling and characterised by high methyl:ethyl nitrate ratios (Atlas et al., 1993; Thompson et al., 1993; Chuck et al., 2002; Blake et al., 2003; Dahl et al., 2005; Dahl et al., 2007). Saturation anomalies of up to 800% for methyl and ethyl nitrate have been reported in the Atlantic Ocean (Chuck et al, 2002) and supersaturations of C_1-C_3 ANs as high as 2000% with respect to the atmosphere have been observed in the Pacific Ocean (Dahl et al., 2005). Within the corresponding marine boundary layer, ANs have also been found to compose 20-80% of the total NO_y (Talbot et al., 2000).

Model calculations, using only photolysis and OH initiated oxidation of ANs as major loss terms, suggests that export of ANs to the surrounding atmosphere is a significant removal mechanism (Dahl et al., 2005). This highlights the importance of the sea to air flux as a source of ANs in environments sufficiently remote from anthropogenic and terrestrial impact, with implications for local O_3 regimes. For example, total emissions of methyl and ethyl nitrate are estimated to be equivalent to 0.35 Tg N yr^{-1} and responsible for ~3% of the global tropospheric oxidative capacity (Neu et al., 2008).

Laboratory studies have found that aqueous phase AN formation follows reactions 2.9-2.11 (Dahl et al., 2003). However the branching ratio for reaction 2.11b were found to be much higher than those reported in the gaseous phase (Atkinson et al., 1982). Dahl et al (2003) propose that photolysis of nitrite (NO_2^-) acts as a source

of NO (2.13) and photochemical reactions of coloured dissolved organic matter (CDOM) provides RO_2 (2.14).

$$NO_2^- \xrightarrow{H_2O,\ h\upsilon} NO + OH + OH^- \qquad 2.13$$

$$CDOM \xrightarrow{O_2,\ h\upsilon} RO_2 \qquad 2.14$$

In support of this mechanism, Dahl et al (2008) observed *in situ* photochemical production of ANs in tropical Pacific surface water samples following the addition of NO_2^-. The relative rates of production were similar to the concentration ratios in the ambient water, indicating that photochemistry may be the dominant source. Production showed saturation behaviour when NO_2^- concentrations were added in excess, suggesting that AN formation became limited by the availability of RO_2. Furthermore, higher concentrations were required to reach saturation in those areas that are typically NO_2^- deplete, i.e. within gyre systems, suggesting that although different water masses have similar potential for AN production, NO_2^- concentrations control AN distribution in the surface oceans.

While this is consistent with photochemical production, it does not discriminate between photochemical or a biological production mechanism. There is evidence for the latter, for example, Atlas et al (1993) found that isopropyl nitrate correlated with the biogenic halocarbon bromoform. Dahl et al (2007) also found that on the scale of different water masses, the spatial distribution of ANs was correlated with chlorophyll concentrations.

Another source of ANs first described by Simpson et al (2002) is emission following biomass burning. Emission ratios (ERs) are often used to express trace gas emissions from biomass burning, where the background mixing ratio of the target compound is subtracted from the elevated concentration within a plume and then divided by the mixing ratio of a reference compound such as CO or CO_2. The conversion efficiency (CE), which is calculated using equation 2.15 is a factor that affects ERs and gives an indication to the state of the fire. For example, a $\Delta CO/\Delta CO_2 < 0.1$ ppmv ppmv^{-1} indicates a high CE, meaning the fire is flaming, whereas a $\Delta CO/\Delta CO_2 > 0.1$ ppmv ppmv^{-1} indicates a low CE associated with a smouldering fire (Bonsang et al., 1995).

$$CE = \frac{CO_{plume} - CO_{background}}{CO_{2\ plume} - CO_{2\ background}} \quad 2.15$$

Simpson et al (2002) found that methyl nitrate dominated during the flaming stage with peak mixing ratios of > 3 ppbv, whereas C_2-C_4 ANs were primarily emitted during the smoldering phase. The authors proposed that following peroxy radical self-reactions (2.16a) or reactions with NO (2.16b), the resultant hydroxy radical oxidises NO_2 to form the AN (2.16c).

$$RO_2 + RO_2 \rightarrow 2RO + O_2 \quad 2.16a$$
$$RO_2 \rightarrow RO + NO_2 \quad 2.16b$$
$$RO + NO_2 \rightarrow RONO_2 \quad 2.16c$$

This pathway allowed for the higher mixing ratios of methyl nitrate observed, as its formation is no longer constrained by oxidation of the parent hydrocarbon by OH or of NO by a peroxy radical. It is also consistent with the better correlation of larger ANs with CO than with CO_2 as the cooler temperatures during the smouldering phase favour larger radicals (Simpson et al., 2002). Although it is well understood that biomass burning is a source of ANs, their emissions are heavily dependent on the fuel source and therefore the environment (Akagi et al., 2011; Simpson et al., 2011)

Many of the simple ANs are both thermally stable (Hiskey et al., 1991; Politzer et al., 1997) and only slightly soluble in water (Luke et al., 1989), meaning thermal decomposition and wet deposition are minor loss mechanisms for this class of compounds. However, by analogy with the 'missing NO_y', discrepancies in the surface deposition rates also exist when calculated from the sum of deposition rates for individual species in comparison with surface deposition rates calculated for total NO_y, suggesting a missing loss term in the NO_y budget (Nielsen et al., 1995; Horii et al., 2006). Again, this discrepancy is often greatest in photochemically aged air masses and has therefore been attributed to the AN reservoir and has received greater research interest in recent years (Cornell et al., 2003; Russo et al., 2010). A recent study found evidence that this disagreement could partly be due to dry deposition of methyl nitrate, which has a higher solubility than other AN species (Russo et al., 2010), thereby also providing another pathway of possible terrestrial-atmospheric cycling of nitrogen.

The dominant sinks for ANs in the atmosphere however are via photolysis (He et al., 2011) and OH initiated oxidation (Aschmann et al., 2011). Both cause

comparable loss rates with AN lifetimes calculated to be approximately 2-5 weeks (Aschmann et al., 2011; He et al., 2011). Photolysis dominates for short chain ANs (C_1-C_3) whereas OH oxidation typically affects larger ANs (Talukdar et al., 1997a, Talukdar et al., 1997b). The longevity of ANs facilitates long distance transport to remote regions, where these loss processes can lead to the release of NO_x and subsequent O_3 formation.

Photolysis of ANs results in the formation of an alkoxy radical (RO) and NO_2 (2.17) (Talukdar et al., 1997a). The ratio of ANs to the parent hydrocarbon can be employed as a photochemical tracer and measure of age of an air mass during transport (Bertman et al., 1995). As the photochemical lifetimes of the C_2 and C_3 ANs are shorter than that of their parent hydrocarbon, the ratio of the two is expected to reach steady state over long processing times (weeks). In contrast for larger ANs, this ratio will increase indefinitely with time as they are longer lived than their parent hydrocarbons (Bertman et al., 1995). This relationship was first tested by Bertman et al (1995) who developed a simple kinetic analysis based on two sequential first order reactions and assumed that all peroxy radicals react with NO. This compared well with observations, though deviations from the predicted values have been observed in many studies for smaller ANs (Bertman et al., 1995; Simpson et al., 2003; Russo et al., 2010). It has been postulated that this deviation is due to an additional source of smaller ANs, which may be a result of decomposition of larger species, specifically alkoxy radicals (Bertman et al., 1995).

$$RONO_2 \xrightarrow{h\upsilon} RO + NO_2 \qquad 2.17$$

The products of OH initiated AN oxidation, including whether or not NO_2 is released, are not well known and direct evidence is ambiguous (Farmer and Cohen, 2008). The three known pathways are shown by reactions 2.18, where 2.18b and 2.18c represent a loss of alkyl nitrate functionality and are estimated to account for 6-30 % of reaction 2.1 in total (Farmer and Cohen, 2008).

$$RONO_2 + OH \rightarrow R'ONO_2 + H_2O \qquad 2.18a$$
$$\rightarrow R'O + HNO_3 \qquad 2.18b$$
$$\rightarrow ROOH + NO_2 \qquad 2.18c$$

Recent studies have provided a better understanding of the reaction pathways involved in 2.18, the fates of AN oxidation products and the consequences this has on the release of NO_x. The OH initiated oxidation of monofunctional, branched (Aschmann et al., 2011) and linear (Aschmann et al., 2012) ANs was found to proceed via H-atom abstraction, producing H_2O and a nitrooxy radical (2.19). If an ∝-nitrooxy radical is formed (2.19a), i.e. abstraction removes an H-atom from the same carbon bonded to the nitrate group, then a significant fraction of the NO_x contained within the AN is released due to rapid decomposition of the ∝-nitrooxy radical to form a carbonyl and NO_2 (2.20) (Vereecken et al., 2008).

$RONO_2 + OH$	→	$RC•ONO_2 + H_2O$	2.19a
	→	$C•RONO_2 + H_2O$	2.19b
$RC•ONO_2$	→	$RC(O)R + NO_2$	2.20
$C•RONO_2 + O_2$	→	$R(OO•)RONO_2$	2.21
$R(OO•)RONO_2 + NO$	→	$RONO_2RONO_2$	2.22a
	→	$RONO_2RO• + NO_2$	2.22b

For all other nitrooxy radicals, H-atom abstraction is followed by oxidation (2.21) before reaction with NO to form either a dinitrate (2.22a) or an alkoxy radical and NO_2 (2.22b). The amount of NO_x released from the AN following this pathway depends predominantly on the subsequent reactions of this alkoxy intermediate.

$RONO_2RO•$	→	$C•RONO_2ROH$	2.23
$C•RONO_2ROH + O_2 + NO$	→	$O•RONO_2ROH + NO_2$	2.24a
$O•RONO_2ROH$	→	$OHRONO_2R•OH$	2.24b
$OHRONO_2R•OH + O_2$	→	$OHRONO_2RO + HO_2$	2.24c
$RONO_2RO• + O_2$	→	$RONO_2RO + HO_2$	2.25
O•RONO2ROH	→	HCHO + ROHRO + NO2	2.26

The alkoxy radicals can undergo isomerization (2.23-24), reaction with O_2 (2.25) and / or decomposition (2.26). Recent kinetic (Atkinson, 2007) and experimental analysis (Aschmann et al., 2012) suggests that isomerization is the dominant pathway (2.23), which in the presence of NO, forms hydroxycarbonyl-

nitrates (2.24). Reaction of the alkoxy radical with O_2 results in the formation of multifunctional carbonyl-nitrates (2.25) and decomposition will eventually lead to the formation of carbonyls and NO_2 (2.26). Dinitrates may also be produced during alkyl nitrate oxidation, although this is thought to be a minor pathway (less than 5%) (Perring et al., 2009; Aschmann et al., 2012).

In low NO environments, RO_2 self-reactions (reactions with RO_2 and HO_2) dominate over RO_2 + NO (2.11a) and a greater yield of multifunctional hydroperoxy-, carbonyl- and hydroxycarbonyl- nitrates is expected (Aschmann et al., 2012). These multifunctional products will also undergo OH oxidation, photolysis or wet and/or dry deposition, but their exact fate and whether or not their degradation results in the release of NO_2 or the maintenance of alkyl nitrate functionality in the system is still unknown. For this reason, further investigation into these processes is merited to allow quantification of the contribution of alkyl nitrates as a NO_x source in remote environments.

Another important subgroup of alkyl nitrates are isoprene nitrates (INs), which have been found to represent a significant fraction of the alkyl nitrate group and up to 5% of total NO_y in environments such as forests where emissions are especially high (Grossenbacher et al., 2004; Perring et al., 2009). Isoprene is the dominant VOC accounting for ~44% of total global VOC emissions, estimated at 440-660 Tg yr^{-1} (Guenther et al., 2006). Therefore, any minor changes to isoprene chemistry can have major influences on global atmospheric chemistry.

OH oxidation of isoprene proceeds via reactions 2.9-2.11 to produce six chemically distinct hydroxynitrates with the branching ratio for reaction 2.11b estimated to be between 4.4-12% (Chen et al., 1998; Sprengnether et al., 2002). Oxidation of isoprene at night by NO_3 in high NO_x environments, produces another set of isoprene nitrates and has been found to be a dominant isoprene sink (Stroud et al., 2002; Warneke et al., 2004), accounting for >20% of isoprene losses (Rollins et al., 2009). The reaction pathways are identical to that of OH initiated oxidation, only with nitrooxyalkyl peroxy radicals formed as an intermediate (2.10) and the production of aldehydic or ketonic nitrates (2.11b) instead of a hydroxynitrate as described above. The branching ratio of isoprene nitrate formation and the relative importance of NO_3 oxidation compared with OH is unknown, though recent product analysis has found the organic nitrate yield of NO_3 initiated oxidation of isoprene to be 65 ± 12 % (Perring et al., 2009b). Although this is significantly lower than early findings of 80 % yields (Barnes et al., 1990), it confirms the importance of isoprene oxidation by NO_3, not only as an important contributor to the total alkyl nitrate pool, but also as an important isoprene sink as a result of their high solubility.

The deposition velocity of isoprene nitrates is thought to be comparable to that of HNO_3 (Giacopelli et al., 2005). For example in a pine forest in the eastern US where isoprene nitrates are dominant (Dreyfus et al., 2002), the deposition velocity of ΣANs was calculated to be 0.027 m s^{-1}, 80 % of HNO_3 (Farmer and Cohen, 2008). Additionally, isoprene nitrate abundance is strongly constrained by NO_x due to its control of OH concentrations, with greater rates of isoprene nitrate production at higher NO_x concentrations (Barket et al., 2001; Grossenbacher et al., 2001). This highlights the need to quantify the role of multifunctional alkyl nitrates and their associated products and their potential for sequestration of atmospheric NO_x and possible biosphere-atmosphere feedbacks.

2.2.4. Nitric Acid, HNO_3

Nitric acid (HNO_3) is the dominant form of reactive nitrogen in the atmosphere, though it is mainly found in the stratosphere at polar latitudes where it plays an important role in regulating O_3 concentrations and the development of the O_3 hole in polar springtime, through both the sequestration of NO_x and formation of Type 1 Nitric Acid Trihydrate (NAT) polar stratospheric clouds (PSCs) (Solomon, 1999). In contrast, it is estimated that only 10-15 % on a column basis is present in the troposphere (Wespes et al, 2009). Here it is formed predominantly via OH initiated oxidation of NO_2 as shown in reaction 2.27. However it should be noted that the heterogeneous hydrolysis reaction of N_2O_5, which will be discussed in section 2.27, is also thought to be a major source of HNO_3 (Dentener and Crutzen, 1993)

$$OH + NO_2 \rightarrow HNO_3 \qquad 2.27$$

Typically it is assumed that due to its high solubility, HNO_3 is lost from the system predominantly via wet or dry deposition and has a deposition velocity (V_g) in the range of 1-5 cm s^{-1} (Lovett, 1994), resulting in a tropospheric lifetime on the order of hours (Neuman et al., 2006). This loss rate precludes its relatively slow reaction with OH and photolysis, due to its absorption cross section decreasing rapidly within the actinic region (Finlayson-Pitts and Pitts, 2000). Consequently, this prevents reformation and long-range transport of NO_x and makes HNO_3 an irreversible NO_x sink. This inability to act as a NO_x sink and undergo long-range transport is a controversial subject however. In stratified, low-level emission plumes over oceanic environments, HNO_3 can be contained within an air parcel, thereby preventing precipitation or surface contact losses. By this mechanism there is evidence that

HNO_3 could be transported large distances prior to OH oxidation or photolysis, with subsequent reformation of NO_x concentrations sufficiently high to maintain an O_3 production regime in an otherwise pristine, remote marine boundary layer environment (Neuman et al., 2006).

Despite this on-going discussion, the deposition of HNO_3 is still considered to be the greatest loss mechanism for NO_x in the global atmosphere and has a significant effect on terrestrial systems through the formation of acid rain, which acts to damage the environment through the acidification of soils and waterways. Consequently, understanding its role in the atmosphere and quantifying its sources, sinks and reaction pathways is critical to the understanding of the Earth system as a whole. HNO_3 measurements in the troposphere are difficult and relatively sparse (Wespes et al., 2007) with chemistry and transport models failing to reproduce the limited observations (Staudt et al., 2003). Ground based measurements generally rely on gas sampling but intercomparisons between different techniques have shown discrepancies, mainly a result of losses to the walls of instruments as a consequence of its high solubility (Hering et al., 1988; Fehsenfeld et al., 1998, Day et al., 2002)

It is only recently that spatial, seasonal and inter-annual variations in stratospheric HNO_3 distributions have been detected through the use of limb sounders operating in the infrared (IR) spectral range (Orsolini et al., 2008; von Clarmann et al., 2009) and the first global distribution of HNO_3 in the troposphere was reported only in 2007 following the use of the high-resolution nadir infrared satellite, the Interferometric Monitor for Greenhouse gases (IMG) (Wespes et al., 2007). Clearly more long-term measurements are needed, not only to quantify HNO_3 distributions in the atmosphere, but also to use ground-based measurements to verify satellite measurements, which regarding HNO_3, are currently still in their infancy (Popp et al., 2009).

The biosphere-atmosphere exchange of HNO_3 not only affects terrestrial systems, it is also considered to be an important source of new nitrogen to oligotrophic ocean provinces such as gyre systems, with deposition leading to increases in ecosystem productivity (Paerl, 1985; Owens et al., 1992; Jordan and Talbot, 2000). More recently, it has been suggested that HNO_3 could also increase deposition of iron to high nutrient low chlorophyll (HNLC) surface waters. These iron-limited regions represent approximately 30 % of the world's oceans (de Baar and Boyd, 2000) and increases in productivity have been observed following the deposition of mineral dust, the dominant source of iron for HNLC environments (Jo et al., 2007). This is thought to occur due to the uptake of acids such as HNO_3 onto mineral dust surfaces, thereby creating extremely acidic environments that promote

iron dissolution and increase the amount of bioavailable iron following deposition (Cwiertny et al., 2008).

Nitrous acid (HONO) is another acid that is included in the NO_y definition and of atmospheric importance. This is on account of its role as a major source of OH, predominantly in polluted regions within the troposphere, following photodissociation due to the absorption of radiation with a wavelength of < 400 nm (reaction 2.28). HONO has been found to represent up to 80 % of the OH source during the early morning (Elshorbany et al., 2009) and contribute to between 20-60 % of daily OH production (Acker et al., 2006; Zhou et al., 2007; Villena et al., 2011).

$$HONO + h\upsilon \rightarrow OH + NO \qquad 2.28$$

Its formation can occur via both homogeneous and heterogeneous reaction pathways, though the dominant pathway is still questioned (Yu et al., 2009; Zhang et al., 2012). Heterogeneous production occurs through the reaction of NO_2 with H_2O on a surface as shown in reaction 2.29 and has been observed on surfaces such as soils, vegetation, glass and buildings (Zhou, 2007; Zhang et al., 2012)

$$2NO_2 + H_2O + surface \rightarrow HONO + HNO_3 \qquad 2.29$$

The homogeneous gas phase production of HONO can proceed via four main pathways. Reaction 2.29 can also occur in the absence of surfaces and is thought to dominate the homogeneous production pathways (reaction 2.30) (Yu et al., 2009). However reaction 2.31 has also been found to be significant, accounting for over 60 % of daytime HONO production (Elshorbany et al., 2009). Reaction 2.32 (Indarto, 2012) and the photolysis of HNO_3 (2.33) (Koch and Sodeau, 1995) may also provide important formation pathways.

$$2NO_2 + H_2O \rightarrow HONO + HNO_3 \qquad 2.30$$

$$NO + OH \rightarrow HONO \qquad 2.31$$

$$NO_2 + NO + H_2O \rightarrow 2HONO \qquad 2.32$$

$$HNO_3 \rightarrow HONO + O(^3P) \qquad 2.33$$

Mixing ratios of HONO range from tens of ppbv to tens of pptv in urban (Lee et al., 2002) and remote (Villena et al., 2011) environments respectively. However, it is the consistency of its significant contribution to OH production and therefore effect

on the atmospheric oxidising capacity, that provide the reasoning for further investigation and understanding of this important compound.

2.2.5. NO_3 Aerosol

Further to the role of HNO_3 in the gas phase chemistry of the atmosphere, it also has a significant effect on aerosol chemistry. Radiative forcing is defined as "an externally imposed perturbation in the radiative energy budget of the Earth's climate" (Forster, 2007) and aerosols can impact the radiative balance directly through both scattering and absorption and indirectly, predominantly through cloud formation. Forster et al (2007) estimate that globally, total direct aerosol radiative forcing derived from models and observations is approximately -0.5 ± 0.4 W m^{-2} (has a net cooling effect) as shown earlier in figure 1.2 and the inclusion of the cloud-albedo effect increases this cooling effect to -2.2 W m^{-2} (Forster, 2007).

Nitrate (NO_3^-) and ammonium (NH_4^+) ions are major constituents of atmospheric aerosols contributing up to 13 % of the global anthropogenic forcing (Xu and Penner, 2012) and in some instances, have been found to be more important than the sulfate aerosol loading (ten Brink et al., 1997; Malm et al., 2004). However the gas-aerosol partitioning of nitrate depends strongly on temperature, relative humidity and the availability of its precursors, with cooler temperatures and higher humidity favouring the aerosol phase (Dall'Osto et al., 2009). Their formation can occur via heterogeneous hydrolysis of N_2O_5 on the surface of aqueous aerosol particles (Brown et al., 2006) (2.34), adsorption of HNO_3 onto pre-existing particles with a sufficient water content (Seinfeld and Pandis, 2006) (2.35) and reaction between HNO_3 and ammonia (NH_3) to form ammonium nitrate (NH_4NO_3) (Nowak et al., 2010) (2.36). The latter is often the dominant fraction of nitrate aerosol and is formed if sulfate aerosols become irreversibly neutralised and excess NH_3 is available to react with HNO_3.

$$N_2O_5 + H_2O_{aerosol} \rightarrow 2HNO_3 \quad (2.34)$$

$$HNO_3 \leftrightarrow NO_3^- + H^+ \quad (2.35)$$

$$NH_3 + HNO_3 \leftrightarrow NH_4NO_3 \quad (2.36)$$

Although the present day aerosol loading and direct radiative forcing from nitrate aerosols is considerably smaller than that of sulfate aerosols (Liao et al., 2004), sulphur dioxide (SO_2) emissions are reducing due to restrictions whereas NO_x emissions are predicted to stabilize or continue to rise throughout the next century

(Makkonen et al., 2012). As a result of the predicted increase in NO_x:SO_2, it is thought that nitrate aerosols may grow increasingly important for the global aerosol budget and partially offset the loss of aerosol due to restricitons of SO_2 emissions through a compensatory effect caused by reaction 2.36 (Adams et al., 2001; Makkonen et al., 2012). This increasing importance of nitrogen oxides could also have significant consequences for cloud formation.

HNO_3 condenses onto aqueous aerosols at relative humidities close to and exceeding 100 % (Kulmala et al., 1997). With increasing humidity, large aerosols begin to activate to cloud droplets and as humidity continues to increase, so smaller aerosols are able to activate until peak relative humidity is reached, leaving any still smaller particles unactivated. Depending on conditions, the fraction of total aerosol that is activated can vary from 1 % to almost 100 % (Makkonen et al., 2012). The condensation of HNO_3 can increase an aerosols hygroscopic mass allowing activation at lower relative humidities and increase the total fraction of aerosol that is activated as it is more efficient at condensing onto smaller particles that have a greater surface area to volume ratio (Xue and Feingold, 2004). This effect of HNO_3 has been shown to be enhanced following the co-condensation of ammonia, which as a base acts to neutralise the solution resulting in condensation at lower relative humidities (Romakkaniemi et al., 2005). Although this potential shift in aerosol dynamics and the associated repercussions for atmospheric processes could occur within the next century, the scientific understanding of aerosol impacts is currently rated as medium-low (Forster, 2007) and consequently, further investigation is warranted to allow the effective incorporation of aerosol processes into global climate predictive models.

2.2.6. Halogen Nitrates

Halogen nitrates (HNs) of the form $XONO_2$, where 'X' represents a halogen molecule are another important class within NO_y. They are formed through the recombination of XO and NO_2 (reaction 2.37) and serve as an important reservoir for both NO_x and active halogens.

$$XO + NO_2 \rightarrow XONO_2 \qquad 2.37$$

Upon photolysis in the stratosphere and subsequent formation of X and NO, HNs can take part in stratospheric O_3 depletion through a catalytic destruction regime. This release of active halogens can also occur via the heterogeneous

hydrolysis of HNs on the surfaces of polar stratospheric clouds (PSCs) as shown in reaction 2.38. The catalytic O_3 destruction cycle for active halogens is shown in reaction scheme (2.39).

$$XONO_2 + H_2O_{(S)} \rightarrow HOX + HNO_3 \quad 2.38$$

$$X + O_3 \rightarrow XO + O_2 \quad 2.39a$$
$$XO + HO_2 \rightarrow HOX + O_2 \quad 2.39b$$
$$HOX + h\upsilon \rightarrow X + OH \quad 2.39c$$

$$\textit{Net: } 2O_3 + h\upsilon \rightarrow 3O_2 \quad 2.39$$

Halogen chemistry has also been shown to have a significant effect on O_3 chemistry in the remote marine boundary layer (Read et al., 2008). Halogen species in this environment include chloride (Cl^-), bromide (Br^-) and iodide (I^-). Whilst Cl^- is a major component of seawater, Br^- and I^- have biological sources, being produced by phytoplankton and macro algae in the surface ocean waters. These compounds undergo sea-to-air transfer where they can then undergo chemical reaction in the atmosphere and also form a major component of sea salt aerosol (SSA).

When incorporated into SSA, they have been shown to undergo reaction with dinitrogen pentoxide (N_2O_5) to form nitryl halides (2.40) (Finlayson-Pitts et al., 1989). Nitryl halides all absorb in the actinic region resulting in the production of reactive halogen radicals and whilst the relative importance of these reactions is uncertain, there remains the potential for an additional mechanism for O_3 destruction.

$$N_2O_5 + NaCl \rightarrow ClNO_2 + NaNO_3 \quad 2.40a$$
$$N_2O_5 + NaBr \rightarrow BrNO_2 + NaNO_3 \quad 2.40b$$
$$N_2O_5 + NaI \rightarrow INO_2 + NaNO_3 \quad 2.40c$$

2.2.7. Nocturnal Chemistry, NO_3 and N_2O_5

Owing to their photochemical source, OH and O_3 are the dominant oxidising species in the atmosphere during the day. However at night with the absence of solar radiation driving OH production, concentrations diminish due to reactions with atmospheric constituents. During the night, although O_3 still plays an important role, the nitrate radical (NO_3) becomes the dominant oxidising species and plays a key role in the nocturnal chemistry within the troposphere, with oxidation rates

comparable to that of OH for some VOCs (Wayne et al, 1991). NO_3 is formed via reaction 2.41 and upon further reaction with NO_2, produces and exists in thermal equilibrium with dinitrogen pentoxide (N_2O_5) as shown by reaction 2.42.

$$NO_2 + O_3 \rightarrow NO_3 + O_2 \qquad 2.41$$

$$NO_3 + NO_2 \rightarrow N_2O_5 \qquad 2.42$$

Although the rate of reaction 2.41 does not change significantly between day and night, NO_3 and N_2O_5 concentrations are small during the day. This is due to the loss of NO_3 via photolysis (2.43), which has a branching ratio of 0.13 and 0.87 for NO and NO_2 respectively (Sander et al., 2006) and a rapid $j[NO_3]$ rate of $\sim 0.2\ s^{-1}$ in direct sunlight (Stark et al., 2007), and reaction with NO (2.44), which as previously discussed is a primarily daytime species.

$$NO_3 + h\nu \rightarrow NO \qquad 2.43a$$

$$\rightarrow NO_2 \qquad 2.43b$$

$$NO_3 + NO \rightarrow 2NO_2 \qquad 2.44$$

As described in section 2.2.5, loss of N_2O_5 can proceed via heterogeneous hydrolysis resulting in the formation of HNO_3 and can occur in gas phase and on wet surfaces, the latter of which also catalyse the reaction.

Despite being typically nighttime species, in certain conditions such as those in heavily polluted environments where both O_3 and NO_x concentrations are high, daytime concentrations of NO_3 and N_2O_5 have been found to be up to 5 pptv (Geyer et al., 2003; Osthoff et al., 2006). This arises due to enhanced O_3 concentrations that act to increase NO_3 production (2.41), which in turn can perturb the photostationary steady state that exists for NO and NO_2 and lead to elevated N_2O_5 concentrations (2.42). However, this only led to significant NO oxidation during sunrise and sunset, or in fresh pollution plumes, when the photostationary steady state approximation is of questionable accuracy because of the increased time required to achieve a steady state (Geyer et al., 2003; Osthoff et al., 2006)

References

Acker, K., Möller, D., Wieprecht, W., Meixner, F. X., Bohn, B., Gilge, S., Plass-Dülmer, C. and Berresheim, H. (2006) Strong Daytime Production of OH from HNO_2 at a Rural Mountain Site, Geophysical Research Letters. 33, L02809.

Aschmann, S.M., Tuazon, E.C., Arey, J. and Atkinson, R. (2011) Products of the OH radicalinitiated reactions of 2-propyl nitrate, 3-methyl-2-butyl nitrate and 3-methyl-2-pentyl nitrate. *Atmospheric Environment*. **45**, 1695-1701.

Aschmanna, S.M., Areya, J. and Atkinson, R. (2012) Products of the OH radical-initiated reactions of 2- and 3-hexyl nitrate. *Atmospheric Environment*. **46**, 264-270.

Atkinson, R., Ashmann, S.M., Carter, W.P.L. and Winer, A.M. (1982) Kinetics of the gas-phase reactions of OH radicals with alkyl nitrates at 299 ± 2K. *International Journal of Chemical Kinetics*. **14**, 919-926.

Atkinson, R., Carter, W.P.L. and Winer, A.M. (1983) Effects of temperature and pressure of alkyl nitrate yields in the photo oxidations of n-pentane and n-heptane. *Journal of Physical Chemistry*. **87**, 2012-2018.

Atkinson, R. (2007) Rate constants for the atmospheric reactions of alkoxy radicals: An updated estimation method. *Atmospheric Environment.* **41**, 8468-8485.

Atlas, E., Pollock, W., Greenberg, J. and Heidt, L. (1993) Alkyl nitrates, nonmethane hydrocarbons and halocarbon gases over the equatorial Pacific Ocean during Saga 3. *Journal of Geophysical Research.* **98**, 16933-16,947.

Barket, D.J., Hurst, J.M., Couch, T.L., Colorado, A., Shepson, P.B., Riemer, D.D., Hills, A.J., Apel, E.C., Hafer, R., Lamb, B.K., Westberg, H.H., Farmer, C.T., Stabenau, E.R. and Zika, R.G. (2001) Intercomparison of automated methodologies for determination of ambient isoprene during the PROPHET 1998 summer campaign. *Journal of Geophysical Research - Atmospheres.* **106**, D20 24301-24313.

Barnes, I., Bastian, V., Becker, K.H. and Tong, Z. (1990) Kinetics and products of the reactions of NO3 with monoalkenes, dialkenes, and monoterpenes. *Journal of Physcial Chemistry*. **94**, 2413-2419.

Bertman, S.B., Roberts, J.M., Parrish, D.D., Buhr, M.P., Goldan, P.D., Kuster,W.C., Fehsenfeld, F.C., Montzka, S.A., and Westberg, H. (1995) Evolution of alkyl nitrates with air-mass age *Journal of Geophysical Research*. **100**, 22805-22813.

Blake, N.J., et al., 2003. Latitudinal, vertical, and seasonal variations of C1–C4 alkyl nitrates in the troposphere over the Pacific Ocean during PEM-Tropics A and B: oceanic and continental sources. *Journal of Geophysical Research.* **108**, D2 8242.

Brown, S.S., Ryerson, T.B., Wollny, A.G., Brock, C.A., Peltier, R., Sullivan, A.P., Weber, R.J., Dube, W.P., Trainer, M., Meagher, J.F., Fehsenfeld, F.C. and Ravishankara, A.R. (2006) Variability in nocturnal nitrogen oxide processing and its role in regional air quality. *Science*. **311**, 67-70.

Chen, X.H., Hulbert, D. and Shepson, P.B. (1998) Measurement of the organic nitrate yield from OH reaction with isoprene. *Journal of Geophysical Research - Atmospheres.* ***103****,* D19 25563-25568.

Cleary, P.A., Wooldridge, P.J., Millet, D.B., McKay, M., Goldstein, A.H. and Cohen, R.C. (2007) Observations of total peroxy nitrates and aldehydes: Measurement interpretation and inference of OH radical concentrations. *Atmospheric Chemistry and Physics*. **7**, 1947-1960.

Cornell, S.E., Jickells, T.D., Cape, J.N., Rowland, A.P. and Duce, R.A. (2003) Organic nitrogen deposition on land and coastal environments: A review of methods and data. *Atmospheric Environment*. **37**, 2173-2191.

Cwiertny, D.M., Baltrusaitis, J., Hunter, G.J., Laskin, A., Scherer, M.M. and Grassian, V.H. (2008) Characterization and acid-mobilization study of iron-containing mineral dust source materials. *Journal of Geophysical Research - Atmospheres*. **113**, D05202.

Dahl, E.E., Saltzman, E.S. and de Bruyn, W.J. (2003) The aqueous phase yield of alkyl nitrates from ROO + NO: Implications for photochemical production in seawater. *Geophysical Research Letters.* 30, 1271.

Dahl, E.E., Yvon-Lewis, S.A. and Saltzman, E.S. (2005) Saturation anomalies of alkyl nitrates in the tropical Pacific Ocean. *Geophysical Research Letters*. **32**, L20817.

Dahl, E.E., Yvon-Lewis, S.A. and Saltzman, E.S. (2007) Alkyl nitrate (C1–C3) depth profiles in the tropical Pacific Ocean. *Journal of Geophysical Research*. **112**, C01012.

Dahl, E.E. and Saltzman, E.S. (2008) Alkyl nitrate photochemical production rates in North Pacific seawater. *Marine Chemistry*. **112**, 137-141.

Dall'Osto, M., Harrison, R.M., Coe, H., Williams, P.I. and Allan, J.D. (2009) Real time chemical characterization of local and regional nitrate aerosols. *Atmospheric Chemistry and Physics*. **9**, 3709-3720.

Day, D.A., Wooldridge, P.J., Dillon, M.B., Thornton, J.A. and Cohen, R.C. (2002) A thermal dissociation laser-induced fluorescence instrument for in situ detection of NO2, peroxy nitrates, alkyl nitrates, and HNO_3. *Journal of Geophysical Research*. **107**, D64046.

Day, D.A., Dillon, M.B., Wooldridge, P.J., Thornton, J.A., Rosen, R.S., Wood, E.C. and Cohen, R.C. (2003) On alkyl nitrates, O3, and the "missing NOy,". *Journal of Geophysical Research*. **108**, D16 4501.

Day, D.A., Wooldridge, P.J. and Cohen, R.C. (2009) Observations of the effects of temperature on atmospheric HNO_3, ΣANs, ΣPNs, and NO_x: Evidence for a temperature-dependent HO_x source. *Atmospheric Chemistry and Physics*. **8**, 1867-1879.

Deyfrus, G.B., Schade, G.W. and Goldstein, A.H. (2002) Observational constraints on the contribution of isoprene oxidation to ozone production on the western slope of the Sierra Nevada, California. *Journal of Geophyscial Research - Atmospheres.***107**, D19 4365.

Elshorbany, Y.F., Kurtenbach, R., Wiesen, P., Lissi, E., Rubio, M., Villena, G., Gramsch, E., Rickard, A. R., Pilling, M. J. and Kleffmann, J. (2009) Oxidation

capacity of the city air of Santiago, Chile. *Atmospheric Chemistry and Physics*. **9**, 2257-2273.

Fahey, D.W., Hubler, G., Parrish, D.D., Williams, E.J., Norton, R.B., Ridley, B.A., Singh, H.B., Liu, S.C. and Fehsenfeld, F.C. (1986) Reactive nitrogen species in the troposphere: Measurements of NO, NO_2, HNO_3, particulate nitrate, peroxyacetyl nitrate (PAN), O3, and total reactive odd nitrogen (NOy) at Niwot Ridge, Colorado. *Journal of Geophysical Research*. **91**, 9781-9793.

Farmer, D.K. and Cohen, R.C. (2008) Observations of HNO3, ΣAN, ΣPN and NO_2 fluxes: evidence for rapid HO_x chemistry within a pine forest canopy. *Atmospheric Chemistry and Physics*. **8**, 3899-3917.

Finlayson-Pitts, B. J., Pitts, J. N., 2000. Chemistry of the Upper and Lower Atmosphere (1st Edition). Academic Press.

Fischer, R.G., Kastler, J. and Ballschmiter, K. (2000) Levels and pattern of alkyl nitrates, multifunctional alkyl nitrates, and halocarbons in the air over the Atlantic Ocean. *Journal of Geophysical Research - Atmospheres.* **105**, D11 14473-14494.

Forster, P., Ramaswamy, V., Artaxo, P., Berntsen, T., Betts, R., Fahey, D.W., Haywood, J., Lean, J., Lowe, D.C., Myhre, G., Nganga, J., Prinn, R., Raga, G., Schulz, M. and Van Dorland. R. (2007) Changes in Atmospheric Constituents and in Radiative Forcing, *In*, Climate Change 2007: The Physical Science Basis. Contribution of Working Group I to the Fourth Assessment Report of the Intergovernmental Panel on Climate Change. (Solomon, S., Qin, D., Manning, M., Chen, Z., Marquis, M., Averyt, K.B., Tignor, M. and Miller, H.L. Eds.). Cambridge University Press, Cambridge.

Geyer, A., Alicke, B., Ackermann, R., Martinez, M., Harder, H., Brune, W., di Carlo, P., Williams, E., Jobson, T., Hall, S., Shetter, R. and Stutz, J. (2003) Direct observations of daytime NO_3: Implications for urban boundary layer chemistry. *Journal of Geophysical Research - Atmospheres.* **108**, D12 4368.

Giacopelli, P., Ford, K., Espada, C. and Shepson, P.B. (2005) Comparison of the measured and simulated isoprene nitrate distributions above a forest canopy. *Journal of Geophysical Research*. **110**, D01304.

Grossenbacher, J.W., Barket, D.J., Shepson, P.B., Carroll, M.A., Olszyna, K. and Apel, E. (2004) A comparison of isoprene nitrate concentrations at two forest-impacted sites. *Journal of Geophysical Research*. **109**, D11311.

He, S., Chen, Z. and Zhang, X. (2011) Photochemical reactions of methyl and ethyl nitrate: A dual role for alkyl nitrates in the nitrogen cycle. *Environmental Chemistry*. **8**, 529-542.

Hiskey, M.A., Brower, K.R. and Oxley, J.C. (1991) Thermal decomposition of nitrate esters. *Journal of Physical* Chemistry. 95, 3955.

Hering, S.V., Lawson, D.R., Allegrini, I., Febo, A., Perrino, C., Possanzini, M., Sickles, J.E., Anlauf, K.G., Wiebe, A., Appel, B.R., John, W., Ondo, J., Wall, S., Braman, R.S., Sutton, R., Cass, G.R., Solomon, P.A., Eatough, D.J., Eatough, N.L., Ellis, E.C., Grosjean, D., Hicks, B.B., Womack, J.D., Horrocks, J., Knapp, K.T., Ellestad, T.G., Paur, R.J., Mitchell, W.J., Pleasant, M., Peake, E., Maclean, A., Pierson, W.R., Brachaczek, W., Schiff, H.I., Mackay, G.I., Spicer, C.W., Stedman, D.H., Winer, A.M., Biermann, H.W. And Tuazon, E.C. (1988) The nitric acid shootout - field comparison of measurement methods. *Atmospheric Environment*. **22**, 1519-1539.

Horowitz, L.W., Fiore, A.M., Milly, G.P., Cohen, R.C., Perring, A., Wooldridge, P.J., Hess, P.G., Emmons, L.K. and Lamarque, J.F. (2007) Observational constraints on the chemistry of isoprene over the Eastern U.S. *Journal of Geophysical Research - Atmospheres.* **112**, D12S08.

Horii, C.V., Munger, J.W., Wofsy, S.C., Zahniser, M., Nelson, D. and McManus, J.B. (2006) Atmospheric reactive nitrogen concentration and flux budgets at a Northeastern US forest site. *Agricultural and. Forest Meteorology*. **136**, 159-174.

Hudman, R.C., Jacob, D.J., Cooper, O.C., Evans, M.J., Heald, C.L. Park., R.J., Fehsenfeld, F., Flocke, F., Holloway, J., Hubler, G., Kita, K., Koike, M., Kondo, Y., Neuman, A., Nowak, J., Oltmans, S., Parrish, D., Roberts, J.M. and Ryerson, T. (2004) Ozone production in transpacific Asian pollution plumes and implications for ozone air quality in California. *Journal of Geophysical Research.* **109**, D23S10.

Indarto, A. (2012) Heterogeneous reactions of HONO formation from NO2 and HNO3: A review. *Research Chemistry Intermediates*. 38, 1029-1041.

Jacob, D.J., Logan, J.A., Gardner, G.M., (1993) factors regulating ozone over the united-states and its export to the global atmosphere. *Journal of Geophysical Research - Atmospheres*. **98**, D8 14817-14826.

Jo, C.O., Lee, J.Y., Park, K.A., Kim, Y.H. and Kim, K.R. (2007) Asian dust initiated early spring bloom in the northern East/Japan Sea. *Geophysical Research Letters*. **34**, L05602.

Jordan, C.E. and Talbot, R.W. (2000) Direct atmospheric deposition of water-soluble nitrogen to the Gulf of Maine. *Global Biogeochemical Cycles*. **14**, 1315-1329.

Kulmala, M., Laaksonen, A., Charlson, R.J. and Korhonen, P. (1997) Clouds without supersaturation. *Nature*, **338**, 336-337.

LaFranchi, B.W., Wolfe, G.M., Thornton, J.A., Harrold, S.A., Browne, E.C., Min, K.E., Wooldridge, P.J., Gilman, J.B., Kuster, W.C., Goldan, P.D., deGouw, J.A., McKay, M., Goldstein, A.H., Ren, X., Mao, J. and Cohen, R.C. (2009) Closing the peroxy acetyl (PA) radical budget: observations of acyl peroxy nitrates (PAN, PPN, and MPAN) during BEARPEX 2007. *Atmospheric Chemistry and Physics* Discussions. **9**, 9879-9926.

Liao, H., Seinfeld, J.H., Adams, P.J. and Mickley, L.J. (2004) Global radiative forcing of coupled tropospheric ozone and aerosols in a unified general circulation model. *Journal of Geophysical Research*. **109**, D16207.

Liu, S.C., Trainer, M., Fehsenfeld, F.C., Parrish, D.D., Williams, E.J., Fahey, D.W., Hubler, G. And Murphy, P.C. (1987) Ozone production in the rural troposphere and the implications for regional and global ozone distributions. *Journal of Geophysical Research – Atmospheres*. **92**, D4 4191-4207.

Lovett, G.M. (1994) Atmospheric deposition of nutrients and pollutants in North America: An ecological perspective. *Ecological Applications*. **4**, 629-650.

Luke, W.T., Dickerson, R.R. and Nunnermacker, L.J. (1989) Direct measurements of the photolysis rate cofficients and Henry's Law constants of several alkyl nitrates. *Journal of Geophysical Research.* **94**, 14905.

Makkonen, R., Romakkaniemi, S., Kokkola, H., Stier, P., aisänen, P.R., Rast, S., Feichter, J., Kulmala, M. and Laaksonen, A. (2012) Brightening of the global cloud field by nitric acid and the associated radiative forcing. *Atmospheric Chemistry and Physics*. **12**, 7625-7633.

Malm, W.C., Schichtel, B.A., Pitchford, M.L., Ashbaugh, L.L. and Eldred, R.A. (2004) Spatial and monthly trends in speciated fine particle concentration in the United States. *Journal of Geophysical Research - Atmospheres*. **109**, D03306.

Min, K.E., Pusede, S.E., Browne, E.C., LaFranchi, B.W., Wooldridge, P.J., Wolfe, G.M., Harrold, S.A., Thornton, J.A. and Cohen, R.C. (2012) Observations of atmosphere-biosphere exchange of total and speciated peroxynitrates: nitrogen fluxes and biogenic sources of peroxynitrates. *Atmospheric Chemistry and Physcis*. **12**, 9763-9773.

Montanya, J., Soula, S. and Pineda, N. (2007) A study of the total lightning activity in two hailstorms. *Journal of Geophysical Research - Atmospheres*. **112**, D13118.

Moxim, W.J., Levy, H. and Kasibhatla, P.S. (1996) Simulated global tropospheric PAN: Its transport and impact on NO_x. *Journal of Geophysical Research - Atmospheres.* **101**, D7 12621-12638.

Murphy, J.G., Thornton, J.A., Wooldridge, P.J., Day, D.A., Rosen, R.S., Cantrell, C., Shetter, R.E., Lefer, B. and Cohen, R.C. (2004) Measurements of the sum of HO_2NO_2 and $CH_3O_2NO_2$ in the remote troposphere. *Atmospheric Chemistry and Physcis.* **4**, 377-384.

Neu, J.L., Lawler, M.J., Prather, M.J. and Saltzman, E.S. (2008) Oceanic alkyl nitrates as a natural source of tropospheric ozone. *Geophysical Research Letters.* **35**, L13814.

Neuman, J.A., et al. (2006) Reactive nitrogen transport and photochemistry

in urban plumes over the North Atlantic Ocean. *Journal of Geophysical Research.* **111**, D23S54.

Nielsen, T., Egelov, A.H., Granby, K. and Skov, H. (1995) Observations on particulate organic nitrates and unidentified components of NO_y. *AtmosphericEnvironment*. **29**, 1757-1769.

Nowak, J.B., Neuman, J.A., Bahreini, R., Brock, C.A., Middlebrook, A.M., Wollny, A.G., Holloway, J.S., Peischl, J., Ryerson, T.B. and Fehsenfeld, F.C. (2010) Airborne observations of ammonia and ammonium nitrate formation over Houston, Texas. *Journal of Geophysical Research - Atmospheres*. **115**, D22304.

Orlando, J.J. and Tyndall, G.S. (2002) Mechanisms for the reactions of OH with two unsaturated aldehydes: Crotonaldehyde and acrolein. *Journal of Physical Chemistry*. **106**, 12252-12259.

Orsolini, Y.J., Urban, J. and Murtagh, D.P. (2008) Nitric acid in the stratosphere based on Odin observations from 2001 to 2007 – Part 2: High-altitude polar enhancements, *Atmospheric Chemistry and Physics.* **8**, 9591, 9605.

Osthoff, H., Brown, S., Ryerson, T., Fortin, T., Lerner, B., Williams, E., Pettersson, A., Baynard, T., Dube, W., Ciciora, S. and Ravishankara, A. (2006) Measurement of atmospheric NO_2 by pulsed cavity ring-down spectroscopy. *Journal of Geophysical Research - Atmospheres*. **111**, D12305.

Owens, N.J.P., Galloway, J.N. and Duce, R.A. (1992) Episodic atmospheric nitrogen deposition to oligotrophic ocEANS. *Nature*. **357**, 397-399.

Paerl, H.W. (1985) Enhancement of marine primary production by nitrogen-enriched acid-rain. *Nature*. **6022**, 747-749.

Parrish, D.D., Millet, D.B. and Goldstein, A.H. (2009) Increasing ozone in marine boundary layer inflow at the west coasts of North America and Europe. *Atmospheric Chemistry and Physics*. **9**, 1303-1323.

Parton, W.J., Hartman, M., Ojima, D. and Schimel, D. (1998) DAYCENT and its land surface submodel: Description and testing. *Global and Planetary Change*. **19**, 35-48.

Perring, A.E., Wisthaler, A., Graus, M., Wooldridge, P.J., Lockwood, A.L., Mielke, L.H., Shepson, P.B., Hansel, A. and Cohen, R.C. (2009) A product study of the isoprene + NO_3 reaction. *Atmospheric chemistry and Physics Discussions*. **9**, 5231-5261.

Politzer, P., Seminario, J.M., Concha, M.C. and Zacarias, A.G. (1997) Densityfunctional investigation of some decomposition routes of methyl nitrate. *International Journal of Quantum Chemistry*. **64**, 205.

Popp, P.J., Marcy, T.P., Gao, R.S., Watts, L.A., Fahey, D.W., Richard, E.C., Oltmans, S.J., Santee, M.L., Livesey, N.J., Froidevaux, L., Sen, B., Toon, G.C., Walker, K.A., Boone, C.D. and Bernath, P.F. (2009) Stratospheric correlation between nitric acid and ozone. *Journal of Geophysical Research - Atmospheres*. **114**, D03305.

Postgate, J. R. (1982) The fundamentals of nitrogen fixation. Cambridge University Press.

Ravishankara, A.R. Daniel, J.S. Portmann, R.W. (2009) Nitrous Oxide (N_2O): The Dominant Ozone-Depleting Substance Emitted in the 21st Century. *Science*. **326**, 123-125.

Read, K., Mahajan, A., Carpenter, L., Evans, M., Faria, B., Heard, D., Hopkins, J., Lee, J.D, Moller, S.J, Mendes, L.A., McQuaid, J., Oetjen, H., Saiz-Lopez, A., Pilling, M. and Plane, J.M.C. (2008) Extensive halogen-mediated ozone destruction over the tropical Atlantic Ocean. Nature. 453, 1232-1235.

Roberts, J.M. (1990) The atmospheric chemistry of organic nitrates. Atmospheric Environment. 24, 243-287.

Roberts, J.M. and Bertman, S.B. (1992) The Thermal Decomposition of PeroxyAcetic Nitric Anhydride (PAN) and Peroxymethacrylic Nitric Anhydride (MPAN). *International Journal of Chemical Kinetics*. **24**, 297-307.

Roberts, J.M., Williams, J., Baumann, K., Buhr, M.P., Goldan, P.D., Holloway, J., Hubler, G., Kuster, W.C., McKeen, S.A., Ryerson, T.B., Trainer, M., Williams, E.J., Fehsenfeld, F.C., Bertman, S.B., Nouaime, G., Seaver, C., Grodzinsky, G., Rodgers,

M. and Young, V.L. (1998) Measurements of PAN, PPN, and MPAN made during the 1994 and 1995 Nashville Intensives of the Southern Oxidants Study: Implications for regional ozone production from biogenic hydrocarbons. *Journal of Geophysical Research*. **103**, 22473-22490.

Roberts, J.M., Stroud, C.A., Jobson, B.T., Trainer, M., Hereid, D., Willaims E., Fehsenfeld, F., Brune, W., Martinez, M. and Harder. H. (2001) Application of sequential reaction model to PANs and aldehyde measurements in two urban areas. *Geophysical Research Letters*. **28**, 4583-4596.

Roberts, J.M., Marchewka, M. and Bertman, S.B. (2007) Measurements of PANs during the New England air quality study 2002. *Journal of Geophysical Research - Atmospheres.* **112**, D20306.

Rollins, A.W., Kiendler-Scharr, A., Fry, J.L., Brauers, T., Brown, S.S., Dorn, H.P., Dube, W.P., Fuchs, H., Mensah, A., Mentel, T.F., Rohrer, F., Tillmann, R., Wegener, R., Wooldridge, P.J. and Cohen, R.C. (2009) Isoprene oxidation by nitrate radical: alkyl nitrate and secondary organic aerosol yields. *Atmospheric Chemistry and Physics*. **18**, 6685-6703.

Romakkaniemi, S., Kokkola, H., and Laaksonen, A. (2005) Parameterization of the nitric acid effect on CCN activation. *Atmospheric Chemistry and Physics*. **5**, 879-885.

Russo, R.S., Zhou, Y., Haase, K.B., Wingenter, O.W., Frinak, E.K., Mao, H., Talbot, R.W. and Sive, B.C. (2010) Temporal variability, sources, and sinks of C1-C5 alkyl nitrates in coastal New England. *Atmospheric Chemistry and Physics*. **10**, 1865-1883.

Sander, S., Ravishankara, A., Golden, D., Kolb, C., Kurylo, M., Molina, M., Moortgat, G., Finlayson-Pitts, B., Wine, P., Huie, R. and Orkin, V. (2006) Chemical kinetics and photochemical data for use in atmospheric studies, evaluation number 15. National Aeronautics and Space Administration, Jet Propulsion Laboratory.

Simpson, I.J., Meinardi, S., Blake, D.R., Blake, N.J., Rowland, F.S., Atlas, E. and Flocke, F. (2002) A biomass burning source of C1-C4 alkyl nitrates. *Geophysical Research Letters*. **29**, 2168.

Simpson, I.J., Blake, N.J., Blake, D.R., Atlas, E., Flocke, F., Crawford, J.H., Fuelberg, H.E., Kiley, C.M., Meinardi, S. and Rowland, F.S. (2003) Photochemical production and evolution of selected C2–C5 alkyl nitrates in tropospheric air influenced by Asian outflow. *Journal of Geophysical Research*. **108**, D20 8808.

Singh, H.B. and Hanst, P.L. (1981) Peroxyacetyl nitrate (pan) in the unpolluted atmosphere: an important reservoir for nitrogen oxides. *Geophysical Research Letters*. **8**, 941-944,

Solomon, S. (1999) Stratospheric Ozone Depletion: A review of concepts and history. *Reviews in Geophysics.* **37**, 275-316.

Sparks, J.P., Roberts, J.M. and Monson, R.K. (2003) The uptake of gaseous organic nitrogen by leaves: A significant global nitrogen transfer process. *Geophysical Research Letters*. **30**, 2189.

Sparks, J.P. (2009) Ecological ramifications of the direct foliar uptake of nitrogen. *Ocealogia*. **159**, 1-13.

Sprengnether, M., Demerjian, K.L., Donahue, N.M. and Anderson, J.G. (2002) Product analysis of the OH oxidation of isoprene and 1,3-butadiene in the presence of NO. *Journal of Geophysical Research - Atmospheres.* **107**, D15 4269.

Stark, H., Lerner, B.M., Schmitt, R., Jakoubek, R., Williams, E.J., Ryerson, T.B., Sueper, D.T., Parrish, D.D. and Fehsenfeld, F.C. (2007) Atmospheric in situ measurement of nitrate radical (NO_3) and other photolysis rates using spectroradiometry and filter radiometry. *Journal of Geophysical Research - Atmospheres.* **112**, D10S04.

Staudt, A.C., Jacob, D.J., Ravetta, F., Logan, J.A., Bachiochi, D., Krishnamurti, T.N., Sandholm, S., Ridley, B., Singh, H.B. and Talbot, B. (2003) Sources and chemistry of nitrogen oxides over the tropical Pacific. *Journal of Geophysical Research - Atmospheres*. **108**, D2 8239.

Stroud, C.A., Roberts, J.M., Williams, E.J., Hereid, D., Angevine, W.M., Fehsenfeld, F.C., Wisthaler, A., Hansel, A., Martinez Harder, M., Harder, H., Brune, W.H.,

Hoenninger, G., Stutz, J. and White, A.B. (2002) Nighttime isoprene trends at an urban forested site during the 1999 Southern Oxidant Study. *Journal of Geophysical Research - Atmospheres.***107**, 4291.

Talbot, R.W., Dibb, J.E., Scheuer, E.M., Bradshaw, J.D., Sandholm, S.T., Singh, H.B., Blake, D.R., Blake, N.J., Atlas, E. and Flocke, F. (2000) Tropospheric reactive odd nitrogen over the South Pacific in austral springtime. *Journal of Geophysical Research.***105**, D5 6681-6694.

Talukdar, R.K., Burkholder, J.B. and Schmoltner, A.M. (1995) Investigation of the loss processes for peroxyacetyl nitrate in the atmosphere - uv photolysis and reaction with oh. *Journal of Geophysical Research - Atmospheres.* **100**, D7 14163-14173.

Talukdar, R.K., Herndon, S.C., Burkholder, J.B., Roberts, J.M. and Ravishankara, A.R. (1997a). Atmospheric fate of several alkyl nitrates, Part 2: UV absorption cross-sections and photodissociation quantum yields. *Journal of the Chemical Society, Faraday Transactions.* **93**, 2797-2805.

Talukdar, R.K., Herndon, S.C., Burkholder, J.B., Roberts, J.M. and Ravishankara, A.R. (1997b) Atmospheric fate of several alkyl nitrates, Part 1: Rate coefficients of the reactions of alkyl nitrates with isotopically labeled hydroxyl radicals. *Journal of the ChemicalSociety, Faraday Transactions.* **93**, 2787-2796.

Teklemariam, T.A. and Sparks , J.P. (2004) Gaseous fluxes of peroxyacetyl nitrate (PAN) into plant leaves. *Plant Cell and Environment*. **27**, 1149-1158.

ten Brink, H.M., Kruisz, C., Kos, G.P.A. and Berner, A. (1997) Composition/size of the light-scattering aerosol in the Netherlands. *Atmospheric Environment*. **31**, 3955-3962.

Thompson, A.M. et al. (1993) Ozone observations and a model of marine boundary layer photochemistry during SAGA-3. *Journal of Geophysical Research*. **98**, 16955-16968.

Turnipseed, A.A., Huey, L.G., Nemitz, E., Stickel, R., Higgs, J., Tanner, D.J., Slusher, D.L., Sparks, J.P., Flocke, F. and Guenther, A. (2006) Eddy covariance

fluxes of peroxyacetyl nitrates (PANs) and NO_y to a coniferous forest. *Journal of Geophysical Research*. **111**, D09304.

Vereecken, L. (2008) Computational study of the stability of a-nitroxy-substituted alkyl radicals. *Chemical Physics Letters*. **466**, 127-130.

Villena, G., Kleffmann, J, Kurtenbach, R.,Wiesen, P., Lissi, E., Rubio, M.A., Croxatto, J. and Rappenglück, B. (2011) Vertical gradients of HONO, NO_x and O_3 in Santiago de Chile. *Atmospheric Environment*. **45**, 3867-3873.

Wayne, R.P., Barnes, I., Biggs, P., Burrows, J.P., Canosamas, C.E., Hjorth, J., Lebras, G., Moortgat, G.K., Perner, D., Poulet, G., Restelli, G. and Sidebottom, H. (1991) The nitrate radical - Physics, chemistry, and the atmosphere. *Atmospheric Environment*. **25**, 1-203.

Wayne, R. P., 2000. Chemistry of Atmospheres (3rd Edition). Oxford University Press.

Wespes, C., Hurtmans, D., Herbin, H., Barret, B., Turquety, S., Hadji-Lazaro, J., Clerbaux, C., and Coheur, P.F. (2007) First global distributions of nitric acid in the troposphere and the stratosphere derived from infrared satellite measurements. *Journal of Geophysical Research*. **112**, D13311.

Williams, E.J., Roberts, J.M., Baumann, K., Bertman, S.B., Buhr, S., Norton, R.B. and Fehsenfeld, F.C. (1997) Variations in NOy composition at Idaho Hill, Colorado, *Journal of Geophysical Research*. **102**, D5 6297-6314.

Wolfe, G.M., Thornton, J.A., Yatavelli, R.L.N., McKay, M., Goldstein, A.H., LaFranchi, B., Min, K.E. and Cohen, R.C. (2009) Eddy covariance fluxes of acyl peroxy nitrates (PAN, PPN and MPAN) above a Ponderosa pine forest. *Atmospheric Chemistry and Physics*. **9**, 615-634.

Wooldridge, P.J., Perring, A.E., Bertram, T.H., Flocke, F.M., Roberts, J.M., Singh, H.B., Huey, L.G., Thornton, J.A.,Wolfe, G.M., Murphy, J.G., Fry, J.L., Rollins, A.W., LaFranchi, B.W. and Cohen, R.C. (2010) Total Peroxy Nitrates (6PNs) in the atmosphere: The Thermal Dissociation-Laser Induced Fluorescence

(TD-LIF) technique and comparisons to speciated PAN measurements. *Atmospheric Measurement Techniques*. **3**, 593-607.

Zhang, K., O'Donnell, D., Kazil, J., Stier, P., Kinne, S., Lohmann, U., Ferrachat, S., Croft, B., Quaas, J., Wan, H., Rast, S. and Feichter, J. (2012) The global aerosol-climate model ECHAMHAM, version 2: Sensitivity to improvements in process representations. *Atmospheric Chemistry and Physicas Discussions*. **12**, 7545-7615.

Chapter 3

NO_x Measurements

3.1. Measurement Techniques

3.1.1. Differential Optical Absorption Spectrometry (DOAS)

Many atmospheric constituents have absorption cross-sections in the UV and visible region of the spectrum. Although the abundance of compounds that do absorb in this region creates a limitation to the application of differential optical absorption spectrometry (DOAS), many have species-specific narrow band absorption structures that allow them to be identified. Species that can be measured and are relevant to this work include; NO_2, O_3, HONO and NO_3. Concentrations are determined by comparing light intensity in a given path length, both with and without the presence of the compound of interest, or by comparing the light intensity from two different path lengths. These measurements give values for I and I_0 from the Beer-Lambert law (3.1.) respectively and the compounds absorption spectrum can then also be used to calculate its concentration.

$$ln\left(\frac{I(\lambda)}{I_o(\lambda)}\right) = -L \sum_i \sigma_i(\lambda)\,\beta_i \qquad 3.1$$

where

λ	=	wavelength
$I(\lambda)$	=	light intensity in the presence of absorbers
$I_0(\lambda)$	=	light intensity without absorbers
L	=	optical path length
$\sigma_i(\lambda)$	=	absorption cross section of the i^{th} absorber
β_i	=	concentration of the i^{th} absorber

NO_2 has multiple absorption bands that can be measured using DOAS; 310-340 nm, 421-437 nm and 437-449 nm. Limits of detection for NO_2 using long-path DOAS (where the path length is on the order of tens of kilometres or greater) have been in the region of 30-200 pptv (Platt, 1994; Plane and Smith, 1995), making it a good candidate for measurements in more remote regions. Additional advantages of this system are that it does not require calibration due to the high specificity to its target molecule. However, there are major drawbacks in that not all molecules have the absorbance structure required for identification. The large path lengths required also causes problems due to non-uniform air masses when working on the scale of

tens of kilometres and its use is restricted by meteorological conditions such as fog which increase scattering, thereby affecting transmission (Finlayson-Pitts and Pitts, 2000).

3.1.2. Cavity Ring-Down Spectroscopy (CRDS)

Cavity ring-down spectroscopy (CRDS) is a laser absorption technique used to measure NO_2. A light pulse is emitted from a tunable laser into a reaction cell and is reflected repeatedly within the cell between two mirrors. The light is then turned off and the exponential loss of light intensity through the end mirror is then measured over time to give a ring-down time constant. Similar to the DOAS technique, this time constant is measured both with (τ) and without (τ_0) the target molecule present. Concentrations can then be determined via equation 3.2.

$$[\mathrm{NO_2}] = \frac{R_L}{c\,\sigma_{\mathrm{NO2}}}\left(\frac{1}{\tau} - \frac{1}{\tau_0}\right) \qquad 3.2$$

where

R_L = ratio of total cavity length to length over which absorber is present

c = speed of light

σ_{NO2} = absorption cross section of NO_2

Due to the many reflections involved in this technique, the path length can become very long for high quality mirrors with minimal intensity loss. As a result, this technique has a high sensitivity with a limit of detection in the range of tens of pptv and has been shown to agree well with the established chemiluminescence technique (Osthoff et al., 2006).

3.1.3. Laser Induced Fluorescence (LIF)

Laser induced fluorescence (LIF) is a technique that has been shown to measure both NO and NO_2. NO can be measured using a two-photon LIF technique. This involves excitation of the NO by a laser with a wavelength of 226 nm. A second laser with a wavelength of 1.1 μm then excites the NO to a higher energy state, which, as it relaxes back to ground state, fluoresces with a wavelength of 187-220 nm. Although it has a sensitivity of tens of pptv (Sandholm et al., 1997), the complexity and size of the instrument means that it is generally unsuitable for use in field studies. More recently, this has technique has been developed further so that NO has also been measured using a single photon excitation, whilst maintaining sensitivity (Miyazaki et al., 2008).

There are many measurements of NO_2 using the LIF technique (Thornton et al., 2000; Cleary et al., 2002; Dari-Salisburgo et al., 2009). NO_2 can be selectively excited using a narrow band laser, the resultant fluorescence detected and interference from alternative sources of radiation removed through the use of optical filters. This is a highly sensitive method, capable of measuring concentrations lower than 5 pptv. This method has the added benefit of being a direct NO_2 measurement, thereby removing the need for conversion of NO_2 to NO before detection and the interferences and problems associated with this process.

3.1.4. Chemiluminescence

The method used for measuring NO_x at the Cape Verde Atmospheric Observatory (CVAO) and during laboratory calibration of the NO_y inlet in this study is via chemiluminescence. Chemiluminescence is the emission of electromagnetic radiation in the form of light following a chemical reaction. It occurs when an excited molecule transitions from a higher to a lower energy state, causing the release of excess energy (Finlayson-Pitts and Pitts, 2000). For the measurement of NO, gas phase oxidation by the addition of O_3 creates excited state NO_2 as shown in reaction 3.3. Electronically excited NO_2 can then undergo either subsequent relaxation causing the emission of chemiluminscence as shown by reaction 3.4, or the energy can be quenched via reaction with M as shown in reaction 3.5.

$$NO + O_3 \rightarrow NO_2^* + O_2 \quad 3.3$$

$$NO_2^* \rightarrow NO_2 + h\upsilon \quad 3.4$$

$$NO_2^* + M \rightarrow NO_2 + M \quad 3.5$$

The intensity of the light emitted via reaction 3.4 is proportional to the concentration of the reactant, therefore providing a direct measure of NO concentrations. However it should be noted that reaction 3.5 represents interference in the measurement that will cause an underestimation of actual NO concentrations as this pathway does not fluoresce. This interference can be minimised by reducing the pressure in the reaction chamber, and therefore the concentration of M.

Following conversion to NO prior to detection, NO_2 concentrations can also be measured using this method. This conversion can be either photolytic, which is a more selective method (Kley and McFarland, 1980), or through the use of catalytic reduction. For the latter, the most common catalysts used are molybdenum oxide heated to 350 °C or gold heated to 300 °C accompanied by a small flow of CO to act as a reducing agent. However, it is has been shown that these catalysts reduce all –NO containing species to NO, thereby giving a measure of total NO_y rather than just NO. Indeed, these catalysts are widely used for this purpose and both show near 100 % conversion (Williams et al., 1998).

Owing to the techniques versatility and selectivity, it has become the most widely used for the measurements of NO and NO_2. Due to its high sensitivity, it is also able to detect concentrations lower than 5 pptv, making it suitable for determining the concentrations of trace gases in pristine environments.

3.1.5. O_3 Measurements

Although O_3 measurements were not carried out as part of this report, data from the CVAO is used for analysis and therefore the method of detection merits a brief description. O_3 measurements at the CVAO are carried out using UV absorption (TEI 49 C), which analyses the proportion of incident UV light produced by a mercury lamp that passes through a sample of O_3. An O_3 scrubber is used to filter ambient air and produce a zero measurement that can be used as a reference light intensity for measurements of ambient air that bypass this scrubber. A photodetector then measures the reduction in light intensity at 254 nm, the wavelength of maximum O_3 absorption, with the difference in light intensity being related to the O_3 concentration and can be calculated using the Beer-Lambert Law as shown in equation 3.6, where,

$$I = I_0 \exp(-\alpha L C) \qquad 3.6$$

where,

I = light intensity following O_3 absorption
I_0 = light intensity at zero O_3 concentration
α = O_3 molar absorption coefficient
L = pathlength
C = O_3 concentration

3.2. CVAO NO_x Instrument

3.2.1. NO_x Inlet

As stated, the technique used for measuring NO_x at the CVAO and during laboratory calibration of the NO_y inlet is via chemiluminescence. Both the CVAO and laboratory instruments used are essentially identical and so will be described as one in this report, with any major differences made clear in the text. It is a single-channel chemiluminescence instrument, manufactured by Air Quality Design Inc., USA (Lee et al., 2009), which uses O_3 oxidation to measure NO concentrations, as shown in reactions 3.3 and 3.4. The NO_2 converter used in this system is photolytic, using two light emitting diode (LED) arrays that produce radiation with a wavelength of 385-405 nm. The NO_2 to NO conversion efficiency of this setup is typically in the range of 35-40 % for a residence time of 1 second (Lee et al., 2009). The LEDs can be turned off and on to give a measure of NO and of NO+ NO_2 respectively, within the same channel. The former can then be subtracted from the latter to give a signal that corresponds to NO_2 only (Lee et al, 2009).

Figure 3.1 is a schematic drawing of the NO_x inlet and table 3.1 describes the parameter settings of the instrument and all models and manufacturers of instrument parts are listed in appendix 3.1. Each compartment of the NO_x inlet is shown in greater detail in figures 3.2-4 with parts described in tables 3.2-3.4**.**

Table 3.1. Parameter settings during instrument operation.

Parameter	Setting
PMT temperature	-30 °C
Zero volume temperature	40 °C
Reaction cell temperature	40 °C
Control (laboratory) temperature	25 °C
Reaction cell pressure	5 Torr
Oxygen flow	0.1 L min^{-1}
Sample flow	1 L min^{-1}

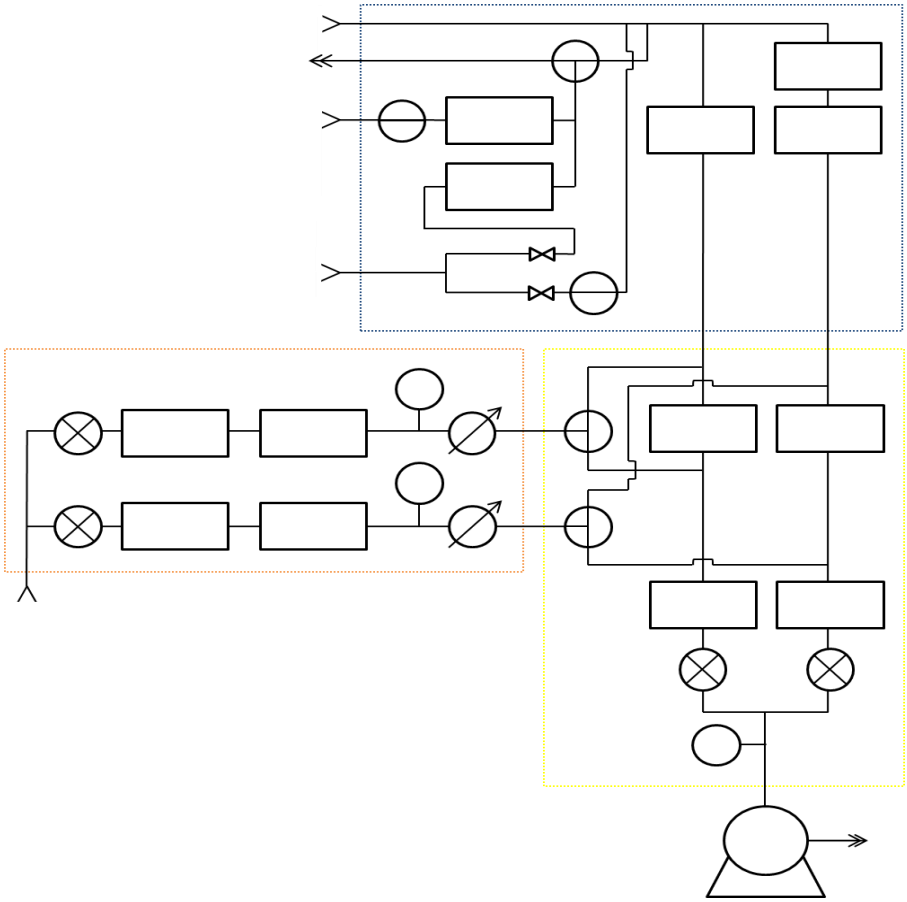

Figure 3.1. Schematic of the NO_x instrument. ■ = NO_x inlet, ■ = Ozonizer box, ■ = Snooper box.

The NO_x chemiluminescence instrument can be divided into three regions; the inlet, the ozonizer and the snooper (figure 3.1). An external vacuum pump draws air in through the systems inlet at a flow rate of 2.5 L min^{-1} (figure 3.2). The sample is then divided and controlled by separate mass flow controllers, to provide a sample flow in each channel of 1 L min^{-1} with a small overflow to prevent the sampling of laboratory air. The inlet also contains two tee junctions prior to the channel separation. These allow a known amount of NO calibration gas or zero air, generated by an Ecophysics PAG 003 pure air generator (PAG), to be introduced for the purposes of calibrating and zeroing the instrument as will be discussed below.

The ozonizer box (figure 3.3) comprises of an O_3 generator that allows O_3 to be introduced into both sample lines in the snooper box. This is used to generate NO_2 via NO oxidation as shown in reaction 3.3, therefore allowing the measurement of both NO and NO_2. The O_3 can be added directly before the main reaction chamber, or further upstream into a pre-chamber. As will be described below, adding O_3 to the pre-chamber allows the quantification of interferences in the NO and NO_2 measurements.

The snooper box (figure 3.4) contains both the pre-chamber where chemical interferences are quantified as well as the main reaction chamber where NO and NO_2 are measured. The chemiluminescence method used is described in detail in section 3.2.2.

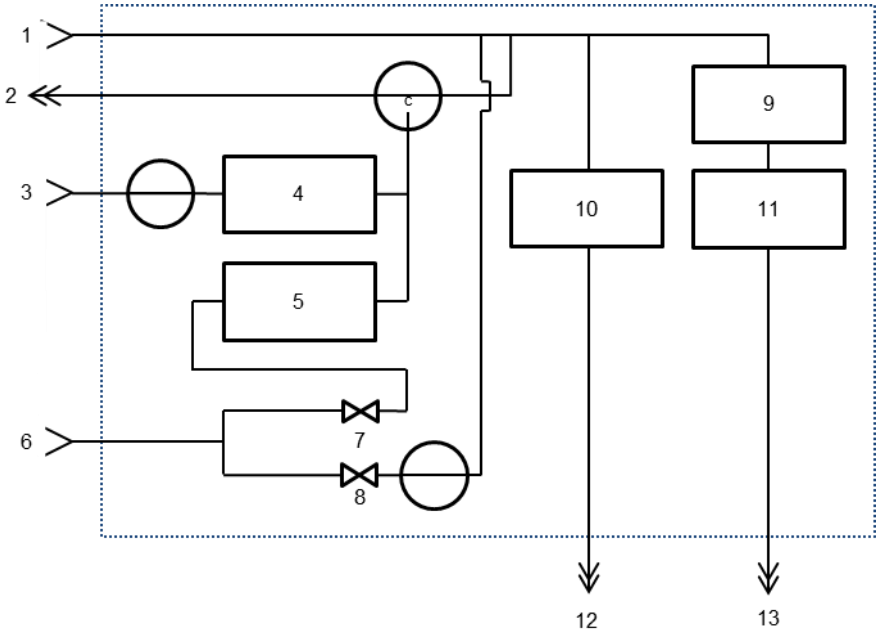

Figure 3.2. Schematic of the NO_x inlet. Numbered parts are described in table 3.2.

Table 3.2. Descriptions of parts numbered in figure 3.2.

Number	Part
1	Sample line
2	Waste
3	NO calibration gas inlet
4	NO calibration MFC
5	Titration cell
6	Zero air inlet
7	Critical orifice (10 sccm)
8	Critical orifice (3 slpm)
9	NO_2 converter
10	Channel 1 MFC
11	Channel 2 MFC
12	NO sample outlet
13	NO_x sample outlet

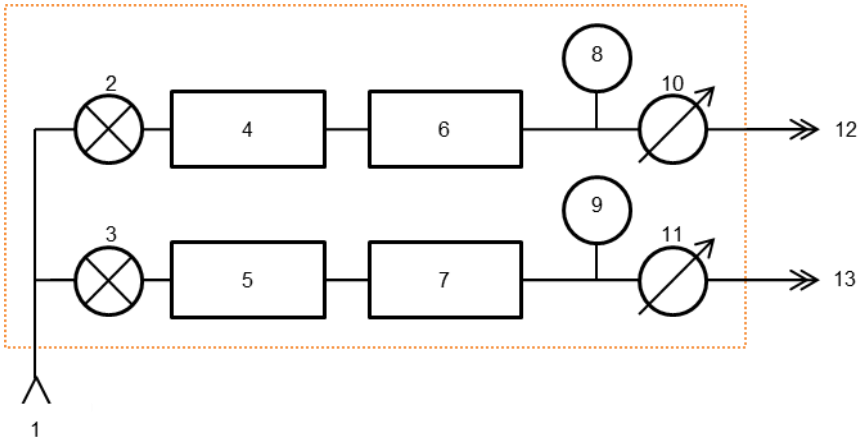

Figure 3.3. Schematic of the ozonizer box. Numbered parts are described in table 3.3.

Table 3.3. Descriptions of parts numbered in figure 3.3.

Number	Part
1	Oxygen inlet
2	Channel 1 solenoid valve
3	Channel 2 solenoid valve
4	Channel 1 MFC (500 sccm)
5	Channel 2 MFC (500 sccm)
6	Channel 1 O_3 generator
7	Channel 2 O_3 generator
8	Channel 1 transformer
9	Channel 2 transformer
10	Channel 1 valve
11	Channel 2 valve
12	Channel 1 O_3 outlet
13	Channel 2 O_3 outlet

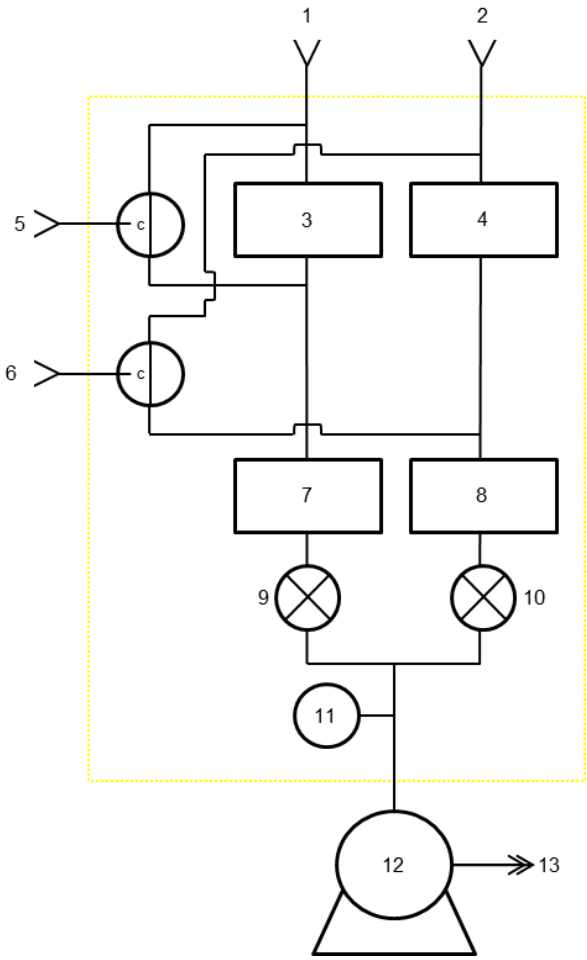

Figure 3.4. Schematic of the snooper box. Numbered parts are described in table 3.4.

Table 3.4. Descriptions of parts numbered in figure 3.4.

Number	Part
1	NO sample inlet
2	NO_x sample inlet
3	Channel 1 teflon prechamber (250 ml)
4	Channel 2 teflon prechamber (250 ml)
5	Channel 1 O_3 inlet
6	Channel 2 O_3 inlet
7	Channel 1 reaction volume
8	Channel 2 reaction volume
9	Channel 1 solenoid valve
10	Channel 2 solenoid valve
11	Transformer
12	Vacuum pump
13	Exhaust

3.2.2. Measurements

NO and NO_x are measured in turn during a five minute cycle as illustrated in figure 3.5. This cycle consists of 60 seconds of a prechamber zero signal during which, the sample bypasses the NO_2 converter and O_3 is added to the prechamber reaction vessel. This is followed by 120 seconds of adding O_3 to the main reaction chamber, before 120 seconds of the sample going through the NO_2 converter prior to O_3 titration in the main reaction chamber. This cycle gives measurements of the instruments zero signal, NO and NO_x mixing ratios.

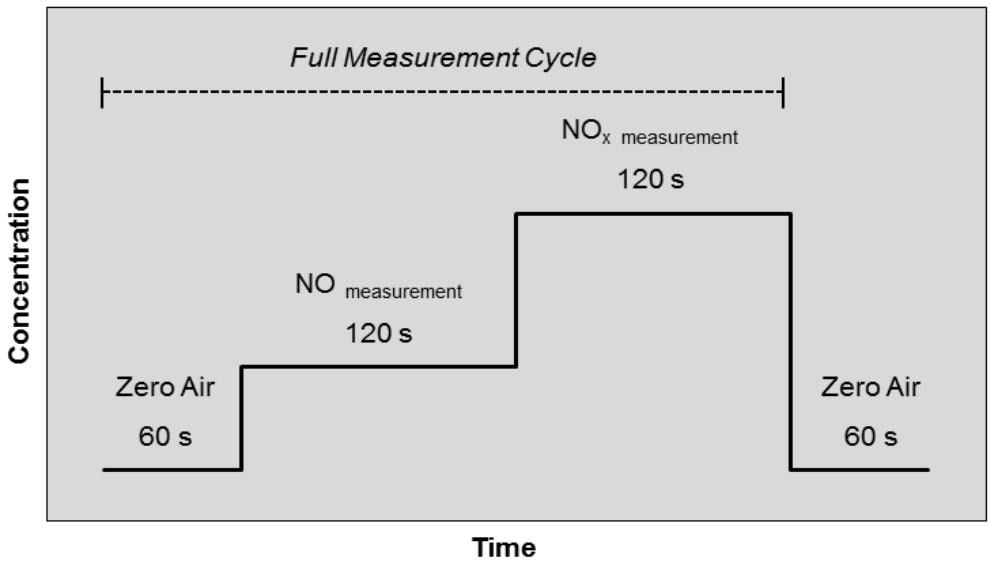

Figure 3.5. The measurement cycle used by the CVAO instrument. Values are for illustration only and do not represent real values.

It is important to note that the signal (*S*) detected by the instrument is made up of several components (equation 3.7.), all of which must be quantified in order to get an accurate measure of the NO signal (S_{NO}). These are described in turn below.

$$S = S_{NO} + S_{Int} + S_D + S_{Art} \qquad 3.7$$

where,

S = total signal

S_{NO} = signal due to NO chemiluminescence

S_{Int} = signal due to chemical interference

S_D = signal due to anode dark current in PMT

S_{Art} = signal due to ‘fake NO’

Light emitted from reaction 3.4 is detected by a photomultiplier tube (PMT) that converts light energy to an electrical impulse. This is achieved by the production of electrons when photons hit a photocathode inside the PMT. The electrons are then accelerated by an electric field and are directed to an electron multiplier. The build-up of charge at the anode results in a current pulse and the number of these pulses over a specified integration time produces a signal that corresponds to the NO concentration (S_{NO}). The PMT is also cooled to a temperature of -30 °C which acts to reduce the anode dark current and therefore improves the signal-to-noise (S/N) ratio. The dark current signal (S_D or zero counts) is a constant offset to the measurement. This is particularly important to quantify when measuring NO_x in an environment where concentrations are low, such as at the CVAO (Lee et al., 2009).

As described, during measurement mode O_3 is added to the main reaction chamber where the resultant chemiluminescence (3.4) is detected by the PMT. O_3 can also be added upstream of the main reactor into a prechamber system. Most chemical interference reactions are slower than that of reaction 3.3 and so when O_3 is added to the prechamber, the residence time is extended and the resultant signal detected is a measure of the sum of interferences (S_{Int}), thereby providing an instrument zero. This can then be subtracted from the main chamber signal to give a signal measure that is the result solely of the NO chemiluminescence (Lee et al, 2009).

In the CVAO setup, calibrations of the system are carried out in ambient air using the standard addition method every 37 hours. Calibrations in ambient air are beneficial as the sensitivity of the instrument can be calculated under conditions of equal humidity. This is important as water vapour is an efficient quencher of excited state NO_2 (3.5) and therefore changes in humidity can significantly affect the instrument sensitivity. However in the laboratory setup, the ambient sample flow is replaced with NO_x free zero air (ZA). This provides a stable baseline allowing a more accurate calculation of the instruments sensitivity. The CVAO calibration cycle consists of nine 5 minute measurement cycles. The first three cycles calibrate for the instruments NO sensitivity using a 4 sccm flow of 5 ppmv NO gas in nitrogen (BOC, UK), added to a an ambient sample flow of 1600 sccm giving an NO concentration of ~ 12 ppbv. The following three cycles add O_3 to titrate approximately 90 % of the NO calibration gas to NO_2, giving a known NO_2 concentration. This allows the calculation of the instruments conversion efficiency (CE) of NO to NO_2 by titrating with O_3 both with and without the NO_2 converter on. The CE is then calculated using equation 3.8. The output of this is shown in figure 3.6.

$$CE = 1 - \frac{(NO_c\,1 - NO_c\,2)}{NO\,1 - NO\,2} \qquad 3.8$$

where,

CE = NO to NO_2 conversion efficiency

NO 1 = NO concentration in calibration gas

NO 2 = NO concentration in calibration gas once titrated (~ 80 % of NO 1)

NO_c 1 = NO concentration in calibration gas with NO_2 converter on

NO_c 2 = NO concentration in calibration gas with NO_2 converter on once titrated

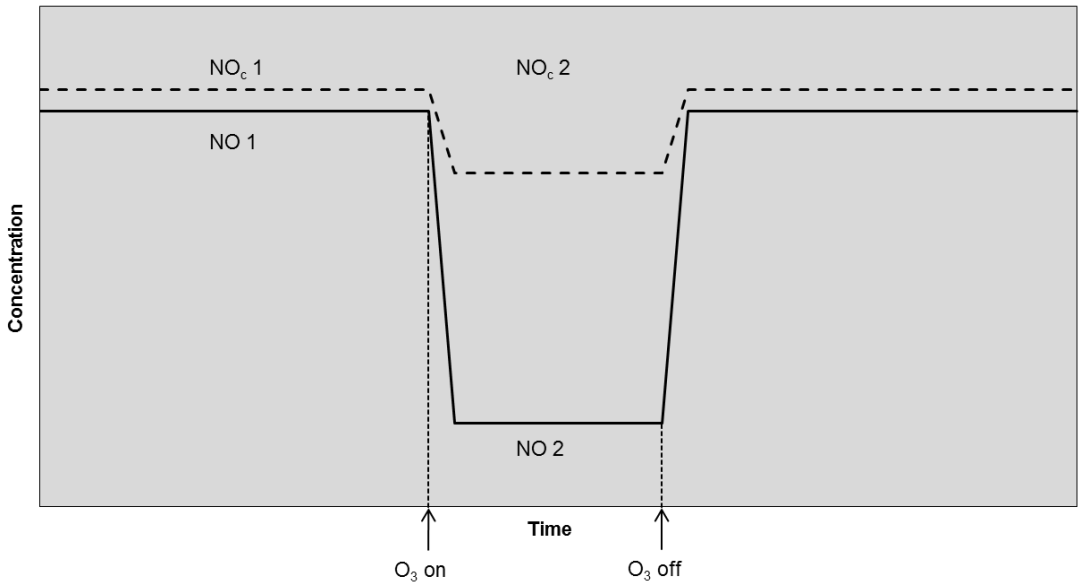

Figure 3.6. Schematic showing the signal output during the calculation of the conversion efficiency.

The final three cycles sample NO_x free zero air, produced by a PAG 003 generator (Ecophysics, UK), to give a measure of the instruments artefact (Lee et al., 2009). The artefact of the instrument is caused by a so called “fake NO” signal (Drummond et al., 1985). This component (S_{Art}) is a background measure in the instrument which is not removed by subtraction of the S_{Int} signal. This can be calculated using the following method. As NO is produced via NO_2 photolysis, at night time when production has stopped but losses continue, NO concentrations decrease to zero. The other potential source of NO is anthropogenic emissions, however, CVAO is sufficiently distant from any such source and so the artefact of this system can be taken to be the NO signal measured by the instrument between 0000-0400 (Lee et al., 2009).

Quantifying all of the components of equation 3.6 allows the accurate measurement of NO and NO_2 following conversion. Using the average raw and zero counts from the calibration during which the NO standard and ZA is being sampled respectively, the instrument sensitivity can also be determined using equation 3.9.

$$\text{Sensitivity} = \frac{\text{raw counts - zero counts - artefact in counts}}{\text{[NO] in standard}} \qquad 3.9$$

To assess the reliability of the data collected by the instrument, error analysis must be carried out. To characterise the errors, both the precision and the accuracy of the measurements must be evaluated. Precision is a measure of reproducibility regardless of the determined values proximity to the actual value. To quantify this, the zero count rate variability can be used as this is directly related to the precision of the photon-counting detector. It is calculated by plotting a frequency distribution of the zero counts, before fitting a Gaussian distribution (Silvia and Skilling, 2006) and using this to then find the standard deviation (full width half maximum (FWHM)) of this population (Figure 3.7). The standard deviation is then divided by the instruments sensitivity, as determined through instrument calibrations, to obtain the precision in parts per trillion. For the CVAO instrument using a sensitivity of 2.1 Hz $pptv^{-1}$ (Lee et al., 2009), this was calculated to be 40.7 pptv for 1 second frequency data.

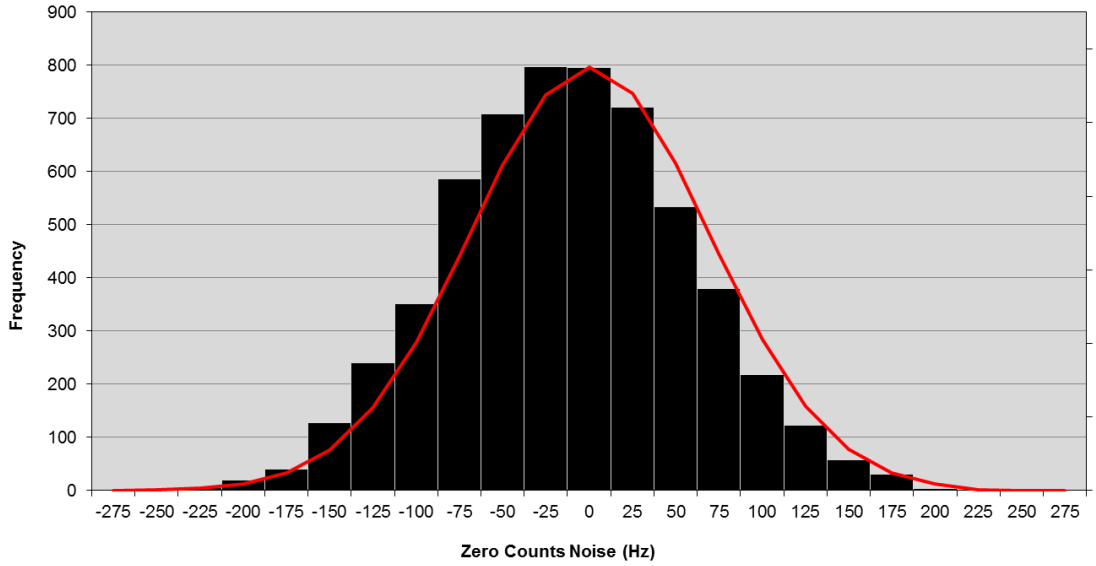

Figure 3.7. Frequency distribution plot of zero count variability with fitted Gaussian distribution. Mean = 0.33 ± 69.38 Hz. 2σ standard deviation = 24.70 Hz for 1 minute frequency data.

Accuracy is a measure of how close to the actual value a measurement is and is quantified using equation 3.10 to calculate the combined uncertainty. This includes both the systematic uncertainty (U_s), which is due to that of the sites gas standard and is typically 0.5-2 %, and random uncertainty (U_r), which is a result of uncertainties in the analyser, the calibration standard and the flows and dilutions of the system used. The individual components of U_r were either determined through measurement or as stated by the manufacturer and total U_r was calculated using equation 3.11.

$$U_c = (U_r^2 + U_s^2)^{0.5} \quad 3.10$$

where,

U_c = combined uncertainty
U_r = random uncertainty
U_s = systematic uncertainty

$$U_r = [US] * 2 * \left(A^2 + \left(\frac{\frac{\bar{x}([LS_{SD}])}{(LS_{\#})^{0.5}}}{\bar{x}([LS])} \right)^2 \right) + \left(B^2 + \left(\frac{\frac{[US_{SD}]}{(US_{\#})^{0.5}}}{[US]^2} \right)^{0.5} \right) \quad 3.11$$

where,

U_r = random uncertainty
A = uncertainty due to dilution factor drift (typically 0.5-2 %)
LS_{SD} = standard deviation of laboratory standard (ppbv)
US_{SD} = standard deviation of unknown standard (ppbv)
$LS_{\#}$ = number of high time-resolution laboratory standard measurements
$US_{\#}$ = number of high time-resolution unknown standard measurements
[LS] = mixing ratio of laboratory standard measured (ppbv)
[US] = mixing ratio of unknown standard measured (ppbv)
$\bar{x}$ = Mean
B = uncertainty due to analyser drift or deviation from equilibrium value (typically 0.5-2 %)

The accuracy can then be propagated through the root sum of squares (RSS) equation along with the measure of precision to reach a value for total uncertainty in the measurement. For NO measurements at the CVAO, total uncertainty was calculated to be 12, 6 and 3 % for mixing ratios of 5, 10 and 20 pptv respectively. There is the added uncertainty of the conversion efficiency for NO_2. The total uncertainty in the NO_2 measurements was found to be 33 and 29 % for 10 and 20 pptv respectively and had a precision of 58.1 pptv for 1 second frequency data.

3.3. ACTRIS

The Aerosols, Clouds, and Trace gases Research InfraStructure Network (ACTRIS) is a European project aiming at integrating European ground-based stations equipped with advanced atmospheric probing instrumentation for aerosols, clouds, and short-lived gas-phase species. Its role is to develop our understanding as well as policy issues on climate change, air quality, and long-range transport of pollutants. As part of this consortium (table 3.5.), the laboratory instrument took part in two separate workshops that aimed to calibrate NO_x measuring instruments from 13 institutions across Europe, to a common NO standard.

The first of these was a blind standard round robin that involved a measurement schedule alternating between zero air, the individual institution or sites (table 3.5.) NO standard and a NO standard of unknown concentration. The concentration of the unknown standard was determined to be 2.01 ± 0.03 ppbv, with an actual concentration of 2.07 ± 0.01 ppbv (NPL, UK). As can be seen in the results from the blind standard round robin (figure 3.8), the instrument provided an accurate measure of the unknown standard. However the variation in the measurement is relatively large in comparison with the other institutes, most likely a result of fluctuating laboratory conditions.

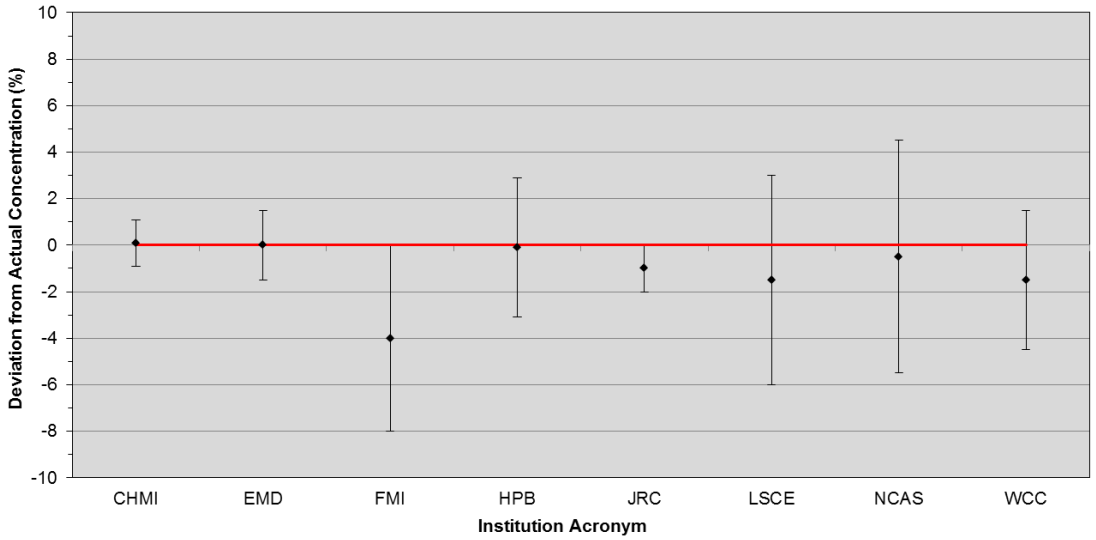

Figure 3.8. Graph of results from the blind standard round robin. Red line indicates zero deviation from the standard concentration and the y-axis represents each institutions estimates and total uncertainty, U_t. Institution acronyms are shown in table 3.5 and highlighted in grey.

Table 3.5. Details of all the institutions involved in the NO_x comparison as part of the ACTRIS programme and the technique used for measurements. Institutions highlighted in grey also took part in the blind standard round robin. CLD = Chemiluminescence, Mo converter = Molybdenum converter, BLC = Blue light converter, PLC = Photolytic converter, DOAS = Differential Optical Absorption Spectrometry, LIF = Laser induced fluorescence.

Institution	Acronym	Country	Method
Czech Hydrometeorolocical Institute	CHMI	Czech Republic	CLD / Mo converter
Ecole des Mines de Douai	EMD	France	CLD / BLC
Energy, Environment and Water Research Centre	EEWRC	Cyprus	CLD / BLC / Mo Converter
Finnish Meteorological Institute	FMI	Finland	CLD
Hohenpeissenβerg Meteorlogical Observatory	HPB	Germany	CLD / BLC / PLC
Joint Research Centre of European Union	JRC	Italy	CLD / Mo converter
Koninklijk Nederlands Meteorologisch Instituut	KNMI	France	NO2 sonde, Luminol-CLD
Laboratoire des Sciences du Climat et de l'Environnement	LSCE	France	CLD / PLC
Max-Planck Institute for Environmental Research	MPI	Germany	Cavity enhanced DOAS
National Centre for Atmospheric Science	NCAS	UK / Cape Verde	CLD / PLC
Observatoire de Physique du Globe de Clermont-Ferrand	OPGC	France	CLD / Mo converter
Research Centre Jeulich, World Calibration Centre	WCC	Germany	CLD / PLC
University of Heidelberg, Institute for Environmental Physics	IUP	Germany	LIF

The second workshop incorporated a 3-day side-by-side comparison at the Hohenpeiβenberg Observatory, Germany. Hohenpeiβenberg is an atmospheric observatory located at 47°48'N, 011°01'E, 986 m above sea level (Mannschreck et al., 2004; Gilge et al., 2010). Since 1994, it has been part of the Global Atmospheric Watch (GAW) programme, run by the World Meteorological Organisation (WMO). The role of the GAW is to provide scientific data and information on the chemical composition of the atmosphere, natural and anthropogenic induced changes and help to improve the understanding of interactions between the atmosphere, the oceans and the biosphere. As part of this work, the GAW monitoring programme collects data from sites around the world and divides these measurements into six components of the atmospheric system; O_3, UV radiation, greenhouse gases, aerosols, selected reactive gases and precipitation chemistry.

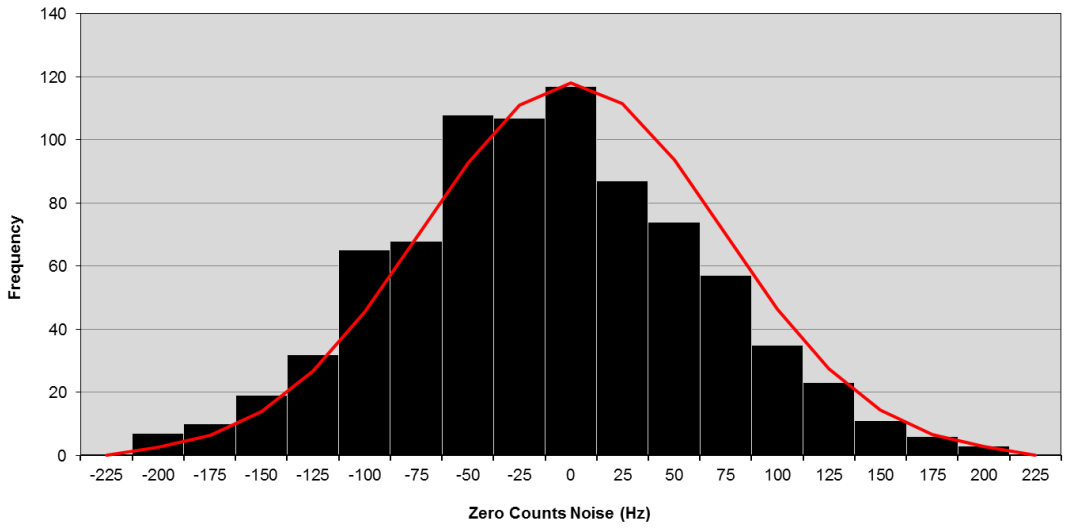

Figure 3.9. Frequency distribution plot of zero count variability with fitted Gaussian distribution. Mean = 0.58 ± 72.83 Hz. 2σ standard deviation = 26.04 Hz for 1 minute frequency data.

As with the CVAO instrument, the precision, accuracy and total uncertainty in the measurements were calculated for this campaign (Figure 3.9). Using an average sensitivity of 4.7 Hz $pptv^{-1}$ determined from all calibrations carried out during the workshop, the precision was calculated as 42.9 pptv and 65.9 pptv for NO and NO_2 respectively using 1 second frequency data. The accuracy of the instrument was determined to be 27, 14 and 7 % for NO mixing ratios of 5, 10 and 20 pptv respectively and 42 and 33 % for 10 and 20 pptv of NO_2.

Institutions listed in table 3.5 sampled from a common inlet (PFA tubing), to which synthetic air, spiked ambient air and other complex mixtures were added. The complete sampling log from the workshop is listed in appendix 1. Examples of the sampling routines

are shown in figures 3.10-12, including the results from an NO concentration ramp, a NO_x mixture in which the NO was titrated by varying O_3 concentrations and an overnight of ambient sampling respectively. Figures 3.10 and 3.11 demonstrate that following a brief initial stabilization period induced by alterations in the sample composition, the instrument gave an accurate measure of the actual NO and NO_2 concentrations being introduced into the common inlet.

Figure 3.12 demonstrates clearly the boundary layer dynamics described in section 1.2. Following the formation of a stable nocturnal boundary, increased solar radiation causes surface heating (~ 0700) and leads to the development of vertical thermal convection in the boundary layer and subsequent release of high NO_x concentrations. This pronounced diurnal cycle is typical of Hohenpeiβenberg (Mannschreck et al., 2004).

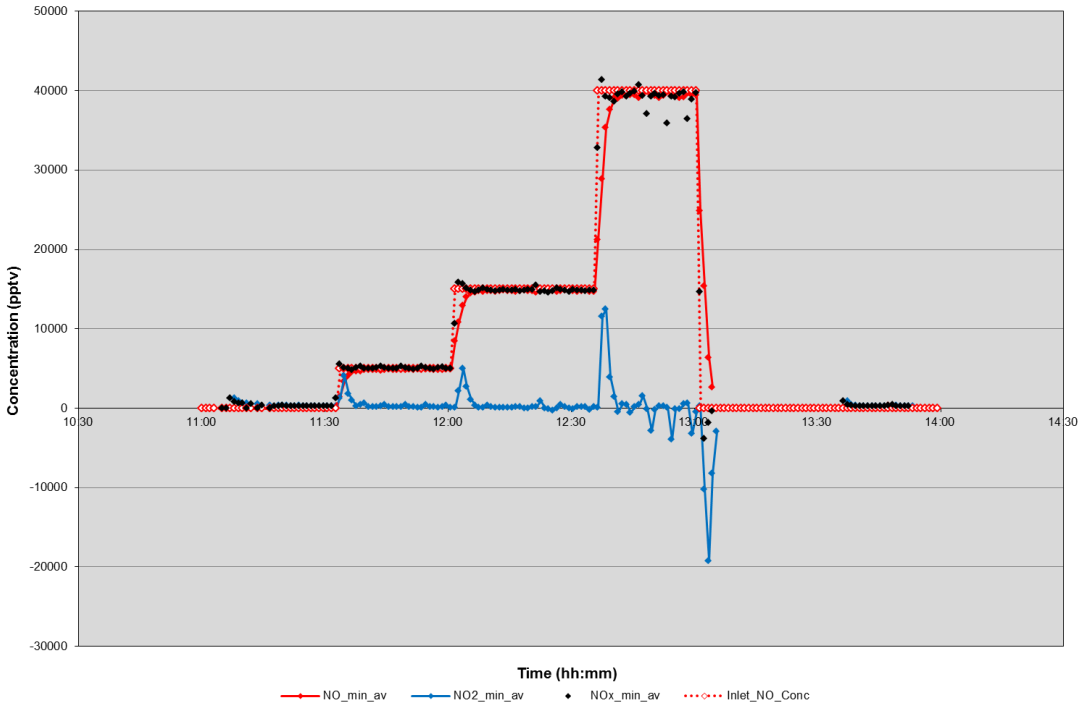

Figure 3.10. Results from the NO concentration ramping experiment. Common inlet concentrations are shown as open diamonds. Briefly; 1100-1130 = zero air, 1130-1200 = 5 ppbv NO, 1200-1230 = 15 ppbv, 1230-1300 = 40 ppbv NO, 1300-1330 = Calibration in zero air (data not shown), 1330-1400 = zero air.

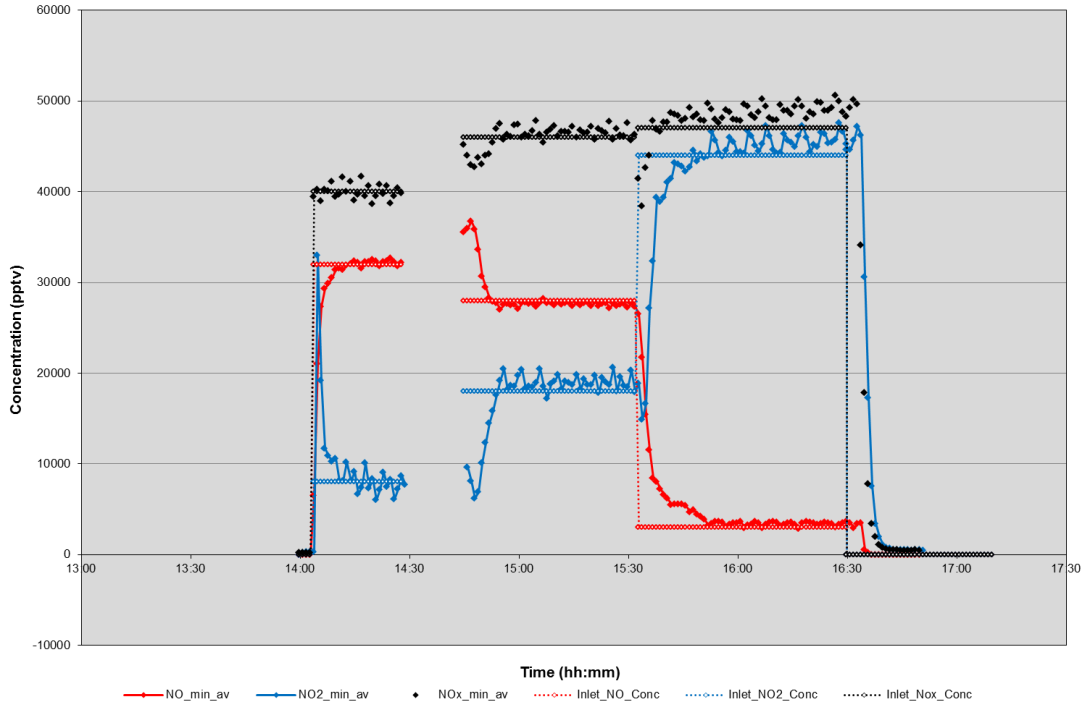

Figure 3.11. Results from the NO titration ramping experiment. Common inlet concentrations are shown as open diamonds. Briefly; 1400-1430 = 40 ppbv NO and 8 ppbv O_3, 1430-1445 = calibration in zero air (data not shown), 1500-1530 = 46 ppbv NO and 18 ppbv O_3, 1530-1630 = 47 ppbv NO and 44 ppbv O_3, 1630-1700 = zero air.

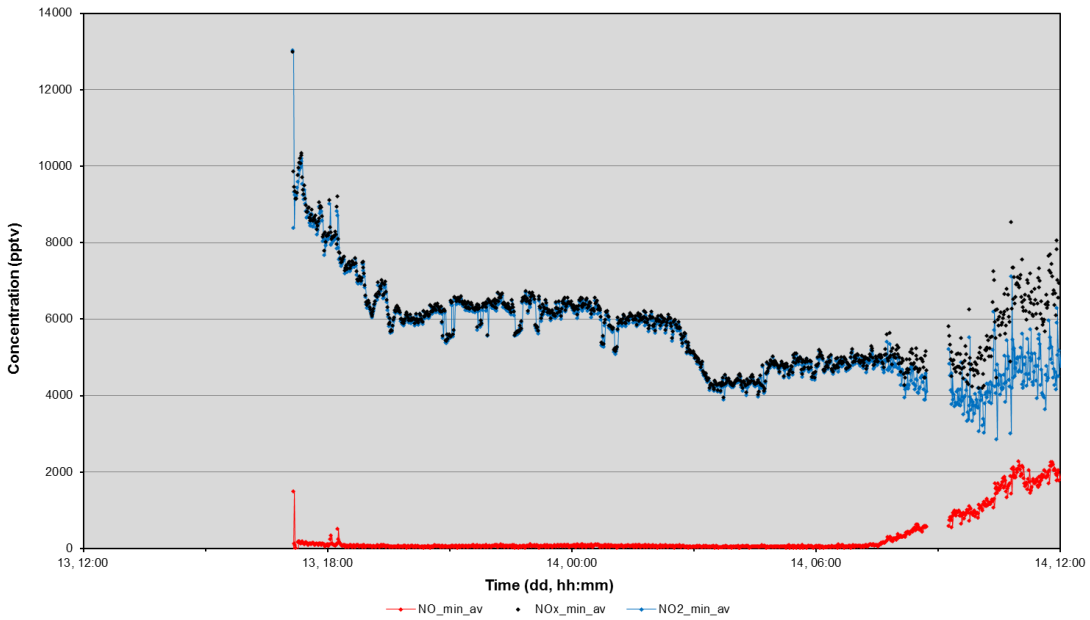

Figure 3.12. Overnight ambient air sample. A calibration was run from 0845-0915 (data not shown). Boundary layer dynamics as a result of solar radiation can be seen starting to develop at approximately 0730 on the 14th.

3.4. Summary

The chemiluminescence NO_x instruments installed at the Cape Verde Atmospheric Observatory (CVAO) and used in laboratory studies have been shown to be highly sensitive for the detection of low NO_x mixing ratios. Measurements of the CVAO and laboratory instruments uncertainty and precision are summarised in table 3.6.

Table 3.6. Uncertainty and precision measurements of the CVAO and laboratory NO_x chemiluminescence instruments.

	CVAO Instrument	**Laboratory Instrument**
Uncertainty:		
5 pptv of NO	12 %	27 %
10 pptv of NO	6 %	14 %
20 pptv of NO	3 %	7 %
10 pptv of NO_2	33 %	42 %
20 pptv of NO_2	29 %	33 %
Precision:		
1 second frequency data	58.1 pptv	65.9 pptv

Data from the CVAO instrument will be described in detail in Chapter 4. The laboratory instrument has been involved in the European project, The Aerosols, Clouds, and Trace gases Research InfraStructure Network (ACTRIS). This involved two workshops, a blind standard calibration and a side-by-side 3-day comparison, which both aimed to calibrate NO_x measuring instruments from 13 institutions across Europe to a common standard. The instrument performed well, estimating the blind standard to + 2.98 % of its actual concentration. It also accurately traced the NO and NO_2 concentrations manually introduced into the common inlet throughout the 3-day side-by-side comparison under a range of conditions including varying humidity, O_3 mixing ratios and complex mixtures.

References

Cleary, P., Wooldridge, P. and Cohen, R. (2002) Laser-induced fluorescence detection of atmospheric NO_2 with a commercial diode laser and a supersonic expansion. *Applied Optics*. **41**, 6950-6956.

Dari-Salisburgo, C., Di Carlo, P., Giammaria, F., Kajii, Y., D'Altorio, A. (2009) Laser induced fluorescence instrument for NO_2 measurements: Observations at a central Italy background site. *Atmospheric Environments.* **43**, 970-977.

Drummond, J., Volz, A. and Ehhalt, D. (1985) An optimized chemiluminescence detector for tropospheric NO measurements. *Journal of Atmospheric Chemistry*. **2**, 287-306.

Finlayson-Pitts, B.J. and Pitts, J.N. (2000) Chemistry of the Upper and Lower Atmosphere. Academic Press, London.

Gilge. S., Plass-Duelmer, C., Fricke, W., Kaiser, A., Ries, L., Buchmann, B. and Steinbacher, M. (2010) Ozone, carbon monoxide and nitrogen oxides time series at four alpine GAW mountain stations in central Europe. *Atmospheric Chemistry and Physics*. **10**, 12295-12316.

Kley, D. and McFarland, M. (1980) Chemiluminescence detector for NO and NO2. *Atmospheric Technology*. **12**, 63-69.

Lee, J.D., Moller, S.J., Read, K.A., Lewis, A.C., Mendes, L. and Carpenter, L.J. (2009) Year-round measurements of nitrogen oxides and ozone in the tropical
North Atlantic marine boundary layer. *Journal of Geophysical Research*. **114**,
D21302.

Mannschreck, K., Gilge, S., Plass-Duelmer, C., Fricke, W. and Berresheim, H. (2004) Assessment of the applicability of $NO\text{-}NO_2\text{-}O_3$ photostationary state to long-term measurements at the Hohenpeissenberg GAWStation, Germany. *Atmospheric Chemistry and Physics.* 4, 1265-1277.

Miyazaki,K., Matsumoto, J., Kato, S. and Kajii, Y. (2008) Development of atmospheric NO analyser by using a laser-induced fluorescence NO_2 detector. *Atmospheric Environment*. **42**, 7812-7820.

Osthoff, H., Brown, S., Ryerson, T., Fortin, T., Lerner, B., Williams, E., Pettersson, A., Baynard, T., Dube, W., Ciciora, S. and Ravishankara, A. (2006) Measurement of atmospheric NO_2 by pulsed cavity ring-down spectroscopy. *Journal of Geophysical Research - Atmospheres*. **111**, D12305.

Plane, J.M.C. and Smith, N. (1995) Atmospheric monitoring by differential optical absorption spectroscopy, *In*, Spectroscopy in Environmental Science. Wiley, New York.

Platt, U. (1994) Differential Optical Absorption Spectroscopy (DOAS), *In*, Air Monitoring by Spectroscopic Techniques. (Sigrist, M.W., Ed.), Wiley, New York. *Chemical Analysis Series*. **127**, 27-84.

Sandholm, S., Smyth, S., Bai, R. and Bradshaw, J. (1997) Recent and future improvements in two-photon laser-induced fluorescence NO measurement capabilities. *Journal of Geophysical Research - Atmospheres*. **102**, D23 28651-28661.

Silvia, D. and Skilling, J. (2006). Data analysis: A bayesian tutorial. 2nd edition.

Thornton, J., Wooldridge, P. and Cohen, R.C (2000) Atmospheric NO_2: In situ laser-induced fluorescence detection at parts per trillion mixing ratios. *Analytical Chemistry*. **72**, 528-539.

Williams, E.J., Baumann, K., Roberts, J.M., Bertman, S.B., Norton, R.B., Fehsenfeld, F.C., Springston, S.R., Nunnermacker, L.J., Newman, L., Olszyna, K., Meagher, J., Hartsell, B., Edgerton, E., Pearson, J.R. and Rodgers, M.O. (1998) Intercomparison of ground-based NOy measurement techniques. *Journal of Geophysical Research*. **103**, D17 22261-22280.

Chapter 4

Cape Verde Atmospheric Observatory (CVAO)

4.1. Remote, Tropical Marine Boundary Layer

The remote marine boundary layer represents approximately 25 % of the Earth's surface and plays an important role in the chemical processing of the atmosphere (Monks et al., 2000). It also provides optimal conditions for the study of baseline photochemical processes. As previously described in Chapter 1, the tropical, remote, marine boundary layer is characterised by high solar radiation and abundance of water vapour, leading to high OH concentrations (Crutzen, 1998) and has important implications for the oxidative capacity of the atmosphere. For example, a large proportion of tropospheric O_3 loss (Horowitz et al., 2003) and approximately 80 % of global CH_4 oxidation occurs here (Bloss et al., 2005). Another important process that dominates the tropical troposphere is the presence of the strong vertical transport of compounds due to the ITCZ as described in section 1.2 and shown in figure 1.4. Therefore, those compounds that have the potential to disrupt O_3 chemistry in the stratosphere, such as halogen radicals and N_2O, must first be processed in this region of the atmosphere (Bridgeman et al., 2000).

Background O_3 levels in the northern hemisphere have more than doubled since pre-industrial times believed to be a result of an increase in anthropogenic NO_x emissions and distribution (Lelieveld et al., 2004). Due to the presence of longer lived NO_y species able to undergo long-range transport as described in Chapter 2, this increase in anthropogenic emissions has the potential to impact O_3 regimes in countries downwind of source regions, impairing their ability to meet their air quality standards (Derwent et al., 2004). As NO_x emissions from remote uninhabited and oceanic regions are generally very small (Jacob et al., 1996), the O_3 regime in these areas is highly sensitive to NO_x concentrations, with small increases leading to mixing ratios in excess of the compensation point resulting in a switch of the system from net O_3 destruction to one exhibiting photochemical O_3 production (Jacob et al., 1993). Despite the obvious importance of NO_x in these remote regions of the troposphere and for atmospheric chemistry in general, measurements of these compounds in the remote tropical marine boundary layer are sparse, with long-term measurements even more so (Lee et al., 2009). As a result, models are used to make up for this gap in scientific knowledge. However, any seasonal and longer term variability is still relatively unknown or unverified.

4.2. Cape Verde Atmospheric Observatory, CVAO

4.2.1. CVAO

The Cape Verde Islands are an archipelago situated in the North Atlantic Ocean off the west coast of Africa (figure 4.1). The Cape Verde Atmospheric Observatory (CVAO) is situated on the north-east facing coast of the island of São Vicente at 16.848 °N, 24.871 °W (figure 4.2). It was installed to further the understanding of sea-air interactions and trends in atmospherically important species in the tropical remote marine boundary layer. This site is ideally located for the measurement of compounds in a variety of air masses, as the north easterly trade winds that arrive here have multiple sources yet provide a constant wind direction ~ 95 % of the time, thereby minimising interference from local pollution and anthropogenic activity (figure 4.3) (Lee et al., 2009). Due to the volcanic origins of the archipelago, the continental shelf in this region is steep and acts to also reduce coastal influences, such as biogenic emissions (Carpenter et al., 2010). Appendix 2 lists the compounds measured at the CVAO as well as the method and duration of the measurements. However the scope of this report is confined to that of the NO and NO_2 measurements, with some reference to the concurrent O_3 data.

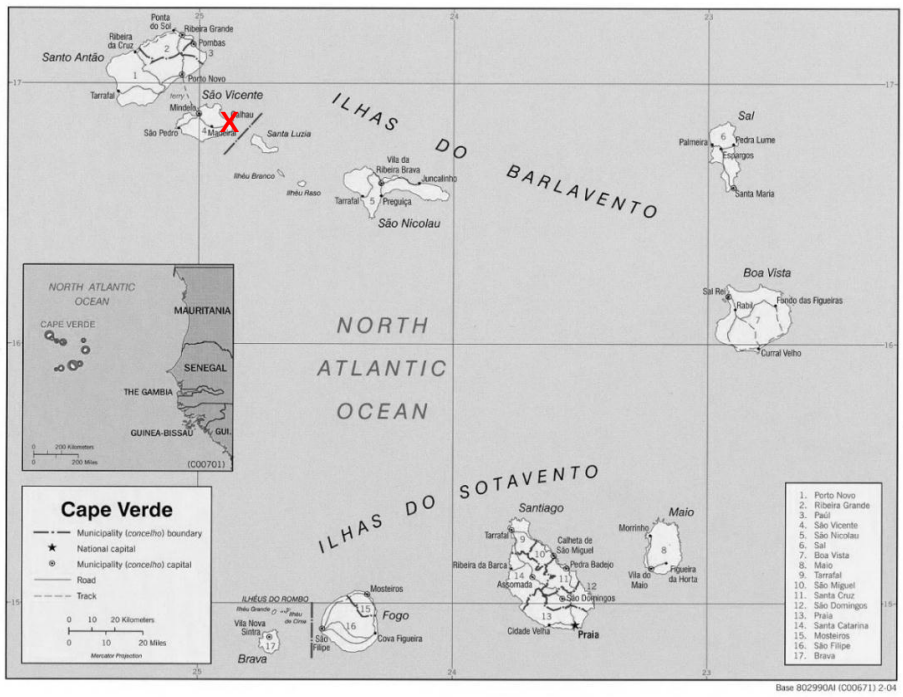

Figure 4.1. Map of the Cape Verde Islands. X = location of the CVAO.

Figure 4.2. The Cape Verde Atmospheric Observatory, CVAO. Located at 16.848 °N, 24.871 °W. Picture shown is facing north east.

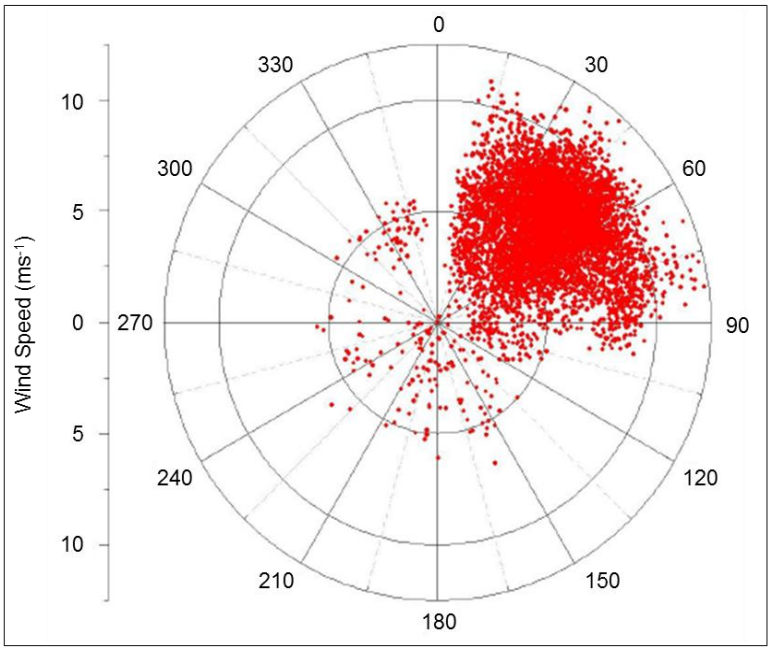

Figure 4.3. Wind direction and speed measured at the CVAO.

4.2.2. Air Mass Classification

Although wind direction is predominantly from the north-east, the origins of the air masses that are sampled at the CVAO can vary widely and consequently, wind sector analysis is an invalid method of identification. Trajectory models are an estimate of the transport pathway of an infinitesimally small air parcel, which is then transposed to the centreline of an advected air mass, taking into account both the vertical and horizontal dispersal of the air parcel modelled (Stohl et al., 2002).

Dispersion models differ in that this air parcel is represented by multiple, small, inert, tracer particles and are back calculated from the point of measurement. This added complexity has the advantage over trajectory models as the particles can be treated individually and allow a more accurate representation of factors such as turbulence, resulting in a more realistic growth in the volume of influence (Fleming et al., 2012). The output is a series of integrations based on the number of particles per grid cell and represents the probability that the air mass encounters a given area. At the CVAO, air mass back trajectories are calculated every three hours using the NAME dispersion model (Numerical Atmospheric Dispersion Modelling Environment) (Ryall et al., 2001) and are assigned a classification according to its trajectory in the past ten days. An example of each are shown in figure 4.4.

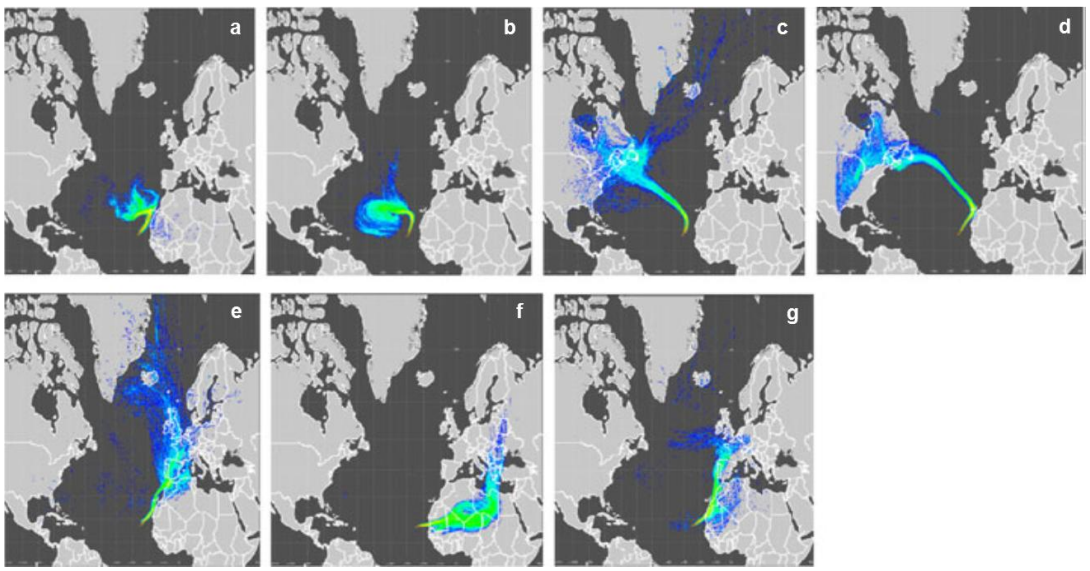

Figure 4.4. Examples of 10-day back trajectories using the NAME dispersion model for the most common air masses sampled at the CVAO. a= Atlantic and Coastal Africa, b= Atlantic, c = Atlantic and North America, d = North America and Coastal Africa, e = Europe, f = Continental Africa, g = Europe and Coastal Africa (adapted from Carpenter et al., 2010).

It is important to note that there are a number of variable errors inherent in calculating air mass trajectories. Due to the complexity of these errors, models are often evaluated through the use of a 'true' reference trajectory that can be used to estimate the error. This involves tagging an air parcel, for example using a chemical tracer (Stohl et al., 2002) or through the use of balloons (Knudsen et al., 1996). Meteorological data can also be used. For example, Lee et al. (2009) used potential vorticity calculations to estimate the horizontal position error of trajectories performed for studies of seasonal NO_x trends at the CVAO to be < 20 % (in distance) for air parcels that had spent more than 24 hours in the free troposphere.

4.2.3. NO_x and O_3 Measurements

The NO, NO_2, NO:NO_2 ratio and O_3 hourly averages from the CVAO data set measured between the 1st October 2006 to the 31st December 2011 are shown in figure 4.5 (top to bottom). As described in Chapter 3, NO_x measurements are made using the chemiluminescence technique and O_3 is measured via UV absorption (Lee et al., 2009; Carpenter et al., 2010). NO_x data is filtered for outliers using a three-day running average of the 5 minute data. Any points greater than 3 standard deviations from the mean were removed prior to hourly averaging and are believed to be a result of local pollution events such as visiting vehicles or passing ship emissions (Lee et al., 2009). Raw, 1 second data, shows that > 95 % of these pollution events last less than 30 seconds. Due to the 5 minute measurement cycle, spikes can exist solely within the NO measurement period and lead to a negative NO_2 value caused by the subtraction of this NO spike. This NO_2 data is also removed from the data set (Lee et al., 2009). Data coverage for the entire period is 59, 58 and 86 % for NO, NO_2 and O_3 respectively, with missing data also associated with power failure and instrument maintenance.

The monthly day and night time averages for NO, NO_2 and O_3 are shown in tables 4.1-4.3 respectively, along with the standard deviation and median values. Daytime is classified as 1100-1500 local time, which is approximately 2 hours either side of solar noon (figure 4.6) and should therefore represent average daytime mixing ratios. Nighttime values are considered to be those between 0000-0400, the same time period as that used to calculate the NO artefact.

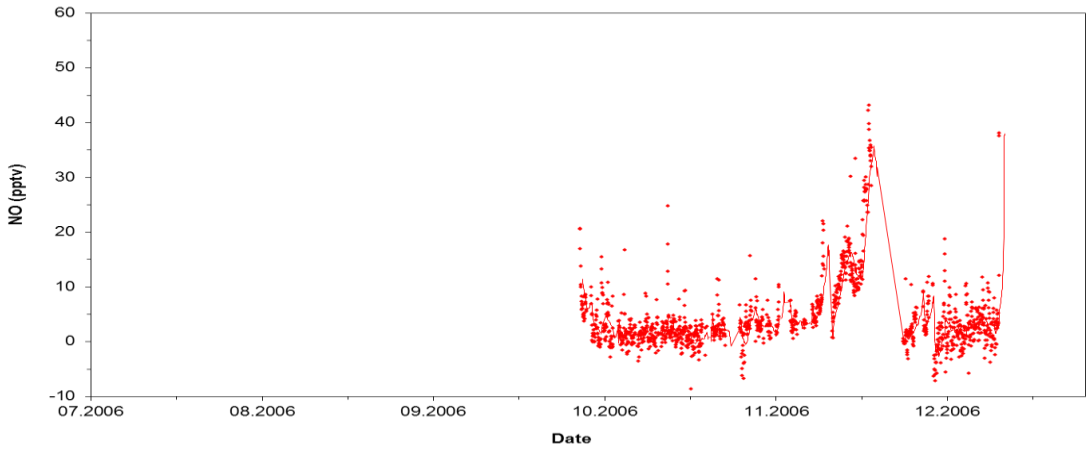
NO (pptv)
60
50
40
30
20
10
0
-10
07.2006
08.2006
09.2006
10.2006
11.2006
12.2006
Date

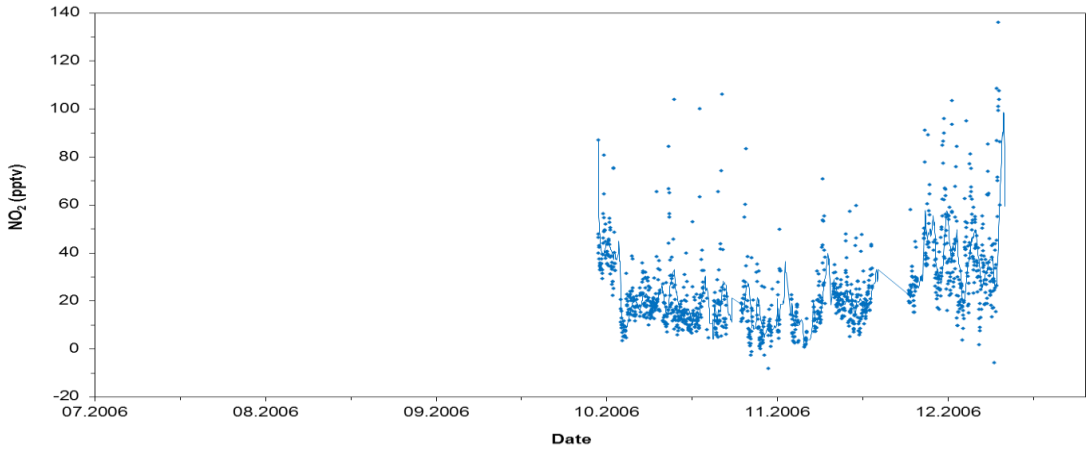
NO2 (pptv)
140
120
100
80
60
40
20
0
-20
07.2006
08.2006
09.2006
10.2006
11.2006
12.2006
Date

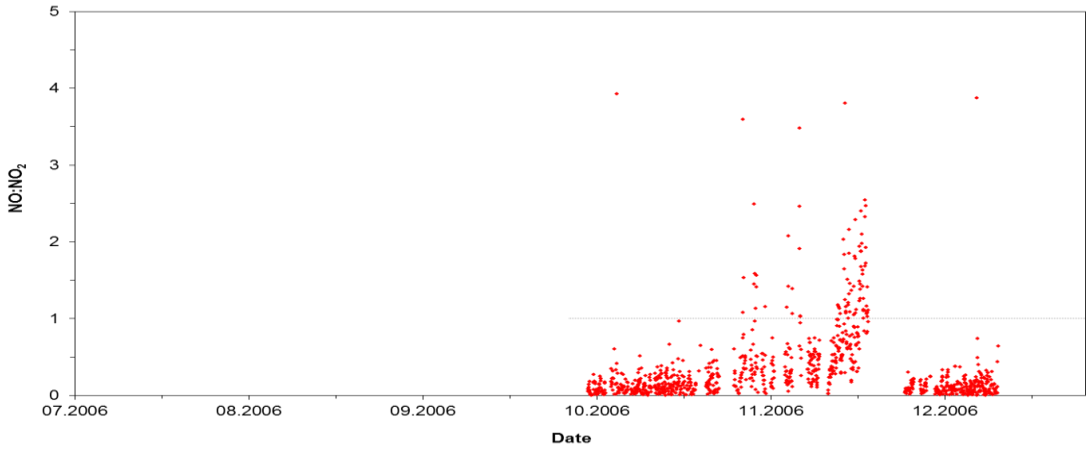
NO:NO2
5
4
3
2
1
0
07.2006
08.2006
09.2006
10.2006
11.2006
12.2006
Date

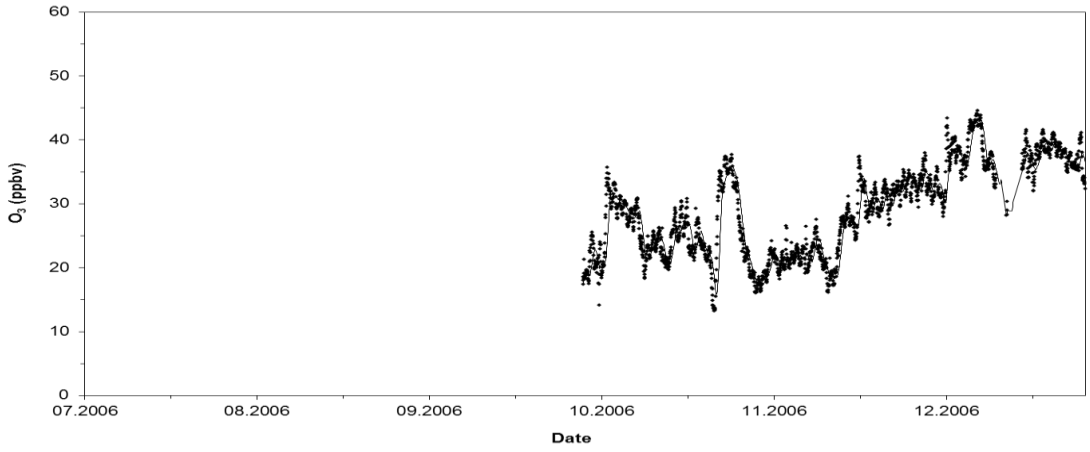
O3 (ppbv)
60
50
40
30
20
10
0
07.2006
08.2006
09.2006
10.2006
11.2006
12.2006
Date

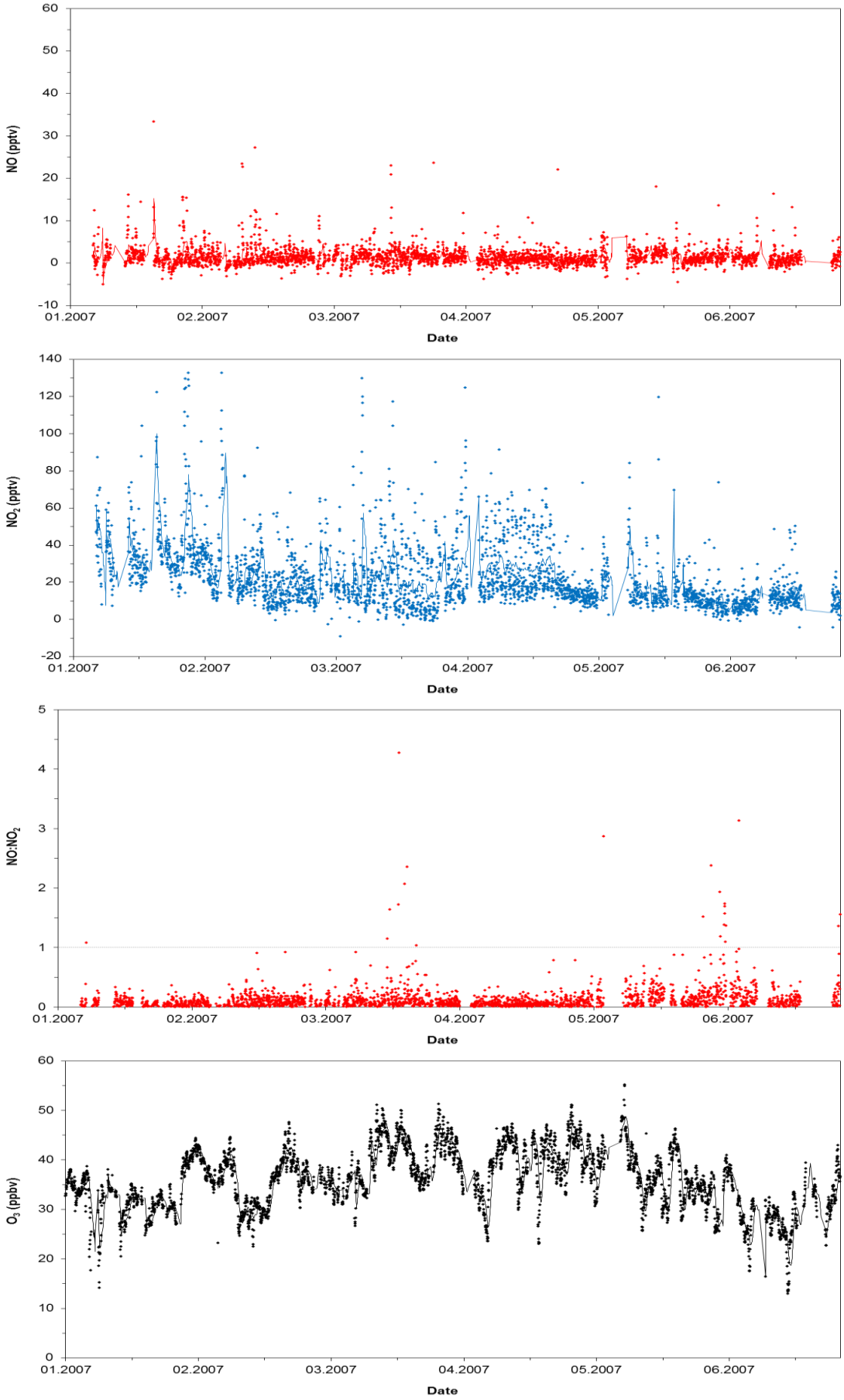
NO (pptv)
60
50
40
30
20
10
0
-10
01.2007
02.2007
03.2007
04.2007
05.2007
06.2007
Date
NO2 (pptv)
140
120
100
80
60
40
20
0
-20
01.2007
02.2007
03.2007
04.2007
05.2007
06.2007
Date
NO:NO2
5
4
3
2
1
0
01.2007
02.2007
03.2007
04.2007
05.2007
06.2007
Date
O3 (ppbv)
60
50
40
30
20
10
0
01.2007
02.2007
03.2007
04.2007
05.2007
06.2007
Date

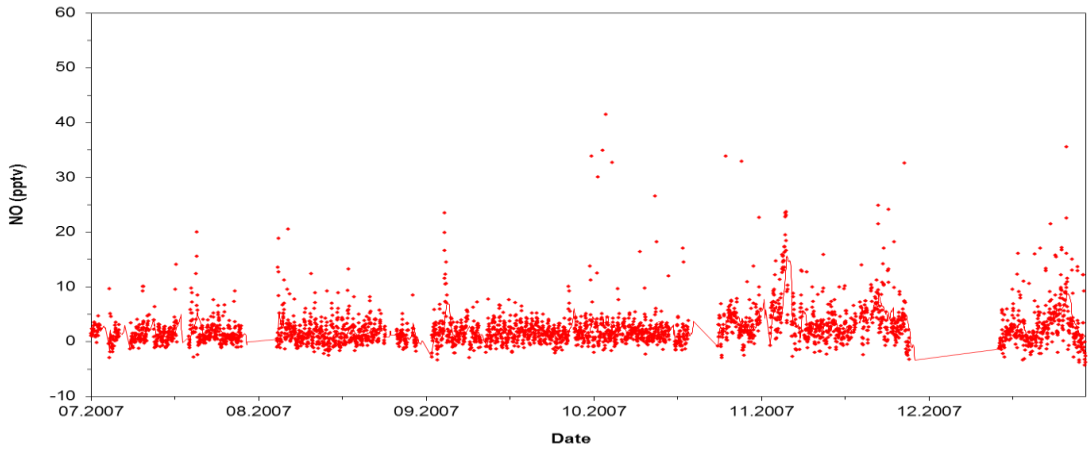
NO (pptv)
60
50
40
30
20
10
0
-10
07.2007
08.2007
09.2007
10.2007
11.2007
12.2007
Date

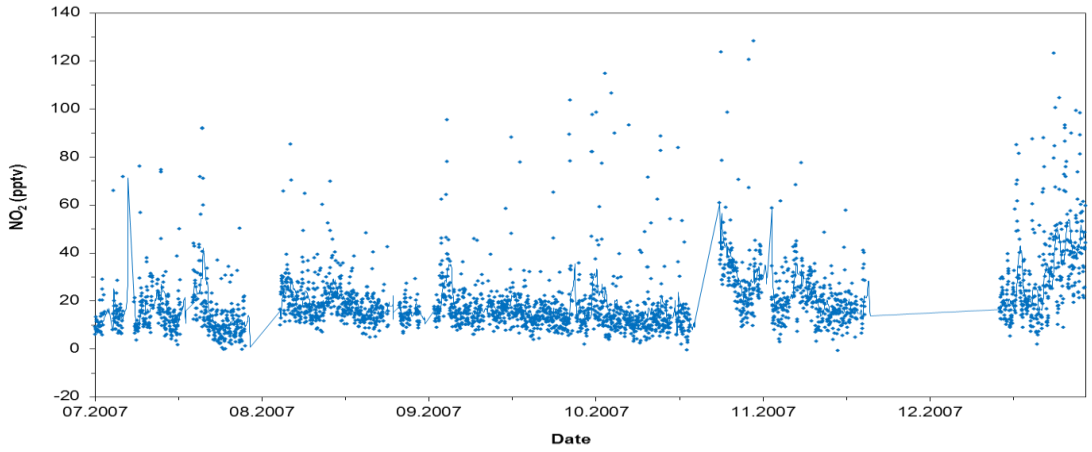
NO2 (pptv)
140
120
100
80
60
40
20
0
-20
07.2007
08.2007
09.2007
10.2007
11.2007
12.2007
Date

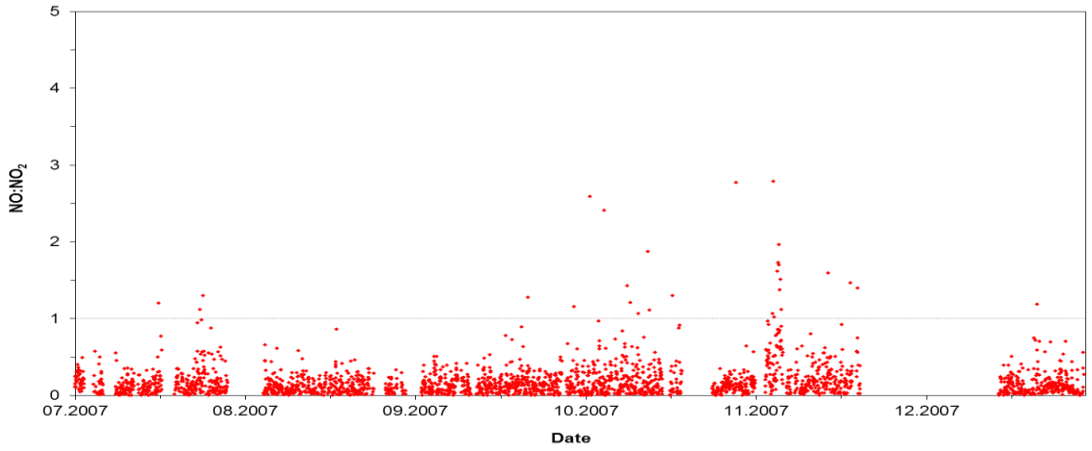
NO:NO2
5
4
3
2
1
0
07.2007
08.2007
09.2007
10.2007
11.2007
12.2007
Date

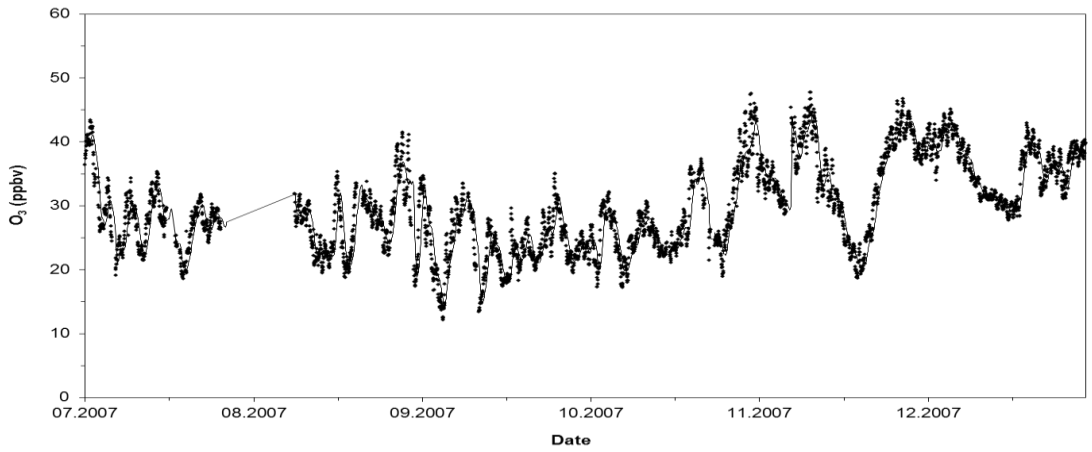
O3 (ppbv)
60
50
40
30
20
10
0
07.2007
08.2007
09.2007
10.2007
11.2007
12.2007
Date

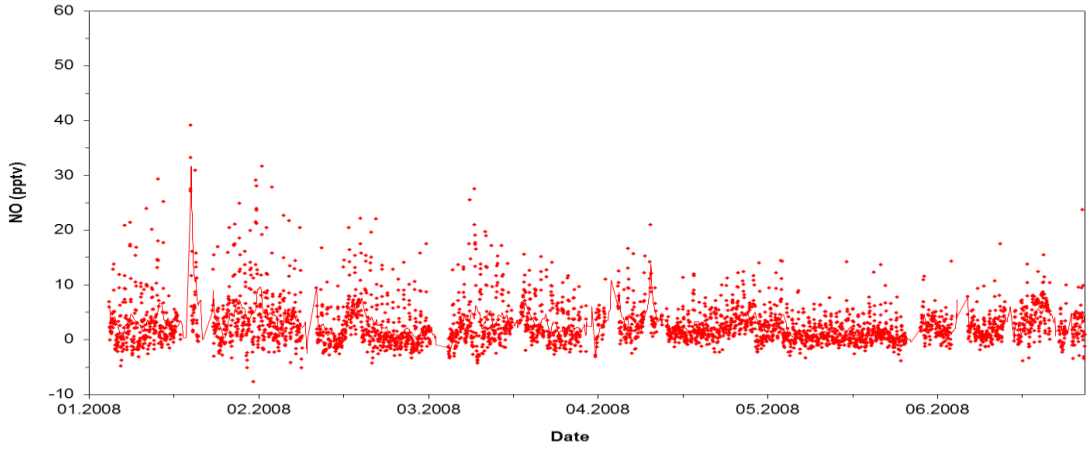
NO (pptv)
60
50
40
30
20
10
0
-10
01.2008
02.2008
03.2008
04.2008
05.2008
06.2008
Date

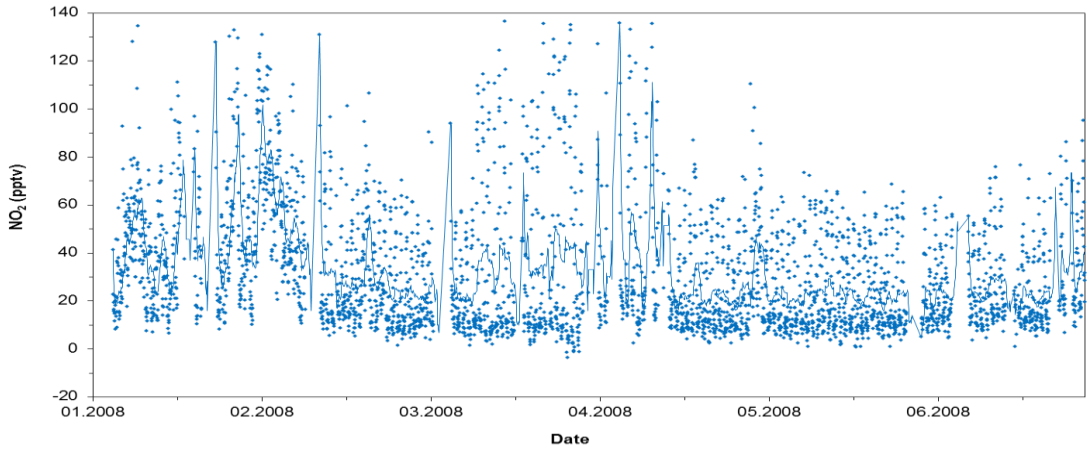
NO2 (pptv)
140
120
100
80
60
40
20
0
-20
01.2008
02.2008
03.2008
04.2008
05.2008
06.2008
Date

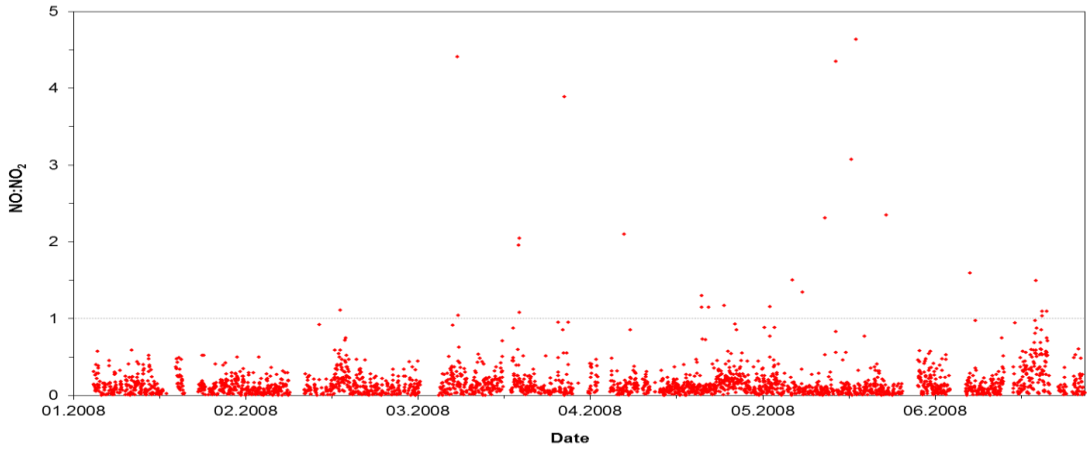
NO:NO2
5
4
3
2
1
0
01.2008
02.2008
03.2008
04.2008
05.2008
06.2008
Date

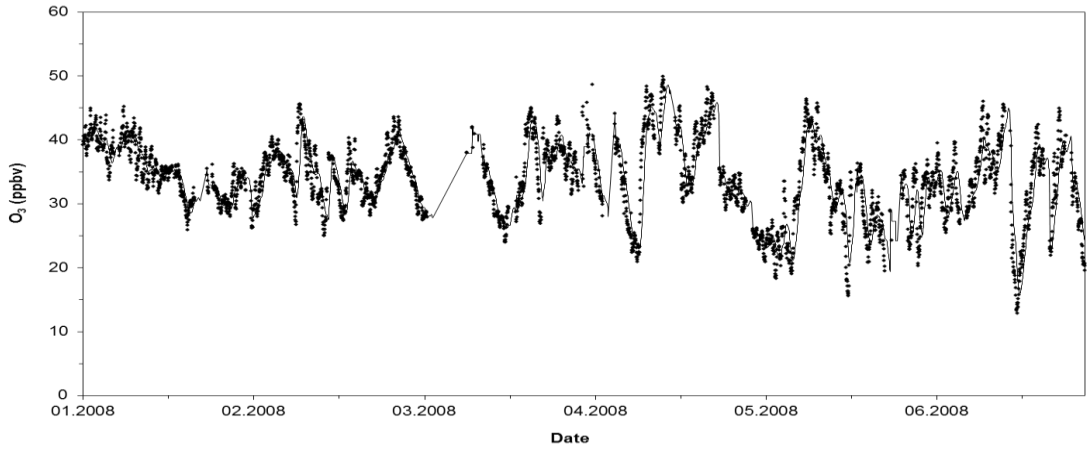
O3 (ppbv)
60
50
40
30
20
10
0
01.2008
02.2008
03.2008
04.2008
05.2008
06.2008
Date

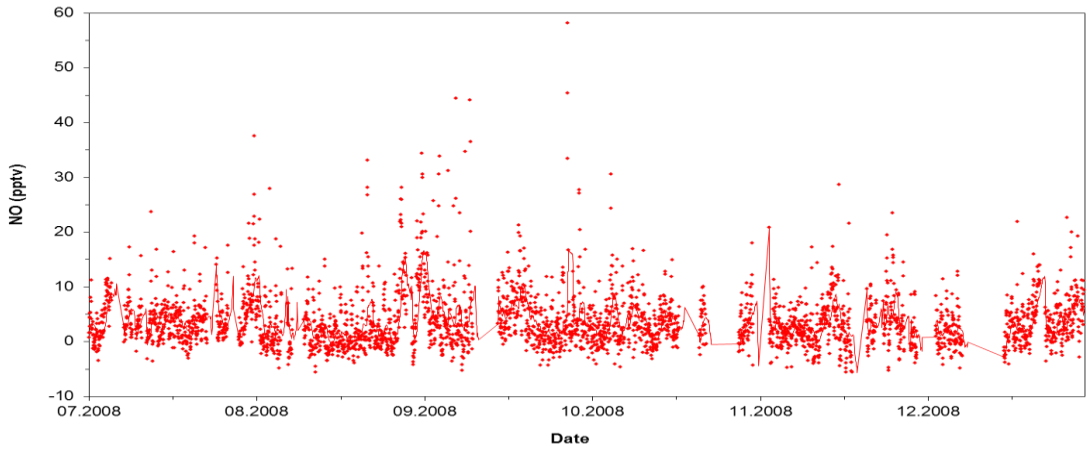
NO (pptv)
60
50
40
30
20
10
0
-10
07.2008
08.2008
09.2008
10.2008
11.2008
12.2008
Date

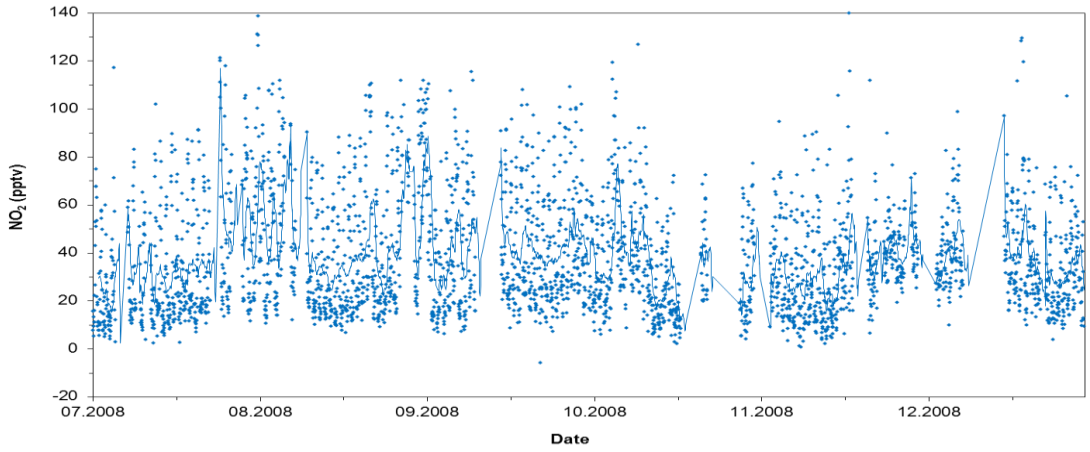
NO2 (pptv)
140
120
100
80
60
40
20
0
-20
07.2008
08.2008
09.2008
10.2008
11.2008
12.2008
Date

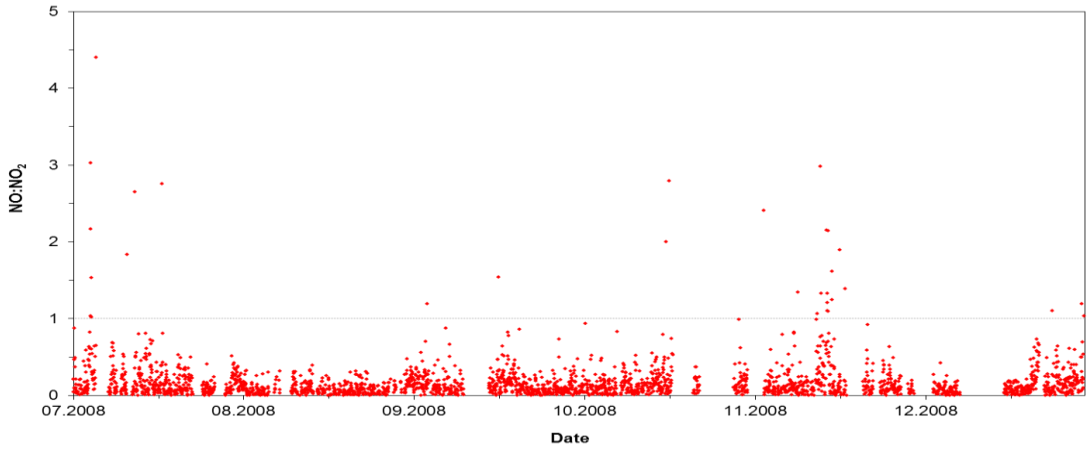
NO:NO2
5
4
3
2
1
0
07.2008
08.2008
09.2008
10.2008
11.2008
12.2008
Date

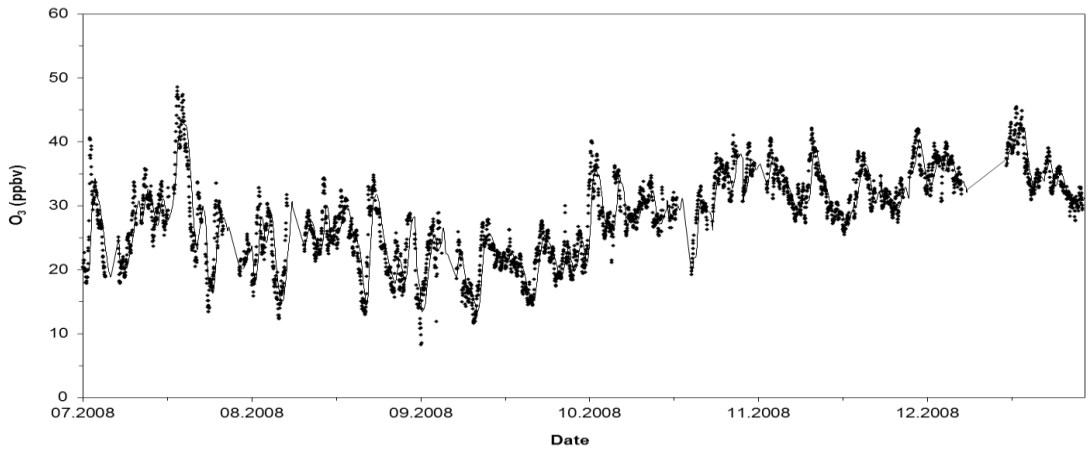
O3 (ppbv)
60
50
40
30
20
10
0
07.2008
08.2008
09.2008
10.2008
11.2008
12.2008
Date

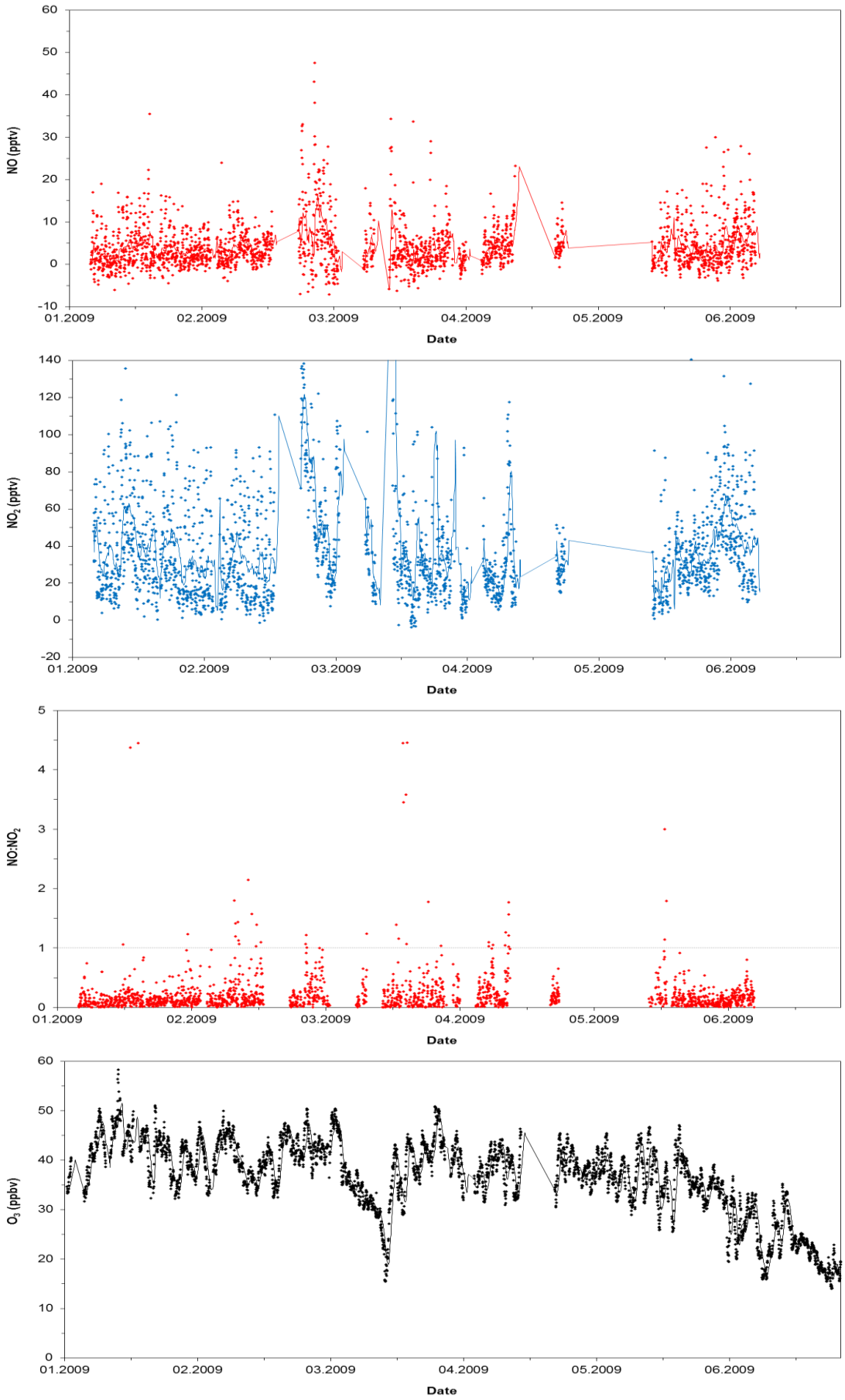
NO (pptv)
60
50
40
30
20
10
0
-10
01.2009
02.2009
03.2009
04.2009
05.2009
06.2009
Date
NO2 (pptv)
140
120
100
80
60
40
20
0
-20
01.2009
02.2009
03.2009
04.2009
05.2009
06.2009
Date
NO:NO2
5
4
3
2
1
0
01.2009
02.2009
03.2009
04.2009
05.2009
06.2009
Date
O3 (ppbv)
60
50
40
30
20
10
0
01.2009
02.2009
03.2009
04.2009
05.2009
06.2009
Date

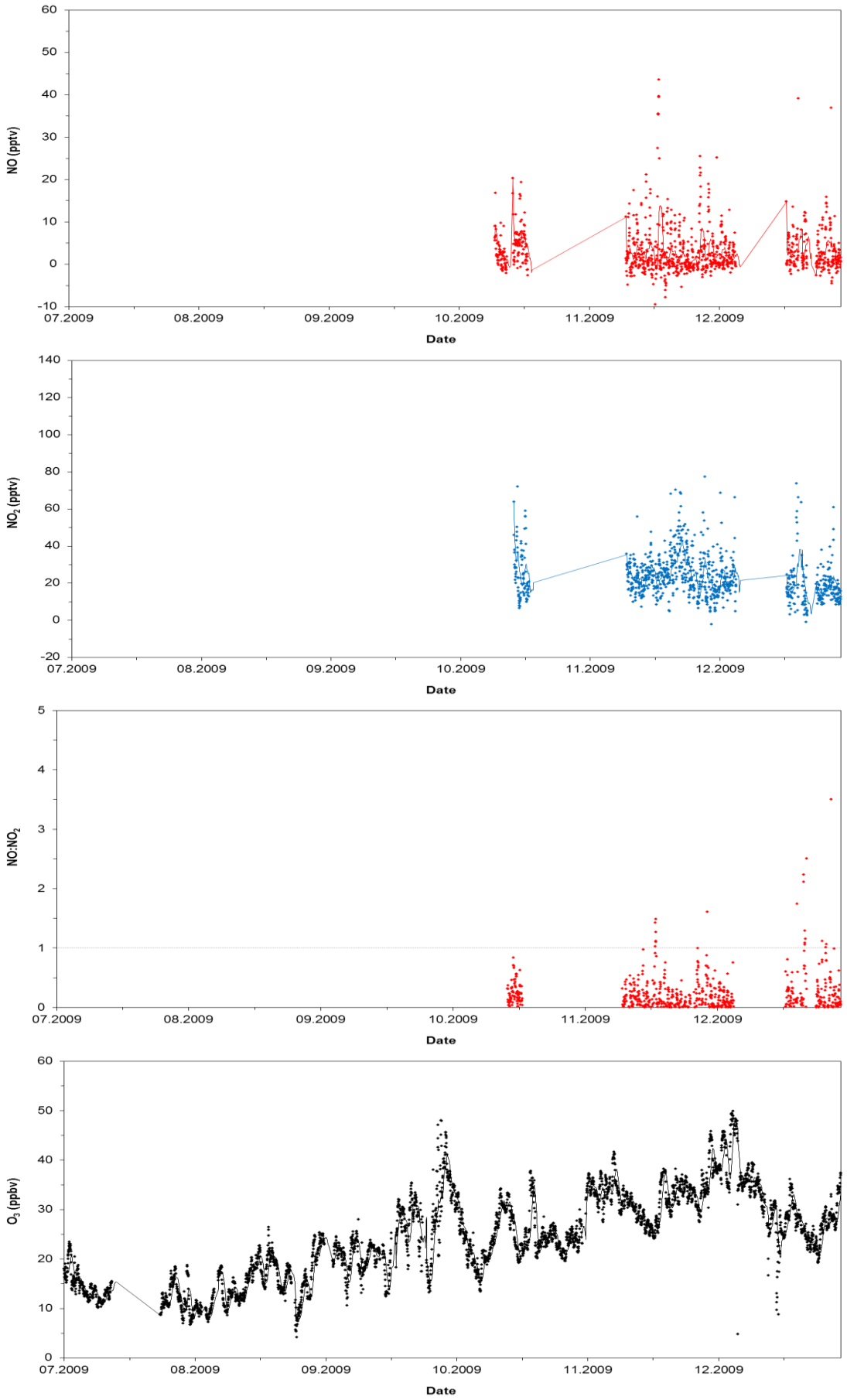
NO (pptv)
60
50
40
30
20
10
0
-10
07.2009
08.2009
09.2009
10.2009
11.2009
12.2009
Date
NO2 (pptv)
140
120
100
80
60
40
20
0
-20
07.2009
08.2009
09.2009
10.2009
11.2009
12.2009
Date
NO:NO2
5
4
3
2
1
0
07.2009
08.2009
09.2009
10.2009
11.2009
12.2009
Date
O3 (ppbv)
60
50
40
30
20
10
0
07.2009
08.2009
09.2009
10.2009
11.2009
12.2009
Date

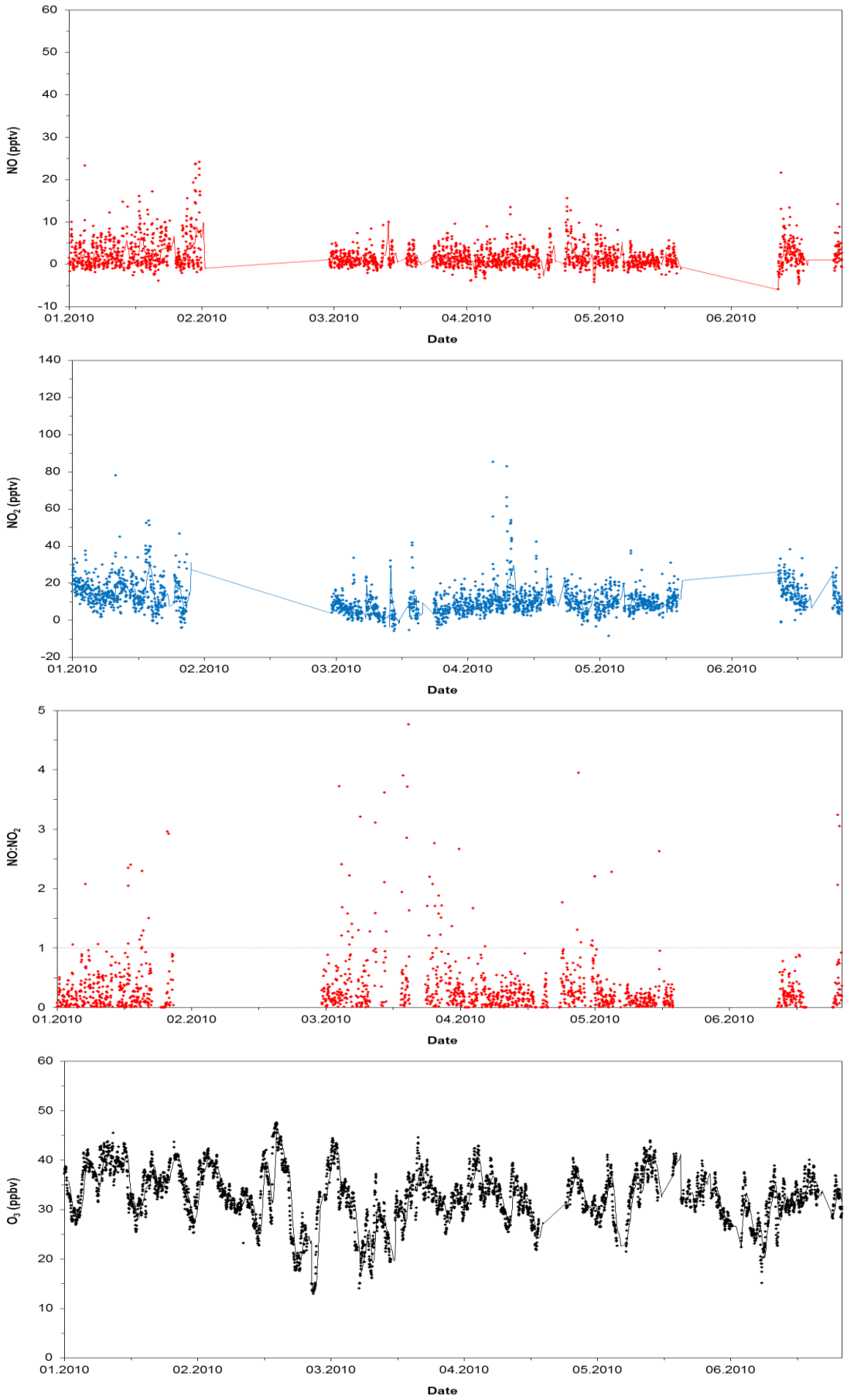
NO (pptv)
60
50
40
30
20
10
0
-10
01.2010
02.2010
03.2010
04.2010
05.2010
06.2010
Date
NO2 (pptv)
140
120
100
80
60
40
20
0
-20
01.2010
02.2010
03.2010
04.2010
05.2010
06.2010
Date
NO:NO2
5
4
3
2
1
0
01.2010
02.2010
03.2010
04.2010
05.2010
06.2010
Date
O3 (ppbv)
60
50
40
30
20
10
0
01.2010
02.2010
03.2010
04.2010
05.2010
06.2010
Date

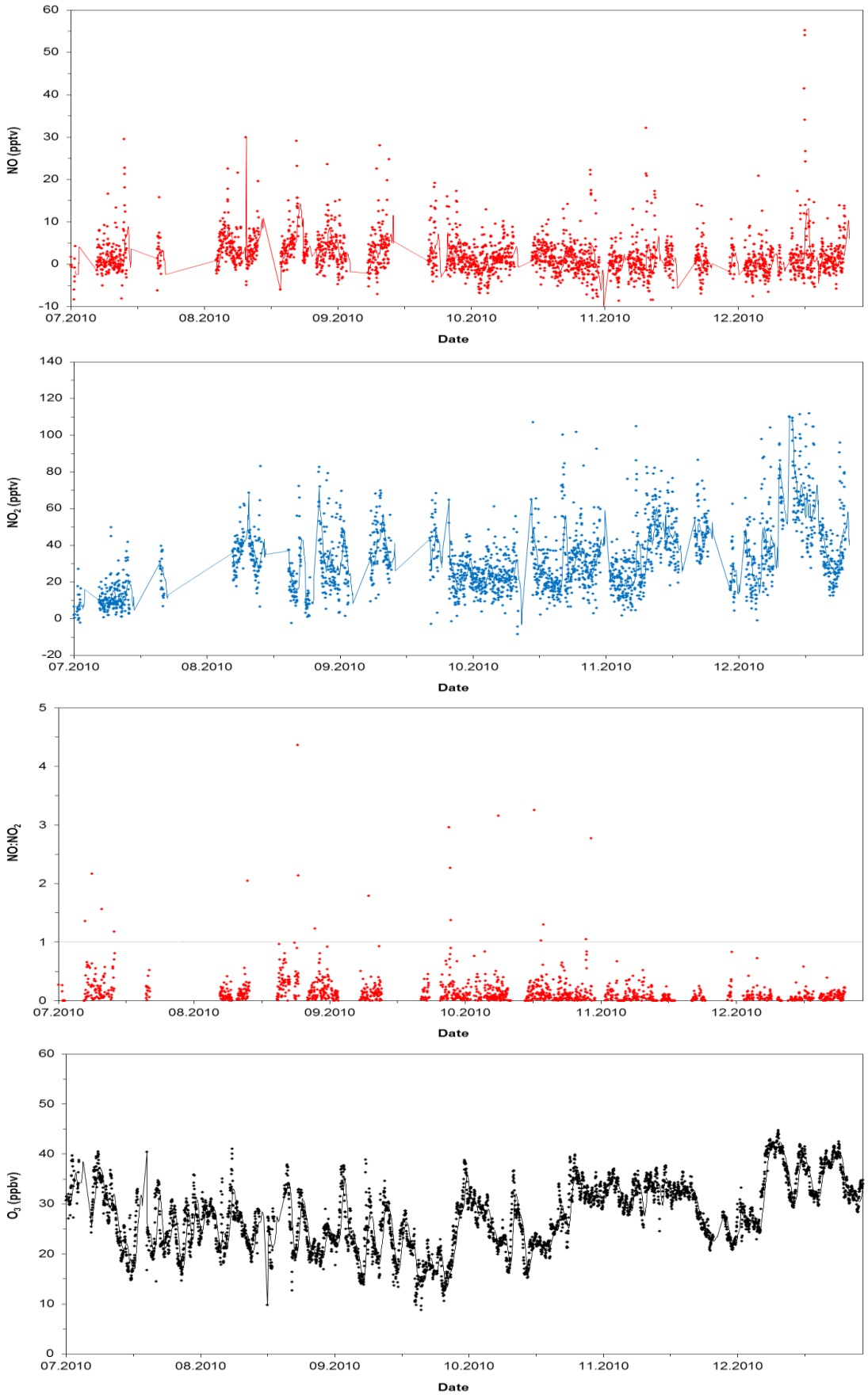

Figure 4.5. NO (top), NO_2 (second top), NO:NO_2 (second bottom) and O_3 measurements from the CVAO made between the 1st October 2006 and the 31st December 2010. Each plot represents 6 months of data.

Table 4.1. Monthly day and night time average O_3 mixing ratios along with standard deviation, median and number of measurements. Day = 1100-1500, night =0000-0400.

Date	Night time			Day time		
	Mean ± SD	Median	N	Mean ± SD	Median	N
Oct 06	25.7 ± 0.6	25.7	143	25.6 ± 1.1	25.6	145
Nov 06	24.6 ± 0.7	24.5	150	24.5 ± 0.8	24.5	150
Dec 06	37.6 ± 0.5	37.6	130	36.2 ± 0.8	36.2	132
Jan 07	32.9 ± 1.0	32.7	101	32.5 ± 1.0	32.6	118
Feb 07	36.4 ± 0.7	36.3	130	35.8 ± 1.3	35.8	132
Mar 07	40.6 ± 0.8	40.6	110	38.7 ± 1.2	38.7	129
Apr 07	40.6 ± 1.0	40.6	125	38.9 ± 1.3	38.8	130
May 07	38.1 ± 0.8	38.1	134	37.4 ± 1.5	37.4	135
Jun 07	30.0 ± 0.7	29.9	91	29.5 ± 1.4	29.7	107
Jul 07	28.7 ± 0.6	28.8	105	28.4 ± 1.0	28.4	118
Aug 07	27.3 ± 0.9	27.3	100	27.8 ± 1.1	28.0	108
Sep 07	23.8 ± 0.7	23.8	133	24.5 ± 1.2	24.6	150
Oct 07	26.7 ± 0.8	26.7	135	26.5 ± 1.1	26.6	137
Nov 07	34.5 ± 0.6	34.5	144	34.6 ± 1.5	34.8	144
Dec 07	36.7 ± 0.5	36.7	155	35.8 ± 0.9	35.8	155
Jan 08	35.9 ± 0.7	35.9	135	35.4 ± 1.0	35.5	132
Feb 08	34.6 ± 0.5	34.5	125	33.5 ± 1.0	33.5	128
Mar 08	34.5 ± 0.6	34.5	101	34.9 ± 1.2	34.9	92
Apr 08	36.4 ± 0.8	36.4	105	37.6 ± 1.5	37.4	107
May 08	29.4 ± 0.9	29.4	130	29.4 ± 1.1	29.4	121
Jun 08	32.7 ± 0.9	32.7	135	32.3 ± 1.4	32.2	125
Jul 08	27.7 ± 1.1	27.5	110	27.9 ± 1.3	27.8	118
Aug 08	23.7 ± 0.8	23.7	139	24.3 ± 0.9	24.3	128
Sep 08	21.1 ± 0.7	21.1	133	20.7 ± 1.2	20.7	129
Oct 08	30.2 ± 0.5	30.3	121	30.1 ± 1.2	30.1	119
Nov 08	32.9 ± 0.6	32.8	127	31.9 ± 1.0	31.9	134
Dec 08	35.5 ± 0.5	35.5	108	35.4 ± 0.8	35.4	102
Jan 09	42.6 ± 0.8	42.6	119	40.3 ± 0.8	40.3	121
Feb 09	40.4 ± 0.7	40.3	133	39.8 ± 0.9	39.8	129
Mar 09	37.9 ± 0.5	37.9	155	37.6 ± 1.1	37.5	150
Apr 09	38.8 ± 0.9	38.8	89	38.6 ± 1.1	38.7	90
May 09	37.0 ± 1.0	37.0	140	36.8 ± 1.3	36.9	150
Jun 09	26.4 ± 0.7	26.3	150	26.3 ± 1.0	26.2	147
Jul 09	14.0 ± 0.6	14.0	100	14.1 ± 0.8	14.1	91
Aug 09	14.7 ± 0.5	14.7	140	14.7 ± 0.8	14.7	145
Sep 09	22.5 ± 1.0	22.5	125	23.1 ± 1.3	23.1	125
Oct 09	25.3 ± 0.6	25.3	155	24.5 ± 1.0	24.5	155
Nov 09	32.2 ± 0.6	32.1	145	30.8 ± 1.1	30.7	147
Dec 09	32.5 ± 0.6	32.5	150	31.1 ± 1.6	31.1	154
Jan 10	35.8 ± 0.9	35.9	150	35.5 ± 1.0	35.4	154
Feb 10	34.1 ± 0.6	34.1	140	34.5 ± 1.3	34.6	138
Mar 10	31.0 ± 0.8	31.0	144	30.4 ± 1.5	30.4	132
Apr 10	32.7 ± 0.9	32.9	120	32.2 ± 1.4	32.2	106
May 10	34.2 ± 0.6	34.2	112	33.2 ± 1.2	33.1	106
Jun 10	30.6 ± 0.8	30.5	125	30.7 ± 1.3	30.6	110
Jul 10	26.3 ± 0.8	26.3	124	27.3 ± 1.9	27.4	117
Aug 10	25.2 ± 1.0	25.3	131	25.1 ± 1.4	25.1	138
Sep 10	21.6 ± 1.0	21.6	146	21.8 ± 1.5	21.5	145
Oct 10	27.1 ± 0.5	27.1	155	26.5 ± 1.2	26.4	155
Nov 10	31.3 ± 0.8	31.3	142	31.6 ± 0.9	31.6	132
Dec 10	33.4 ± 0.6	33.4	152	33.8 ± 0.8	33.9	153

Table 4.2. Monthly day and night time average NO mixing ratios along with standard deviation, median and number of measurements. Day = 1100-1500, night =0000-0400.

Date	Night time			Day time		
	Mean ± SD	Median	N	Mean ± SD	Median	N
Oct 06	0.7 ± 1.4	0.7	105	4.6 ± 2.1	4.4	125
Nov 06	8.8 ± 1.1	8.9	79	9.1 ± 2.0	8.8	84
Dec 06	1.4 ± 1.5	1.3	69	7.2 ± 3.0	7.0	65
Jan 07	0.5 ± 0.6	0.5	86	4.6 ± 2.8	3.6	82
Feb 07	0.4 ± 0.9	0.4	128	3.9 ± 2.1	3.5	128
Mar 07	1.1 ± 0.9	1.0	131	2.7 ± 1.6	2.6	119
Apr 07	0.4 ± 0.8	0.4	134	2.3 ± 1.9	2.0	127
May 07	0.8 ± 0.8	0.9	113	2.4 ± 1.4	2.3	97
Jun 07	0.5 ± 0.6	0.5	99	2.2 ± 1.3	2.0	94
Jul 07	0.5 ± 0.7	0.4	104	3.3 ± 1.5	3.2	116
Aug 07	0.2 ± 0.8	0.2	109	3.6 ± 1.9	3.2	114
Sep 07	0.3 ± 0.9	0.4	133	3.6 ± 1.3	3.5	128
Oct 07	1.3 ± 0.9	1.3	116	4.1 ± 3.3	3.1	109
Nov 07	3.4 ± 1.3	3.5	124	5.9 ± 3.5	5.1	128
Dec 07	2.1 ± 1.1	2.1	74	6.8 ± 4.9	5.7	72
Jan 08	1.4 ± 1.3	1.3	109	11.8 ± 4.9	10.9	105
Feb 08	1.9 ± 1.4	1.8	104	11.7 ± 5.3	10.5	101
Mar 08	0.6 ± 0.9	0.7	133	8.9 ± 3.9	8.4	110
Apr 08	1.5 ± 1.2	1.5	109	6.2 ± 2.8	5.9	92
May 08	0.4 ± 0.9	0.3	149	4.4 ± 2.1	4.2	134
Jun 08	2.2 ± 1.0	2.3	109	4.6 ± 3.0	4.1	99
Jul 08	3.2 ± 1.3	3.0	112	7.1 ± 4.1	6.3	115
Aug 08	1.0 ± 1.3	1.1	133	8.1 ± 3.8	7.5	131
Sep 08	3.1 ± 2.1	3.2	118	9.8 ± 5.8	8.5	123
Oct 08	2.5 ± 2.2	2.5	99	5.8 ± 3.5	6.0	102
Nov 08	2.7 ± 1.9	2.6	113	5.9 ± 4.0	5.6	111
Dec 08	2.1 ± 1.7	1.9	94	5.9 ± 3.8	5.8	93
Jan 09	0.7 ± 1.5	0.8	120	8.7 ± 3.3	8.2	118
Feb 09	1.8 ± 1.5	1.7	104	6.5 ± 2.3	6.5	95
Mar 09	1.8 ± 2.4	1.7	103	8.3 ± 3.4	8.0	103
Apr 09	3.0 ± 1.3	3.1	63	8.3 ± 1.9	8.2	62
May 09	1.7 ± 1.7	1.8	54	6.9 ± 3.8	6.4	47
Jun 09	2.0 ± 2.0	2.2	64	12.4 ± 6.0	11.2	63
Jul 09			0			0
Aug 09			0			0
Sep 09			0			0
Oct 09	2.0 ± 1.6	1.8	35	6.8 ± 3.2	6.8	29
Nov 09	-0.3 ± 1.5	-0.4	83	10.2 ± 3.4	10.1	80
Dec 09	0.3 ± 1.6	0.2	75	7.6 ± 1.9	7.5	74
Jan 10	0.3 ± 1.2	0.2	137	6.7 ± 2.1	6.5	136
Feb 10	0.8 ± 2.6	-0.1	22	13.5 ± 2.4	13.7	23
Mar 10	0.4 ± 0.6	0.4	99	3.4 ± 1.1	3.4	83
Apr 10	0.0 ± 0.9	-0.1	122	3.9 ± 1.3	3.9	108
May 10	0.1 ± 0.7	0.1	98	3.4 ± 1.4	3.4	82
Jun 10	0.7 ± 1.9	0.6	29	4.3 ± 2.9	4.0	30
Jul 10	0.8 ± 2.2	0.5	46	5.2 ± 3.3	5.1	41
Aug 10	2.6 ± 1.6	2.5	86	8.3 ± 2.9	8.1	83
Sep 10	1.1 ± 2.7	1.2	63	6.5 ± 4.2	6.1	68
Oct 10	0.0 ± 2.0	0.0	127	2.8 ± 2.2	2.7	129
Nov 10	-1.1 ± 2.1	-1.2	79	3.8 ± 3.9	4.2	81
Dec 10	-0.4 ± 1.7	-0.5	100	5.1 ± 3.4	4.7	99

Table 4.3. Monthly day and night time average NO_2 mixing ratios along with standard deviation, median and number of measurements. Day = 1100-1500, night =0000-0400.

Date	Night time			Day time		
	Mean ± SD	Median	N	Mean ± SD	Median	N
Oct 06	20.8 ± 7.1	19.2	95	24.1 ± 7.2	23.2	114
Nov 06	14.4 ± 5.5	13.5	75	21.9 ± 5.7	21.3	79
Dec 06	40.0 ± 10.3	38.0	69	38.9 ± 8.5	38.0	65
Jan 07	38.2 ± 11.4	36.3	86	43.9 ± 9.0	41.8	82
Feb 07	27.4 ± 8.6	26.2	128	33.9 ± 7.3	32.2	128
Mar 07	16.7 ± 8.9	15.0	130	37.3 ± 7.0	37.0	119
Apr 07	17.0 ± 5.2	16.0	134	45.2 ± 8.3	44.2	127
May 07	17.9 ± 7.4	16.6	113	13.4 ± 4.7	13.3	95
Jun 07	9.6 ± 5.3	8.0	99	12.3 ± 4.0	11.7	94
Jul 07	12.6 ± 7.2	10.0	102	17.9 ± 5.4	17.5	116
Aug 07	16.4 ± 4.4	16.4	109	22.8 ± 5.6	21.7	114
Sep 07	17.0 ± 6.6	15.6	133	17.4 ± 4.3	16.9	128
Oct 07	21.4 ± 11.0	17.7	116	20.5 ± 10.5	18.0	115
Nov 07	18.5 ± 7.3	17.7	89	24.5 ± 7.7	22.6	90
Dec 07	37.6 ± 14.4	36.1	72	34.6 ± 9.2	32.5	72
Jan 08	43.7 ± 12.6	41.2	105	59.9 ± 12.8	61.2	105
Feb 08	53.6 ± 13.2	51.0	99	72.7 ± 14.1	73.0	102
Mar 08	12.2 ± 6.7	10.8	133	81.6 ± 16.5	82.8	107
Apr 08	14.5 ± 7.6	12.3	109	68.5 ± 13.7	69.8	89
May 08	12.9 ± 6.1	11.7	149	49.6 ± 9.2	51.1	134
Jun 08	13.8 ± 5.2	13.1	109	48.8 ± 10.2	49.6	99
Jul 08	18.6 ± 7.3	16.9	111	63.2 ± 12.9	64.6	115
Aug 08	28.9 ± 7.3	28.6	126	74.2 ± 11.6	75.1	126
Sep 08	28.1 ± 11.3	25.9	116	68.6 ± 13.5	66.4	120
Oct 08	30.1 ± 16.4	25.8	96	52.8 ± 10.6	52.4	102
Nov 08	27.9 ± 12.9	24.8	113	45.6 ± 11.1	44.9	111
Dec 08	30.6 ± 9.5	29.3	94	56.6 ± 10.8	56.7	93
Jan 09	26.4 ± 10.3	25.0	120	70.2 ± 15.5	70.9	118
Feb 09	16.1 ± 9.6	14.0	104	62.1 ± 14.0	64.1	95
Mar 09	73.0 ± 27.6	72.0	104	36.6 ± 13.4	33.4	104
Apr 09	26.9 ± 8.2	27.4	63	29.3 ± 7.6	29.2	62
May 09	22.1 ± 8.6	20.0	54	48.9 ± 8.0	48.5	47
Jun 09	34.3 ± 13.6	29.9	64	73.5 ± 10.5	73.0	63
Jul 09			0			0
Aug 09			0			0
Sep 09			0			0
Oct 09	18.7 ± 3.6	18.3	20	46.7 ± 7.8	46.6	15
Nov 09	26.4 ± 6.0	26.3	83	29.3 ± 6.6	29.6	80
Dec 09	18.8 ± 7.8	16.7	74	24.6 ± 8.1	24.4	74
Jan 10	17.8 ± 6.5	16.7	119	14.8 ± 4.9	14.0	114
Feb 10	7.8 ± 3.6	5.8	5	16.3 ± 12.5	9.2	3
Mar 10	6.3 ± 3.6	6.5	94	7.9 ± 3.1	8.1	81
Apr 10	11.7 ± 5.1	11.4	124	13.2 ± 2.3	13.2	104
May 10	6.9 ± 2.7	7.1	98	14.7 ± 2.7	14.2	82
Jun 10	13.3 ± 2.5	13.1	33	19.9 ± 6.1	21.4	32
Jul 10	9.9 ± 4.1	9.3	51	19.3 ± 5.5	18.5	42
Aug 10	34.4 ± 10.1	32.4	66	31.3 ± 8.9	30.7	63
Sep 10	36.1 ± 12.2	35.5	57	35.0 ± 8.7	34.0	67
Oct 10	26.4 ± 9.8	24.7	132	28.8 ± 7.8	28.2	133
Nov 10	35.3 ± 8.6	33.9	99	45.1 ± 7.3	44.8	96
Dec 10	39.3 ± 8.2	38.0	94	57.3 ± 10.3	57.4	95

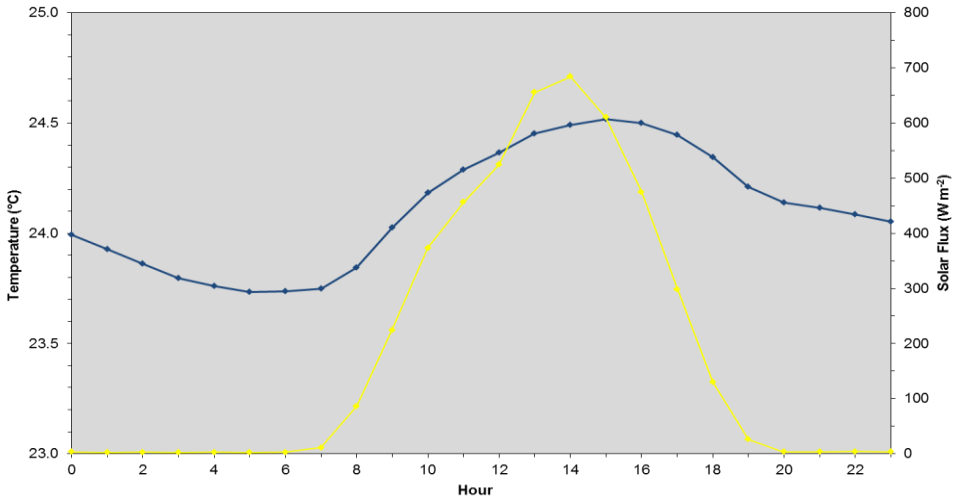

Figure 4.6. Diurnal cycle of temperature and solar flux at the CVAO.

NO_x levels display seasonality on the annual scale, peaking between November and February as shown by figure Figure 4.7. Rather than a result of photochemistry, this is believed to be a result of changes in the air mass origin (Lee et al., 2009). Figure 4.8 shows the percentage contribution of each air mass sampled at CVAO from October 2006 to March 2010. During the months of November to February, continental African air masses comprise a significant proportion of that sampled and are almost exclusively sampled within this four month period. The lower NO_x levels measured from mid-March to July correspond with predominantly marine or coastal air masses and the elevated levels from late July to October occur as the contribution of European air masses increases.

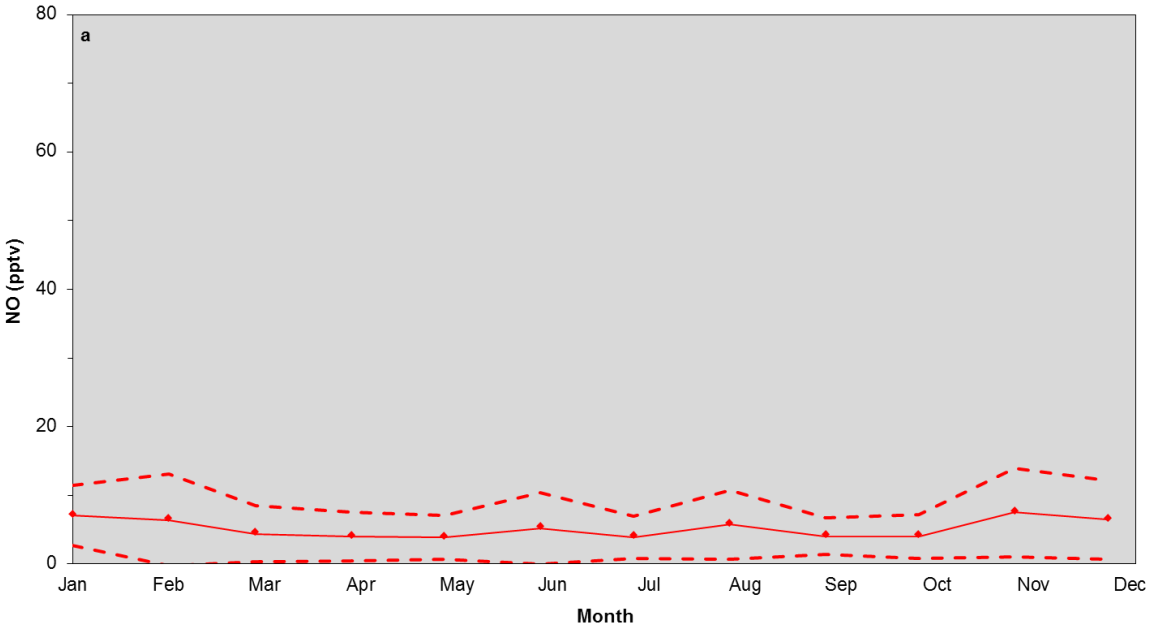

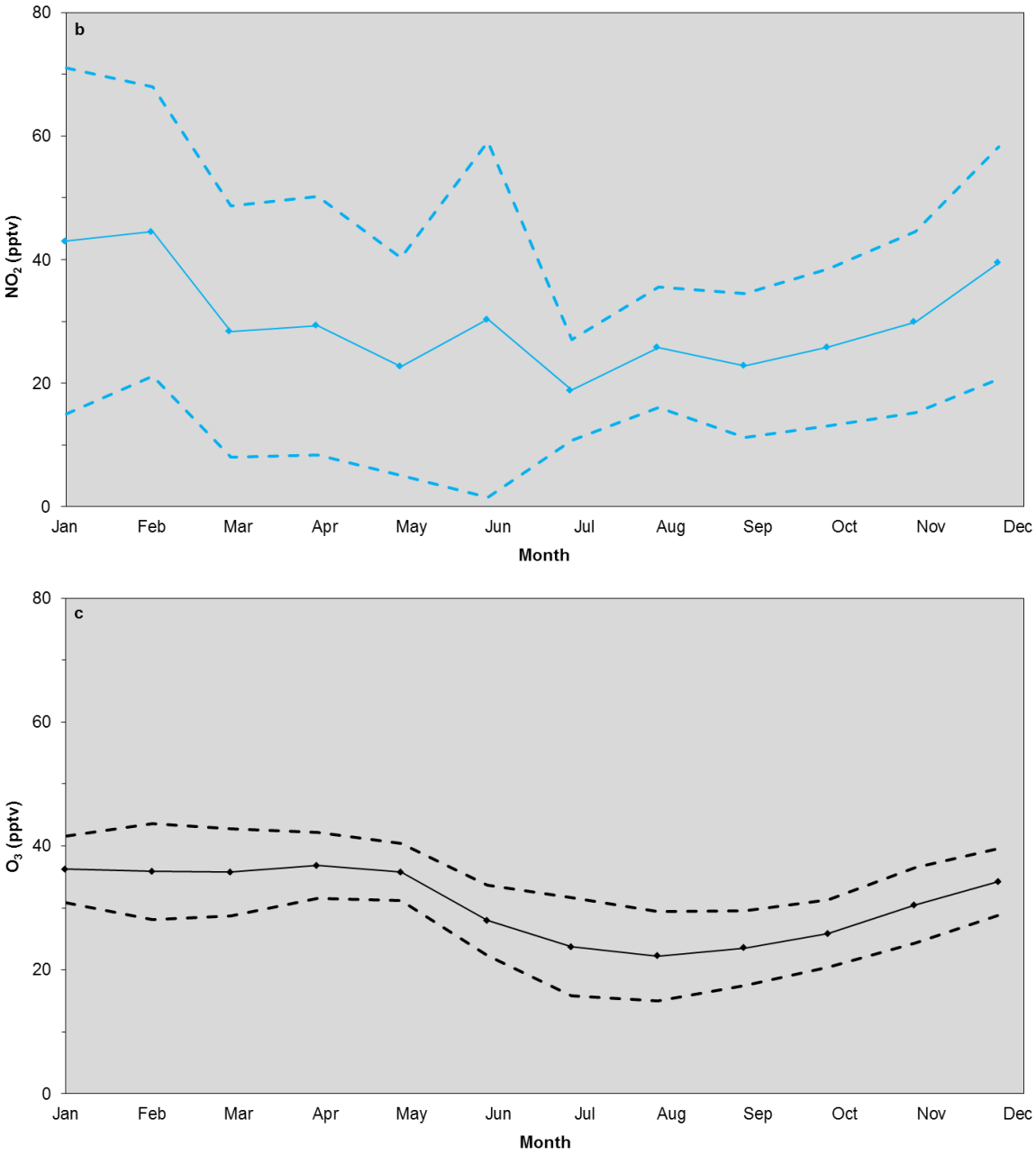

Figure 4.7. The annual cycle shown by average monthly daytime mixing ratios over all years, a = NO (red line), b = NO_2 (blue line), c = O_3 (black line). Dashed lines are standard deviation from mean.

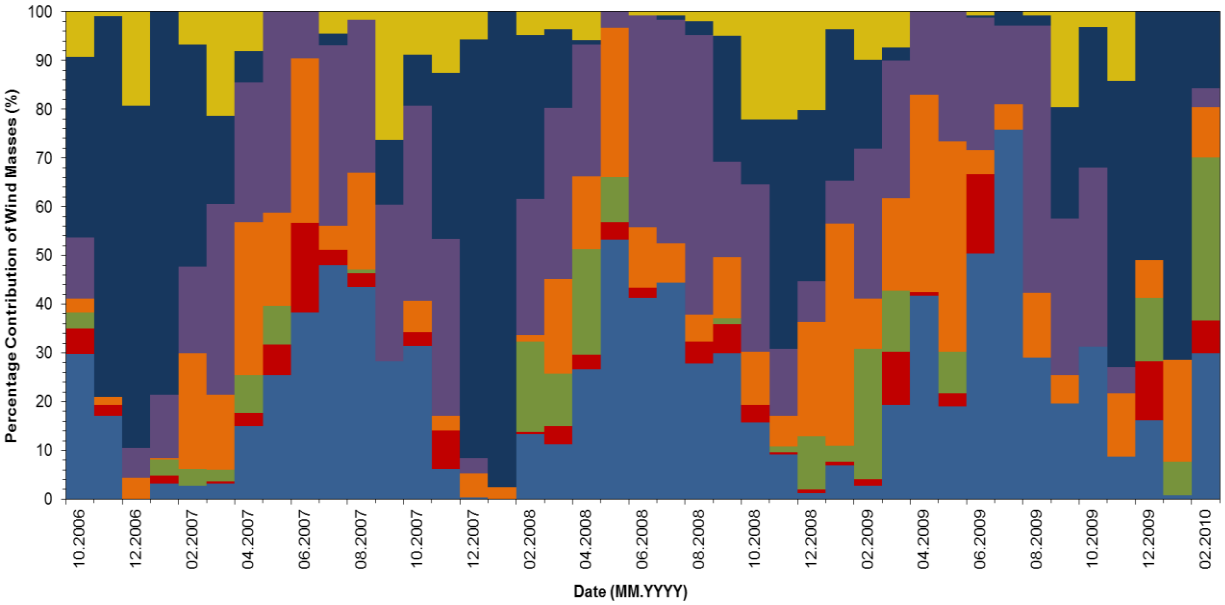

Figure 4.8. Seasonality of air masses sampled at CVAO during 1.10.2006 to 31.3.2010. Light blue = ACA, red = A, green = NACA, orange = ANA, purple = ECA, dark blue = CA, gold = E. (adapted from Carpenter et al., 2010).

This is further supported by the frequency distribution of NO_x measurements in the different air masses shown in figures 4.9a-g. Examples of their respective back trajectories are shown in figure 4.4. The plots in figure 4.9 can be subdivided by the amount of processing time spent in the marine boundary layer with reduced continental interference. Figures 4.9a-c represent air masses that have spent a significant amount of time in the marine boundary layer, which is reflected in the lower NO_x levels and fewer occurrences of high pollution events. Of these air masses, purely Atlantic air (figure 4.9b) shows a marked reduction in median NO_x levels of just 16.53 pptv in comparison with those originating from coastal African and North American sources (figures 4.9a and 4.9c). This is most likely due to residual NO_x that has been transported from these regions in the form of longer lived reservoir species prior to reformation.

Figures 4.9d-g represent those air masses that have a greater contribution from continental regions and consequently, have increased NO_x loadings. As would be expected, air masses transported from North America via coastal Africa (figure 4.9d) have greater NO_x levels than those from the same source which have not encountered fresh plumes to replenish NO_x levels (figure 4.9c). As processing of the air mass is not linear with time however, this air mass (figure 4.9d) also shows high variability in the NO_x mixing ratios encountered at the CVAO. This is similar for that of European and coastal African air masses which display an almost log normal distribution (figure 4.9g), with 12-15 pptv being the most common mixing ratios. European air masses also show a near normal distribution, but exhibit both greater levels and variation in the NO_x content. Of a similar NO_x burden is

that of continental African air, which although it shows a reduced average and variation of NO_x in comparison with European air, it shows the greatest median NO_x levels of 26.26 pptv and a greater proportion of high NO_x events, either as a result of direct transport or via the transport of reservoir species and subsequent reformation close to the CVAO.

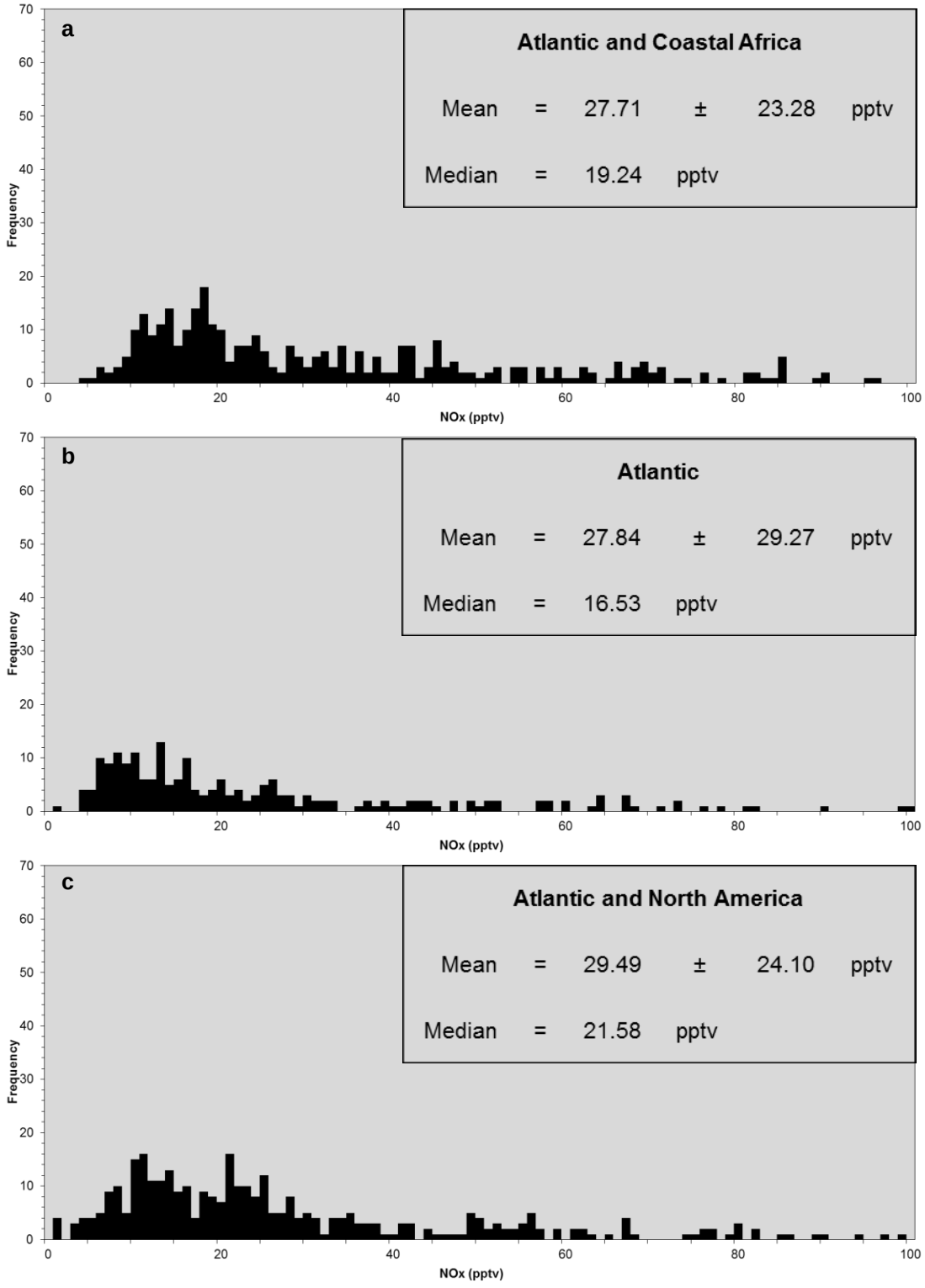

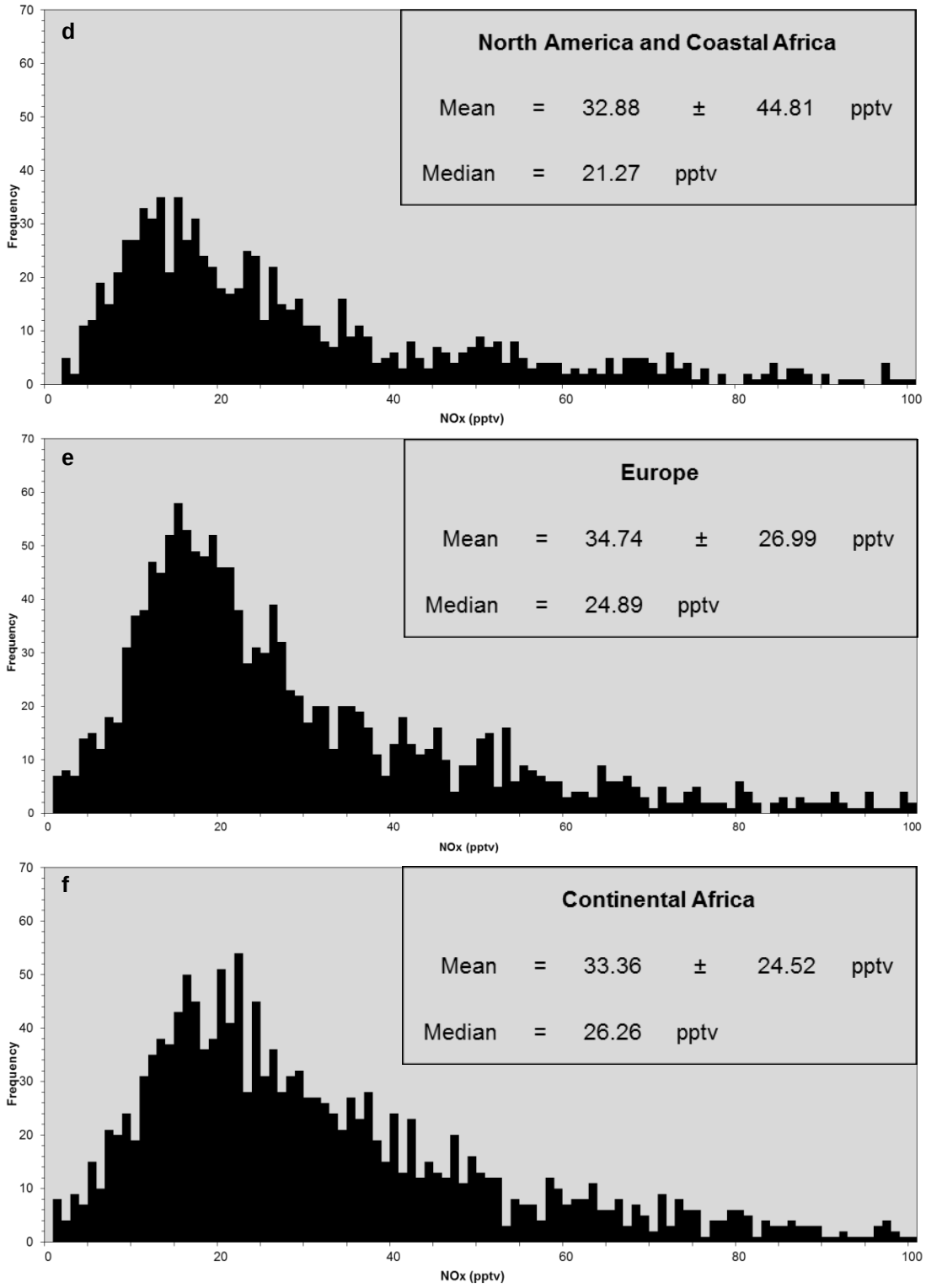
d
North America and Coastal Africa
Mean = 32.88 ± 44.81 pptv
Median = 21.27 pptv
Frequency
NOx (pptv)
e
Europe
Mean = 34.74 ± 26.99 pptv
Median = 24.89 pptv
Frequency
NOx (pptv)
f
Continental Africa
Mean = 33.36 ± 24.52 pptv
Median = 26.26 pptv
Frequency
NOx (pptv)

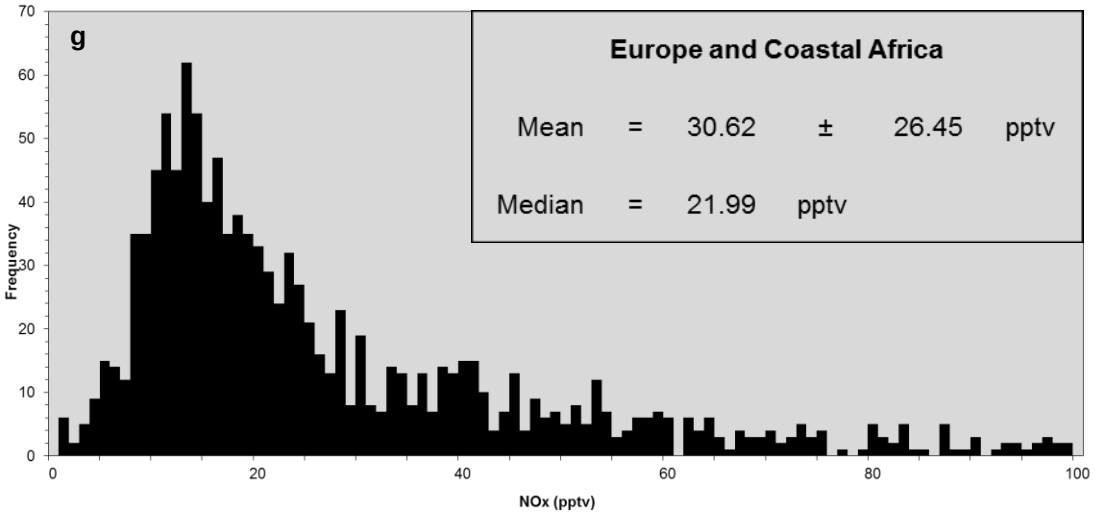

Figure 4.9. NO_x frequency distribution for different wind masses sampled at CVAO between October 2006 and December 2009. Mean, standard deviation and median for each dataset also displayed. a= Atlantic and Coastal Africa, b= Atlantic, c = Atlantic and North America, d = North America and Coastal Africa, e = Europe, f = Continental Africa, g = Europe and Coastal Africa.

Individually, both NO and NO_2 display diurnal cycles as shown in figure 4.10. NO values peak around solar noon and are typically less than 10 pptv. This trend is consistent with a pristine, remote environment and with current understanding of NO production as a result of NO_2 photolysis. Although a significant proportion of the NO data is close to the instrument detection limit, statistical analysis comparing the day and night time data found that they were significantly different at the 99.9 % confidence level (students *t*-test, $P < 0.1$), giving confidence in the NO data and the trends observed (Lee et al., 2009). The NO_2 mixing ratio varies between 15-80 pptv and exhibits a diurnal cycle with stable nighttime values and peaking a few hours after solar noon. As it is believed that NO_2 undergoes photolysis during the day to form NO, the source of this diurnal cycle is currently unknown and will be the subject of discussion in section 4.2.4.

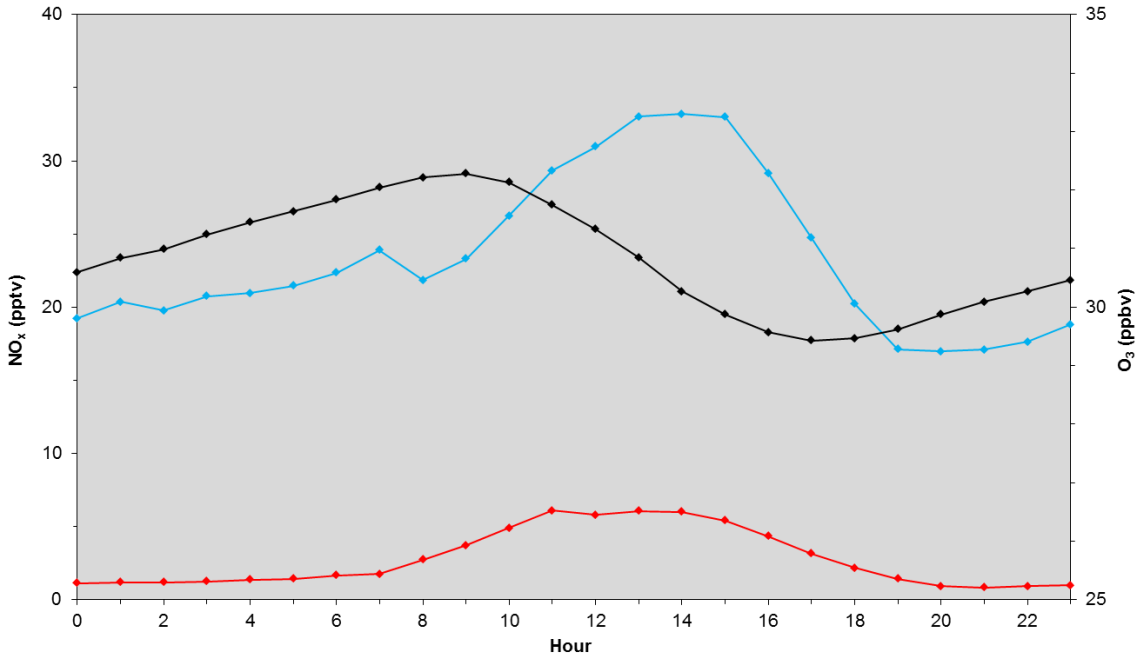

Figure 4.10. Average diurnal cycle, for all data, of NO (red line), NO_2 (blue line) and O_3 (black line) at the CVAO.

O_3 also exhibits both a clear annual and diurnal cycle as shown in figures 4.7 and 4.10 respectively. Annually, O_3 displays a maximum in spring and a minimum in late summer that is consistent with previous studies in remote boundary layer sites in the Northern Hemisphere (Ayers et al., 1996; Carpenter et al., 1997). Although the reason for this seasonality is not completely understood, it is thought that changes in STE combined with a lower stratospheric O_3 maximum due to the build-up of O_3 precursors over the winter is responsible (Penkett et al., 1998; Monks et al., 2000).

The diurnal cycle peaks around 0800-0900, with daily O_3 destruction varying between 1-8 ppbv until approximately 1800, when a gradual overnight increase in O_3 occurs due to advection and / or entrainment from the free troposphere (figure 4.10) (Lee et al., 2009). Although this diurnal is rare in the northern hemisphere due to greater pollution from anthropogenic activity, it is typical of areas with very low NO_x levels (Monks et al., 1998; Parrish et al., 1998).

Lee et al (2009) developed a zero-dimensional box model to look at the dependence of O_3 on NO mixing ratios at the CVAO. ΔO_3 was defined as the change in the O_3 mixing ratio from 0900-1700 each day, with a negative ΔO_3 value indicating net O_3 destruction. ΔO_3 for each day is plotted alongside the daytime average NO mixing ratio as measured at CVAO in figure 4.11, as this would be expected to correspond to the highest NO mixing ratios. As demonstrated by figure 4.11, NO is typically lower than 15 pptv and instances of O_3 production throughout the 5-year dataset are relatively rare.

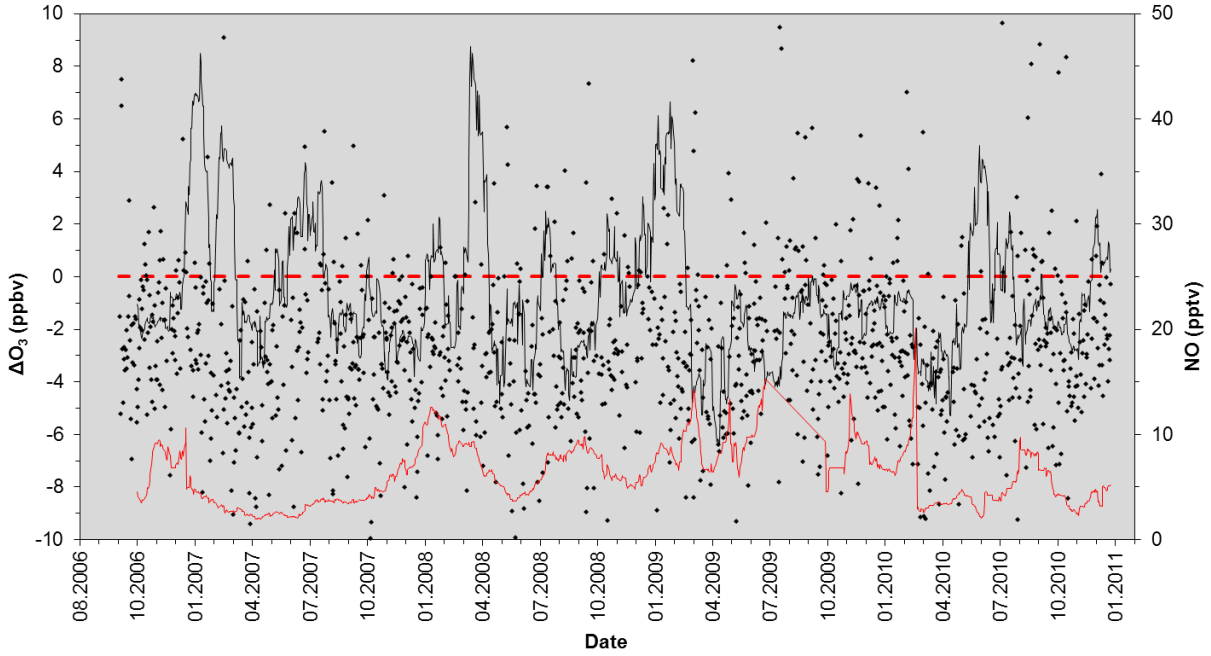

Figure 4.11. ΔO_3 values and daytime NO showing dependency of O_3 dynamics on NO. Black dots = ΔO_3, black line = 30-day running average of O_3, solid red line = 30-day running average of daytime NO mixing ratio, dashed red line = O_3 compensation point.

As O_3 dynamics are controlled by a range of factors, of which NO_x mixing ratios are just one, Lee et al (2009) modelled monthly data separately maintaining the months average conditions with only the rate of increase and maximum NO concentrations being varied, thereby calculating a range of O_3 compensation points. The results of this analysis are shown in figure 4.12 with each month being represented by a different coloured line and the x-intercept representing the O_3 compensation point. The corresponding coloured diamond is the predicted compensation point based solely on the measured NO mixing ratio for that month. The compensation point calculated for each month however, ranged from 17 to 34 pptv with all but 4 months clustered within the NO mixing ratio of 23 to 27 pptv. The difference between these higher compensation points and the values calculated using only the average NO values, is due to other factors that contribute to daily O_3 dynamics including halogen chemistry, which contributes approximately 30 % to the O_3 loss at the CVAO (Read et al., 2008). Lee et al (2009) found that daily ΔO_3 values (y-intercept) at the CVAO are controlled predominantly by water vapour concentration and solar radiation and that the strength of the relationship between ΔO_3 and the NO mixing ratio (the gradient) is controlled by HO_2 concentrations. Consequently, the O_3 compensation point at CVAO displays significant temporal variation (Lee et al., 2009).

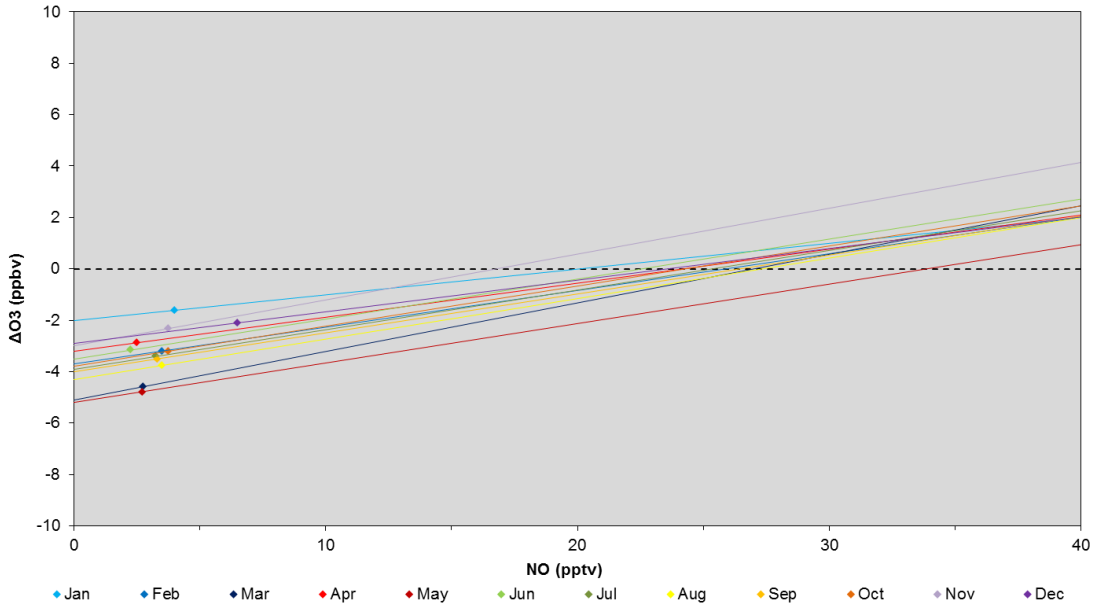

Figure 4.12. Modelled ΔO_3 values constrained by NO mixing ratios ranging from 1-40 pptv and using averaged conditions for each month in 2007. Actual NO measurements with the corresponding ΔO_3 values for each month during 2007 are shown as coloured diamonds (Lee et al., 2009).

Similar O_3 destruction regimes have been demonstrated in a variety of remote marine boundary layer sites globally. As can be seen in table 4.4, measurements from the CVAO show some of the greatest ΔO_3 values, further supporting the description of the CVAO location as a pristine environment. Lower ΔO_3 values found in other studies can be attributed to a number of sources including; lower photolysis rates due to the latitude of the study (Heikes et al., 1996; Ayers et al., 1997; Galbally et al., 2000), halogen chemistry (Galbally et al., 2000; Dickerson et al., 1999; Read et al., 2008) and proximity to continental source regions (Carsey et al., 1997; Parrish et al., 1998; Jacobi et al., 1999). As evidence for the latter, during a study by Carsey et al (1997) at 29° N, 25° W, located near to the CVAO, ΔO_3 values and NO mixing ratios were similar to those observed at CVAO (table 4.5) with O3 destruction rates reduced on days that coincided with sampling of continental African air masses, similar to the findings of Lee et al (2009) at the CVAO. Of additional interest due to the scope of this report, is a study by Jacobi et al (1999) to the east of the CVAO at 15° W. These authors found that O_3 displayed a diurnal cycle with production peaking mid-afternoon and corresponding with a large diurnal cycle in PAN mixing ratios. This highlights the importance of NO_x transport in the form of reservoir species and the role that proximity of the CVAO to continental source regions plays.

Table 4.4. Studies showing O_3 destruction regimes in remote boundary layer environments. * = studies from or near the CVAO.

Reference	Region	NO (pptv)	ΔO_3 (ppbv d^{-1})
Liu et al., 1983	Equatorial Pacfic Ocean	3.7	0.13
Thompson et al., 1993	Equatorial Pacfic Ocean	1.3	0.1-0.2
Heikes et al., 1996	South Atlantic Ocean	< 5	0.08
Singh et al., 1996	West Pacific Ocean	5.5	0.23
Ayers et al., 1997	South Pacific Ocean	2.0	0.12
Carsey et al., 1997	*North Atlantic Ocean	5.0	8.0
Dickerson et al., 1999	Equatorial Indian Ocean	5.0	4.0
Galbally et al., 2000	Cape Grim, Tasmania	6.0	2.0
Lee et al., 2009	*North Atlantic Ocean (CVAO)	1.8	1.0-8.0
Conley et al., 2011	Equatorial Pacfic Ocean	2.7	0.18

4.2.4. NO_2 Diurnal, ΔNO_2

As described in section 4.2.3, both NO and NO_2 display diurnal cycles at the CVAO (figure 4.10). Whereas the NO diurnal, which peaks around solar noon, agrees well with its known formation pathway of NO_2 photolysis, the apparent NO_2 diurnal seen at CVAO remains an unexplained feature of remote marine boundary layer chemistry at this site. As illustrated previously, this diurnal shows a reasonably stable nighttime value and peaks a few hours after solar noon reaching maximum mixing ratios of approximately 80 pptv. This phenomenon has been termed ΔNO_2 and was calculated for all days between the 1st of October 2006 and the 31st of December 2010 where data was available. ΔNO_2 was determined by subtracting the NO_2 nighttime average from that of the daytime average, both of which are defined as in section 4.2.3.

One aim of this project was to investigate the source of this NO_2 diurnal and determine whether it is a 'real' trend. Given the timing of its peak values, this would suggest a thermal or photolytic source (figure 4.6) such as the thermal decomposition of PAN which is known to act as dominant NO_x reservoir and lead to alterations in O_3 regimes (Carsey et al., 1997), or whether it is a fake signal due to instrumental error.

Hourly data of both NO and NO_2 were averaged over annual time scales to create a series of diurnal cycles as shown in figures 4.13 and 4.14 respectively. NO diurnals showed no deviation greater than that expected due to interannual variation (figure 4.13) further consolidating confidence in the NO data. Although the NO_2 diurnals showed that nighttime

NO_2 data did not vary significantly either, there was a distinct increase in the ΔNO_2 values for the year of 2008 as shown in figure 4.15.

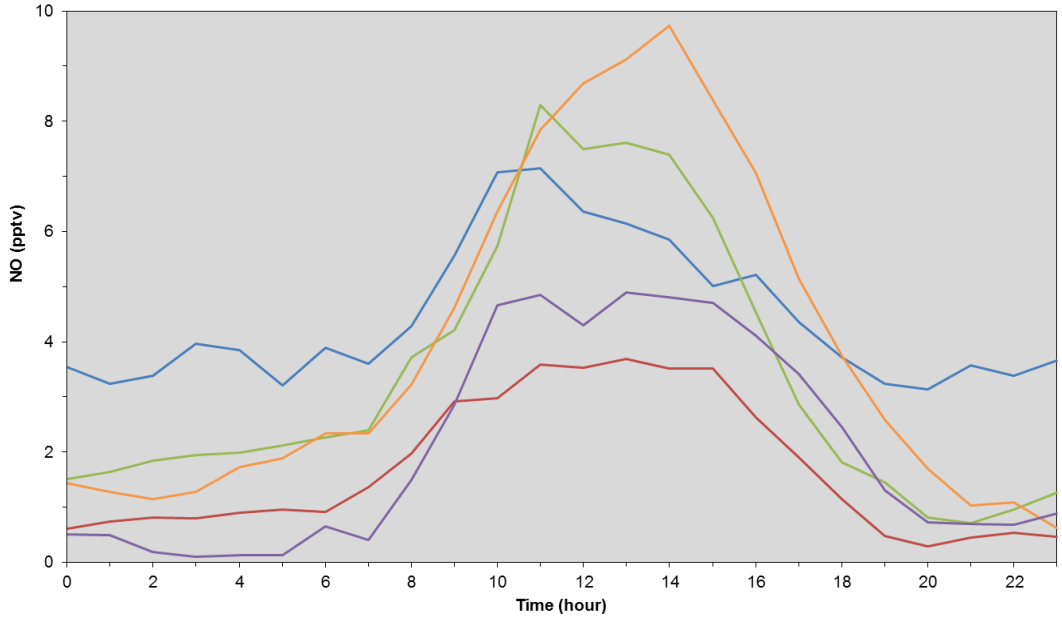

Figure 4.13. Yearly averaged NO diurnal cycle. Blue line = 2006, red line = 2007, green line = 2008, orange line = 2009, purple line = 2010.

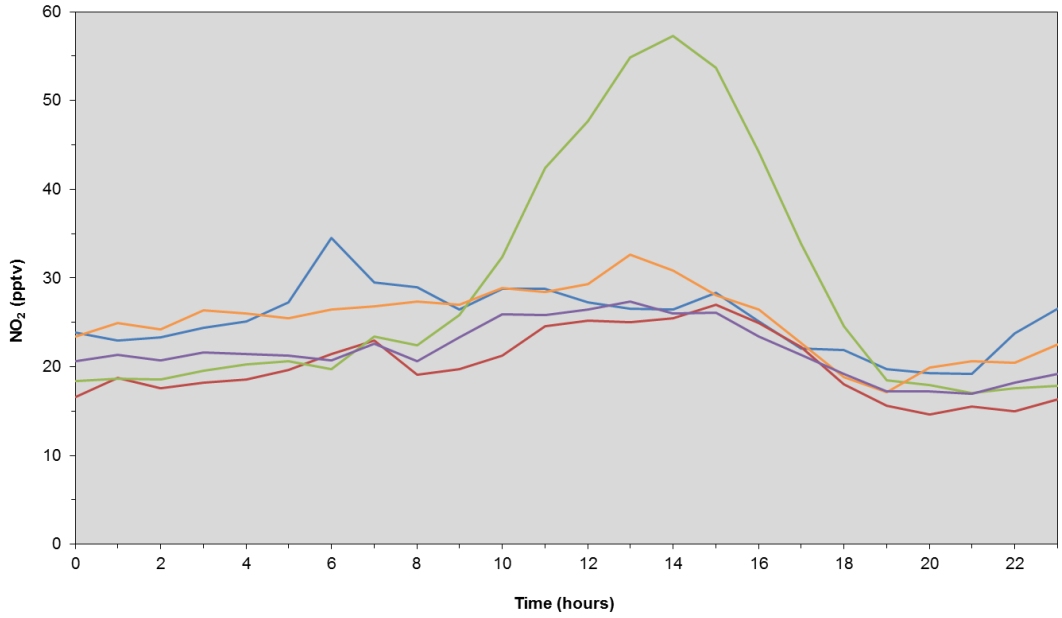

Figure 4.14. Yearly average NO_2 annual cycle. Blue line = 2006, red line = 2007, green line = 2008, orange line = 2009, purple line = 2010.

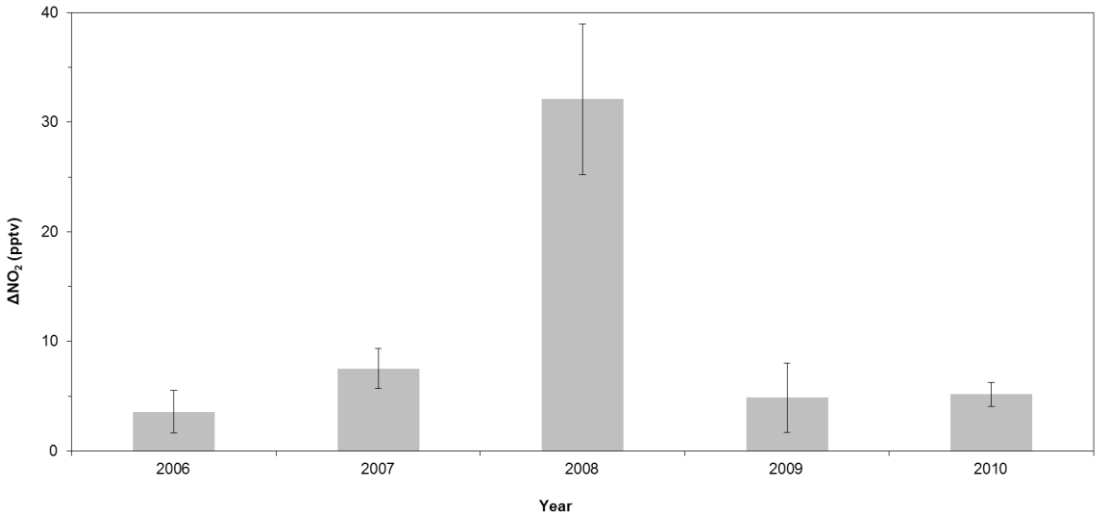

Figure 4.15. Average ΔNO_2 values and standard deviation for each year.

Although seasonally grouped data produced diurnals that showed higher NO_x levels in periods between December to February in all years (figures 4.16 and 4.17), as described previously in section 4.2.3, this can be explained by changes in air mass origins with a greater contribution from continental African sources during this period. Aside from this known seasonality, there is no fundamental change in the NO_2 diurnal profile that would suggest that the cause of the ΔNO_2 observed is a result of natural seasonal variation (figure 4.18).

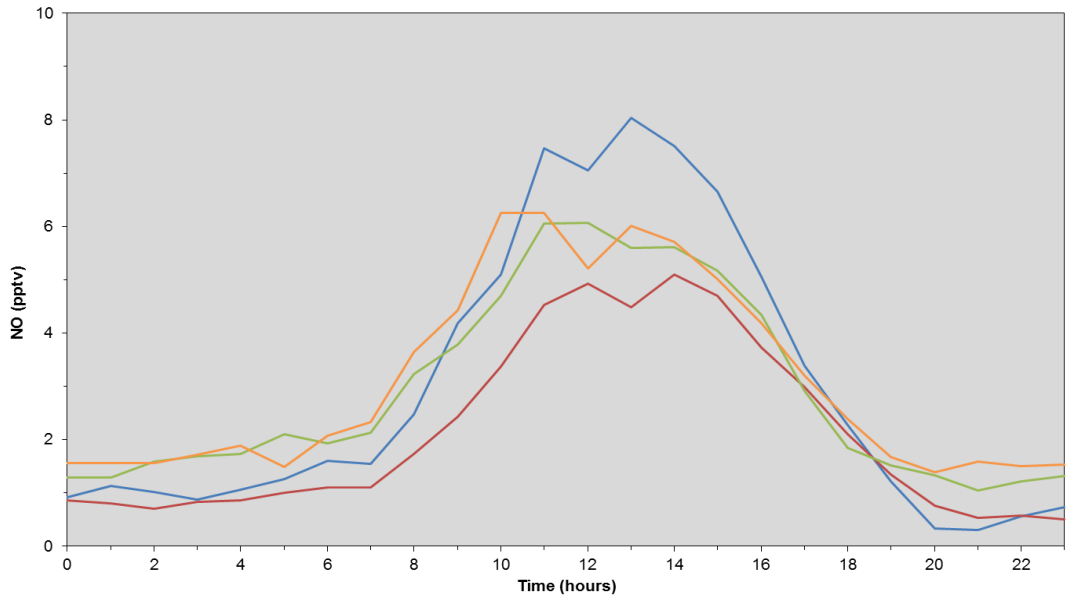

Figure 4.16. Seasonally averaged NO diurnal cycle. Blue line = Dec-Feb, red line = Mar-May, green line = Jun-Aug, orange line = Sep-Nov.

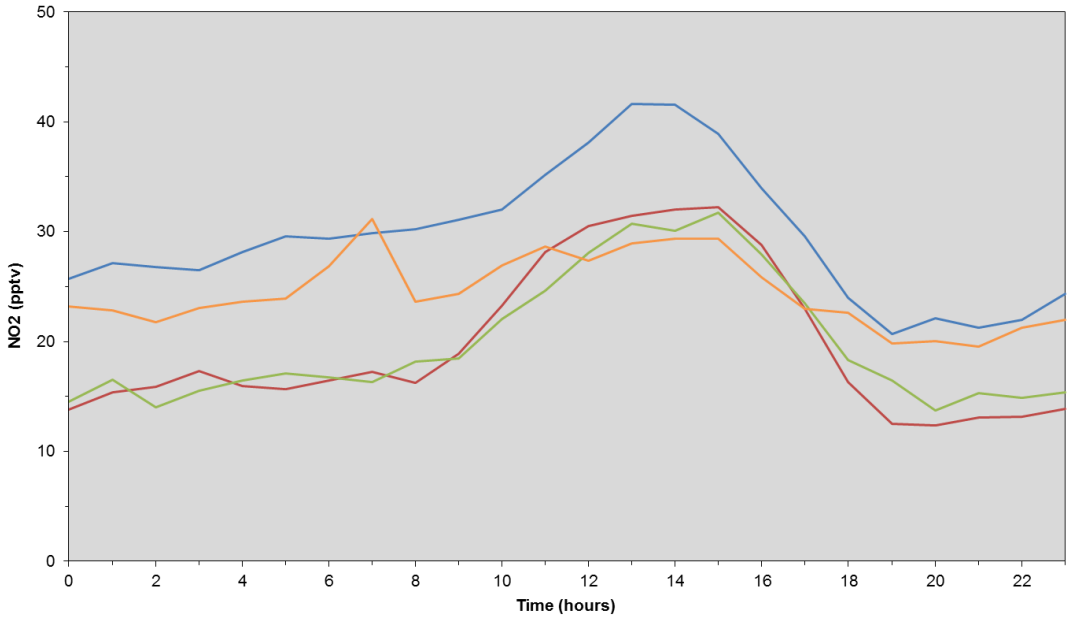

Figure 4.17. Seasonally averaged NO_2 diurnal cycle. Blue line = Dec-Feb, red line = Mar-May, green line = Jun-Aug, orange line = Sep-Nov.

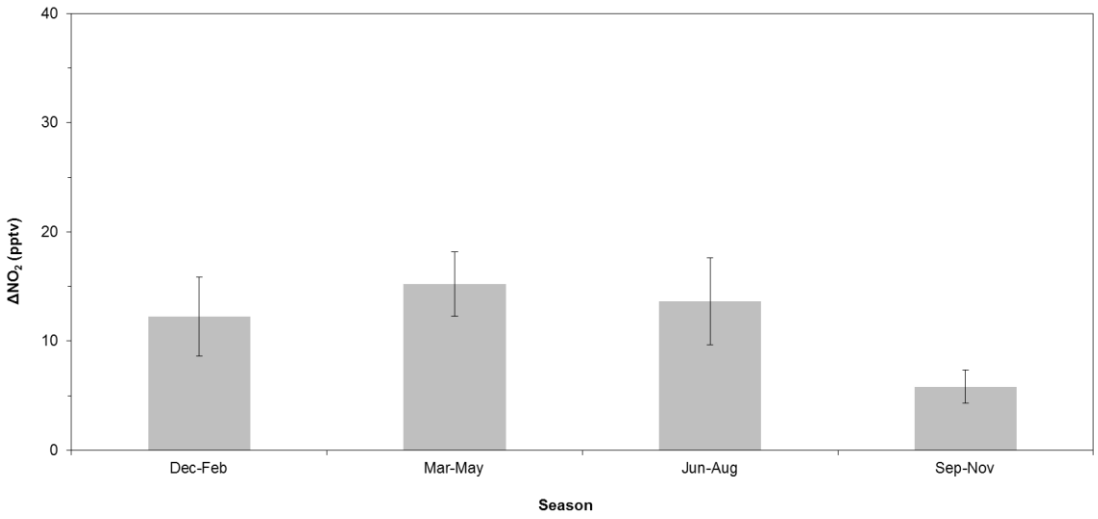

Figure 4.18. Average ΔNO_2 values and standard deviation for each season.

This is further supported by the lack of variation in the NO and NO_2 diurnals from within air masses as shown in figures 4.19 and 4.20, suggesting that the cause of the ΔNO_2 varies temporally rather than spatially and that the cause was particularly strong during the year 2008.

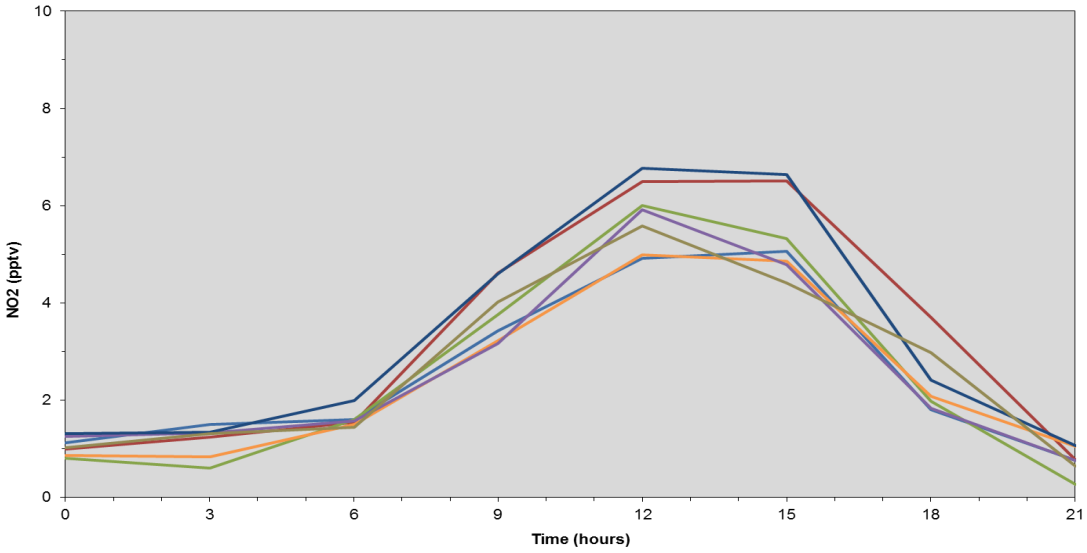

Figure 4.19. NO diurnal cycle averaged by air mass. Light blue = ACA, red = A, green = NACA, orange = ANA, purple = ECA, dark blue = CA, gold = E.

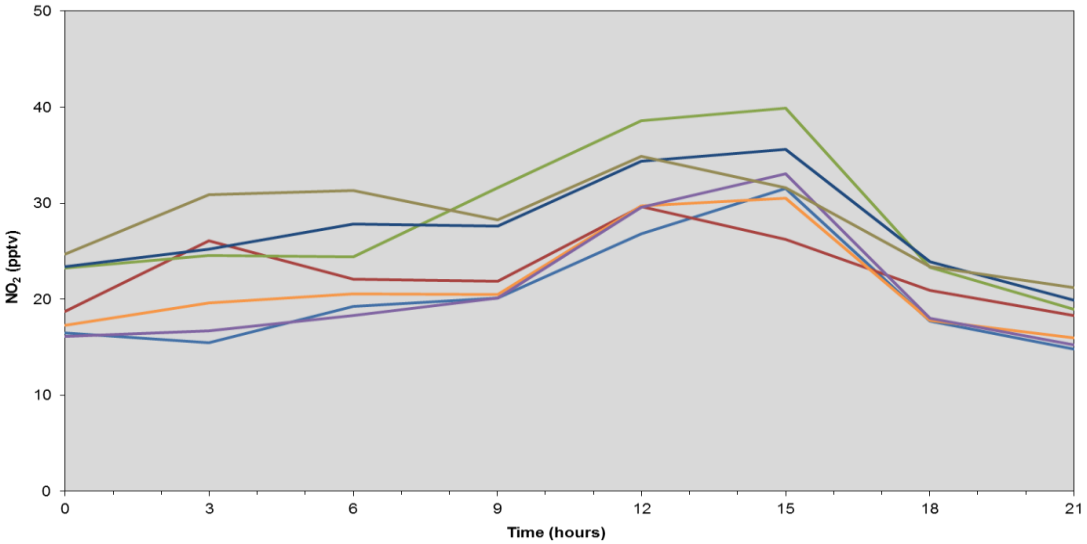

Figure 4.20. NO_2 diurnal cycle averaged by air mass. Light blue = ACA, red = A, green = NACA, orange = ANA, purple = ECA, dark blue = CA, gold = E.

Another parameter by which the data was analysed is using different instrument maintenance periods. Over the course of the 5 years, the instrument has undergone 5 distinct periods in its inlet design and setup as described in table 4.5. Whilst the ΔNO variation was consistent between these periods (figure 4.21), the NO_2 diurnal showed a significant increase in the ΔNO_2 observed during P_2 as shown in figures 4.22 and 4.23. The data within P_2 that was not obtained during 2008 was analysed separately and was also shown to display this high ΔNO_2 value, proving that although present in late 2007 and early 2009, this was not detected during the analysis of the data on an annual time scale as the averaging of the data dampened the appearance of the ΔNO_2.

Table 4.5. Table showing dates of changes to inlet design and setup. $P_{\#}$ = period of inlet design or setup where '#' represents the period number.

Period (*P#*)	Date			Inlet Design
	Start		End	
1	1st Oct. 2006	-	4th Dec. 2007	- Start of operation. Uncooled inlet mounted outside facing northeast.
2	4th Dec. 2007	-	28th Feb. 2009	- Inlet mounted outside facing directly upwards. New BLC installed.
3	28th Feb. 2009	-	16th Oct. 2009	- Cooled inlet mounted outside.
4	16th Oct. 2009	-	8th Aug. 2010	- Cooled inlet mounted inside. Samples taken from main glass sampling manifold.
5	8th Aug. 2010	-	30th Jun. 2011	- New BLC installed

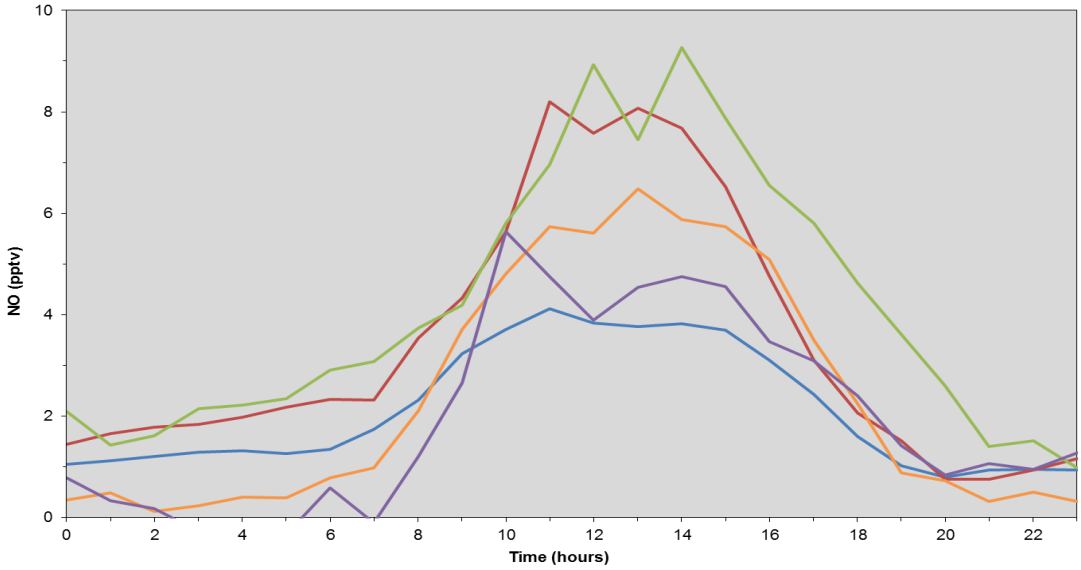

Figure 4.21. NO diurnal averaged by maintenance period. Blue line = P_1, red line = P_2, green line = P_3, orange line = P_4, purple line = P_5.

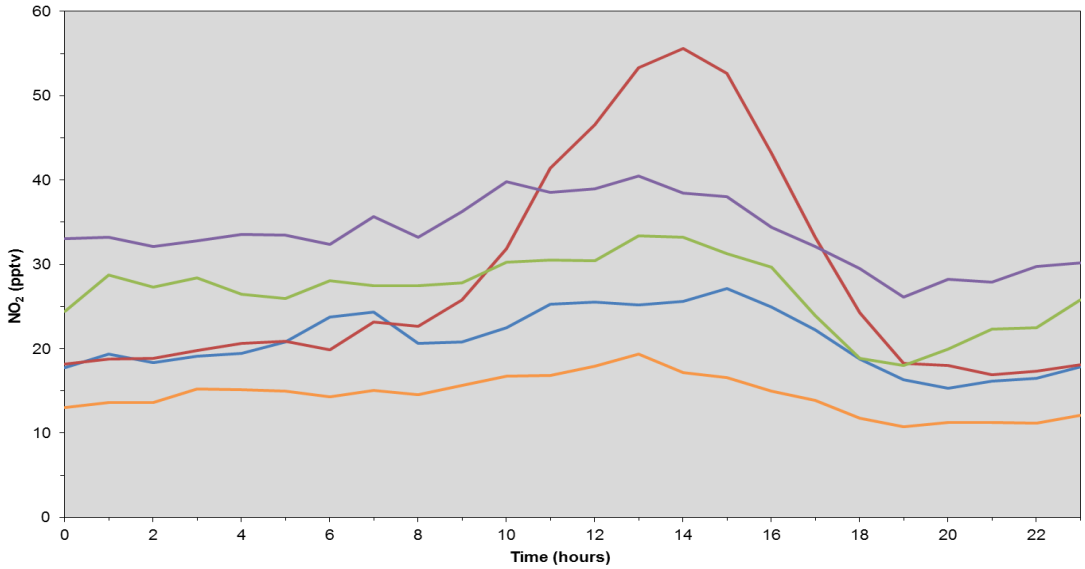

Figure 4.22. NO_2 diurnal averaged by maintenance period. Blue line = P_1, red line = P_2, green line = P_3, orange line = P_4, purple line = P_5.

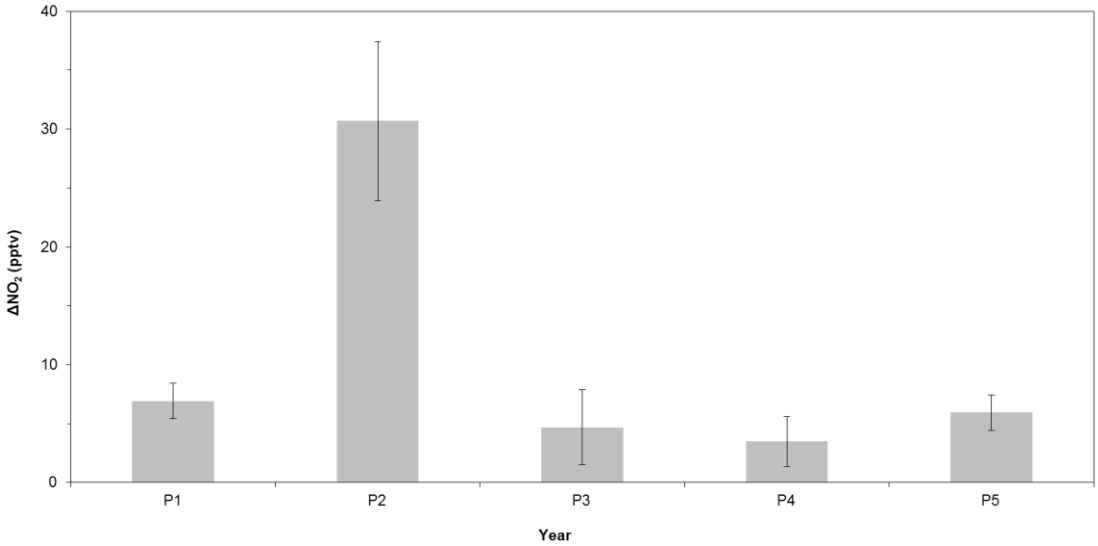

Figure 4.23. Average ΔNO_2 values and standard deviation for each maintenance period.

By comparing the ΔNO_2 values over the entire dataset for diurnals both with and without the P_2 data included as shown in figure 4.24, this allowed the contribution of the P_2 data to the ΔNO_2 value to be estimated and found that P_2 caused an overall increase in ΔNO_2 of approximately 5.09 ± 0.94 pptv.

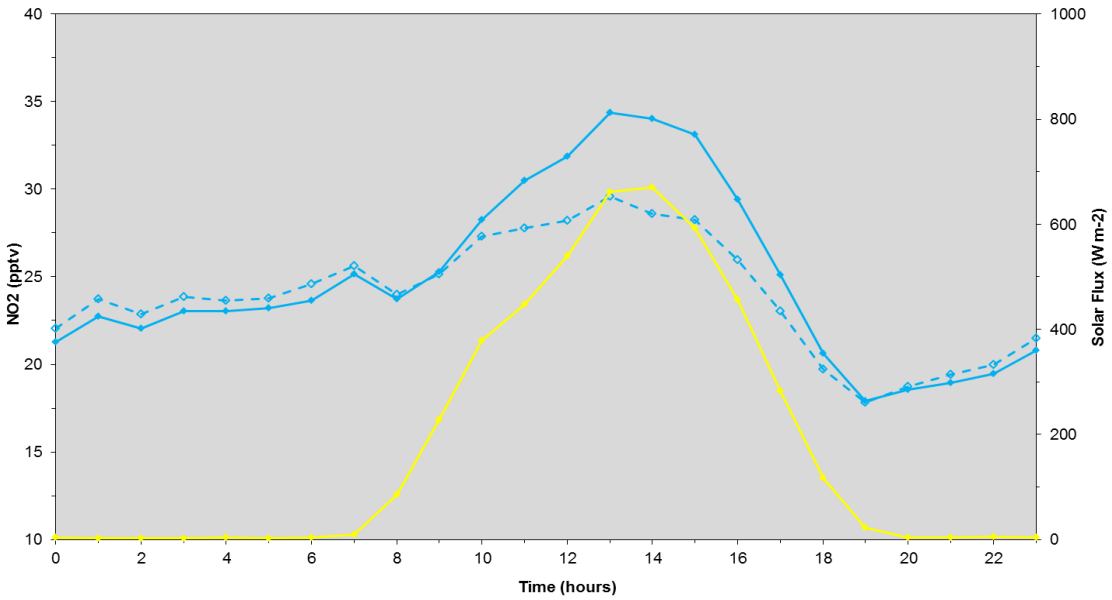

Figure 4.24. NO_2 diurnal averaged for all data (solid blue line) and all data except P_2 (dashed blue line). Average solar flux diurnal also plotted (yellow line) for comparison.

It was postulated that the positioning of the inlet led to increased exposure to solar radiation, resulting in a significant temperature increase within the inlet. As there is no temperature data corresponding to the inlet temperature, solar flux (SF) was used as a proxy and plotted against ΔNO and ΔNO_2 values (figure 4.25-26). Monthly averages of ΔNO, ΔNO_2 and ΔSF were grouped into the relevant period bins and compared.

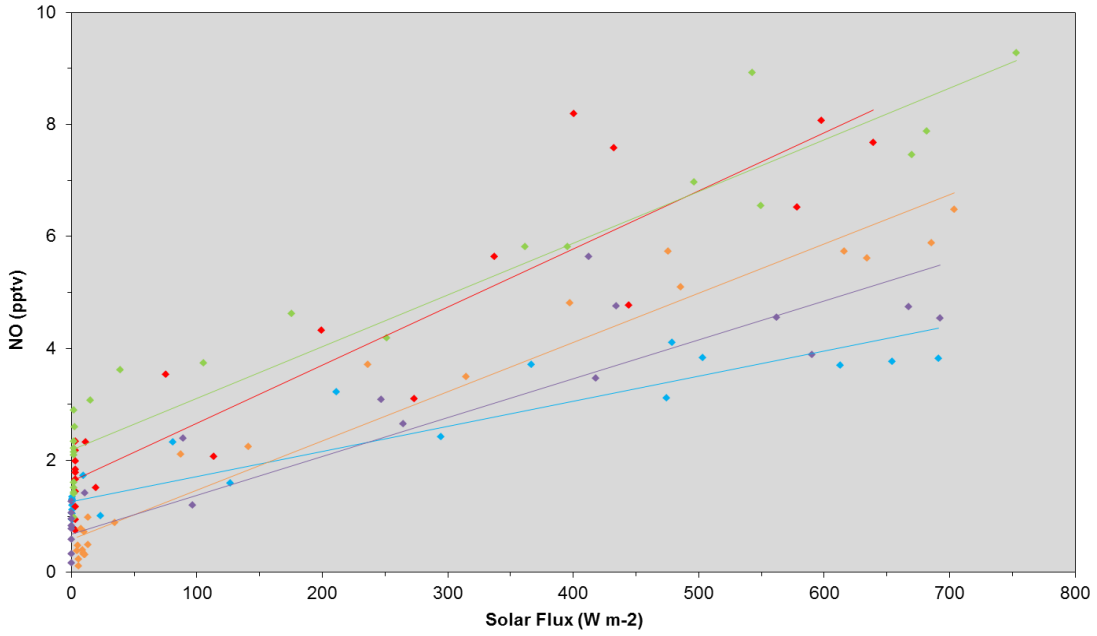

Figure 4.25. Hourly NO and solar flux values averaged for each maintenance period. Blue line = P_1, red line = P_2, green line = P_3, orange line = P_4, purple line = P_5.

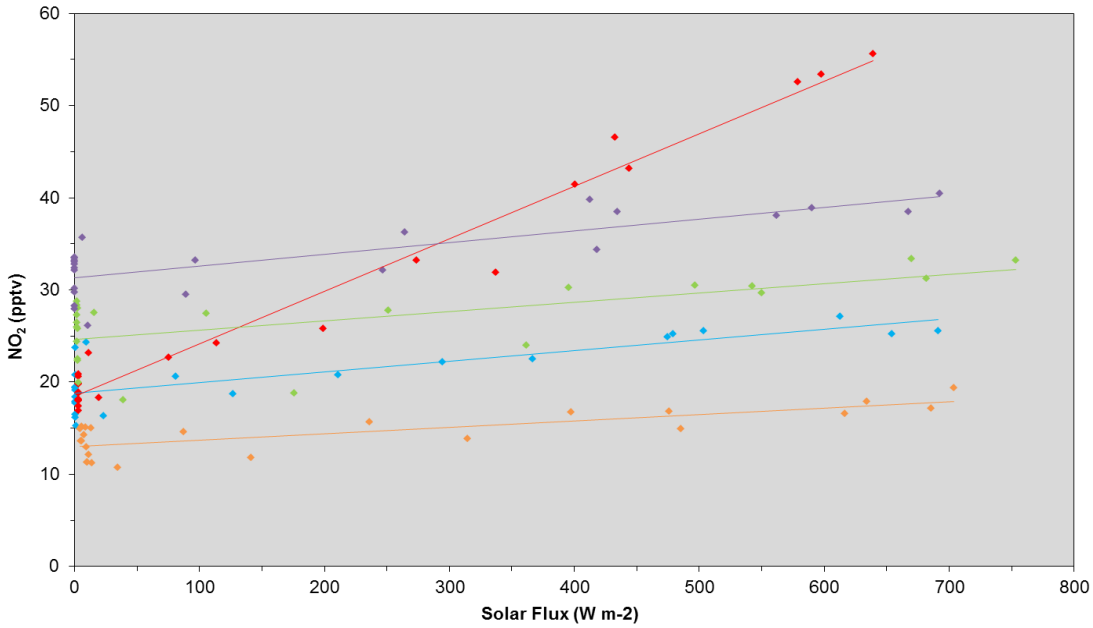

Figure 4.26. Hourly NO_2 and solar flux values averaged for each maintenance period. Blue line = P_1, red line = P_2, green line = P_3, orange line = P_4, purple line = P_5.

Multiple linear regression analysis showed that the ΔNO_2 dependency on solar flux was significantly greater during P_2 ($P < 0.01$), supporting the hypothesis that inlet positioning and resultant temperature fluctuations contributed to the ΔNO_2 values observed. This suggests that the large ΔNO_2 observed during P_2 is an instrumental artefact rather than a real trend. Temperature measurements within the inlet would help analyse this relationship fully and quantify its importance, however, despite the ΔNO_2 being significantly greater, the ΔNO_2 cycle is observed in all of the data to some degree.

Similarly, previous studies have also found deviations from the Leighton Ratio ($\varphi > 1$) where NO_2 mixing ratios are greater than those expected from theoretical calculation (Parrish et al., 1986; Hauglustaine et al., 1999; Volz-Thomas et al., 2003; Mannschreck et al., 2004; Hosaynali-Beygi et al., 2011). As described in section 1.3, reactions 4.1-4.3 represent the NO_x cycle. This is a null cycle, which when reaction 4.1 dominates the conversion of NO to NO_2, reaches photostationary steady state (PSS) within minutes (Leighton, 1961). This is also known as the Leighton ratio (φ) and is calculated via equation 4.4.

$$NO + O_3 \rightarrow NO_2 + O_2 \qquad 4.1$$

$$NO_2 + h\upsilon \rightarrow NO + O(^3P) \qquad 4.2$$

$$O(^3P) + O_2 + M \rightarrow O_3 + M \qquad 4.3$$

$$\varphi = \frac{J_{NO_2}[NO_2]}{k_{4.1}[O_3][NO]} \qquad 4.4$$

where

J_{NO_2} = photodissociation frequency of NO_2

$k_{4.1}$ = reaction coefficient of reaction 4.1

This disagreement could stem from an unknown or unquantified photochemically driven oxidation pathway that would cause additional NO to NO_2 conversion and therefore suggests an incomplete understanding of the oxidative budget under low NO_x conditions in the troposphere. Beygi et al (2011) found that for NO_x mixing ratios ranging between 5-25 pptv, this deviation increased by up to a factor of ~7 with NO_x mixing ratio and J_{NO_2} intensity, indicating the importance of NO_x mediated photochemistry.

When NO_x mixing ratios are very low, peroxy radicals HO_2 and RO_2 become increasingly important and compete with O_3 in the oxidation of NO (reaction 4.1). In the tropical remote boundary layer, the alkyl group 'R', is mostly of the form CH_3O_2 following the oxidation of CH_4, the dominant hydrocarbon in this environment (Crutzen et al., 1994). It is therefore important that under low NO_x conditions, NO oxidation by peroxy radicals is taken into consideration as this will significantly affect the calculated Leighton ratio. Furthermore, uncertainties in the reaction rates of NO with peroxy radicals will also effect calculations. It is a common assumption that the reaction rate coefficient of RO_2 with NO is similar to that of HO_2 and it has been postulated that this assumption is critical to PSS calculations and requires more validation (Matsumoto et al., 2006; Hosaynali-Beygi et al., 2011).

Other criteria which if not met invalidate the steady state assumption include additional O_3 loss processes such as photolysis or the reaction of O_3 with NO_2, alkenes and radicals. In relation to the former, steady state is invalidated at sunrise and sunset due to lower J_{NO_2} values. Insufficient reaction time following perturbations to gas concentrations such as source pollution from shipping emissions, which have been shown to interfere with measurements at the CVAO, can also result in deviations from PSS. However at the CVAO, the data filtering process previously described removes this source of error. Other perturbations however can be caused by the oxidation of NO by halogen monoxides (Carpenter et al., 1998; Read et al., 2008) or via the decomposition of reservoir species such as PAN as previously been shown (Jacobi et al., 1999). Measurements of J_{NO_2}, O_3, NO, NO_2 and radical concentrations can also contribute to the uncertainty of the measurement.

As well as unknown or unquantified chemistry being the possible cause of the deviation seen, instrumental error may also play a role as shown with the analysis of the

maintenance periods and inlet positioning. For example, the BLC wavelength used for the detection of NO_2 is 385-405 nm with the peak absorption cross section for NO_2 at 390-400 nm as shown in figure 4.27. Of all tropospheric species with the potential to cause interference in the BLC measurement resulting in the ΔNO_2 observed, Beygi et al (2011) found that $BrONO_2$ had the greatest overlap in absorption cross section, but that 26 pptv would be required to recreate a ΔNO_2 value of 7 pptv. The BLC used in the CVAO instrument does exhibit temperature dependence with increases in temperature resulting in a decrease in optical power and increase in the wavelength emitted by the LEDs (Martin Buhr, personal communication). This shift in output would act to reduce the possible interference of $BrONO_2$ which absorbs at lower wavelengths and would increase the interference of NO_3. However, this is an unlikely source of interference being a nighttime species with detectable daytime concentrations only in close proximity to large emission sources as described in Chapter 2.

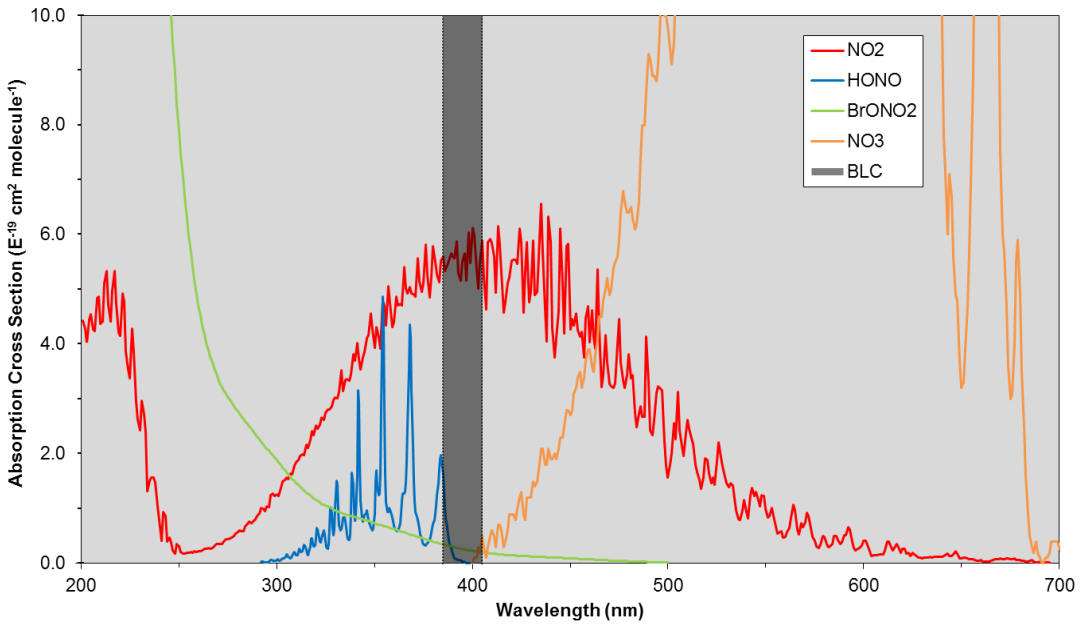

Figure 4.27. Absorption cross sections of NO_2 and all potentially interfering species at 298 K. Emission wavelength band of BLC used in the instrument also shown for comparison.

4.3. Summary

Measurements of NO, NO_2 and O_3 were made at the Cape Verde Atmospheric Observatory (CVAO) in the remote, tropical, North Atlantic, marine boundary layer between October 2006 and December 2010. O_3 shows an annual cycle with a maximum in spring and minimum in late summer, and a clear diurnal cycle, with photochemical destruction rates of 1-8 ppbv d^{-1} during the day. NO_x levels are dependent on air mass origin, with higher NO_x observed in air masses originating from the African continent. This elevated mixing ratio results in a reduced net O_3 destruction rate in air masses that have been influenced by African sources with an average of 2.8 ppbv d^{-1}, compared to 3.5 ppbv d^{-1} in clean Atlantic air.

For all data, independent of air mass origin, NO displays a clear diurnal cycle peaking around solar noon with maximum mixing ratios between 3 and 10 pptv. NO_2 also displays a diurnal cycle with maximum mixing ratios of between 15 and 30 pptv, coinciding with solar noon. However, as it is thought that NO_2 photolysis should dominate NO_2 dynamics in clean environments, an NO_2 minimum would be expected to coincide with solar maximum. This discrepancy in NO_2 dynamics, referred to as ΔNO_2, was investigated for potential sources. Although ΔNO_2 was observed throughout the measurement period, data between 4.12.2007 and 28.2.2009 showed a significantly elevated daytime NO_2 signal and was responsible for an average increase in ΔNO_2 across the dataset of 5.09 ± 0.94 pptv. During this period, the inlet was mounted facing directly upwards and would therefore be susceptible to high levels of heating. One potential source of this elevated NO_2 signal is NO_y species that can undergo thermal dissociation upon heating resulting in the formation of NO_2. Of these NO_y species, peroxyacteyl nitrate (PAN), which exists in thermal equilibrium with its' precursors and is believed to be the main NO_y reservoir for the long range transport of NO_x, has the lowest thermal dissociation temperature of just 60 °C and can rapidly dissociate. Future studies that will enable the characterisation of the NO_y composition at the CVAO will help address this observed anomaly in full.

References

Ayers, G., Penkett, S., Gillett, R., Bandy, B., Galbally, I., Meyer, C., Elsworth, C., Bentley, S. and Forgan, B. (1996) The annual cycle of peroxides and ozone in marine air at Cape Grim, Tasmania. *Journal of Atmospheric Chemistry*. **23**, 221-252.

Ayers, G.P., Granek, H. and Boers, R. (1997) Ozone in the marine boundary layer at Cape Grim: Model simulation. *Journal of Atmospheric Chemistry*. **27**, 179-175.

Hosaynali-Beygi. Z., Fischer. H., Harder. H.D., Martinez, M., Sander, R., Williams, J., Brookes, D.M., Monks, P.S. and Lelieveld, J. (2011) Oxidation photochemistry in the Southern Atlantic boundary layer: Unexpected deviations of photochemical steady state. *Atmospheric Chemistry and Physics*. **11**, 8497-8513.

Bloss, W., Evans, M., Lee, J.D., Sommariva, R., Heard, D. and Pilling, M. (2005) The oxidative capacity of the troposphere: Coupling of field measurements of OH and a global chemistry transport model. *Faraday Discussions*. **130**, 425-436.

Bridgeman, C., Pyle, J. and Shallcross, D. (2000) A three-dimensional model calculation of the ozone depletion potential of 1-bromopropane (1-C_3H_7Br). *Journal of Geophysical Research - Atmospheres*. **105**, D21 26493-26502.

Carpenter, L.J, Monks, P.S, Bandy, B., Penkett, S., Galbally, I. and Meyer, C. (1997) A study of peroxy radicals and ozone photochemistry at coastal sites in the northern and southern hemispheres. *Journal of Geophysical Research - Atmospheres*. **102**, D21 25417-25427.

Carpenter, L.J., Clemitshaw, K.C., Burgess, R.A., Penkett, S.A., Cape, J.N. and McFadyen, G.C. (1998) Investigation and evaluation of the NO_x/O_3 photochemical steady state. *Atmospheric Environment.* **32**, 3353-3365.

Carpenter, L.J., Fleming, Z.L., Read, K.A., Lee, J.D., Moller, S.J., Hopkins, J.R., Purvis, R.M., Lewis, A.C., Müller, K., Heinold, B., Herrmann, H., Wadinga Fomba, K., van Pinxteren, D., Müller. C., Tegen, I., Wiedensohler, A., Müller, T., Niedermeier, N., Achterberg, E.P., Patey, M.D., Kozlova, E.A., Heimann, M., Heard, D.E., Plane, J.M.C., Mahajan, A., Oetjen, H., Ingham, T., Stone, D., Whalley, L.K., Evans, M.J., Pilling, M.J., Leigh, R.J., Monks, P.S., Karunaharan, A., Vaughan, S., Arnold, S.R., Tschritter, J., Pöhler, D., Frieß, U., Holla, R.,

Mendes, L.M., Lopez, H., Faria, B., Manning, A.J. and Wallace, D.W.R. (2010) Seasonal characteristics of tropical marine boundary layer air measured at the Cape Verde Atmospheric Observatory. *Journal of Atmospheric Chemistry*. **67**, 87-140.

Carsey, T., Churchill, D., Farmer, M., Fischer, D., Pszenny, A., Ross, V., Saltzmann, E., Springer-Young, M. and Bonsang, B. (1997). Nitrogen oxides and ozone production in the North Atlantic marine boundary layer. *Journal of Geophysical Research - Atmospheres*. **102**, 10653-10665.

Conley, S.A., Faloona, I.C., Lenschow, D.H., Campos, T., Heizer, C., Weinheimer, A., Cantrell. C.A., Mauldin, R.L., Hornbrook, R.S., Pollack, I. and Bandy, A. (2011) A complete dynamical ozone budget measured in the tropical marine boundary layer during PASE. *Journal of Atmospheric Chemistry*. **68**, 55-70.

Crutzen, P.J., Lelieveld, J. and Bruehl, C. (1994) Advances in Environmental Science and Technology. Wiley, New York.

Crutzen, P. (1998) How the atmosphere keeps itself clean and how this is affected by human activities. *Pure and Applied Chemistry*. **70**, 1319-1326.

Derwent, R., Stevenson, D., Collins, W. and Johnson, C. (2004). Intercontinental transport and the origins of the ozone observed at surface sites in Europe. *Atmospheric Environment*. **38**, 1891-1901.

Dickerson, R., Rhoads, K., Carsey, T., Oltmans, S., Burrows, J. and Crutzen, P. (1999) Ozone in the remote marine boundary layer: A possible role for halogens. *Journal of Geophysical Research – Atmospheres*. **104**, D17 21385-21395.

Fleming, Z.L., Monks, P.S. and Manning, A.J. (2012) Review: Untangling the influence of air-mass history in interpreting observed atmospheric composition. *Atmospheric Research*. **104**, 1–39.

Galbally, I., Bentley, S. and Meyer, C. (2000) Mid-latitude marine boundary layer ozone destruction at visible sunrise observed at Cape Grim, Tasmania. *Geophysical Research Letters*. **27**, 3841-3844.

Hauglustaine, D.A., Madronich, S., Ridley, B.A., Flocke, S.J., Cantrell, C.A., Eisele, F.L., Shetter, R.E., Tanner, D.J., Ginoux, P. and Atlas, E.L. (1999) Photochemistry and budget of ozone during the Mauna Loa Observatory Photochemistry Experiment (MLOPEX 2). *Journal of Geophysical Research - Atmospheres*. **104**, 30275–30307.

Heikes, B., Lee, M.H., Jacob, D., Talbot, R., Bradshaw, J., Singh, H., Blake, D., Anderson, B., Fuelberg, H. and Thompson, A.M. (1996) Ozone, hydroperoxides, oxides of nitrogen, and hydrocarbon budgets in the marine boundary layer over the South Atlantic. *Journal of Geophysical Research - Atmospheres*. **101**, 24221–24234.

Horowitz, L., Walters, S., Mauzerall, D., Emmons, L., Rasch, P., Granier, C., Tie, X., Lamarque, J., Schultz, M., Tyndall, G., Orlando, J. and Brasseur, G. (2003) A global simulation of tropospheric ozone and related tracers: Description and evaluation of MOZART, version 2. *Journal of Geophysical Research - Atmospheres*. **108**, D24 4784-4813.

Jacob, D., Heikes, B., Fan, S., Logan, J., Mauzerall, D., Bradshaw, J., Singh, H., Gregory, G., Talbot, R., Blake, D. and Sachse, G. (1996) Origin of ozone and NO_x in the tropical troposphere: A photochemical analysis of aircraft observations over the South Atlantic basin. *Journal of Geophysical Research - Atmospheres*. **101**, D19 24235-24250.

Jacobi, H., Weller, R., Bluszcz, T. and Schrems, O. (1999) Latitudinal distribution of peroxyacetyl nitrate (PAN) over the Atlantic Ocean. *Journal of Geophysical Research - Atmospheres*. **104**, D21 26901-{26912.

Knudsen, B.M., Rosen, J.M., Kjome, N.T. and Whitten, A.T. (1996) Comparison of analysed stratospheric temperatures and calculated trajectories with long-duration balloon data. *Journal of Geophysical Research*. **101**, 19137-19145.

Lee, J.D., Moller, S.J., Read, K.A., Lewis, A.C., Mendes, L. and Carpenter, L.J. (2009) Year-round measurements of nitrogen oxides and ozone in the tropical North Atlantic marine boundary layer. Journal of Geophysical Research. 114, D21302.

Leighton, P. A. (1961) Photochemistry of air pollution. *Physical Chemistry*. **9**, 300.

Lelieveld, J., Van Aardenne, J., Fischer, H., de Reus, M., Williams, J. and Winkler, P. (2004) Increasing ozone over the Atlantic Ocean. *Science*. 304, 1483-1487.

Liu, S.C., McFarland, M., Kley, D., Zafiriou, O. and Huebert, B. (1983) Tropospheric NO_x and O_3 budgets in the Equatorial Pacific. *Journal of Geophysical Research - Atmospheres*. **88**, 1360-1368.

Mannschreck, K., Gilge, S., Plass-Duelmer, C., Fricke, W. and Berresheim, H. (2004) Assessment of the applicability of $NO\text{-}NO_2\text{-}O_3$ photostationary state to long-term measurements at the Hohenpeissenberg GAWStation, Germany. *Atmospheric Chemistry and Physics*. **4**, 1265-1277.

Matsumoto, J., Kosugi, N., Nishiyama, A., Isozaki, R., Sadanaga, Y., Kato, S., Bandow, H. and Kajii, Y. (2006) Examination on photostationary state of NO_x in the urban atmosphere in Japan, *Atmospheric Environment*. **40**, 3230-3239.

Parrish, D.D., Trainer, M., Williams, E.J., Fahey, D.W., Hubler, G., Eubank, C.S., Liu, S.C., Murphy, P.C., Albritton, D.L. and Fehsenfeld, F.C. (1986) Measurements of the $NO_x\text{-}O_3$ Photostationary State at Niwot Ridge, Colorado. *Journal of Geophysical Research - Atmospheres*. **91**, 5361-5370.

Parrish, D., Trainer, M., Young, V., Goldan, P., Kuster, W., Jobson, B., Fehsenfeld, F., Lonneman, W., Zika, R., Farmer, C., Riemer, D. and Rodgers, M. (1998) Internal consistency tests for evaluation of measurements of anthropogenic hydrocarbons in the troposphere. *Journal of Geophysical Research - Atmospheres.***103**, D17 22339-22359.

Penkett, S., Volz-Thomas, A., Parrish, D., Honrath, R. and Fehsenfeld, F. (1998) Special section: North Atlantic Regional Experiment (NARE II) - preface. *Journal of Geophysical Research – Atmospheres.* **103**, D11 13353-13355.

Read, K., Mahajan, A., Carpenter, L., Evans, M., Faria, B., Heard, D., Hopkins, J., Lee, J.D, Moller, S.J, Mendes, L.A., McQuaid, J., Oetjen, H., Saiz-Lopez, A., Pilling, M. and Plane, J.M.C. (2008) Extensive halogen-mediated ozone destruction over the tropical Atlantic Ocean. *Nature*. **453**, 1232-1235.

Ryall, D.B., Derwent, R.G., Manning, A.J., Simmonds, P.G. and O'Doherty, S. (2001) Estimating source regions of European emissions of trace gases from observations at Mace Head. *Atmospheric Environment*. **35**, 2507–2523.

Singh, H.B., Gregory, G.L., Anderson, B., Browell, E., Sachse, G.W., Davis, D.D., Crawford, J., Bradshaw, J.D., Talbot, R., Blake, D.R., Thornton, D., Newell, R. and Merrill, J. (1996) Low ozone in the marine boundary layer of the tropical Pacific Ocean: Photochemical loss, chlorine atoms, and entrainment. *Journal of Geophysical Research - Atmospheres*. **101**, 1907-1917.

Stohl, A., Eckhardt, S., Forster, C., James, P., Spichtinger, N. and Seibert, P. (2002) A replacement for simple back trajectory calculations in the interpretation of atmospheric trace substance measurements. *Atmospheric Environment*. **36**, 4635-4648.

Thompson, A.M., Johnson, J.E., Torres, A.L., Bates, T.S., Kelly, K.C., Atlas, E., Greenberg, J.P., Donahue, N.M., Yvon, S.A., Saltzman, E.S., Heikes, B.G., Mosher, B.W., Shashkov, A.A. and Yegorov, V.I. (1993) Ozone observations and a model of marine boundary layer photochemistry during saga-3. *Journal of Geophysical Research - Atmospheres*. **98**, 16955-16968.

Volz-Thomas, A., Geiss, H., Hofzumahaus, A. and Becker, K.H. (2003) Introduction to special section: Photochemistry experiment in BERLIOZ. *Journal of Geophysical Research - Atmospheres*.,**108**, 8252.

Chapter 5

NO_y Measurements

5.1. NO_x, NO_y and Models

As described in the preceding chapters, NO_x plays a pivotal role in the chemistry of the atmosphere, particularly in the troposphere where it is involved in the only known O_3 production pathway. The remote tropical boundary layer regions are of special interest as the mixing ratios of NO_x are close to the compensation point, where a small increase in NO_x can result in significant O_3 production. Long-range transport of anthropogenically produced NO_x to such environments is thought possible due to longer-lived nitrogen oxides which have lifetimes ranging from weeks to months under free tropospheric conditions. This has important consequences for countries downwind of emissions to adhere to their air quality standards.

Despite their importance, long-term measurements of NO_x and the rest of the reactive nitrogen pool in the remote boundary layer are lacking. To fill the gaps in understanding, global atmospheric models are used to predict NO_y mixing ratios and their resultant impact on O_3 dynamics. GEOS-Chem is one such model. GEOS-Chem is a global 3D chemical transport model for atmospheric composition and is driven by meteorological measurements made by the Goddard Earth Observing System (GEOS). However, as can be seen from the GEOS model outputs for both NO and NO_2 in figures 5.1 and 5.2 respectively, seasonal and longer term variability of NO_x is poorly represented and requires further measurements to help constrain these models.

The main aim of this project is to calibrate an NO_y inlet capable of measuring the NO_y composition in greater detail as shown by figure 5.3, thereby improving the understanding of this important class of compounds in the remote tropical marine boundary layer, as well as supporting the development of global model simulations of the long-term trends of important atmospheric species.

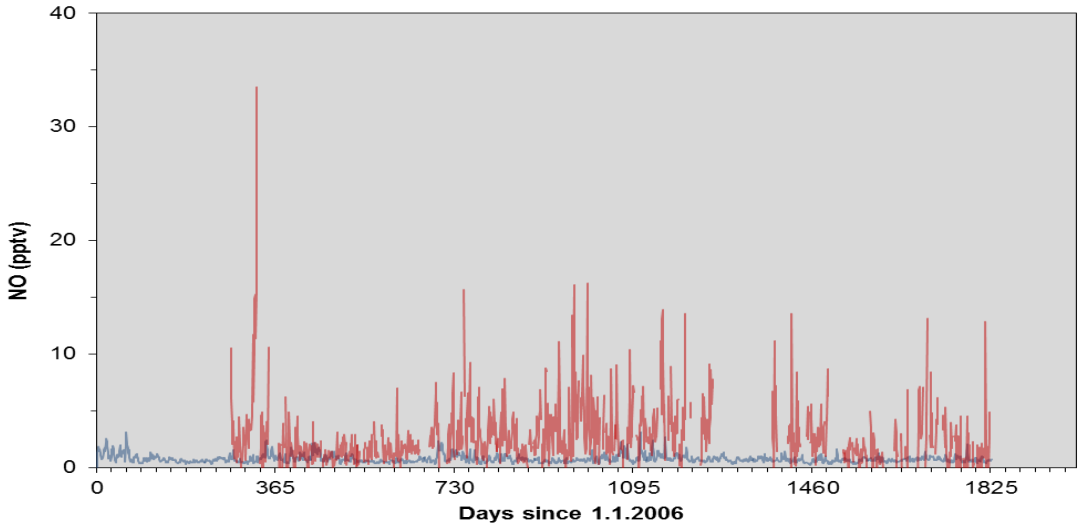

Figure 5.1. Comparison between observed NO mixing ratios at the CVAO (red line) and the predicted values from the GEOS model output (blue line).

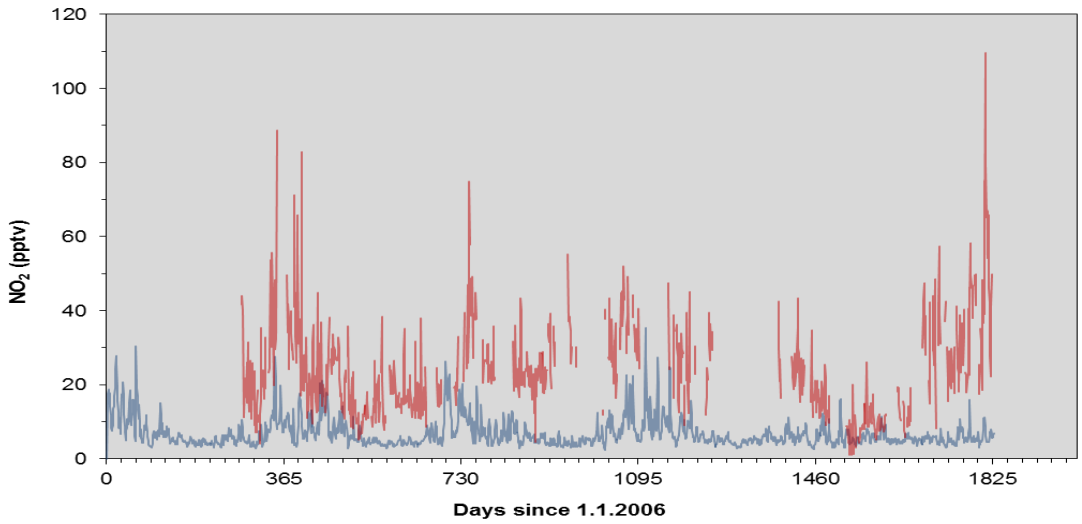

Figure 5.2. Comparison between observed NO_2 mixing ratios at the CVAO (red line) and the predicted values from the GEOS model output (blue line).

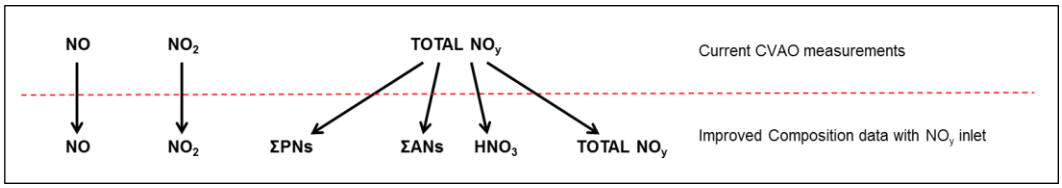

Figure 5.3. Schematic representation of the improved NO_y composition data achieved following the installation of the NO_y inlet in comparison to current measurements at the CVAO.

5.2. NO_y Inlet

5.2.1. NO_y Inlet

The NO_y inlet on which this project is based will be used for the measurement of NO_y reservoirs and will provide a better understanding of the composition of the reactive nitrogen pool in the remote, tropical, marine boundary layer where the CVAO is situated. This technique works on the basis of thermal decomposition of different NO_y species (Day et al., 2002). As the N-O bond strength of each compound is species specific, thermal dissociation occurs over different temperature ranges as shown in figure 5.4. Following rapid heating most NO_y (XNO_2) species undergo thermal dissociation to yield NO_2 and a companion radical as shown in reaction 5.1 and the resultant NO_2 can be detected through various techniques as described in Chapter 3.

$$XNO_2 + \text{heat} \rightarrow X + NO_2 \qquad 5.1$$

At the CVAO, the NO_2 produced will then be measured using the same chemiluminescence instrument previously described. This technique is known as thermal-dissociation chemiluminescence (TD-Chem) and will allow the measurement of NO, NO_2, ΣPNs, ΣANs, HNO_3 and total NO_y (figure 5.3). A schematic representation of the NOy inlet is shown in figure 5.5. Aside from the ozonizer and snooper boxes which will remain the same, all of the individual compartments are shown in greater detail in figures 5.6-5.8 and all parts described in tables 5.1-5.3.

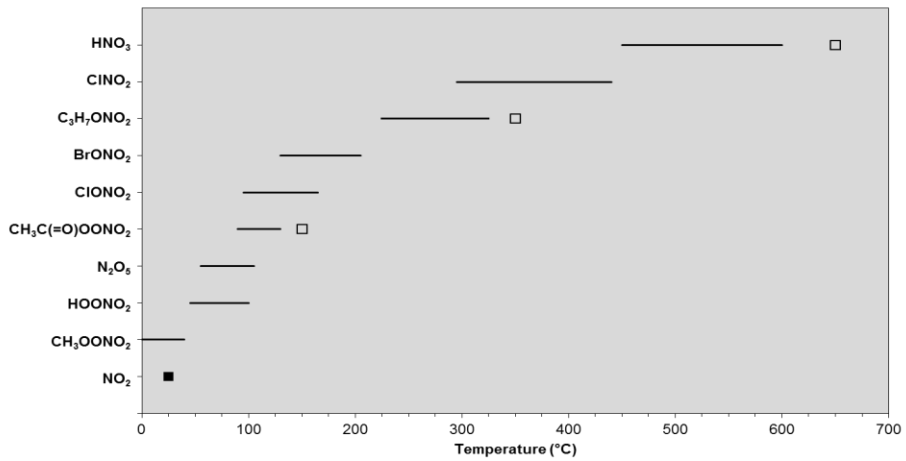

Figure 5.4. Modelled temperature dissociation ranges for a variety of NO_y species. Open squares represent approximate temperature settings of each quartz oven.

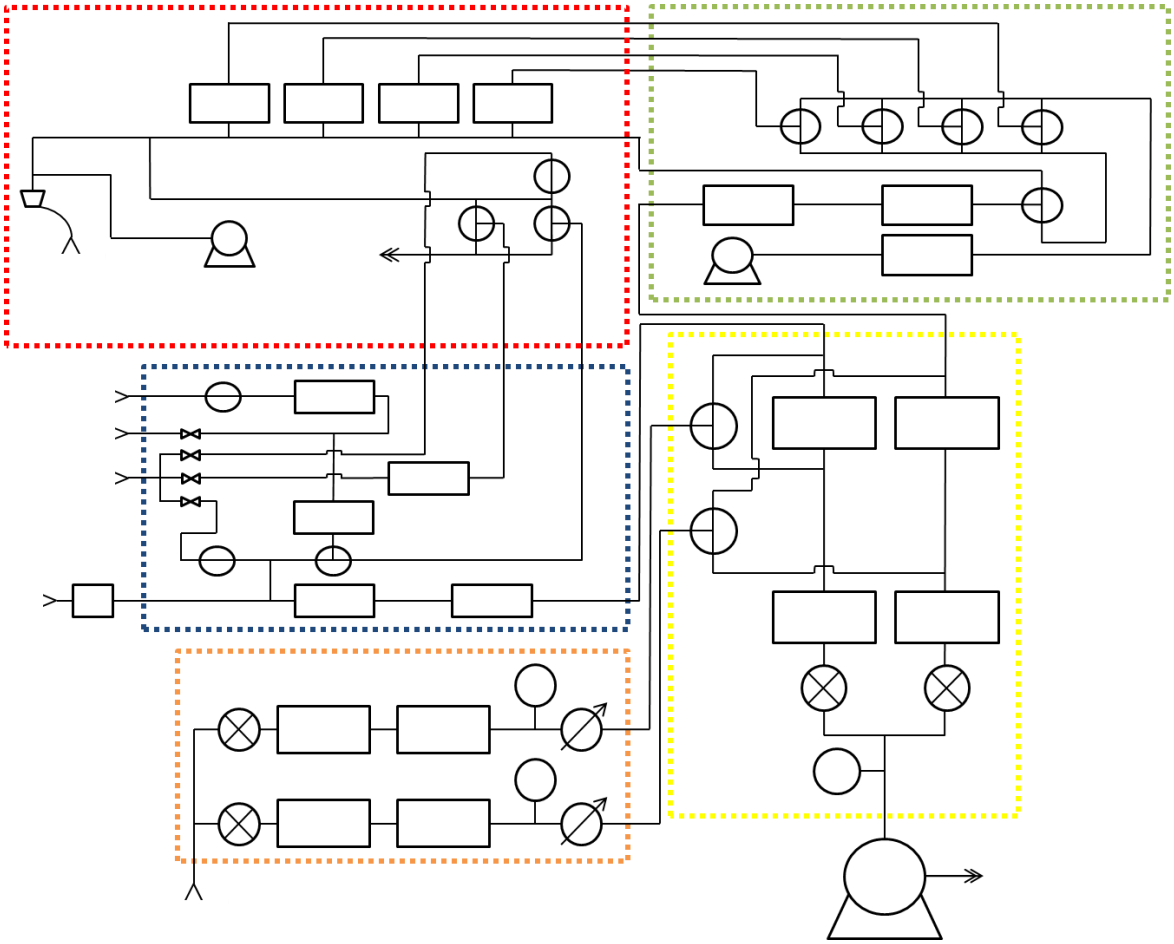

Figure 5.5. Schematic of the NOy inlet. ■ = NO_y inlet, ■ = NO_y controller, ■ = updated NO_x inlet, ■ = Ozonizer box, ■ = Snooper box.

The NO_y inlet when installed will join onto the existing NO_x system, utilising a second channel to measure NO_y and NO_x simultaneously. A detailed description of the measurement cycle will be given in section 5.2.2. This upgrade will result in the addition of two new compartments to the existing system; the NO_y inlet and the NO_y controller and an update of the current NO_x inlet (figure 5.5).

As with the current NO_x instrument, sample air will be drawn into the inlet through the use of a vacuum pump. However, due to the use of high temperatures to measure NO_y reservoirs, aerosol nitrate has the potential to cause interference with NO and NO_2 measurements. For this reason, a cyclone inlet will be placed at the beginning of the inlet that can be switched on and off to quantify the contribution of NO_x from aerosol nitrate (figure 5.6). Sample air is then drawn through one of four ovens heated to different temperatures to measure the total contribution of each reactive NO_y reservoir and total NO_y. Alternatively sample air can proceed via the NO_x bypass with no heating, thereby providing a second measure of NO_x in addition to the NO_x channel. The new NO_y inlet will be controlled by the NO_y inlet controller, which contains a set of valves that will allow the sample flow to

switch between the four ovens and the NO_x bypass (figure 5.7). The NO_x inlet will also be upgraded from its current design to allow the introduction of NO calibration gas, zero air and NO_y standards into the NO_y sample line for calibration and zeroing purposes of the new instrument (figure 5.8).

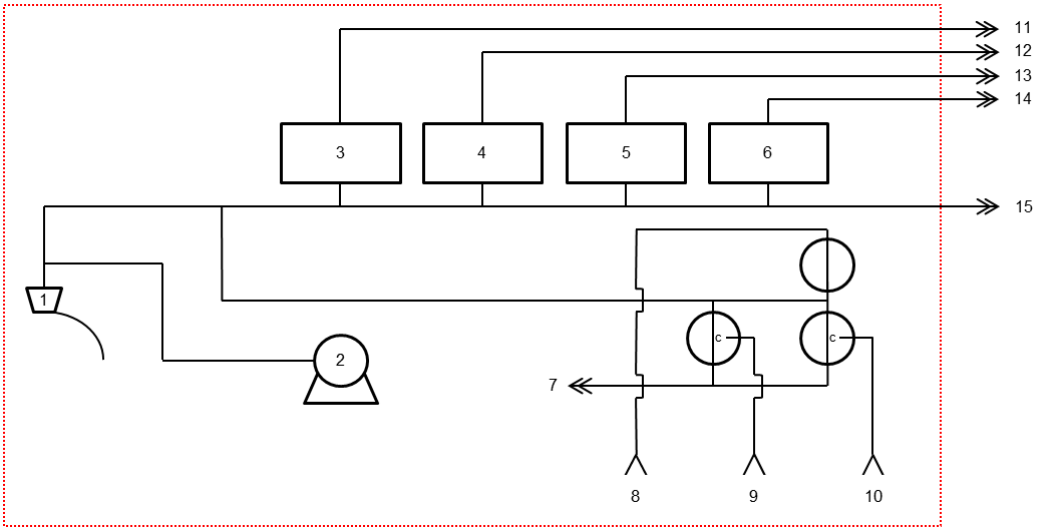

Figure 5.6. Schematic of the NO_y inlet. Numbered parts are described in table 5.1.

Table 5.1. Descriptions of parts numbered in figure 5.6.

Number	Part
1	Cyclone inlet, NO_y sample line
2	Vacuum pump
3	Q1, quartz oven, 150 °C operation temperature, ΣPNs
4	Q3, quartz oven, 350 °C operation temperature, ΣANs
5	Q6, quartz oven, 650 °C operation temperature, HNO_3
6	Mo3, molybdenum oven, 300 °C operation temperature, ΣNO_y
7	Waste
8	Zero air inlet from updated NO_x inlet
9	HNO_3 calibration gas inlet from updated NO_x inlet
10	NO_x sample line from NO_x inlet
11	Q1 outlet
12	Q3 outlet
13	Q6 outlet
14	Mo3 outlet
15	NO_x bypass outlet

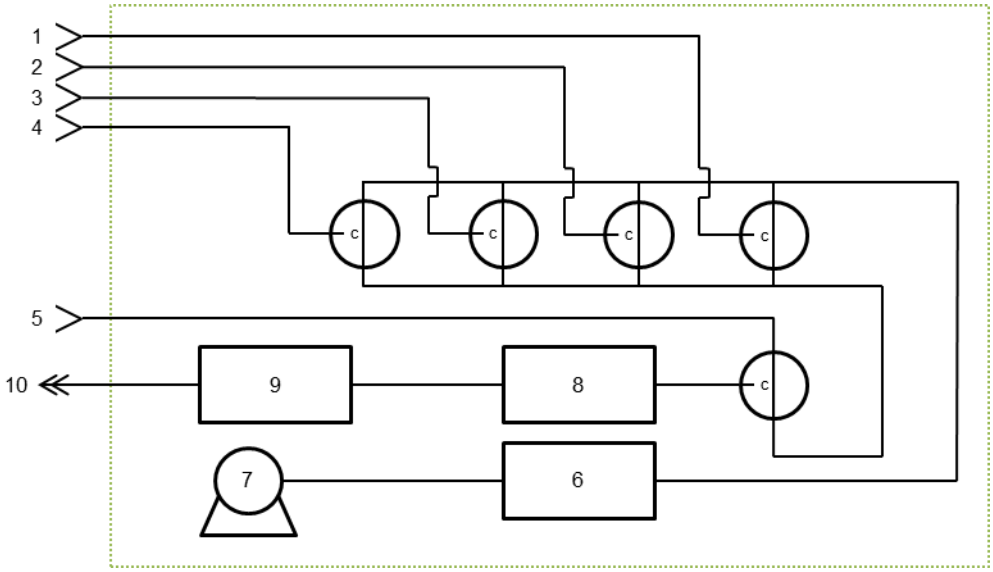

Figure 5.7. Schematic of the NO_y controller. Numbered parts are described in table 5.2.

Table 5.2. Descriptions of parts numbered in figure 5.7.

Number	Part
1	Q1 inlet
2	Q3 inlet
3	Q6 inlet
4	M3 inlet
5	NO_x bypass inlet
6	MFC
7	Vacuum pump
8	Photolytic converter
9	Channel 2 MFC
10	NO_y outlet (Channel 2)

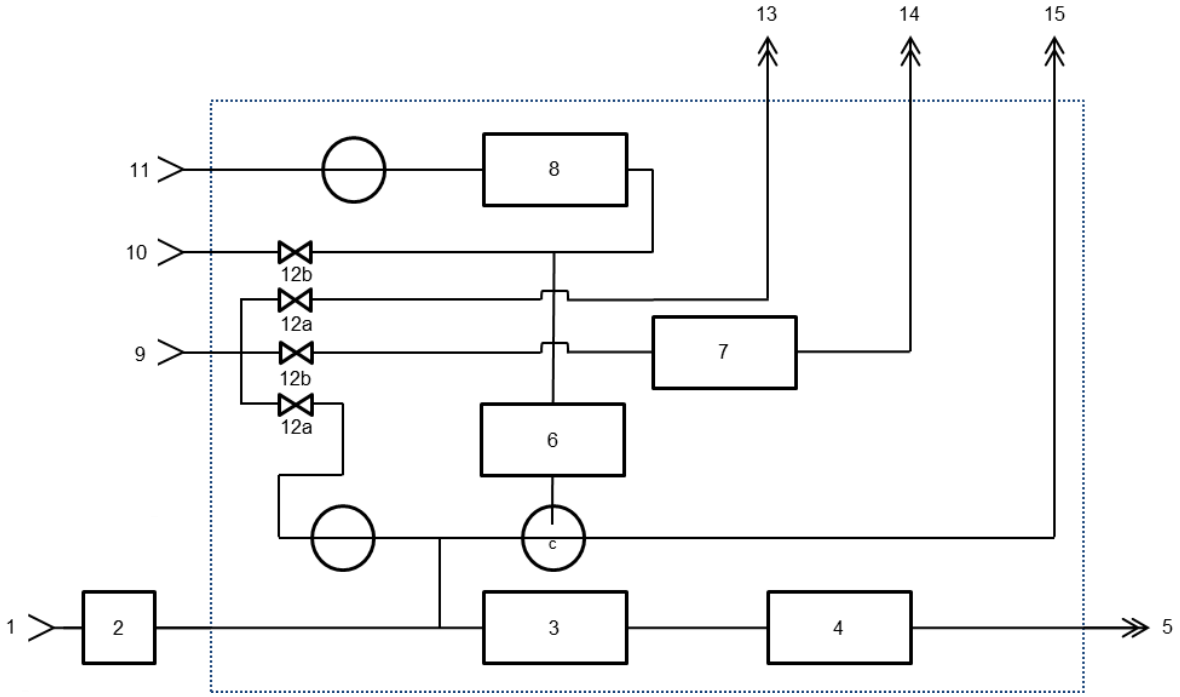

Figure 5.8. Schematic of the updated NO_x inlet. Numbered parts are described in table 5.3.

Table 5.3. Descriptions of parts numbered in figure 5.8.

Number	Part
1	NO_x sample line
2	Filter
3	NO_2 converter
4	MFC
5	NO_x outlet (Channel 1)
6	Titration cell
7	HNO_3 permeation oven
8	NO MFC (10 sccm)
9	Zero air inlet
10	Oxygen inlet
11	NO calibration gas inlet
12a	Critical orifice (10 sccm)
12b	Critical orifice (1000 sccm)
13	Zero air outlet to NO_y inlet
14	HNO_3 calibration gas to NO_y inlet
15	NO_x sample line to NO_y inlet

5.2.2. Measurements

The inlet consists of a bypass line allowing the measurement of ambient levels of NO and NO_2, a series of quartz ovens heated to 150, 350 and 650 °C which will be used to detect ΣPNs, ΣANs and HNO_3 respectively and a molybdenum oven heated to 300 °C for the measurement of total NO_y. Measured thermal decomposition rates of various compounds within two organic nitrate classes ($RC(O)O_2NO_2$, PNs and $RONO_2$, ANs) show little dependence on the R group (Roberts, 1990; Kirchner et al., 1999) The ovens will be referred to as Q1, Q3, Q6 and M3 respectively from here on, unless otherwise stated in the text. Each component of the NO_y pool will be sampled in turn in a single channel system during a measurement cycle as shown in figure 5.9 and includes a prechamber zero signal for the quantification of chemical interference in the sample channel. The updated inlet (figure 5.8.) will also have a second channel allowing the existing instrument to continue measuring ambient NO and NO_2 as described in Chapter 3.

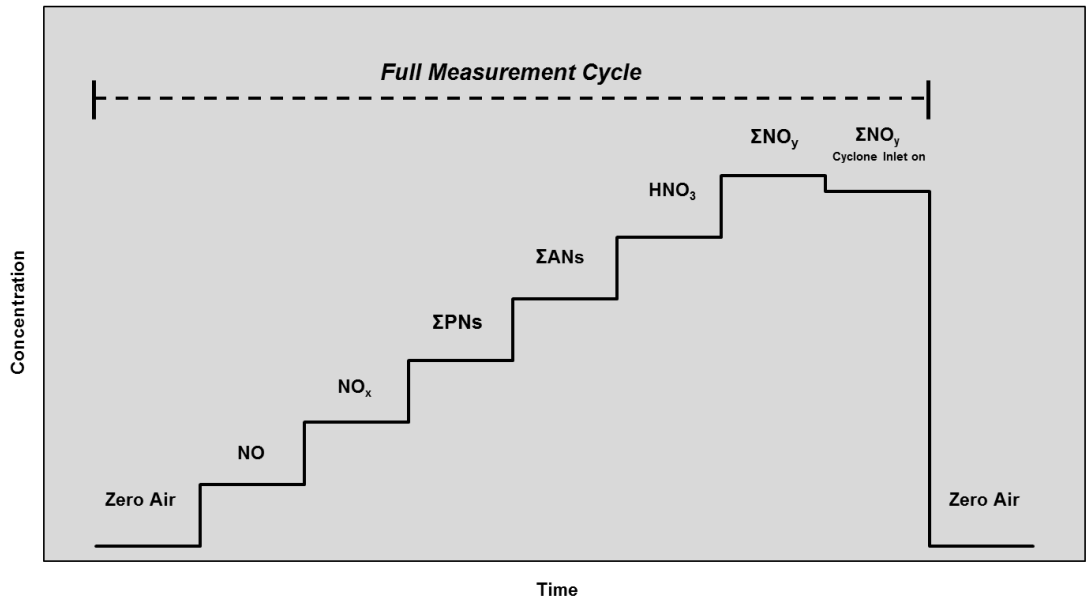

Figure 5.9. The measurement cycle that will be used for the measurements of the NO_y composition at the CVAO instrument. Sampling schedule yet to be finalised. Values are for illustration only and do not represent real values.

For the NO_y inlet, ambient air will be drawn into the inlet which will be situated on the roof of the container at the CVAO, before being rapidly heated in one of the four ovens or will flow through the bypass for the measurement of ambient NO and NO_2 mixing ratios. The residence time in the inlet prior to heating is of upmost importance for the accurate measure of different NO_y species as chemical conversion and loss processes can occur. Of these, the thermal decomposition of PAN and loss of HNO_3 to the walls on account of its high solubility are considered to be the greatest loss mechanisms within the inlet (Day et al., 2002). For example, Val Martin et al (2008) report an NO_2 interference of 4 pptv due to the thermal dissociation of PAN for a residence time of 8 seconds at a temperature of 39 °C in their converter. Neuman et al (1999) investigated HNO_3 wall losses for a range of materials and found that for Teflon tubing, < 5 % of the available HNO_3 adsorbed to the walls in comparison to > 70 % for stainless steel. HNO_3 adsorption was also shown to be dependent on temperature and significantly influenced by relative humidity. For the NO_y inlet reported here, all tubing used is PFA Teflon (PFA) and lines prior to the ovens are heated to ~ 30 °C to minimise wall losses without initiating the thermal dissociation of PAN leading to interference. The potential for this interference is also reduced as the pre-oven residence time is ~ 0.1 second.

All tubing post ovens is collected together in an umbilical and following thermal dissociation, the sample flows through this tubing from the inlet outside to the detector within the container. The production of NO_2 due to NO_y thermal dissociation such as those shown in reactions 5.2-5.4, leads to an elevated signal in comparison to the measured ambient NO_2. Sampling successive ovens allows the quantification of each reservoir by subtracting the signal obtained at the former temperature. For example, a measure of ΣANs is determined by subtracting the average NO_2 mixing ratio when sampling the Q1 oven, from the NO_2 signal measured when sampling from the Q3 oven (Figure 5.9). This is explained schematically using a simplified kinetic model output shown in figure 5.10, which shows the expected NO_2 signal produced from the thermal dissociation of a 1 ppbv mixture of PAN, n-propyl nitrate (NPN) and HNO_3 in equal concentrations under a range of temperatures. The rate constants used in this model are shown in table 5.4.

$$PAN + M + heat \rightarrow CH_3C(O)OO + NO_2 + M \quad 5.2$$

$$NPN + heat \rightarrow CH_3CH_2CH_2O + NO_2 \quad 5.3$$

$$HNO_3 + M + heat \rightarrow OH + NO_2 + M \quad 5.4$$

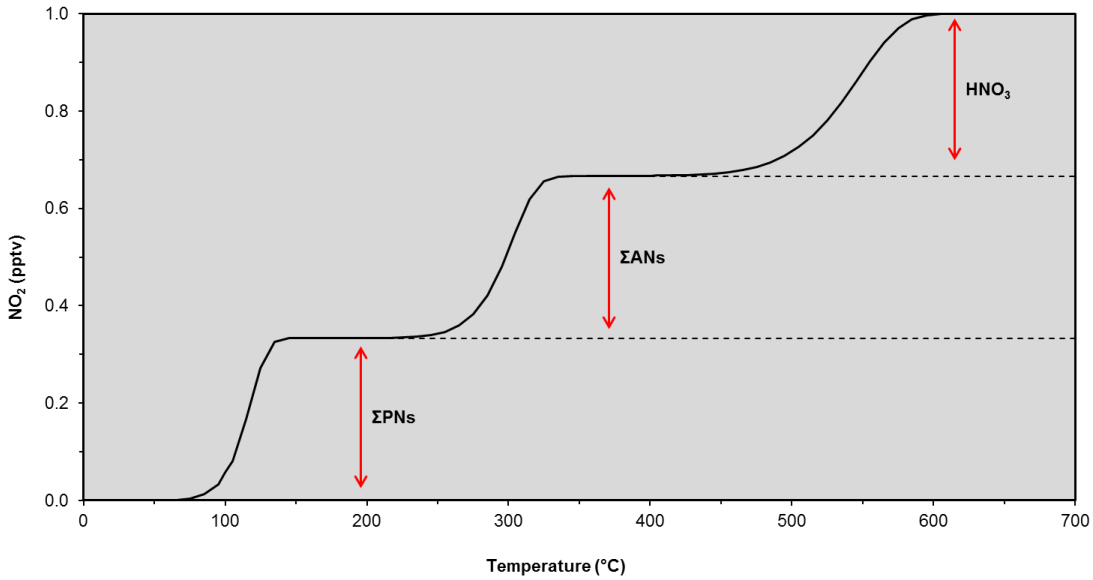

Figure 5.10. Modelled NO_2 yield following temperature ramp of an equal mixture of PAN, NPN and HNO_3 totalling a mixing ratio of 1 ppbv.

Table 5.4. Rate constant parameters for reactions 5.2-5.4 used in the kinetic model described and shown in figure 5.10.

Reaction	Low Pressure Limit k_0 (T) = k_0^* exp (-a / T)		High Pressure Limit k_h (T) = k_h^* exp (-b / T)		Reference
	k_0	a	k_h	b	
5.2	4.9×10^{-3}	12,100	4.0×10^{16}	13,600	Bridier et al. (1991)
5.3			3.16×10^{16}	20,129	Barker et al. (1977)
5.4	$(1.82 \times 10^{-4})(T/298)^{-1.98}$	24,004	2×10^{15}	24658	Glaenzer and Troe (1974)

The model predicts that each compound thermally dissociates over a narrow temperature range and that there are broad regions where dissociation of one class is complete, prior to significant of the next. It is also assumed that each NO_y species thermally dissociates to yield exactly 1 NO_2 molecule as shown in reaction 5.1. Research so far is consistent with this assumption (Day et al., 2009).

Interferences are another possible source of deviation from this expected output. Nonaromatic compounds such as nitromethane can thermally dissociate at high temperatures causing interference in the HNO_3 channel, but if present, are restricted to close proximity of direct emissions and so are not expected to affect the instrument at the CVAO. The oven residence time is long enough to drive any volatile compounds off of the surface of aerosols present and hence the measurement will be the sum of both gas phase and volatile fraction of aerosol nitrate with the corresponding O-N bond energy (Day et al., 2002).

However, as shown in figure 5.6 the inlet will be fitted with a cyclone inlet which can be turned on and off allowing the contribution from aerosol phase nitrate to be quantified.

Further to the interferences listed above caused by the presence of compounds already in the atmosphere, secondary chemistry within the inlet can also result in deviations of the measured value from the true value (Day et al., 2002). There are three classes of such potentially interfering sources shown in reactions 5.5-5.7, though for typical conditions at the CVAO, reaction 5.7c is the only pathway capable of causing a potentially significant interference due to the high mixing ratios of OH. These interference reactions are:

Oxidation of NO

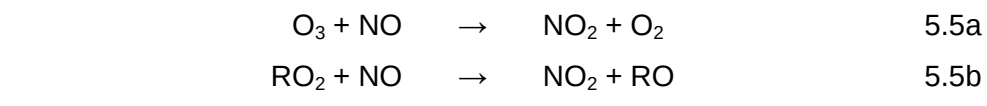

$$O_3 + NO \rightarrow NO_2 + O_2 \quad (5.5a)$$

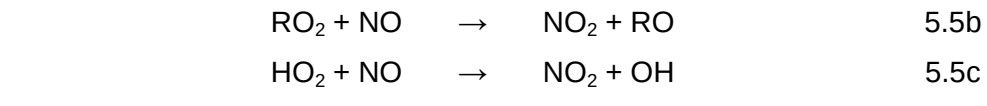

$$RO_2 + NO \rightarrow NO_2 + RO \quad (5.5b)$$

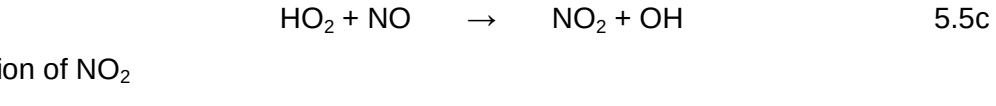

$$HO_2 + NO \rightarrow NO_2 + OH \quad (5.5c)$$

Reduction of NO_2

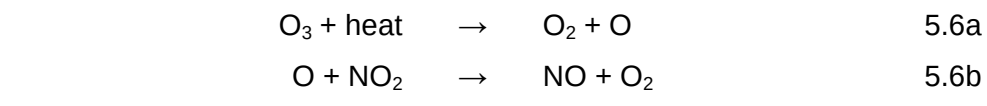

$$O_3 + \text{heat} \rightarrow O_2 + O \quad (5.6a)$$

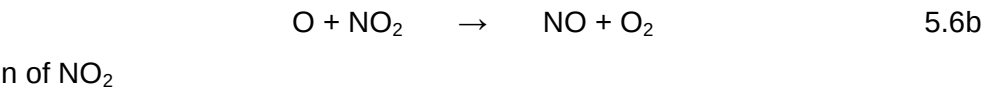

$$O + NO_2 \rightarrow NO + O_2 \quad (5.6b)$$

Oxidation of NO_2

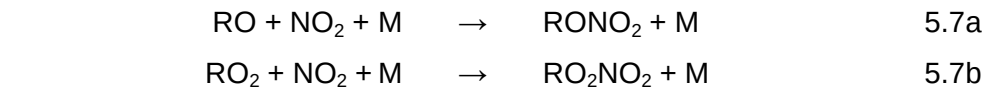

$$RO + NO_2 + M \rightarrow RONO_2 + M \quad (5.7a)$$

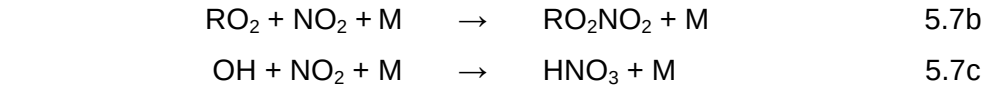

$$RO_2 + NO_2 + M \rightarrow RO_2NO_2 + M \quad (5.7b)$$

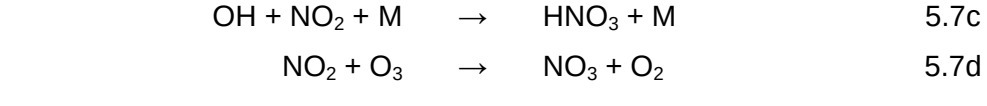

$$OH + NO_2 + M \rightarrow HNO_3 + M \quad (5.7c)$$

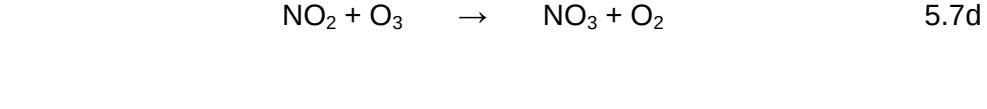

$$NO_2 + O_3 \rightarrow NO_3 + O_2 \quad (5.7d)$$

5.3. NO_y Inlet Calibration

5.3.1. Standards

The method for PAN synthesis is based on the photochemical production of peroxyacetyl (PA) radicals from the photolysis of acetone (285 nm) in the presence of oxygen as shown in reaction 5.8. A small flow of calibration standard NO is added to the gas stream and efficiently converted to NO_2 (reaction 5.9) before reaction with PA radicals to form PAN as shown in reaction 5.10 (Warneck and Zerbach, 1992). This method relies on a large excess of acetone and therefore PA radicals to effect the conversion of NO to NO_2 and suppress reaction 5.11.

$$(CH_3)_2CO + h\upsilon + 2O_2 \rightarrow CH_3O_2 + CH_3C(O)O_2 \quad 5.8$$

$$NO + O_3 \rightarrow NO_2 + O_2 \quad 5.9$$

$$NO_2 + (CH_3)_2C(O)O_2 \rightarrow CH_3C(O)OONO_2 \quad 5.10$$

$$OH + NO_2 \rightarrow HNO_3 \quad 5.11$$

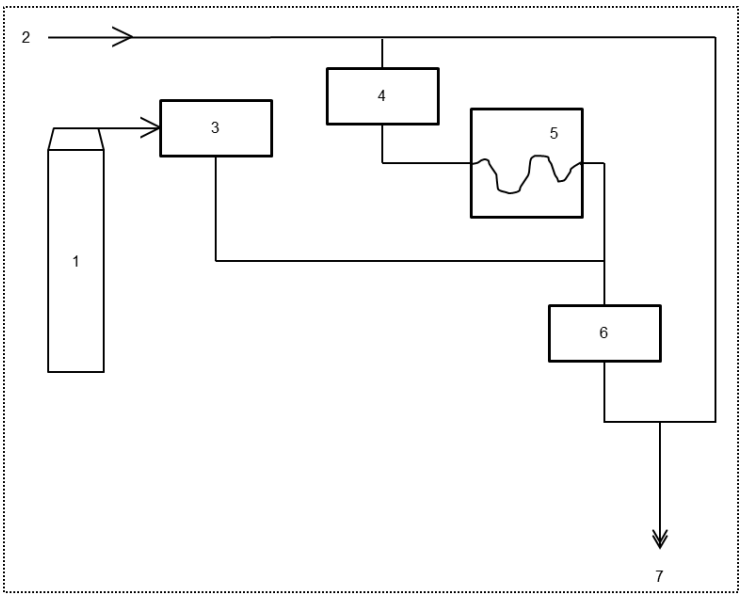

Figure 5.11. Schematic of plumbing used for PAN synthesis and analysis. 1 = NO cylinder, 2 = ZA, 3 = MFC, 4 = MFC, 5 = Permeation cell using acetone excess and maintained at 30 °C, 6 = MFC, 7 = PAN outlet.

For ANs calibrations, a cylinder of 0.997 ± 0.005 ppmv (Scott-Marrin Inc., USA) n-propyl nitrate (NPN) is used. This has a stability of approximately 3 years.

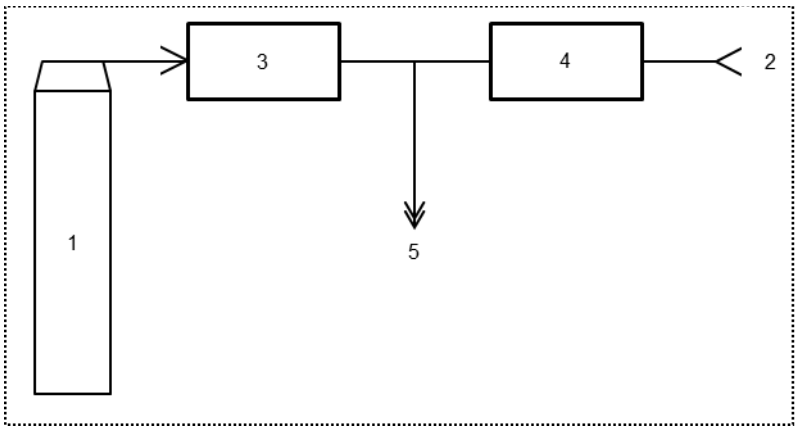

Figure 5.12. Schematic of plumbing used for the NPN standard. 1 = NPN cylinder, 2 = ZA, 3 = MFC, 4 = MFC, 5 = NPN outlet.

The HNO_3 source used for the calibration of the NO_y inlet is a certified permeation tube (EcoScientific, UK). A controlled flow of zero air is passed over a permeation tube filled with high purity HNO_3, which is maintained at a constant temperature of 30 °C. The mixing ratio of the HNO_3 source is then quantified using equation 5.12 and can then be further diluted to the required mixing ratio by using a second controlled flow of zero air.

$$\text{Emission rate (ppmv)} = \frac{(K_0 \times ER)}{F} \qquad 5.12$$

where,

K_0 [1] = constant, 0.355

ER [1] = emission rate, 482 ng min^{-1}

Flow = flow rate, cc min^{-1}

[1] values calibrated for permeation tube held at 30 °C (EcoScientific, UK).

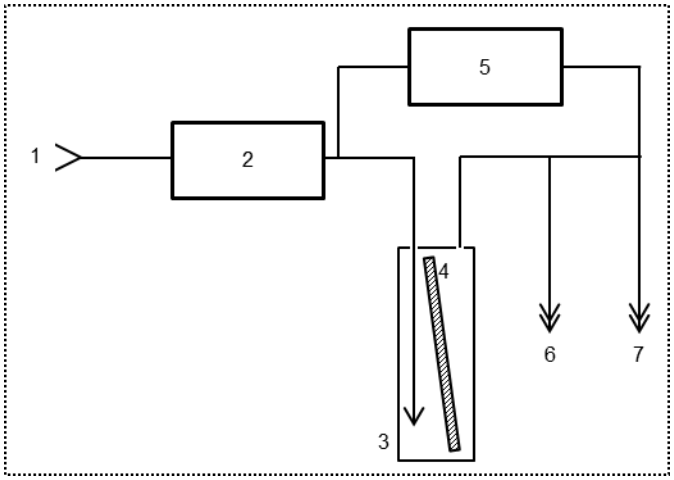

Figure 5.13. Schematic of plumbing used for HNO_3 synthesis and analysis. 1 = ZA, 2 = MFC, 3 = Permeation oven (maintained at 30°C), 4 = certified HNO_3 permeation tube (EcoScientific, UK), 5 = MFC, 6 = Waste, 7 = HNO_3 outlet.

The accuracy of this method can be assessed through periodic weighings of the permeation tube, as provided conditions are maintained and there is a constant gas flow to remove HNO_3 permeating into the oven headspace, the mass loss of the permeation tube should be linear with time. Figure 5.14 shows the weights of the HNO_3 permeation tube recorded over time. The R^2 value shown gives confidence in the accuracy of this as a source of HNO_3.

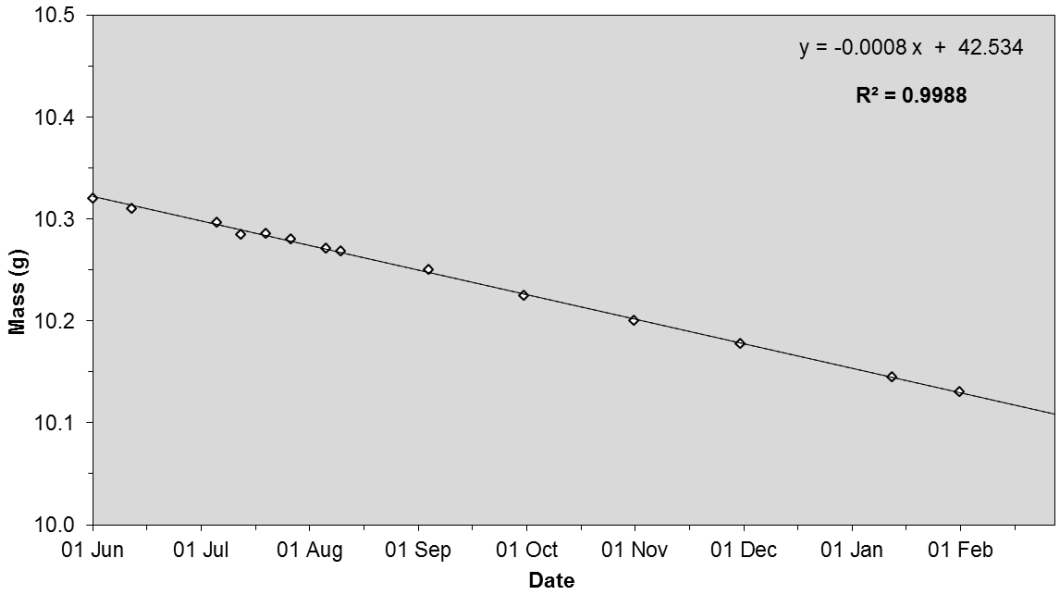

Figure 5.14. HNO_3 permeation tube weighing's plotted against time. R^2 value = 1, gives confidence in the accuracy of the calibration source.

5.3.2. Experimental Methods

5.3.2.a. Standard Calibration

Each standard was calibrated for linearity of detection over a range of mixing ratios. This was done by passing each standard through both the gold (Au_{300}) and molybdenum (Mo_{300}) ovens at a 300 °C. A small flow of CO is added to the Au_{300} oven as a reducing agent. Both of these ovens cause the reduction of O-N containing species to NO with ~100 % efficiency (Williams et al, 1998). Varying the dilution flows allowed a range of mixing ratios to be created. Following stabilisation of the signal, a 10 minute average was compared with the theoretical mixing ratio for the respective dilution being measured. This method therefore allows quantification of the standards actual concentration and a measure of the conversion efficiency of each quartz oven. For example, for 100 % conversion efficiency in the quartz ovens, the mixing ratio of the standard being tested must be equal to that detected by the Au_{300} and Mo_{300} ovens at temperatures above the theoretical temperature at which 100 % thermal decomposition of the respective standard occurs. The results of the PAN, NPN and HNO_3 calibrations are shown in figures 5.15-5.20

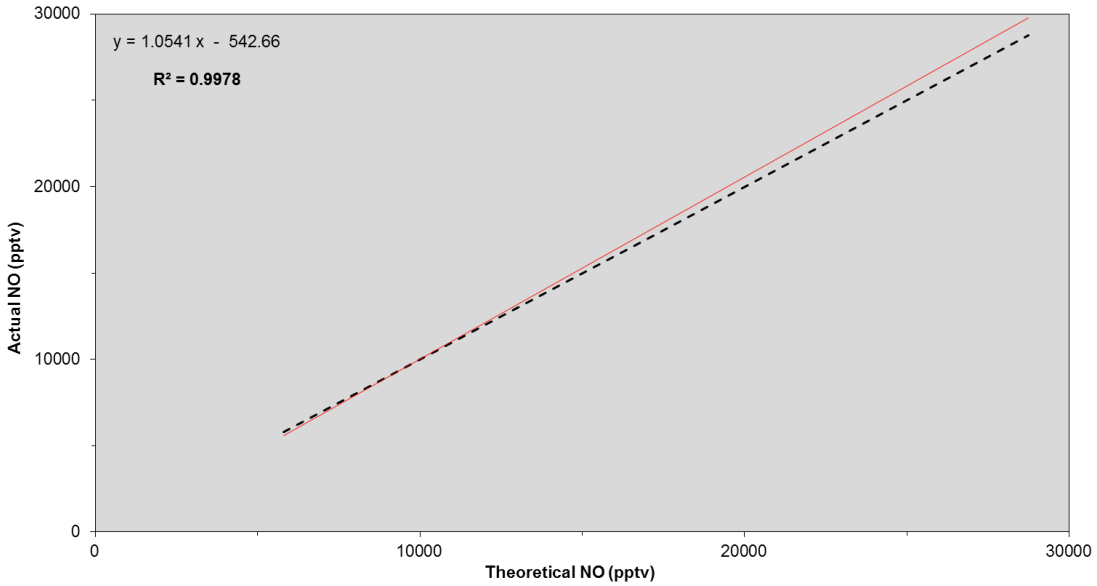

Figure 5.15. NO production following the thermal dissociation of PAN in the Au3 oven over a range of mixing ratios. Dashed black line = theoretical NO mixing ratio expected at each dilution.

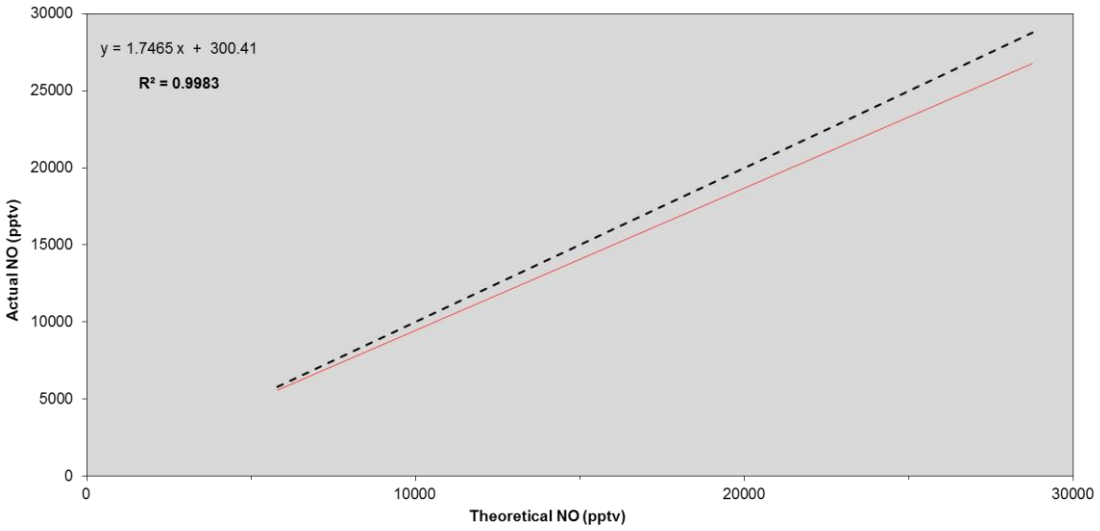

Figure 5.16. NO production following the thermal dissociation of PAN in the Mo3 oven over a range of mixing ratios. Dashed black line = theoretical NO mixing ratio expected at each dilution.

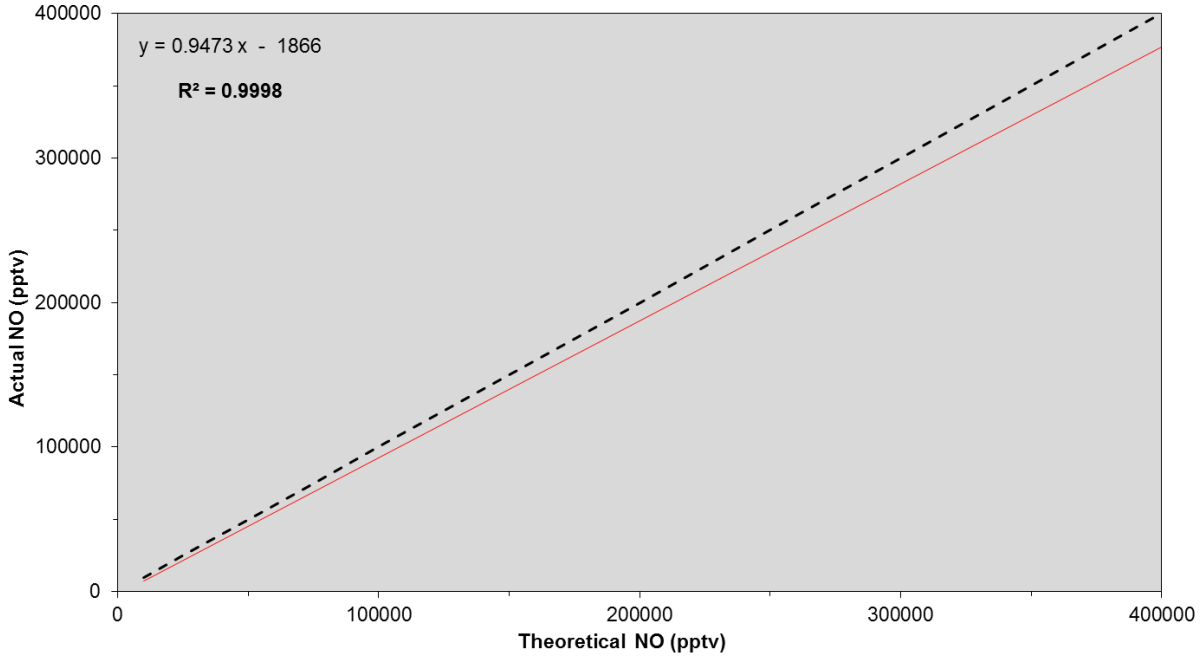

Figure 5.17. NO production following the thermal dissociation of NPN in the Au3 oven over a range of mixing ratios. Dashed black line = theoretical NO mixing ratio expected at each dilution.

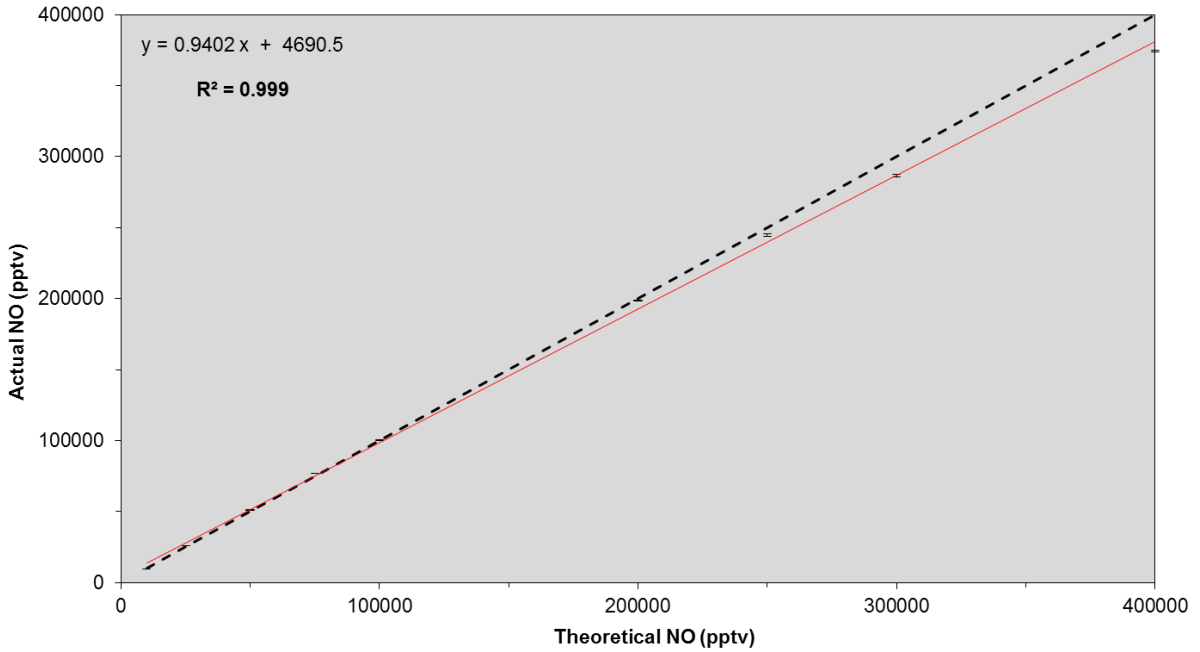

Figure 5.18. NO production following the thermal dissociation of NPN in the Mo3 oven over a range of mixing ratios. Dashed black line = theoretical NO mixing ratio expected at each dilution.

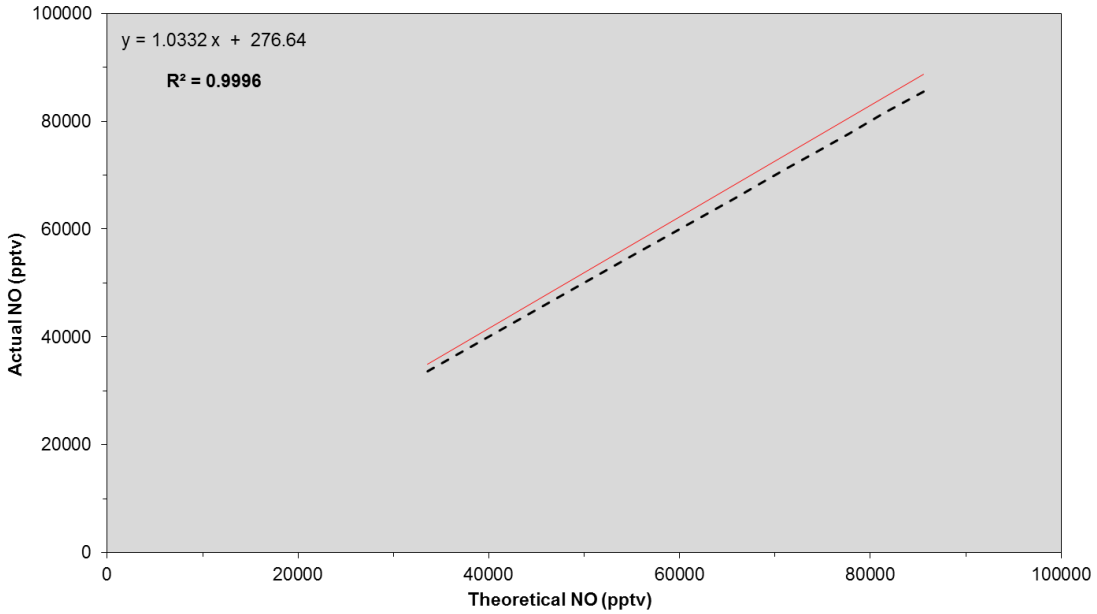

Figure 5.19. NO production following the thermal dissociation of HNO_3 in the Au3 oven over a range of mixing ratios. Dashed black line = theoretical NO mixing ratio expected at each dilution.

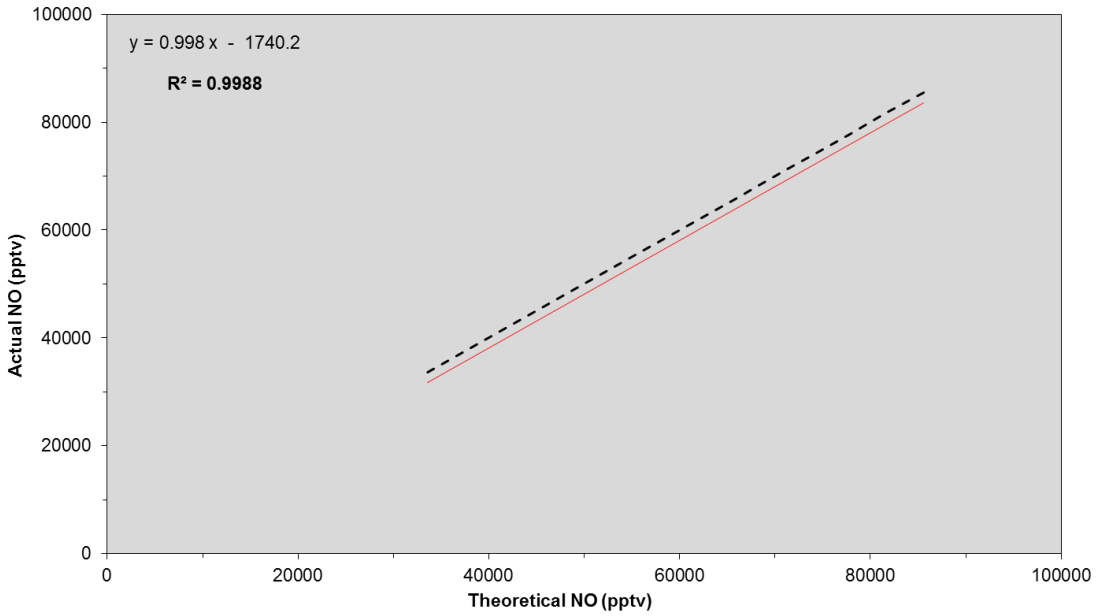

Figure 5.20. NO production following the thermal dissociation of HNO_3 in the Mo3 oven over a range of mixing ratios. Dashed black line = theoretical NO mixing ratio expected at each dilution.

5.3.2.b. Temperature Ramp

The instruments response to the thermal decomposition of each standard was analysed by passing a known mixing ratio of each standard, quantified by the standard calibration procedure, through each quartz oven over a range of temperatures that spanned the temperature range over which 0-100 % of the respective standard thermally dissociates. The temperature of the quartz oven was ramped in increments ranging from 10-50 °C depending on the resolution required. Following stabilisation of the signal, a 10 minute average was calculated along with the variation in the signal. As stated, the temperatures used for calibrating the quartz oven responses covered the thermal decomposition range of each standard and started from ambient air temperature (~25 °C) to ~50 °C higher than that expected for 100 % thermal decomposition, or until the signal stabilised with any increase in temperature resulting in a non-significant increase in the NO_2 signal.

For all results of temperature ramp experiments shown in the following section, unless otherwise stated, the red line represents NO, the blue line represents NO_2, the dashed black line represents total NO_x and the solid black line is the kinetic model output of NO_2 produced following the thermal dissociation of the relevant standard at the theoretical concentration present following dilution.

5.4. Results

5.4.1. Peroxyacetyl Nitrate, PAN

Figures 5.21 and 5.22 show the instrument response to PAN thermal decomposition in the Q3 and Q6 ovens respectively following temperature ramp experiments. As will be shown in all temperature ramps of all standards presented in this report, rather than just NO_2 being produced following thermal dissociation, the NO yield increases with higher temperatures. The cause of this will be discussed in section 5.5. However, what is important is that the NO increase is correlated to that of a decrease in NO_2 meaning that total NO_x is conserved and that the amount detected, is comparable to the total amount of NO_2 expected following 100 % thermal dissociation of each standard predicted by the kinetic model. As the chemiluminescence instrument can provide a measure of both NO and NO_2, this deviation can be accounted for and shows that the quartz ovens have a conversion efficiency of ~100 %.

As can be seen in both plots, NO_x production occurs at temperatures approximately 30 °C lower than those predicted by the kinetic model. Again this feature is consistent in all experiments, though the deviation does vary as will be discussed and is due to the thermocouple that acts as a feedback for temperature control of the ovens being located on the outside of the oven. Therefore all temperatures recorded are lower than the actual temperature of the gas stream. Table 5.6 at the end of this section summarises the temperature deviations between observed and modelled values for each standard in each oven tested.

A particular feature that is specific to PAN thermal dissociation is the large NO_2 artefact as can be seen at lower temperatures when no PAN degradation is occurring. This is a recognised interference in instruments that use the chemiluminescence technique to measure PAN and originates in the use of acetone in its synthesis. It affects the instrument in two ways; chemiluminescence caused by its reaction with O_3 creates a fake NO_2 signal and excited state acetone created during photolysis is longer lived than that for NO_2 and so also causes an increase in the background interference in the instrument. To remove this interference, future work will aim to synthesise PAN using NO in excess and a small flow of acetone. This will remove the acetone interference and the elevated NO signal can be quantified by the instrument. Figure 5.23 shows a schematic of the novel system that will be employed to produce PAN whilst removing the acetone interference observed.

Most importantly, the temperature ranges over which PAN thermal dissociation occurs in the Q3 and Q6 ovens occurs is distinct from the region over which NPN thermal dissociation occurs. The thermal dissociation temperature ranges for all standards and all ovens tested thus far are shown in section 5.5. This is important for the accurate measure of all NO_y reservoirs due to the calculation procedure which subtracts the NO_2 signal of one oven from that of another. Overlap of a thermal dissociation range would cause an overestimation of the reservoir mixing ratio.

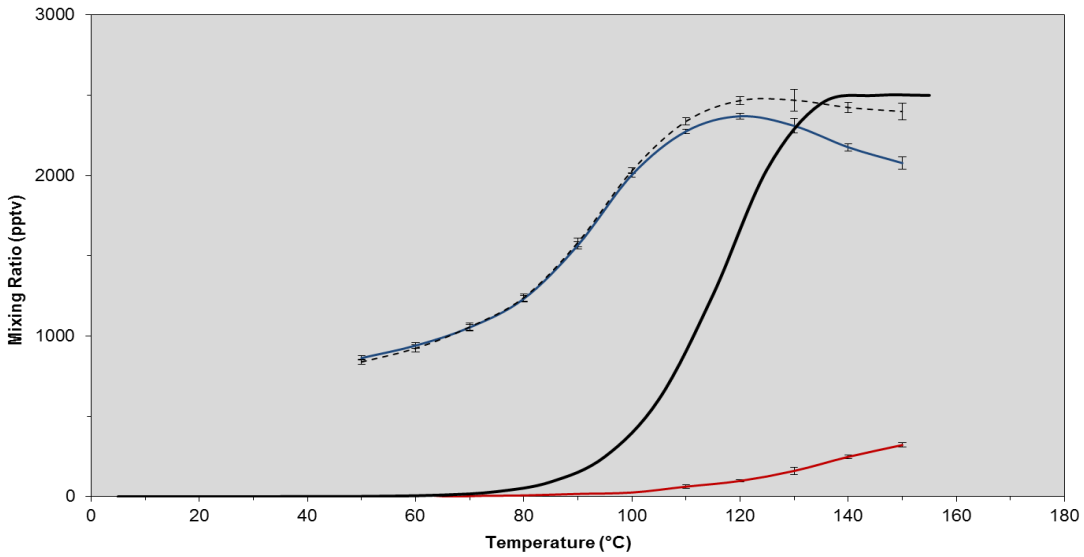

Figure 5.21 . PAN temperature ramp in the Q3 oven. Red line = NO, blue line = NO_2, dashed black line = NO_x, solid black = Modelled NO_2.

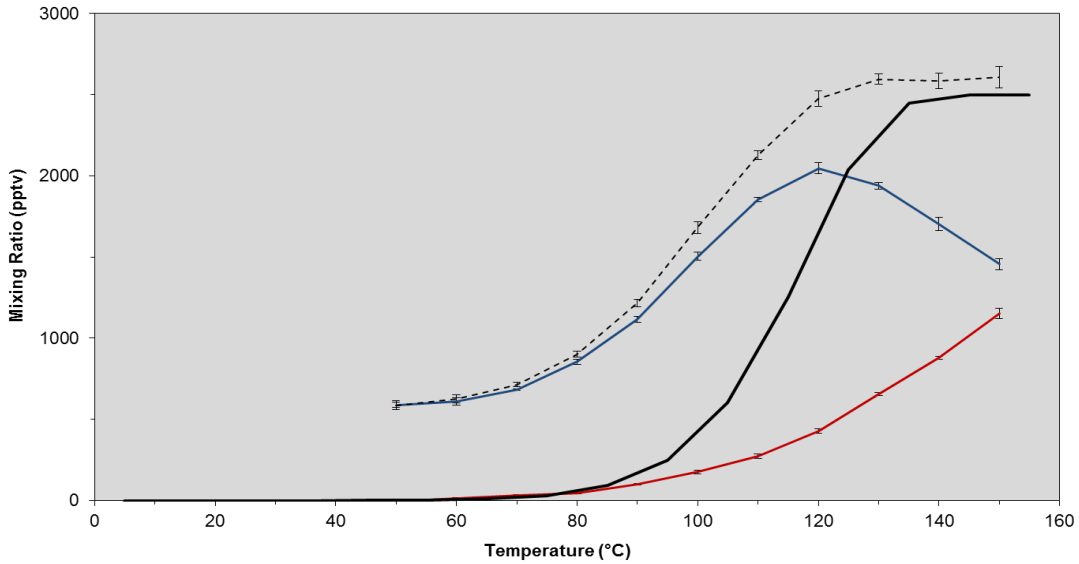

Figure 5.22. PAN temperature ramp in the Q6 oven. Red line = NO, blue line = NO_2, dashed black line = NO_x, solid black = Modelled NO_2.

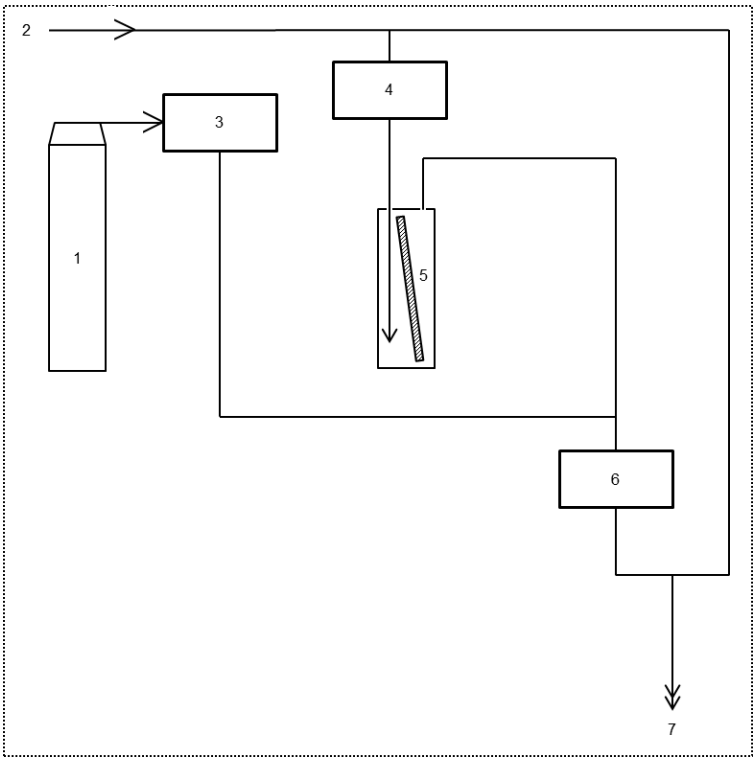

Figure 5.23. Schematic of plumbing used for PAN synthesis and analysis. 1 = NO cylinder, 2 = ZA, 3 = MFC, 4 = MFC, 5 = Permeation tube held in permeation oven creating small acetone mixing ratio and restricting interference (maintained at 30 °C), 6 = MFC, 7 = PAN outlet.

5.4.2. n-Propyl Nitrate, NPN

Figures 5.24-5.26 show the instruments response to a temperature ramp of NPN. As with PAN, NO_2 is converted to NO at higher temperatures but with total NO_x being conserved. NPN thermal dissociation also occurs at temperatures lower than those predicted by the model, however this deviation does vary between the ovens. With an increasing inlet length sampling from the Q1 to the Q6, NPN dissociation occurs at temperatures closer to the modelled values. The source of this result will be discussed in section 5.5. Despite this variation, the temperature range over which NPN exhibits thermal dissociation occurs is similar to the model and distinct from that of PAN allowing accurate quantification.

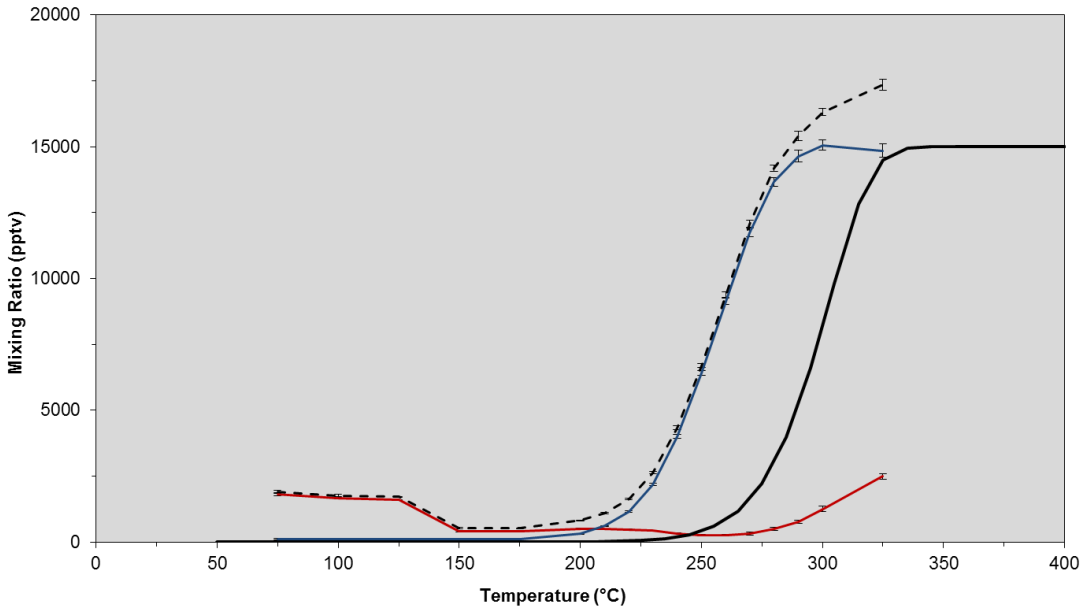

Figure 5.24 . NPN temperature ramp in the Q1 oven. Red line = NO, blue line = NO_2, dashed black line = NO_x, solid black = Modelled NO_2.

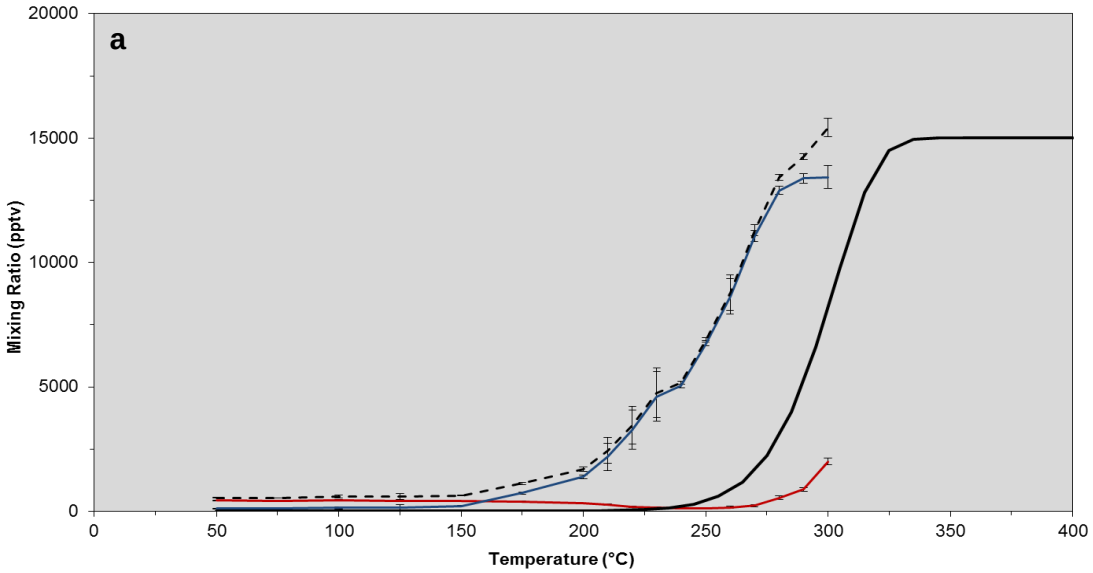

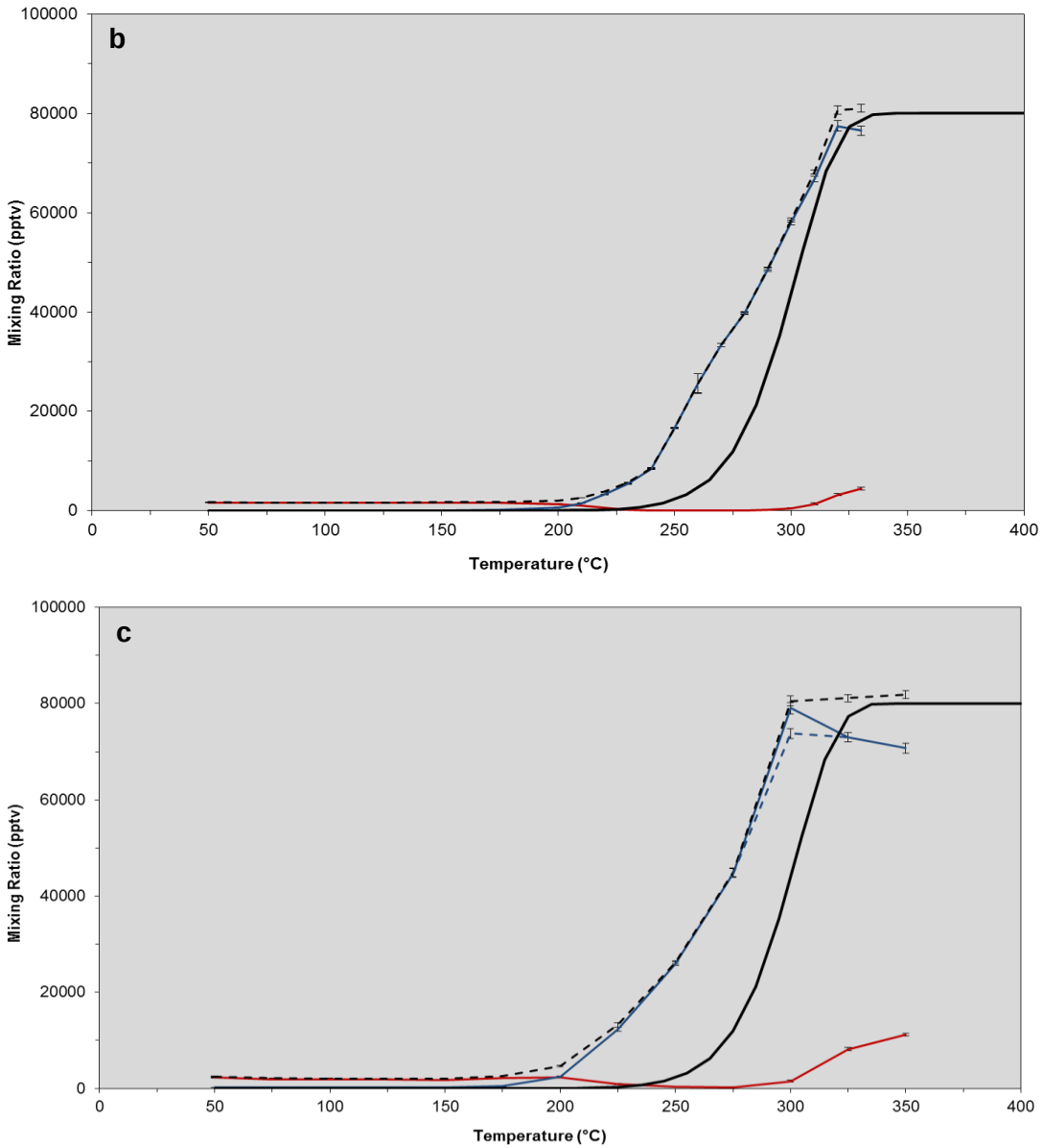

Figure 5.25 . NPN temperature ramps in the Q3 oven. Panels a, b and c refer to repeat results of the temperature ramp experiments using NPN in the Q3 oven. Red line = NO, blue line = NO_2, dashed black line = NO_x, solid black = Modelled NO_2.

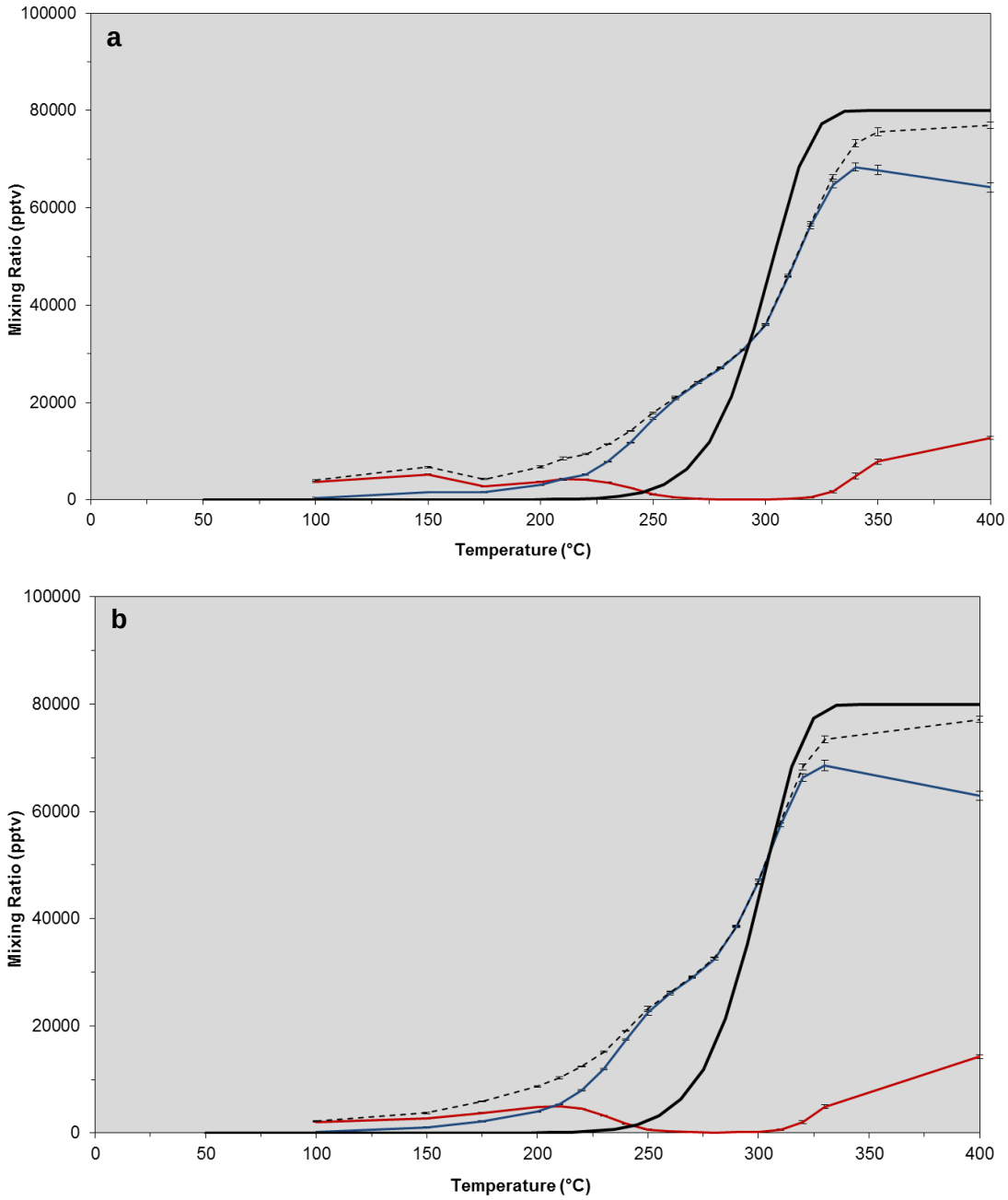

Figure 5.26. NPN temperature ramps in the Q6 oven. Panels a and b refer to repeat results of the temperature ramp experiments using NPN in the Q6 oven Red line = NO, blue line = NO_2, dashed black line = NO_x, solid black = Modelled NO_2.

5.4.3. HNO_3

Figures 5.27 and 5.28 show the results of HNO_3 temperature ramp experiments in the Q3 and Q6 ovens respectively. Similar to PAN and NPN is the production of NO at temperatures comparable to that of NPN temperature ramp experiments. However, the thermal dissociation range observed is much lower than that predicted by the kinetic model resulting in an overlap between NPN and HNO_3 degradation and subsequent NO_x

production. As stated previously, it is important that there is a temperature range during which thermal dissociation of one reservoir is complete prior to the significant dissociation of the next, thereby allowing the accurate quantification of each reservoir. This was clearly not the case and possible reasons for this discrepancy were experimentally verified using the Q6 oven to maintain all other variables, such as oven and inlet length.

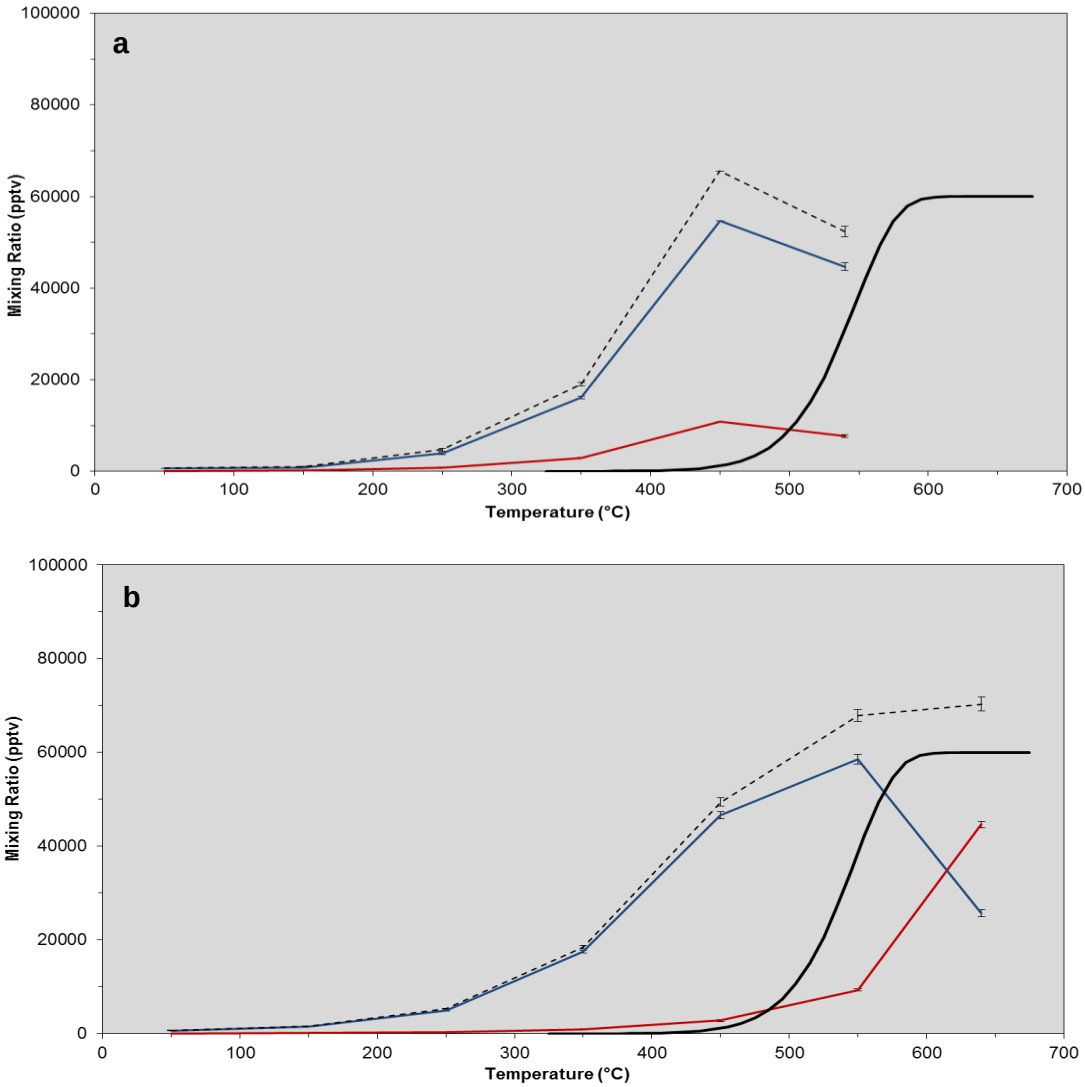

Figure 5.27. HNO_3 temperature ramps in the Q3 oven. Panels a and b refer to repeat results of the temperature ramp experiments using HNO_3 in the Q3 oven. Red line = NO, blue line = NO_2, dashed black line = NO_x, solid black = Modelled NO_2.

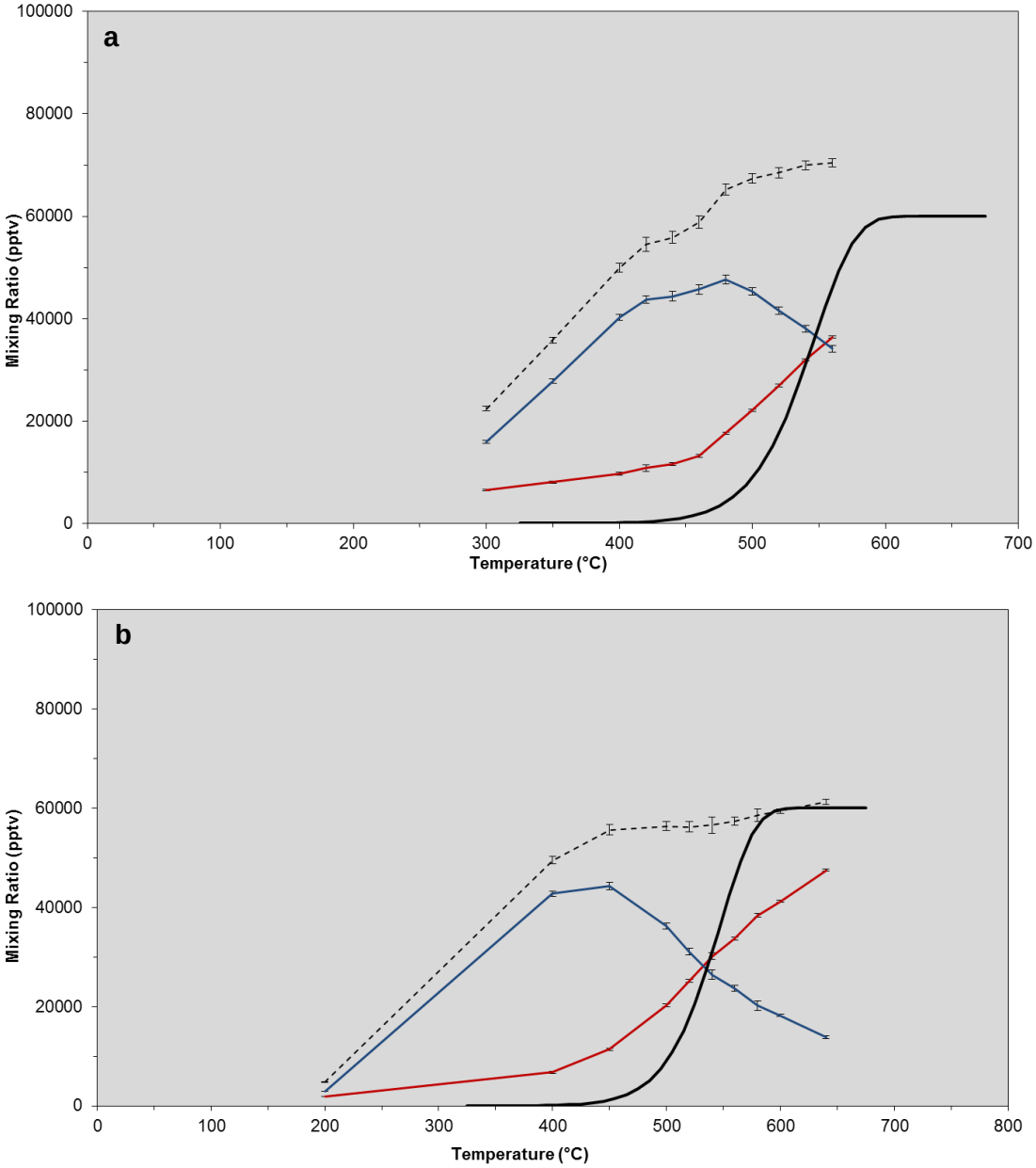

Figure 5.28. HNO_3 temperature ramps in the Q6 oven. Panels a and b refer to repeat results of the temperature ramp experiments using HNO_3 in the Q6 oven. Red line = NO, blue line = NO_2, dashed black line = NO_x, solid black = Modelled NO_2.

The early degradation was initially thought to be due to either direct interference from an acetone permeation tube in the same permeation oven as the HNO_3 source, or due to the reaction between acetone and HNO_3 to form another compound with a lower TD range. The acetone permeation tube is in place to be used for PAN synthesis via the NO excess method as previously described (figure 5.23) and was removed to investigate its effect on the observed result following HNO_3 thermal dissociation. The results of this experiment are shown in figure 5.29. Early degradation was still apparent at approximately 200 °C consistent with the previous temperature ramp experiments suggesting that the acetone permeation tube had no significant effect.

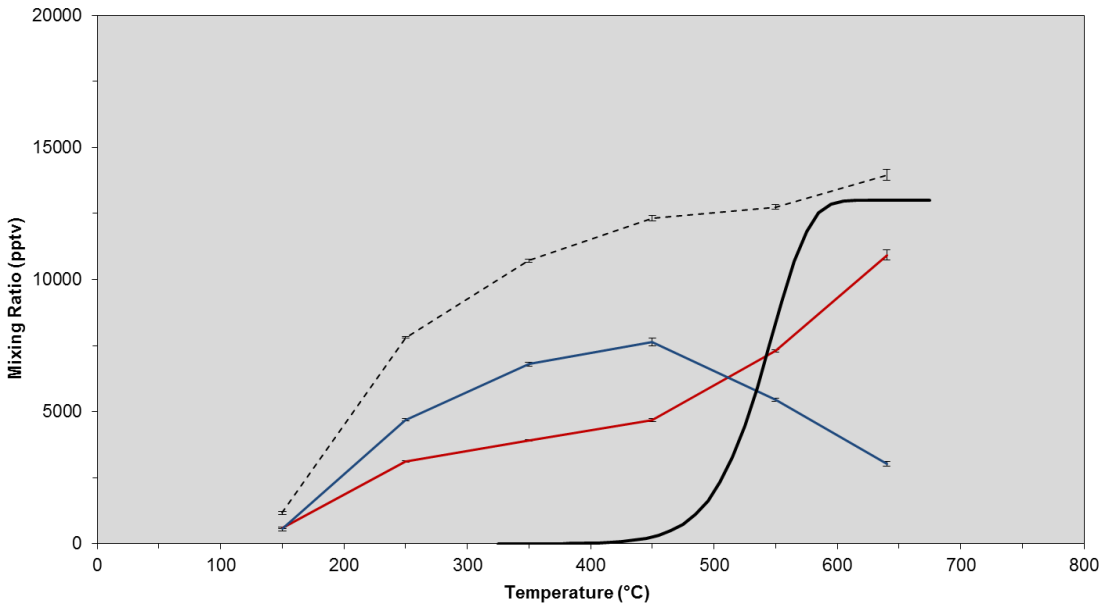

Figure 5.29. HNO_3 temperature ramp in the Q6 oven with the acetone permeation tube removed from the permeation oven. Red line = NO, blue line = NO_2, dashed black line = NO_x, solid black = Modelled NO_2.

Other oven setups used in instruments that measure NO_y reservoirs via thermal dissociation consist of 1.2 m quartz rods with an initial heated section of ~20 cm and a cooling region of ~1 m (Day et al., 2002; Dari-Salisburgo et al, 2009). This means that downstream of the oven, the gas flow encountered by the PFA tubing is of a much lower temperature, thereby suppressing reduction of NO_2 to NO or desorption of chemical species from the walls (Day et al, 2002). In comparison, the ovens used in this inlet have an internal volume of ~ 0.8 m^3 and are filled with glass beads with a diameter of 3 mm with no cooling region. To investigate whether secondary chemistry within the inlet downstream of the ovens caused by leaching of reactants from the PFA, a 1 m length of coiled stainless steel was added downstream of the oven to provide a sufficient cooling region. However as shown by figure 5.30, early degradation still occurred.

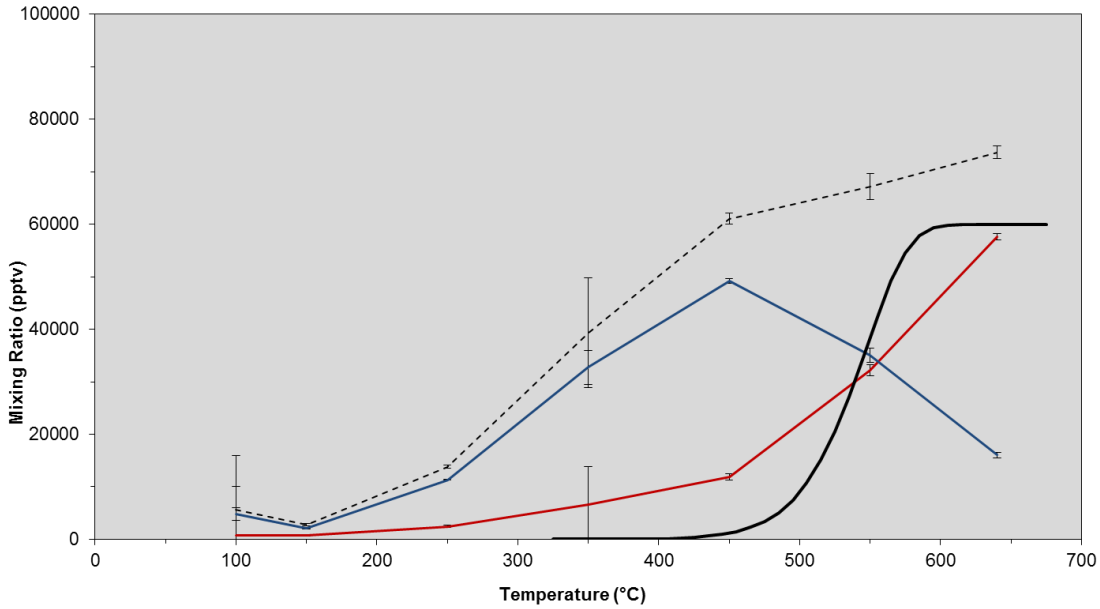

Figure 5.30. HNO_3 temperature ramp in the Q6 oven with a stainless steel cooling region downstream of the Q6 oven. Red line = NO, blue line = NO_2, dashed black line = NO_x, solid black = Modelled NO_2.

Investigation of the source of the early thermal dissociation was then focused on the permeation oven and whether residual HNO_3 and acetone had accumulated over time despite a constant air flow. To quantify the permeation ovens contribution to the measured NO and NO_2, a flow of zero air was first passed through the permeation oven with all permeation tubes removed and then with the permeation oven bypassed completely. The results of these experiments are shown in figures 5.31 and 5.32.

As would be expected, both experiments showed very low levels of NO and NO_2 with a small source of NO and NO_2 originating from the permeation oven (figure 5.32). Although there is a signal from the permeation oven, the level of NO and NO_2 is very much reduced in comparison to temperature ramp experiments using the HNO_3 permeation tube source suggesting that the early degradation seen is due to this source.

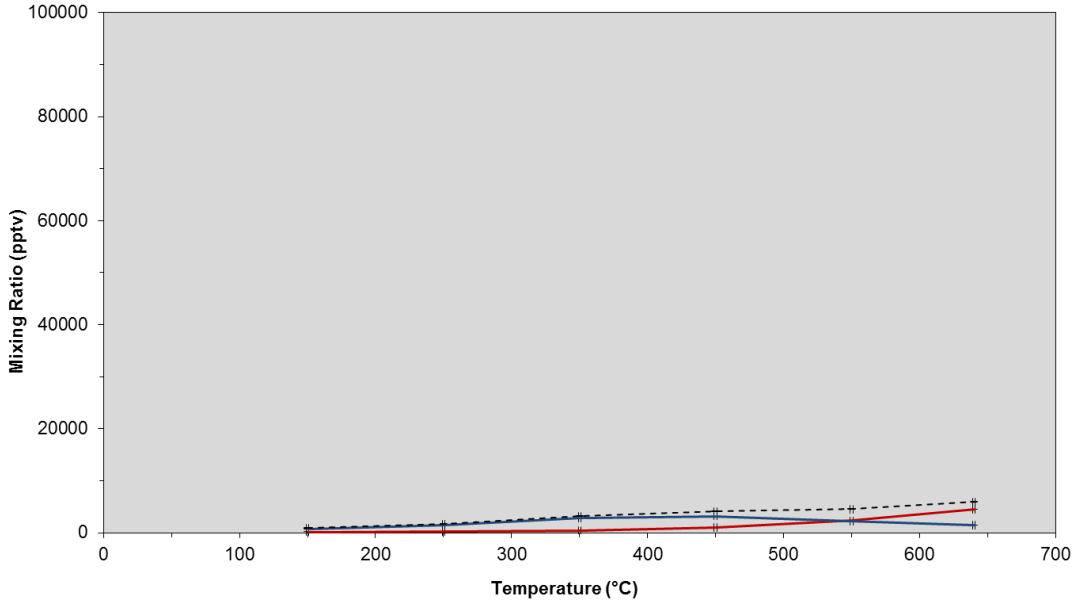

Figure 5.31. ZA temperature ramp in the Q6 oven with the permeation oven in series but empty. Red line = NO, blue line = NO_2, dashed black line = NO_x, solid black = Modelled NO_2.

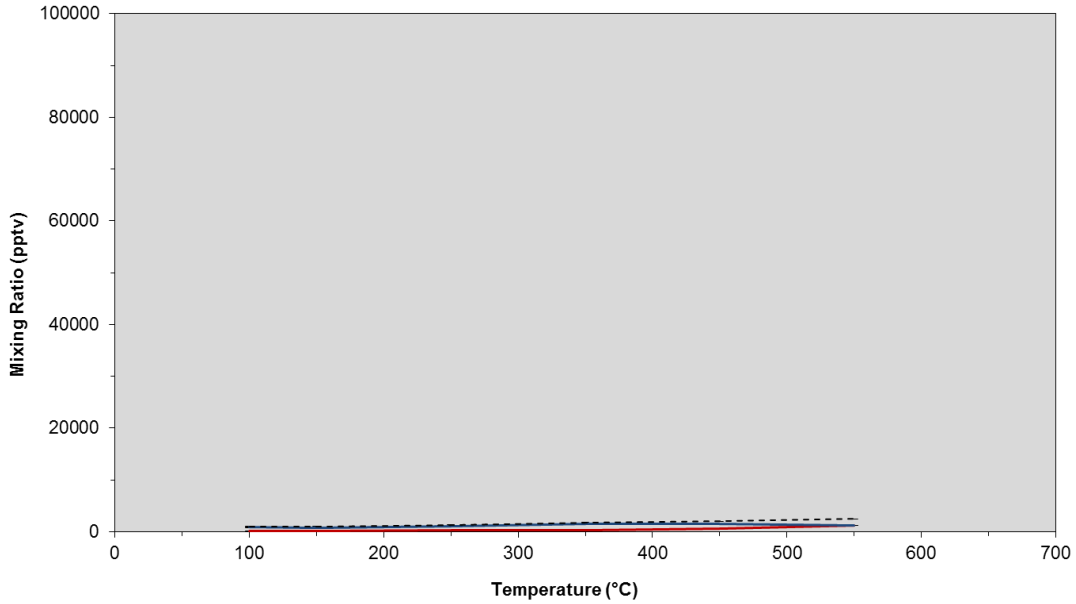

Figure 5.32. ZA temperature ramp in the Q6 oven with the permeation oven bypassed. Red line = NO, blue line = NO_2, dashed black line = NO_x, solid black = Modelled NO_2.

To test the stability of the certified HNO_3 permeation tube, a certified blank permeation tube (EcoScientific, UK) was filled with high purity HNO_3 and left to equilibrate in the permeation oven for 3 weeks. This was then used as the HNO_3 source during a temperature ramp, the results of which are shown in figure 5.33. Again, the thermal dissociation was observed at lower temperatures predicted by the kinetic model and was consistent with all previous HNO_3 experiments.

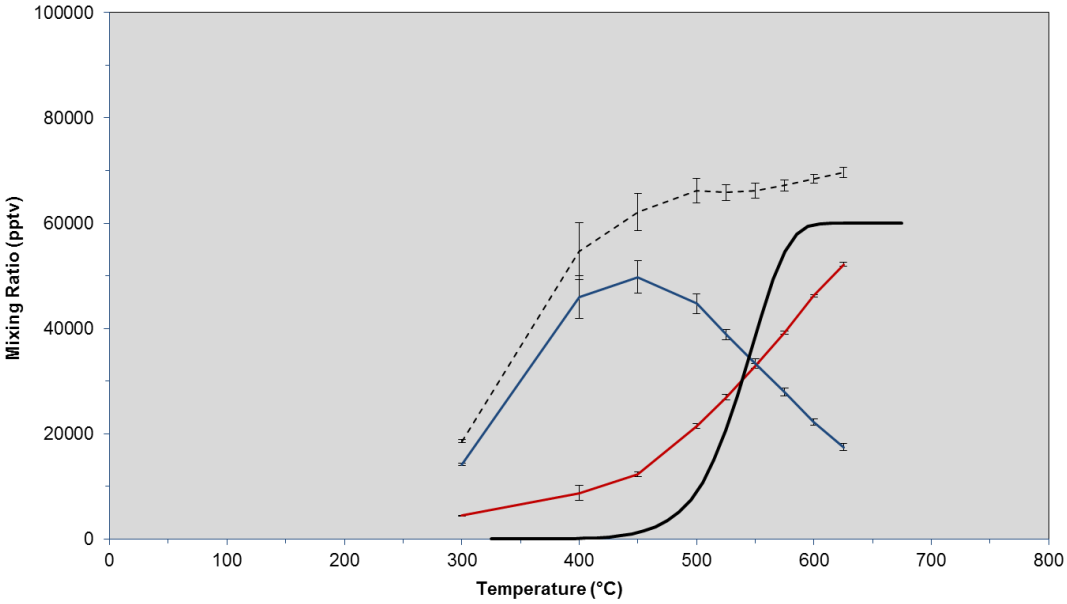

Figure 5.33. HNO_3 temperature ramp in the Q6 oven with a new blank permeation tube filled with high purity HNO_3. Note, this is not an EcoScientific certified HNO_3 permeation tube. Red line = NO, blue line = NO_2, dashed black line = NO_x, solid black = Modelled NO_2.

Table 5.6. Average temperature difference and standard deviation between the observed NO_x and modelled NO_2 for each standard in each of the quartz ovens tested.

Standard	Oven	Temperature Deviation (°C)
PAN	Q1	
	Q3	31.3 ± 13.1
	Q6	28.0 ± 15.2
NPN	Q1	43.3 ± 5.2
	Q3	31.4 ± 16.4
	Q6	11.1 ± 28.6
HNO_3	Q1	
	Q3	156.8 ± 33.6
	Q6	197.2 ± 50.7

5.5. Discussion

The increase in NO observed is correlated to the NO_2 decrease at these higher temperatures as shown in figure 5.34. This feature is not present in other instruments that use thermal decomposition to measure NO_y reservoirs (Day et al., 2002; Dari-Salisburgo et al, 2009). The ovens in these instruments consist of glass rods approximately 1.2 m in length with an initial heating region of ~20 cm. In comparison, the ovens used in this inlet have an internal volume of ~ 0.8 m^3 and are filled with glass beads with a diameter of 3 mm. The purpose of using quartz in the ovens is to provide an inert surface which is able to conduct heat to achieve the temperatures required. The difference between the two systems is a significantly larger surface area in the ovens reported in this study.

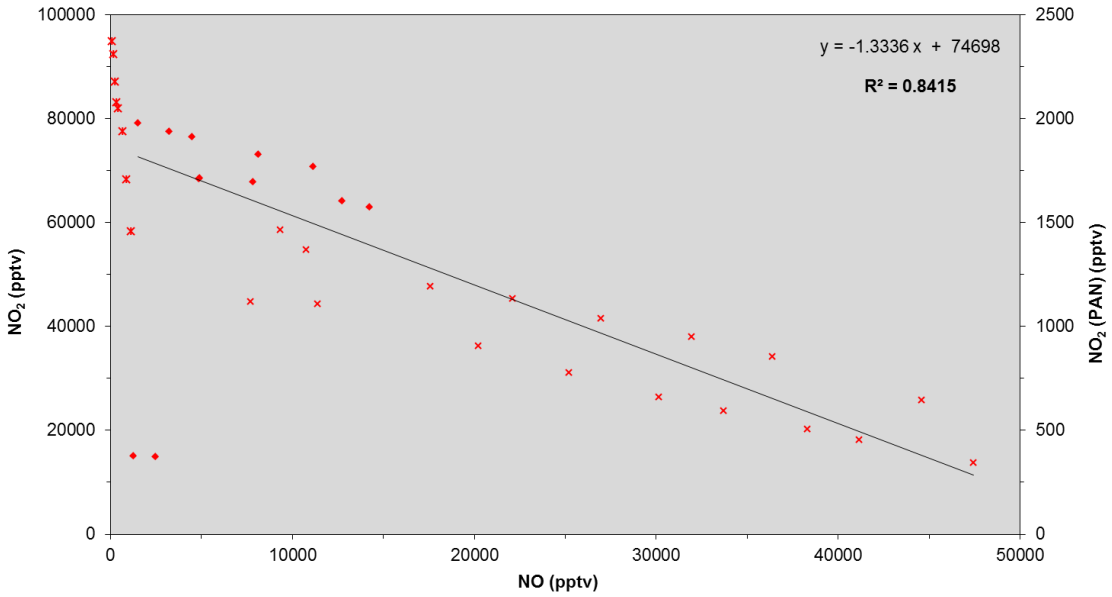

Figure 5.34. Correlation between NO and NO_2 during temperature ramp experiments. Data shown is during NO_2 signal decrease with increasing temperature. Stars = PAN thermal dissociation (plotted on secondary y-axis), diamonds = NPN thermal dissociation, crosses = HNO_3 thermal dissociation. Line of best fit based on all HNO_3 data and NPN data excluding two anomalous NPN data points at ~1.8 NO_2 pptv.

As a result, the increase in NO could be due to surface chemistry within the oven. For example, NO_2 reduction in the ovens or inlet lines downstream can be caused by the presence of free oxygen atoms, which can be produced via the thermal decomposition of O_3. The equilibrium between O_x (O_x = O_3 + O) is controlled by the rate constants for reactions 5.13 and 5.14. Reaction 5.13 is highly temperature dependent so that at 330 °C only 2 % is in the form of O, in comparison to at temperatures of 530 °C, at which nearly all O_x will be

oxygen atoms (Day et al., 2002). However, Perez et al (2007) found that 73 ppbv of O_3 was required to cause a 4 % reduction in NO_2 to NO at 400 °C and is therefore an unlikely cause of the NO production seen.

$$O_3 + M + \text{heat} \rightarrow O_2 + O + M \qquad 5.13$$

$$O_2 + O + M \rightarrow O_3 + M \qquad 5.14$$

HONO is another possible source of NO which has been shown to form on glass surfaces following the heterogeneous reaction between NO_2 and H_2O as shown in reactions 5.15 and 5.16 (Perez et al., 2007; Zhou et al., 2007). Future experiments to establish the cause of NO production should perform temperature ramps using conditions with variable humidities and O_3 mixing ratios in order to ascertain the contribution of each of these possible interferences.

$$2NO_2 + H_2O + \text{surface} \rightarrow HONO + HNO_3 \qquad 5.15$$

$$HONO \rightarrow OH + NO \qquad 5.16$$

Other factors that may contribute to the increasing NO are due to the setup of the inlet for the experiments conducted and the mixing ratios of the standards used. Regarding the inlet setup, the valve system in place to switch sampling between each oven, as will be used during the measurement cycle as shown in figure 5.9, is controlled by a software package that is currently on the CVAO system. As a result, changing of the sampling lines carried out during this work was done manually with all other sample lines having to be capped to sustain an over pressure in the line during the experiments, thereby preventing contamination from laboratory air. To replicate all inlet dynamics as closely as possible, sample lines were capped at the valve system resulting in a dead volume within the ovens and channels not being sampled. Back flushing or production of possible interfering species due to chemistry within the inlet caused by residual sample could therefore lead to the NO production seen. This can be investigated in future studies by capping the sample lines prior to the ovens.

Similarly the sources of each standard lead to high mixing ratios significantly elevated over the levels expected for a remote tropical marine boundary layer environment such as that encountered at the CVAO. Dilution of each standard is carried out to achieve the mixing ratios used, however further dilution without a second dilution point creates a trade-off between final mixing ratio and dilution accuracy. The high mixing ratios used, though unfavourable, are nonetheless unavoidable and may be a contributing factor to the NO increases seen following chemistry of residual sample within the inlet as previously

described. Future experiments would greatly benefit from a second dilution point to achieve mixing ratios that are a realistic representative of those expected at the CVAO.

Finally, the effect of residence time within the inlet as mentioned previously is critical for the accurate measure of NO_y reservoirs. Although the main source of error due to inlet length is thought to be due to thermal decomposition of PAN and loss of HNO_3 to the walls of the inlet due to its high solubility, experiments with NPN shown in figures 5.24-5.26, display a deviation in measured NO_x and predicted NO_2 which decreases with increasing inlet length. Although there is inherent uncertainty in the measured temperature due to the thermocouple being situated on the outside of the oven and not in the gas stream, this deviation could equally be a result of chemistry within the inlet. An in depth kinetic study of each distinct section of the inlet, as described in table 5.5, which includes all relevant reactions for the conditions experienced at the CVAO would help investigate possible sources of the deviation in thermal dissociation temperatures observed (figure 5.35).

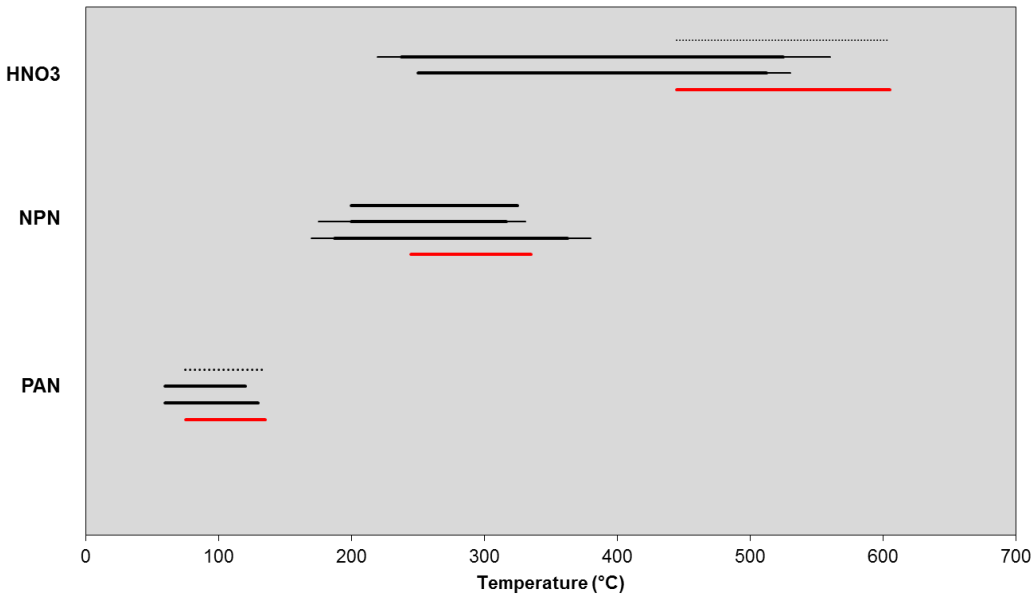

Figure 5.35. Average thermal dissociation ranges (thick black line) and standard deviations (thin black line) for all of the standards in each oven tested. For each standard; top black line = Q1 oven, middle black line = Q3 oven, bottom black line = Q6 oven. Red line indicates modelled temperature range over which significant (*P* > 0.01) thermal dissociation occurs. Dotted black line indicates no data.

5.6. Conclusion

The aim of this project was to calibrate a thermal-decomposition chemiluminescence (TD-Chem) instrument, capable of measuring the composition of reactive nitrogen in the clean, remote, tropical, marine boundary layer at the CVAO. As shown by the results presented in this report, the instrument responds well to the thermal decomposition of species that are representative of the major NO_y reservoirs that exist in the troposphere. All experiments show thermal dissociation kinetics consistent with current understanding and kinetic theory. Deviations that do occur are either known and can be quantified, have been experimentally deduced, or a work schedule is in place in order to quantify them in the near future. Following the completion of the instrument calibration and installation at the CVAO in the summer of 2013, this instrument will provide an exciting, novel data series that will aid the development of global atmospheric models, which currently underestimate NO_x mixing ratios in the remote troposphere, and allow these models to improve and produce accurate simulations of the trends of important atmospheric species in the future.

References

Barker, J.R., Benson, S.W., Mendenhall, G.D. and Goldern, D.M. (1977) Measurment of rate constants of importance in smog. *Report PB-274530, National Technological Information Service*. Springfield, Va., USA.

Bridier, I., Carulp, F., Loirat, H., Lesclaux, R., Veyret, B., Becker, K.H., Reimer, A. and Zabel, F. (1991) Kinetic and theoretical studies of the reactions CH3C(O)O2=NO2 + M → CH3C(O)O2NO2 + M between 248 and 393 K and between 30 and 760 torr. *Journal of Physical Chemistry*. **95**, 3594–3600.

Dari-Salisburgo, C., Di Carlo, P., Giammaria, F., Kajii, Y., D'Altorio, A. (2009) Laser induced fluorescence instrument for NO_2 measurements: Observations at a central Italy background site. *Atmospheric Environments.* **43**, 970-977.

Day, D.A., Wooldridge, P.J., Dillon, M.B., Thornton, J.A. and Cohen, R.C. (2002) A thermal dissociation laser-induced fluorescence instrument for in situ detection of NO2, peroxy nitrates, alkyl nitrates, and HNO_3. *Journal of Geophysical Research*. **107**, D64046.

Day, D.A., Wooldridge, P.J. and Cohen, R.C. (2009) Observations of the effects of temperature on atmospheric HNO_3, ΣANs, ΣPNs, and NO_x: Evidence for a temperature-dependent HO_x source. *Atmospheric Chemistry and Physics*. **8**, 1867-1879.

Glaenzer, K. and Troe, J. (1974) Thermal decomposition of nitrocompounds in shock waves. IV. Decomposition of nitic acid*. Berichte Der Bunsen-Gesellschaft-Physical Chemistry Chemical Physics.* **78**, 71.

Kirchner, F., Mayer-Figge, A., Zabel, F. and Becker, K.H. (1999) Thermal stability of peroxynitrates. *International Journal of Chemical Kinetics*. **31**, 127-144.

Neuman, J.A., Huey, L.G., Ryerson, T.B. and Fahey, D.W. (1999) Study of inlet materials for sampling atmospheric nitric acid. *Environmental Science and Technology*. **33**, 1133-1136.

Perez, I.M., Wooldridge, P.J. and Cohen, R.C. (2007) Laboratory evaluation of a novel thermal dissociation chemiluminescence method for in situ detection of nitrous acid. *Atmospheric Environment*. **41**, 3993-4001.

Roberts, J.M. (1990) The atmospheric chemistry of organic nitrates. *Atmospheric Environment*. **24**, 243-287.

Val Martin, M., Honrath, R.E., Owen, R.C. and Li, Q.B. (2008) Seasonal variation of nitrogen oxides in the central North Atlantic lower free troposphere. *Journal of Geophysical Research*. **113**, D17307.

Warneck, P. and Zerbach, T. (1992) Synthesis of peroxyacetyl nitrate in air by acetone photolysis. *Environmental Science and Technology*. **26**, 74-79.

Williams, E.J., Baumann, K., Roberts, J.M., Bertman, S.B., Norton, R.B., Fehsenfeld, F.C., Springston, S.R., Nunnermacker, L.J., Newman, L., Olszyna, K., Meagher, J., Hartsell, B., Edgerton, E., Pearson, J.R. and Rodgers, M.O. (1998) Intercomparison of ground-based NOy measurement techniques. *Journal of Geophysical Research*. **103**, D17 22261-22280.

Appendices

Appendix 1. The complete sampling log from the ACTRIS workshop at the Hohenpeißenberg Observatory, Germany (see section 3.3).

Date	Time	Sample Mixture
Nov., 12.	1639	10 ppb NO
	1727	Zero air
	1749	5 ppb NO
Nov., 13.	0712	Zero air
	0947	45.4 ± 0.2 ppb NO
	1030	Add O_3 (35 ppb) →7.8 ± 0.1 ppb NO + 38.0±0.3 ppb NO2
	1100	Zero air
	1130	5 ppb NO
	1200	15 ppb NO
	1235	40 ppb NO
	1300	Zero air
	1400	≈ 44 ppb NO + ≈ 8 ppb O_3
	1444	≈ 44 ppb NO + ≈ 17 ppb O_3
	1530	≈ 44 ppb NO + ≈ 42 ppb O_3
	1632	Zero air
	1708	Ambient air
Nov., 14.	1233	Zero air
	1400	Ambient air
	1432	Ambient air + ≈ 8ppb NO
	1501	Ambient air + ≈ 8 ppb NO + ≈ 4 ppb O_3
	1530	Ambient air + ≈ 12 ppb NO + ≈ 6 ppb O_3
	1600	Ambient air
	1630	Zero air
	1655	≈ 1 ppb NO. *Unstable signal due to problems with MFC*
	1734	Ambient air
Nov., 15.	0919	Ambient air + ≈ 4 ppb HNO_3
	0953	Ambient air + ≈ 20 ppb NH_3
	1032	Ambient air (without HNO_3 / NH_3)
	1300	Zero air dew point -7.77°C
	1422	Zero air + ≈ 20 ppb NO + ≈ 14 ppb O_3
	1507	d.p.: -6.50°C
	1510	Add H_2O: 10 L min^{-1} humid air + 2 L min^{-1} NO/O_3 mixture + 33 L min^{-1} dry air. *This resulted in lower mixing ratios due to larger dilution (45 instead of 40 L min^{-1}) by factor of 0.89*
	1510	d.p.: -4.61 °C
	1520	d.p.: -4.42 °C
	1523	d.p.: -4.41 °C
	1528	d.p.: -4.47 °C
	1530	d.p.: between -4.4 and -4.6 °C
	1531	d.p.: -4.5 °C
	1533	d.p.: -4.54 °C
	1535	d.p.: -4.55 °C

Appendix 1. Continued.

Nov., 15.	1536	d.p.: -4.57 °C
	1639	d.p.: -4.62 °C
	1542	20 L min^{-1} humid air + 2 L min^{-1} NO/O_3 mixture + 18 L min^{-1} dry air
	1545	d.p.: -0.26 °C
	1547	dew point: -0.28 °C
	1550	dew point: -0.28 °C
	1551	dew point: -0.30 °C
	1552	dew point: -0.31 °C
	1553	dew point: -0.30 °C
	1555	dew point: -0.29 °C
	1609	dew point: -0.34 °C
	1629	38 L min^{-1} humid air + 2 L min^{-1} NO/O_3 mixture
	1632	dew point: 9.33 °C
	1635	dew point: 9.14 °C
	1646	dew point: 8.79 °C
	1701	dew point: 8.68 °C
	1705	dry zero air
	1715	zero air + ≈ 4 ppb HNO_3
	1738	zero air
	1756	Relaxation experiment for measurement of LOD
	1816	Relaxation experiment for measurement of LOD. *Higher concentration*
	1916	Ambient air
Nov., 16.	0955	Zero air
	1007	Zero air + HNO_3 (≈ 5 ppb)
	1037	d.p.: 7.02 °C
	1038	d.p.: 7.2 °C
	1041	d.p.: 7.12 °C
	1044	d.p.: 7.1 °C
	1103	Only H_2O *(no HNO_3)*
	1116	Dry zero air
	1128	≈ 30 ppb NO + 40 ppb NO_2
	1153	≈ 15 ppb NO + 20 ppb NO_2
	1238	Zero air
	1402	5 ppb NO_2
	1423	2.5 ppb NO_2
	1437	1.25 ppb NO_2
	1449	Zero air
	1500	Ambient air

Appendix 2. List of measurement species, measured permanently at the CVAO by the University of York, including method of detection and duration of measurements (adapted from Caprenter et al., 2011).

Measurements	Instrument	Duration
Meteorological data at 4, 10 and 30 m	Automatic Weather Station	Oct. 2006 - Present
Solar radiation	Spectral Radiometer	Apr. 2008 - Present
JO^1D	Radiometer	Jan. - Feb. 2007, May - Jun. 2007, Apr. 2008 - Present
Ozone	UV Absorption TEI 49 C and 49i	Oct. 2006 - Present
Carbon Monoxide	VUV Fluorescence, Aerolaser 5001	Oct. 2006 - Present
NO_x	Chemiluminescence, Air Quality Design	Oct. 2006 - Present
C_2-C_8 NMVOCs and DMS	Dual Channel GC-FID	Oct. 2006 - Present
Methanol, Acetone and Acetaldehyde	Dual Channel GC-FID	Oct. 2006 - Present
Halocarbons	GC-MS	May 2007, Sep. 2007 - Jan. 2008, Sep. 2009 - Present

Bibliography

Acker, K., Möller, D., Wieprecht, W., Meixner, F. X., Bohn, B., Gilge, S., Plass-Dülmer, C. and Berresheim, H. (2006) Strong Daytime Production of OH from HNO_2 at a Rural Mountain Site, Geophysical Research Letters. 33, L02809.

Alapati, K., Raman, S., 1989. A study of the seasonal migration of ITCZ and the quasi-periodic oscillations in a simple monsoon system using an energy balance model. *Meteorology and Amospheric Physics*. 41, 191-211.

Aschmann, S.M., Tuazon, E.C., Arey, J. and Atkinson, R. (2011) Products of the OH radicalinitiated reactions of 2-propyl nitrate, 3-methyl-2-butyl nitrate and 3-methyl-2-pentyl nitrate. *Atmospheric Environment*. **45**, 1695-1701.

Aschmann, S.M., Areya, J. and Atkinson, R. (2012) Products of the OH radical-initiated reactions of 2- and 3-hexyl nitrate. *Atmospheric Environment*. **46**, 264-270.

Atkinson, R., Ashmann, S.M., Carter, W.P.L. and Winer, A.M. (1982) Kinetics of the gas-phase reactions of OH radicals with alkyl nitrates at 299 ± 2K. *International Journal of Chemical Kinetics*. **14**, 919-926.

Atkinson, R., Carter, W.P.L. and Winer, A.M. (1983) Effects of temperature and pressure of alkyl nitrate yields in the photo oxidations of n-pentane and n-heptane. *Journal of Physical Chemistry*. **87**, 2012-2018.

Atkinson, R. (2007) Rate constants for the atmospheric reactions of alkoxy radicals: An updated estimation method. *Atmospheric Environment.* **41**, 8468-8485.

Atlas, E., Pollock, W., Greenberg, J. and Heidt, L. (1993) Alkyl nitrates, nonmethane hydrocarbons and halocarbon gases over the equatorial Pacific Ocean during Saga 3. *Journal of Geophysical Research.* **98**, 16933-16,947.

Ayers, G., Penkett, S., Gillett, R., Bandy, B., Galbally, I., Meyer, C., Elsworth, C., Bentley, S. and Forgan, B. (1996) The annual cycle of peroxides and ozone in marine air at Cape Grim, Tasmania. *Journal of Atmospheric Chemistry*. **23**, 221-252.

Ayers, G.P., Granek, H. and Boers, R. (1997) Ozone in the marine boundary layer at Cape Grim: Model simulation. *Journal of Atmospheric Chemistry*. **27**, 179-175.

Barket, D.J., Hurst, J.M., Couch, T.L., Colorado, A., Shepson, P.B., Riemer, D.D., Hills, A.J., Apel, E.C., Hafer, R., Lamb, B.K., Westberg, H.H., Farmer, C.T., Stabenau, E.R. and Zika, R.G. (2001) Intercomparison of automated methodologies for determination of ambient isoprene during the PROPHET 1998 summer campaign. *Journal of Geophysical Research - Atmospheres.* **106**, D20 24301-24313.

Barker, J.R., Benson, S.W., Mendenhall, G.D. and Goldern, D.M. (1977) Measurment of rate constants of importance in smog. *Report PB-274530, National Technological Information Service*. Springfield, Va., USA.

Barnes, I., Bastian, V., Becker, K.H. and Tong, Z. (1990) Kinetics and products of the reactions of NO3 with monoalkenes, dialkenes, and monoterpenes. *Journal of Physcial Chemistry*. **94**, 2413-2419.

Bertman, S.B., Roberts, J.M., Parrish, D.D., Buhr, M.P., Goldan, P.D., Kuster,W.C., Fehsenfeld, F.C., Montzka, S.A., and Westberg, H. (1995) Evolution of alkyl nitrates with air-mass age *Journal of Geophysical Research*. **100**, 22805-22813.

Blake, N.J., et al., 2003. Latitudinal, vertical, and seasonal variations of C1–C4 alkyl nitrates in the troposphere over the Pacific Ocean during PEM-Tropics A and B: oceanic and continental sources. *Journal of Geophysical Research.* **108**, D2 8242.

Bloss, W., Evans, M., Lee, J.D., Sommariva, R., Heard, D. and Pilling, M. (2005) The oxidative capacity of the troposphere: Coupling of field measurements of OH and a global chemistry transport model. *Faraday Discussions*. **130**, 425-436.

Brewer, A., 1949. Evidence for a world circulation provided by the measurements of helium and water vapour distribution in the stratosphere. *Quarterly Journal of the Royal Meteorological Society*. 75, 351-363.

Bridgeman, C., Pyle, J. and Shallcross, D. (2000) A three-dimensional model calculation of the ozone depletion potential of 1-bromopropane (1-C_3H_7Br). *Journal of Geophysical Research - Atmospheres*. **105**, D21 26493-26502.

Bridier, I., Carulp, F., Loirat, H., Lesclaux, R., Veyret, B., Becker, K.H., Reimer, A. and Zabel, F. (1991) Kinetic and theoretical studies of the reactions CH3C(O)O2=NO2 + M → CH3C(O)O2NO2 + M between 248 and 393 K and between 30 and 760 torr. *Journal of Physical Chemistry*. **95**, 3594–3600.

Brown, S.S., Ryerson, T.B., Wollny, A.G., Brock, C.A., Peltier, R., Sullivan, A.P., Weber, R.J., Dube, W.P., Trainer, M., Meagher, J.F., Fehsenfeld, F.C. and Ravishankara, A.R. (2006) Variability in nocturnal nitrogen oxide processing and its role in regional air quality. *Science*. **311**, 67-70.

Carpenter, L.J, Monks, P.S, Bandy, B., Penkett, S., Galbally, I. and Meyer, C. (1997) A study of peroxy radicals and ozone photochemistry at coastal sites in the northern and southern hemispheres. *Journal of Geophysical Research - Atmospheres*. **102**, D21 25417-25427.

Carpenter, L.J., Clemitshaw, K.C., Burgess, R.A., Penkett, S.A., Cape, J.N. and McFadyen, G.C. (1998) Investigation and evaluation of the NO_x/O_3 photochemical steady state. *Atmospheric Environment.* **32**, 3353-3365.

Carpenter, L.J., Fleming, Z.L., Read, K.A., Lee, J.D., Moller, S.J., Hopkins, J.R., Purvis, R.M., Lewis, A.C., Müller, K., Heinold, B., Herrmann, H., Wadinga Fomba, K., van Pinxteren, D., Müller. C., Tegen, I., Wiedensohler, A., Müller, T., Niedermeier, N., Achterberg, E.P., Patey, M.D., Kozlova, E.A., Heimann, M., Heard, D.E., Plane, J.M.C., Mahajan, A., Oetjen, H., Ingham, T., Stone, D., Whalley, L.K., Evans, M.J., Pilling, M.J., Leigh, R.J., Monks, P.S., Karunaharan, A., Vaughan, S., Arnold, S.R., Tschritter, J., Pöhler, D., Frieß, U., Holla, R., Mendes, L.M., Lopez, H., Faria, B., Manning, A.J. and Wallace, D.W.R. (2010) Seasonal characteristics of tropical marine boundary layer air measured at the Cape Verde Atmospheric Observatory. *Journal of Atmospheric Chemistry*. **67**, 87-140.

Carsey, T., Churchill, D., Farmer, M., Fischer, D., Pszenny, A., Ross, V., Saltzmann, E., Springer-Young, M. and Bonsang, B. (1997). Nitrogen oxides and ozone production in the North Atlantic marine boundary layer. *Journal of Geophysical Research - Atmospheres*. **102**, 10653-10665.

Chen, X.H., Hulbert, D. and Shepson, P.B. (1998) Measurement of the organic nitrate yield from OH reaction with isoprene. *Journal of Geophysical Research - Atmospheres.* ***103****,* D19 25563-25568.

Cleary, P., Wooldridge, P. and Cohen, R. (2002) Laser-induced fluorescence detection of atmospheric NO_2 with a commercial diode laser and a supersonic expansion. *Applied Optics*. **41**, 6950-6956.

Cleary, P.A., Wooldridge, P.J., Millet, D.B., McKay, M., Goldstein, A.H. and Cohen, R.C. (2007) Observations of total peroxy nitrates and aldehydes: Measurement interpretation and inference of OH radical concentrations. *Atmospheric Chemistry and Physics*. **7**, 1947-1960.

Conley, S.A., Faloona, I.C., Lenschow, D.H., Campos, T., Heizer, C., Weinheimer, A., Cantrell. C.A., Mauldin, R.L., Hornbrook, R.S., Pollack, I. and Bandy, A. (2011) A complete dynamical ozone budget measured in the tropical marine boundary layer during PASE. *Journal of Atmospheric Chemistry*. **68**, 55-70.

Cornell, S.E., Jickells, T.D., Cape, J.N., Rowland, A.P. and Duce, R.A. (2003) Organic nitrogen deposition on land and coastal environments: A review of methods and data. *Atmospheric Environment*. **37**, 2173-2191.

Crawford, J., Davis, D., Chen, G., Bradshaw, J., Sandholm, S., Gregory, G., Sachse, G., Anderson, B., Collins, J., Blake, D., Singh, H., Heikes, B., Talbot, R., Rodriguez, J., 1996. Photostationary state analysis of the NO2-NO system based on airborne observations from the western and central North Pacific. *Journal of Geophysical Research-Atmospheres*. 101, 2053-2072.

Crutzen, P. J., 1986. The role of the tropics in atmospheric chemistry, in Geophysiology of Amazonia. John Wiley, New York.

Crutzen, P.J., Lelieveld, J. and Bruehl, C. (1994) Advances in Environmental Science and Technology. Wiley, New York.

Crutzen, P. (1998) How the atmosphere keeps itself clean and how this is affected by human activities. *Pure and Applied Chemistry*. **70**, 1319-1326.

Cwiertny, D.M., Baltrusaitis, J., Hunter, G.J., Laskin, A., Scherer, M.M. and Grassian, V.H. (2008) Characterization and acid-mobilization study of iron-containing mineral dust source materials. *Journal of Geophysical Research - Atmospheres*. **113**, D05202.

Dahl, E.E., Saltzman, E.S. and de Bruyn, W.J. (2003) The aqueous phase yield of alkyl nitrates from ROO + NO: Implications for photochemical production in seawater. *Geophysical Research Letters.* 30, 1271.

Dahl, E.E., Yvon-Lewis, S.A. and Saltzman, E.S. (2005) Saturation anomalies of alkyl nitrates in the tropical Pacific Ocean. *Geophysical Research Letters*. **32**, L20817.

Dahl, E.E., Yvon-Lewis, S.A. and Saltzman, E.S. (2007) Alkyl nitrate (C1–C3) depth profiles in the tropical Pacific Ocean. *Journal of Geophysical Research*. **112**, C01012.

Dahl, E.E. and Saltzman, E.S. (2008) Alkyl nitrate photochemical production rates in North Pacific seawater. *Marine Chemistry*. **112**, 137-141.

Dall'Osto, M., Harrison, R.M., Coe, H., Williams, P.I. and Allan, J.D. (2009) Real time chemical characterization of local and regional nitrate aerosols. *Atmospheric Chemistry and Physics*. **9**, 3709-3720.

Dari-Salisburgo, C., Di Carlo, P., Giammaria, F., Kajii, Y., D'Altorio, A. (2009) Laser induced fluorescence instrument for NO_2 measurements: Observations at a central Italy background site. *Atmospheric Environments.* **43**, 970-977.

Day, D.A., Wooldridge, P.J., Dillon, M.B., Thornton, J.A. and Cohen, R.C. (2002) A thermal dissociation laser-induced fluorescence instrument for in situ detection of NO2, peroxy nitrates, alkyl nitrates, and HNO_3. *Journal of Geophysical Research*. **107**, D64046.

Day, D.A., Dillon, M.B., Wooldridge, P.J., Thornton, J.A., Rosen, R.S., Wood, E.C. and Cohen, R.C. (2003) On alkyl nitrates, O3, and the "missing NOy,". *Journal of Geophysical Research*. **108**, D16 4501.

Day, D.A., Wooldridge, P.J. and Cohen, R.C. (2009) Observations of the effects of temperature on atmospheric HNO_3, ΣANs, ΣPNs, and NO_x: Evidence for a temperature-dependent HO_x source. *Atmospheric Chemistry and Physics*. **8**, 1867-1879.

Derwent, R., Stevenson, D., Collins, W. and Johnson, C. (2004). Intercontinental transport and the origins of the ozone observed at surface sites in Europe. *Atmospheric Environment*. **38**, 1891-1901.

Deyfrus, G.B., Schade, G.W. and Goldstein, A.H. (2002) Observational constraints on the contribution of isoprene oxidation to ozone production on the western slope of the Sierra Nevada, California. *Journal of Geophyscial Research - Atmospheres.***107**, D19 4365.

Dickerson, R., Rhoads, K., Carsey, T., Oltmans, S., Burrows, J. and Crutzen, P. (1999) Ozone in the remote marine boundary layer: A possible role for halogens. *Journal of Geophysical Research – Atmospheres*. **104**, D17 21385-21395.

Dobson, G. M. B., 1956. Origin and distribution of the plolyatomic molecules in the atmosphere. *Proceedings of the Royal Society of London. Series A, Mathematical and Physical Sciences*. 236, 187-193.

Drummond, J., Volz, A. and Ehhalt, D. (1985) An optimized chemiluminescence detector for tropospheric NO measurements. *Journal of Atmospheric Chemistry*. **2**, 287-306.

Elshorbany, Y.F., Kurtenbach, R., Wiesen, P., Lissi, E., Rubio, M., Villena, G., Gramsch, E., Rickard, A. R., Pilling, M. J. and Kleffmann, J. (2009) Oxidation capacity of the city air of Santiago, Chile. *Atmospheric Chemistry and Physics*. **9**, 2257-2273.

Fahey, D.W., Hubler, G., Parrish, D.D., Williams, E.J., Norton, R.B., Ridley, B.A., Singh, H.B., Liu, S.C. and Fehsenfeld, F.C. (1986) Reactive nitrogen species in the troposphere: Measurements of NO, NO_2, HNO_3, particulate nitrate, peroxyacetyl nitrate (PAN), O3, and total reactive odd nitrogen (NOy) at Niwot Ridge, Colorado. *Journal of Geophysical Research*. **91**, 9781-9793.

Farman, J., Gardiner, B., Shanklin, J., 1985. Large losses of total ozone in Antarctica reveal seasonal ClOx/NOx interaction. Nature. 315, 207-210.

Farmer, D.K. and Cohen, R.C. (2008) Observations of HNO3, ΣAN, ΣPN and NO_2 fluxes: evidence for rapid HO_x chemistry within a pine forest canopy. *Atmospheric Chemistry and Physics*. **8**, 3899-3917.

Finlayson-Pitts, B. J., Pitts, J. N., 2000. Chemistry of the Upper and Lower Atmosphere (1st Edition). Academic Press.

Fischer, R.G., Kastler, J. and Ballschmiter, K. (2000) Levels and pattern of alkyl nitrates, multifunctional alkyl nitrates, and halocarbons in the air over the Atlantic Ocean. *Journal of Geophysical Research - Atmospheres.* **105**, D11 14473-14494.

Fleming, Z.L., Monks, P.S. and Manning, A.J. (2012) Review: Untangling the influence of air-mass history in interpreting observed atmospheric composition. *Atmospheric Research*. **104**, 1–39.

Forster, P., Ramaswamy, V., Artaxo, P., Berntsen, T., Betts, R., Fahey, D.W., Haywood, J., Lean, J., Lowe, D.C., Myhre, G., Nganga, J., Prinn, R., Raga, G., Schulz, M. and Van Dorland. R. (2007) Changes in Atmospheric Constituents and in Radiative Forcing, *In*, Climate Change 2007: The Physical Science Basis. Contribution of Working Group I to the Fourth Assessment Report of the Intergovernmental Panel on Climate Change. (Solomon, S., Qin, D., Manning, M., Chen, Z., Marquis, M., Averyt, K.B., Tignor, M. and Miller, H.L. Eds.). Cambridge University Press, Cambridge.

Galbally, I., Bentley, S. and Meyer, C. (2000) Mid-latitude marine boundary layer ozone destruction at visible sunrise observed at Cape Grim, Tasmania. *Geophysical Research Letters*. **27**, 3841-3844.

Garratt, J. R., 1992. The Atmospheric Boundary Layer. Cambridge University Press.

Geyer, A., Alicke, B., Ackermann, R., Martinez, M., Harder, H., Brune, W., di Carlo, P., Williams, E., Jobson, T., Hall, S., Shetter, R. and Stutz, J. (2003) Direct observations of daytime NO_3: Implications for urban boundary layer chemistry. *Journal of Geophysical Research - Atmospheres.* **108**, D12 4368.

Giacopelli, P., Ford, K., Espada, C. and Shepson, P.B. (2005) Comparison of the measured and simulated isoprene nitrate distributions above a forest canopy. *Journal of Geophysical Research*. **110**, D01304.

Gilge. S., Plass-Duelmer, C., Fricke, W., Kaiser, A., Ries, L., Buchmann, B. and Steinbacher, M. (2010) Ozone, carbon monoxide and nitrogen oxides time series at four alpine GAW mountain stations in central Europe. *Atmospheric Chemistry and Physics*. **10**, 12295-12316.

Glaenzer, K. and Troe, J. (1974) Thermal decomposition of nitrocompounds in shock waves. IV. Decomposition of nitic acid. *Berichte Der Bunsen-Gesellschaft-Physical Chemistry Chemical Physics.* **78**, 71.

Grossenbacher, J.W., Barket, D.J., Shepson, P.B., Carroll, M.A., Olszyna, K. and Apel, E. (2004) A comparison of isoprene nitrate concentrations at two forest-impacted sites. *Journal of Geophysical Research*. **109**, D11311.

Hauglustaine, D.A., Madronich, S., Ridley, B.A., Flocke, S.J., Cantrell, C.A., Eisele, F.L., Shetter, R.E., Tanner, D.J., Ginoux, P. and Atlas, E.L. (1999) Photochemistry and budget of ozone during the Mauna Loa Observatory Photochemistry Experiment (MLOPEX 2). *Journal of Geophysical Research - Atmospheres*. **104**, 30275–30307.

He, S., Chen, Z. and Zhang, X. (2011) Photochemical reactions of methyl and ethyl nitrate: A dual role for alkyl nitrates in the nitrogen cycle. *Environmental Chemistry*. **8**, 529-542.

Heikes, B., Lee, M.H., Jacob, D., Talbot, R., Bradshaw, J., Singh, H., Blake, D., Anderson, B., Fuelberg, H. and Thompson, A.M. (1996) Ozone, hydroperoxides, oxides of nitrogen, and hydrocarbon budgets in the marine boundary layer over the South Atlantic. *Journal of Geophysical Research - Atmospheres*. **101**, 24221–24234.

Hiskey, M.A., Brower, K.R. and Oxley, J.C. (1991) Thermal decomposition of nitrate esters. *Journal of Physical* Chemistry. 95, 3955.

Hering, S.V., Lawson, D.R., Allegrini, I., Febo, A., Perrino, C., Possanzini, M., Sickles, J.E., Anlauf, K.G., Wiebe, A., Appel, B.R., John, W., Ondo, J., Wall, S., Braman, R.S., Sutton, R., Cass, G.R., Solomon, P.A., Eatough, D.J., Eatough, N.L., Ellis, E.C., Grosjean, D., Hicks, B.B., Womack, J.D., Horrocks, J., Knapp, K.T., Ellestad, T.G., Paur, R.J., Mitchell, W.J., Pleasant, M., Peake, E., Maclean, A., Pierson, W.R., Brachaczek, W., Schiff, H.I., Mackay, G.I., Spicer, C.W., Stedman, D.H., Winer, A.M., Biermann, H.W. And Tuazon, E.C. (1988) The nitric acid shootout - field comparison of measurement methods. *Atmospheric Environment*. **22**, 1519-1539.

Horowitz, L., Walters, S., Mauzerall, D., Emmons, L., Rasch, P., Granier, C., Tie, X., Lamarque, J., Schultz, M., Tyndall, G., Orlando, J. and Brasseur, G. (2003) A global simulation of tropospheric ozone and related tracers: Description and evaluation of MOZART, version 2. *Journal of Geophysical Research - Atmospheres*. **108**, D24 4784-4813.

Horowitz, L.W., Fiore, A.M., Milly, G.P., Cohen, R.C., Perring, A., Wooldridge, P.J., Hess, P.G., Emmons, L.K. and Lamarque, J.F. (2007) Observational constraints on the chemistry of isoprene over the Eastern U.S. *Journal of Geophysical Research - Atmospheres.* **112**, D12S08.

Horii, C.V., Munger, J.W., Wofsy, S.C., Zahniser, M., Nelson, D. and McManus, J.B. (2006) Atmospheric reactive nitrogen concentration and flux budgets at a Northeastern US forest site. *Agricultural and. Forest Meteorology*. **136**, 159-174.

Hosaynali-Beygi. Z., Fischer. H., Harder. H.D., Martinez, M., Sander, R., Williams, J., Brookes, D.M., Monks, P.S. and Lelieveld, J. (2011) Oxidation photochemistry in the Southern Atlantic boundary layer: Unexpected deviations of photochemical steady state. *Atmospheric Chemistry and Physics*. **11**, 8497-8513.

Hudman, R.C., Jacob, D.J., Cooper, O.C., Evans, M.J., Heald, C.L. Park., R.J., Fehsenfeld, F., Flocke, F., Holloway, J., Hubler, G., Kita, K., Koike, M., Kondo, Y., Neuman, A., Nowak, J., Oltmans, S., Parrish, D., Roberts, J.M. and Ryerson, T. (2004) Ozone production in transpacific Asian pollution plumes and implications for ozone air quality in California. *Journal of Geophysical Research.* **109**, D23S10.

Indarto, A. (2012) Heterogeneous reactions of HONO formation from NO2 and HNO3: A review. *Research Chemistry Intermediates*. 38, 1029-1041.

IPCC Core Writing Team, Pachauri, R., Reisinger, A., 2007. Intergovernmental Panel for Climate Change (IPCC) Fourth Assessment Report: Climate Change 2007. Technical report.

Jacob, D.J., Logan, J.A., Gardner, G.M., (1993) factors regulating ozone over the united-states and its export to the global atmosphere. *Journal of Geophysical Research - Atmospheres*. **98**, D8 14817-14826.

Jacob, D., Heikes, B., Fan, S., Logan, J., Mauzerall, D., Bradshaw, J., Singh, H., Gregory, G., Talbot, R., Blake, D. and Sachse, G. (1996) Origin of ozone and NO_x in the tropical troposphere: A photochemical analysis of aircraft observations over the South Atlantic basin. *Journal of Geophysical Research - Atmospheres*. **101**, D19 24235-24250.

Jacobi, H., Weller, R., Bluszcz, T. and Schrems, O. (1999) Latitudinal distribution of peroxyacetyl nitrate (PAN) over the Atlantic Ocean. *Journal of Geophysical Research - Atmospheres*. **104**, D21 26901-{26912.

Jaegle, L., Jacob, D., Wang, Y., Weinheimer, A., Ridley, B., Campos, T., Sachse, G., Hagen, D., 1998. Sources and chemistry of NOx in the upper troposphere over the United States. *Geophysical Research Letters*. 25, 1705-1708.

Jo, C.O., Lee, J.Y., Park, K.A., Kim, Y.H. and Kim, K.R. (2007) Asian dust initiated early spring bloom in the northern East/Japan Sea. *Geophysical Research Letters*. **34**, L05602.

Jordan, C.E. and Talbot, R.W. (2000) Direct atmospheric deposition of water-soluble nitrogen to the Gulf of Maine. *Global Biogeochemical Cycles*. **14**, 1315-1329.

Kirchner, F., Mayer-Figge, A., Zabel, F. and Becker, K.H. (1999) Thermal stability of peroxynitrates. *International Journal of Chemical Kinetics*. **31**, 127-144.

Kley, D. and McFarland, M. (1980) Chemiluminescence detector for NO and NO2. *Atmospheric Technology*. **12**, 63-69.

Knudsen, B.M., Rosen, J.M., Kjome, N.T. and Whitten, A.T. (1996) Comparison of analysed stratospheric temperatures and calculated trajectories with long-duration balloon data. *Journal of Geophysical Research*. **101**, 19137-19145.

Kulmala, M., Laaksonen, A., Charlson, R.J. and Korhonen, P. (1997) Clouds without supersaturation. *Nature*, **338**, 336-337.

LaFranchi, B.W., Wolfe, G.M., Thornton, J.A., Harrold, S.A., Browne, E.C., Min, K.E., Wooldridge, P.J., Gilman, J.B., Kuster, W.C., Goldan, P.D., deGouw, J.A., McKay, M., Goldstein, A.H., Ren, X., Mao, J. and Cohen, R.C. (2009) Closing the peroxy acetyl (PA) radical budget: observations of acyl peroxy nitrates (PAN, PPN, and MPAN) during BEARPEX 2007. *Atmospheric Chemistry and Physics* Discussions. **9**, 9879-9926.

Lee, J.D., Moller, S.J., Read, K.A., Lewis, A.C., Mendes, L. and Carpenter, L.J. (2009) Year-round measurements of nitrogen oxides and ozone in the tropical North Atlantic marine boundary layer. *Journal of Geophysical Research*. **114**, D21302.

Leighton, P. A. (1961) Photochemistry of air pollution. *Physical Chemistry*. **9**, 300.

Lelieveld, J., Dentener, F., 2000. What controls tropospheric ozone? *Journal of Geophysical Research - Atmospheres*. 105, 3531-3551.

Lelieveld, J., Van Aardenne, J., Fischer, H., de Reus, M., Williams, J. and Winkler, P. (2004) Increasing ozone over the Atlantic Ocean. *Science*. 304, 1483-1487.

Liao, H., Seinfeld, J.H., Adams, P.J. and Mickley, L.J. (2004) Global radiative forcing of coupled tropospheric ozone and aerosols in a unified general circulation model. *Journal of Geophysical Research*. **109**, D16207.

Liu, S.C., McFarland, M., Kley, D., Zafiriou, O. and Huebert, B. (1983) Tropospheric NO_x and O_3 budgets in the Equatorial Pacific. *Journal of Geophysical Research - Atmospheres*. **88**, 1360-1368.

Liu, S.C., Trainer, M., Fehsenfeld, F.C., Parrish, D.D., Williams, E.J., Fahey, D.W., Hubler, G. And Murphy, P.C. (1987) Ozone production in the rural troposphere and the implications for regional and global ozone distributions. *Journal of Geophysical Research – Atmospheres*. **92**, D4 4191-4207.

Lovett, G.M. (1994) Atmospheric deposition of nutrients and pollutants in North America: An ecological perspective. *Ecological Applications*. **4**, 629-650.

Luke, W.T., Dickerson, R.R. and Nunnermacker, L.J. (1989) Direct measurements of the photolysis rate cofficients and Henry's Law constants of several alkyl nitrates. *Journal of Geophysical Research.* **94**, 14905.

Makkonen, R., Romakkaniemi, S., Kokkola, H., Stier, P., aisänen, P.R., Rast, S., Feichter, J., Kulmala, M. and Laaksonen, A. (2012) Brightening of the global cloud field by nitric acid and the associated radiative forcing. *Atmospheric Chemistry and Physics*. **12**, 7625-7633.

Malm, W.C., Schichtel, B.A., Pitchford, M.L., Ashbaugh, L.L. and Eldred, R.A. (2004) Spatial and monthly trends in speciated fine particle concentration in the United States. *Journal of Geophysical Research - Atmospheres*. **109**, D03306.

Mannschreck, K., Gilge, S., Plass-Duelmer, C., Fricke, W. and Berresheim, H. (2004) Assessment of the applicability of $NO\text{-}NO_2\text{-}O_3$ photostationary state to long-term measurements at the Hohenpeissenberg GAWStation, Germany. *Atmospheric Chemistry and Physics.* 4, 1265-1277.

Matsumoto, J., Kosugi, N., Nishiyama, A., Isozaki, R., Sadanaga, Y., Kato, S., Bandow, H. and Kajii, Y. (2006) Examination on photostationary state of NO_x in the urban atmosphere in Japan, *Atmospheric Environment*. **40**, 3230-3239.

Min, K.E., Pusede, S.E., Browne, E.C., LaFranchi, B.W., Wooldridge, P.J., Wolfe, G.M., Harrold, S.A., Thornton, J.A. and Cohen, R.C. (2012) Observations of atmosphere-biosphere exchange of total and speciated peroxynitrates: nitrogen fluxes and biogenic sources of peroxynitrates. *Atmospheric Chemistry and Physcis*. **12**, 9763-9773.

Miyazaki,K., Matsumoto, J., Kato, S. and Kajii, Y. (2008) Development of atmospheric NO analyser by using a laser-induced fluorescence NO_2 detector. *Atmospheric Environment*. **42**, 7812-7820.

Montanya, J., Soula, S. and Pineda, N. (2007) A study of the total lightning activity in two hailstorms. *Journal of Geophysical Research - Atmospheres*. **112**, D13118.

Moxim, W.J., Levy, H. and Kasibhatla, P.S. (1996) Simulated global tropospheric PAN: Its transport and impact on NO_x. *Journal of Geophysical Research - Atmospheres.* **101**, D7 12621-12638.

Murphy, J.G., Thornton, J.A., Wooldridge, P.J., Day, D.A., Rosen, R.S., Cantrell, C., Shetter, R.E., Lefer, B. and Cohen, R.C. (2004) Measurements of the sum of HO_2NO_2 and $CH_3O_2NO_2$ in the remote troposphere. *Atmospheric Chemistry and Physcis.* **4**, 377-384.

Neu, J.L., Lawler, M.J., Prather, M.J. and Saltzman, E.S. (2008) Oceanic alkyl nitrates as a natural source of tropospheric ozone. *Geophysical Research Letters.* **35**, L13814.

Neuman, J.A., Huey, L.G., Ryerson, T.B. and Fahey, D.W. (1999) Study of inlet materials for sampling atmospheric nitric acid. *Environmental Science and Technology*. **33**, 1133-1136.

Neuman, J.A., et al. (2006) Reactive nitrogen transport and photochemistry in urban plumes over the North Atlantic Ocean. *Journal of Geophysical Research.* **111**, D23S54.

Nielsen, T., Egelov, A.H., Granby, K. and Skov, H. (1995) Observations on particulate organic nitrates and unidentified components of NO_y. *AtmosphericEnvironment*. **29**, 1757-1769.

Nowak, J.B., Neuman, J.A., Bahreini, R., Brock, C.A., Middlebrook, A.M., Wollny, A.G., Holloway, J.S., Peischl, J., Ryerson, T.B. and Fehsenfeld, F.C. (2010) Airborne observations of ammonia and ammonium nitrate formation over Houston, Texas. *Journal of Geophysical Research - Atmospheres*. **115**, D22304.

Orlando, J.J. and Tyndall, G.S. (2002) Mechanisms for the reactions of OH with two unsaturated aldehydes: Crotonaldehyde and acrolein. *Journal of Physical Chemistry*. **106**, 12252-12259.

Orsolini, Y.J., Urban, J. and Murtagh, D.P. (2008) Nitric acid in the stratosphere based on Odin observations from 2001 to 2007 – Part 2: High-altitude polar enhancements, *Atmospheric Chemistry and Physics.* **8**, 9591, 9605.

Osthoff, H., Brown, S., Ryerson, T., Fortin, T., Lerner, B., Williams, E., Pettersson, A., Baynard, T., Dube, W., Ciciora, S. and Ravishankara, A. (2006) Measurement of atmospheric NO_2 by pulsed cavity ring-down spectroscopy. *Journal of Geophysical Research - Atmospheres*. **111**, D12305.

Osthoff, H., Brown, S., Ryerson, T., Fortin, T., Lerner, B., Williams, E., Pettersson, A., Baynard, T., Dube, W., Ciciora, S. and Ravishankara, A. (2006) Measurement of atmospheric NO_2 by pulsed cavity ring-down spectroscopy. *Journal of Geophysical Research - Atmospheres*. **111**, D12305.

Owens, N.J.P., Galloway, J.N. and Duce, R.A. (1992) Episodic atmospheric nitrogen deposition to oligotrophic ocEANS. *Nature*. **357**, 397-399.

Paerl, H.W. (1985) Enhancement of marine primary production by nitrogen-enriched acid-rain. *Nature*. **6022**, 747-749.

Parrish, D.D., Trainer, M., Williams, E.J., Fahey, D.W., Hubler, G., Eubank, C.S., Liu, S.C., Murphy, P.C., Albritton, D.L. and Fehsenfeld, F.C. (1986) Measurements of the NO_x-O_3 Photostationary State at Niwot Ridge, Colorado. *Journal of Geophysical Research - Atmospheres*. **91**, 5361-5370.

Parrish, D., Trainer, M., Young, V., Goldan, P., Kuster, W., Jobson, B., Fehsenfeld, F., Lonneman, W., Zika, R., Farmer, C., Riemer, D. and Rodgers, M. (1998) Internal consistency tests for evaluation of measurements of anthropogenic hydrocarbons in the troposphere. *Journal of Geophysical Research - Atmospheres.***103**, D17 22339-22359.

Parrish, D.D., Millet, D.B. and Goldstein, A.H. (2009) Increasing ozone in marine boundary layer inflow at the west coasts of North America and Europe. *Atmospheric Chemistry and Physics*. **9**, 1303-1323.

Parton, W.J., Hartman, M., Ojima, D. and Schimel, D. (1998) DAYCENT and its land surface submodel: Description and testing. *Global and Planetary Change*. **19**, 35-48.

Penkett, S., Volz-Thomas, A., Parrish, D., Honrath, R. and Fehsenfeld, F. (1998) Special section: North Atlantic Regional Experiment (NARE II) - preface. *Journal of Geophysical Research – Atmospheres.* **103**, D11 13353-13355.

Perez, I.M., Wooldridge, P.J. and Cohen, R.C. (2007) Laboratory evaluation of a novel thermal dissociation chemiluminescence method for in situ detection of nitrous acid. *Atmospheric Environment*. **41**, 3993-4001.

Perring, A.E., Wisthaler, A., Graus, M., Wooldridge, P.J., Lockwood, A.L., Mielke, L.H., Shepson, P.B., Hansel, A. and Cohen, R.C. (2009) A product study of the isoprene + NO_3 reaction. *Atmospheric chemistry and Physics Discussions*. **9**, 5231-5261.

Plane, J.M.C. and Smith, N. (1995) Atmospheric monitoring by differential optical absorption spectroscopy, *In*, Spectroscopy in Environmental Science. Wiley, New York.

Platt, U. (1994) Differential Optical Absorption Spectroscopy (DOAS), *In*, Air Monitoring by Spectroscopic Techniques. (Sigrist, M.W., Ed.), Wiley, New York. *Chemical Analysis Series*. **127**, 27-84.

Politzer, P., Seminario, J.M., Concha, M.C. and Zacarias, A.G. (1997) Densityfunctional investigation of some decomposition routes of methyl nitrate. *International Journal of Quantum Chemistry.* **64**, 205.

Popp, P.J., Marcy, T.P., Gao, R.S., Watts, L.A., Fahey, D.W., Richard, E.C., Oltmans, S.J., Santee, M.L., Livesey, N.J., Froidevaux, L., Sen, B., Toon, G.C., Walker, K.A., Boone, C.D. and Bernath, P.F. (2009) Stratospheric correlation between nitric acid and ozone. *Journal of Geophysical Research - Atmospheres*. **114**, D03305.

Postgate, J. R. (1982) The fundamentals of nitrogen fixation. Cambridge University Press.

Prinn, R., Weiss, R., Miller, B., Huang, J., Alyea, F., Cunnold, D., Fraser, P., Hartley, D., Simmonds, P., 1995. Atmospheric trends and lifetimes of CH3CCl3 and global OH concentrations. *Science*. 269, 187-192.

Ravishankara, A.R. Daniel, J.S. Portmann, R.W. (2009) Nitrous Oxide (N_2O): The Dominant Ozone-Depleting Substance Emitted in the 21st Century. *Science*. **326**, 123-125.

Read, K., Mahajan, A., Carpenter, L., Evans, M., Faria, B., Heard, D., Hopkins, J., Lee, J.D, Moller, S.J, Mendes, L.A., McQuaid, J., Oetjen, H., Saiz-Lopez, A., Pilling, M. and Plane, J.M.C. (2008) Extensive halogen-mediated ozone destruction over the tropical Atlantic Ocean. *Nature*. **453**, 1232-1235.

Roberts, J.M. (1990) The atmospheric chemistry of organic nitrates. Atmospheric Environment. 24, 243-287.

Roberts, J.M. and Bertman, S.B. (1992) The Thermal Decomposition of PeroxyAcetic Nitric Anhydride (PAN) and Peroxymethacrylic Nitric Anhydride (MPAN). *International Journal of Chemical Kinetics*. **24**, 297-307.

Roberts, J.M., Williams, J., Baumann, K., Buhr, M.P., Goldan, P.D., Holloway, J., Hubler, G., Kuster, W.C., McKeen, S.A., Ryerson, T.B., Trainer, M., Williams, E.J., Fehsenfeld, F.C., Bertman, S.B., Nouaime, G., Seaver, C., Grodzinsky, G., Rodgers, M. and Young, V.L. (1998) Measurements of PAN, PPN, and MPAN made during the 1994 and 1995 Nashville Intensives of the Southern Oxidants Study: Implications for regional ozone production from biogenic hydrocarbons. *Journal of Geophysical Research*. **103**, 22473-22490.

Roberts, J.M., Stroud, C.A., Jobson, B.T., Trainer, M., Hereid, D., Willaims E., Fehsenfeld, F., Brune, W., Martinez, M. and Harder. H. (2001) Application of sequential reaction model to PANs and aldehyde measurements in two urban areas. *Geophysical Research Letters*. **28**, 4583-4596.

Roberts, J.M., Marchewka, M. and Bertman, S.B. (2007) Measurements of PANs during the New England air quality study 2002. *Journal of Geophysical Research - Atmospheres.* **112**, D20306.

Rollins, A.W., Kiendler-Scharr, A., Fry, J.L., Brauers, T., Brown, S.S., Dorn, H.P., Dube, W.P., Fuchs, H., Mensah, A., Mentel, T.F., Rohrer, F., Tillmann, R., Wegener, R., Wooldridge, P.J. and Cohen, R.C. (2009) Isoprene oxidation by nitrate radical: alkyl nitrate and secondary organic aerosol yields. *Atmospheric Chemistry and Physics*. **18**, 6685-6703.

Romakkaniemi, S., Kokkola, H., and Laaksonen, A. (2005) Parameterization of the nitric acid effect on CCN activation. *Atmospheric Chemistry and Physics*. **5**, 879-885.

Russo, R.S., Zhou, Y., Haase, K.B., Wingenter, O.W., Frinak, E.K., Mao, H., Talbot, R.W. and Sive, B.C. (2010) Temporal variability, sources, and sinks of C1-C5 alkyl nitrates in coastal New England. *Atmospheric Chemistry and Physics*. **10**, 1865-1883.

Sander, S., Ravishankara, A., Golden, D., Kolb, C., Kurylo, M., Molina, M., Moortgat, G., Finlayson-Pitts, B., Wine, P., Huie, R. and Orkin, V. (2006) Chemical kinetics and photochemical data for use in atmospheric studies, evaluation number 15. National

Ryall, D.B., Derwent, R.G., Manning, A.J., Simmonds, P.G. and O'Doherty, S. (2001) Estimating source regions of European emissions of trace gases from observations at Mace Head. *Atmospheric Environment*. **35**, 2507–2523. Aeronautics and Space Administration, Jet Propulsion Laboratory.

Sandholm, S., Smyth, S., Bai, R. and Bradshaw, J. (1997) Recent and future improvements in two-photon laser-induced fluorescence NO measurement capabilities. *Journal of Geophysical Research - Atmospheres*. **102**, D23 28651-28661.

Secretariat United Nations Environment Programme (Ed.), 2006. Handbook for the Montreal Protocol on substances that deplete the ozone layer, (7th Edition).

Silvia, D. and Skilling, J. (2006). Data analysis: A bayesian tutorial. 2nd edition.

Simpson, I.J., Meinardi, S., Blake, D.R., Blake, N.J., Rowland, F.S., Atlas, E. and Flocke, F. (2002) A biomass burning source of C1-C4 alkyl nitrates. *Geophysical Research Letters*. **29**, 2168.

Simpson, I.J., Blake, N.J., Blake, D.R., Atlas, E., Flocke, F., Crawford, J.H., Fuelberg, H.E., Kiley, C.M., Meinardi, S. and Rowland, F.S. (2003) Photochemical production and evolution of selected C2–C5 alkyl nitrates in tropospheric air influenced by Asian outflow. *Journal of Geophysical Research*. **108**, D20 8808.

Singh, H.B. and Hanst, P.L. (1981) Peroxyacetyl nitrate (pan) in the unpolluted atmosphere: an important reservoir for nitrogen oxides. *Geophysical Research Letters*. **8**, 941-944,

Singh, H.B., Gregory, G.L., Anderson, B., Browell, E., Sachse, G.W., Davis, D.D., Crawford, J., Bradshaw, J.D., Talbot, R., Blake, D.R., Thornton, D., Newell, R. and Merrill, J. (1996) Low ozone in the marine boundary layer of the tropical Pacific Ocean: Photochemical loss, chlorine atoms, and entrainment. *Journal of Geophysical Research - Atmospheres*. **101**, 1907-1917.

Solomon, S. (1999) Stratospheric Ozone Depletion: A review of concepts and history. *Reviews in Geophysics.* **37**, 275-316.

Sparks, J.P., Roberts, J.M. and Monson, R.K. (2003) The uptake of gaseous organic nitrogen by leaves: A significant global nitrogen transfer process. *Geophysical Research Letters*. **30**, 2189.

Sparks, J.P. (2009) Ecological ramifications of the direct foliar uptake of nitrogen. *Ocealogia*. **159**, 1-13.

Sprengnether, M., Demerjian, K.L., Donahue, N.M. and Anderson, J.G. (2002) Product analysis of the OH oxidation of isoprene and 1,3-butadiene in the presence of NO. *Journal of Geophysical Research - Atmospheres.* **107**, D15 4269.

Stark, H., Lerner, B.M., Schmitt, R., Jakoubek, R., Williams, E.J., Ryerson, T.B., Sueper, D.T., Parrish, D.D. and Fehsenfeld, F.C. (2007) Atmospheric in situ measurement of nitrate radical (NO_3) and other photolysis rates using spectroradiometry and filter radiometry. *Journal of Geophysical Research - Atmospheres.* **112**, D10S04.

Staudt, A.C., Jacob, D.J., Ravetta, F., Logan, J.A., Bachiochi, D., Krishnamurti, T.N., Sandholm, S., Ridley, B., Singh, H.B. and Talbot, B. (2003) Sources and chemistry of nitrogen oxides over the tropical Pacific. *Journal of Geophysical Research - Atmospheres*. **108**, D2 8239.

Stohl, A., Eckhardt, S., Forster, C., James, P., Spichtinger, N. and Seibert, P. (2002) A replacement for simple back trajectory calculations in the interpretation of atmospheric trace substance measurements. *Atmospheric Environment*. **36**, 4635-4648.

Stroud, C.A., Roberts, J.M., Williams, E.J., Hereid, D., Angevine, W.M., Fehsenfeld, F.C., Wisthaler, A., Hansel, A., Martinez Harder, M., Harder, H., Brune, W.H., Hoenninger, G., Stutz, J. and White, A.B. (2002) Nighttime isoprene trends at an urban forested site during the 1999 Southern Oxidant Study. *Journal of Geophysical Research - Atmospheres.***107**, 4291.

Talbot, R.W., Dibb, J.E., Scheuer, E.M., Bradshaw, J.D., Sandholm, S.T., Singh, H.B., Blake, D.R., Blake, N.J., Atlas, E. and Flocke, F. (2000) Tropospheric reactive odd nitrogen over the South Pacific in austral springtime. *Journal of Geophysical Research.***105**, D5 6681-6694.

Talukdar, R.K., Burkholder, J.B. and Schmoltner, A.M. (1995) Investigation of the loss processes for peroxyacetyl nitrate in the atmosphere - uv photolysis and reaction with oh. *Journal of Geophysical Research - Atmospheres.* **100**, D7 14163-14173.

Talukdar, R.K., Herndon, S.C., Burkholder, J.B., Roberts, J.M. and Ravishankara, A.R. (1997a). Atmospheric fate of several alkyl nitrates, Part 2: UV absorption cross-sections and photodissociation quantum yields. *Journal of the Chemical Society, Faraday Transactions.* **93**, 2797-2805.

Talukdar, R.K., Herndon, S.C., Burkholder, J.B., Roberts, J.M. and Ravishankara, A.R. (1997b) Atmospheric fate of several alkyl nitrates, Part 1: Rate coefficients of the reactions of alkyl nitrates with isotopically labeled hydroxyl radicals. *Journal of the ChemicalSociety, Faraday Transactions.* **93**, 2787-2796.

Teklemariam, T.A. and Sparks , J.P. (2004) Gaseous fluxes of peroxyacetyl nitrate (PAN) into plant leaves. *Plant Cell and Environment*. **27**, 1149-1158.

ten Brink, H.M., Kruisz, C., Kos, G.P.A. and Berner, A. (1997) Composition/size of the light-scattering aerosol in the Netherlands. *Atmospheric Environment*. **31**, 3955-3962.

Thompson, A.M. et al. (1993) Ozone observations and a model of marine boundary layer photochemistry during SAGA-3. *Journal of Geophysical Research*. **98**, 16955-16968.

Thompson, A.M., Johnson, J.E., Torres, A.L., Bates, T.S., Kelly, K.C., Atlas, E., Greenberg, J.P., Donahue, N.M., Yvon, S.A., Saltzman, E.S., Heikes, B.G., Mosher, B.W., Shashkov, A.A. and Yegorov, V.I. (1993) Ozone observations and a model of marine boundary layer photochemistry during saga-3. *Journal of Geophysical Research - Atmospheres*. **98**, 16955-16968.

Thornton, J., Wooldridge, P. and Cohen, R.C (2000) Atmospheric NO_2: In situ laser-induced fluorescence detection at parts per trillion mixing ratios. *Analytical Chemistry*. **72**, 528-539.

Thornton, J. A., Wooldridge, P. J., Cohen, R. C., Martinez, M., Harder, H., Brune, W. H., Williams, E. J., Roberts, J. M., Fehsenfeld, F. C., Hall, S. R., Shetter, R. E., Wert, B. P., Fried, A., 2002. Ozone production rates as a function of NOx abundances and HOx production rates in the Nashville urban plume. *Journal of Geophysical Research*. 107, 4146-4163.

Turnipseed, A.A., Huey, L.G., Nemitz, E., Stickel, R., Higgs, J., Tanner, D.J., Slusher, D.L., Sparks, J.P., Flocke, F. and Guenther, A. (2006) Eddy covariance fluxes of peroxyacetyl nitrates (PANs) and NO_y to a coniferous forest. *Journal of Geophysical Research*. **111**, D09304.

Val Martin, M., Honrath, R.E., Owen, R.C. and Li, Q.B. (2008) Seasonal variation of nitrogen oxides in the central North Atlantic lower free troposphere. *Journal of Geophysical Research*. **113**, D17307.

Vereecken, L. (2008) Computational study of the stability of a-nitroxy-substituted alkyl radicals. *Chemical Physics Letters*. **466**, 127-130.

Villena, G., Kleffmann, J, Kurtenbach, R.,Wiesen, P., Lissi, E., Rubio, M.A., Croxatto, J. and Rappenglück, B. (2011) Vertical gradients of HONO, NO_x and O_3 in Santiago de Chile. *Atmospheric Environment*. **45**, 3867-3873.

Volz-Thomas, A., Geiss, H., Hofzumahaus, A. and Becker, K.H. (2003) Introduction to special section: Photochemistry experiment in BERLIOZ. *Journal of Geophysical Research - Atmospheres*.,**108**, 8252.

Warneck, P. and Zerbach, T. (1992) Synthesis of peroxyacetyl nitrate in air by acetone photolysis. *Environmental Science and Technology*. **26**, 74-79.

Wayne, R.P., Barnes, I., Biggs, P., Burrows, J.P., Canosamas, C.E., Hjorth, J., Lebras, G., Moortgat, G.K., Perner, D., Poulet, G., Restelli, G. and Sidebottom, H. (1991) The nitrate radical - Physics, chemistry, and the atmosphere. *Atmospheric Environment*. **25**, 1-203.

Wayne, R. P., 2000. Chemistry of Atmospheres (3rd Edition). Oxford University Press.

Wespes, C., Hurtmans, D., Herbin, H., Barret, B., Turquety, S., Hadji-Lazaro, J., Clerbaux, C., and Coheur, P.F. (2007) First global distributions of nitric acid in the troposphere and the stratosphere derived from infrared satellite measurements. *Journal of Geophysical Research*. **112**, D13311.

Williams, E.J., Roberts, J.M., Baumann, K., Bertman, S.B., Buhr, S., Norton, R.B. and Fehsenfeld, F.C. (1997) Variations in NOy composition at Idaho Hill, Colorado, *Journal of Geophysical Research*. **102**, D5 6297-6314.

Williams, E.J., Baumann, K., Roberts, J.M., Bertman, S.B., Norton, R.B., Fehsenfeld, F.C., Springston, S.R., Nunnermacker, L.J., Newman, L., Olszyna, K., Meagher, J., Hartsell, B., Edgerton, E., Pearson, J.R. and Rodgers, M.O. (1998) Intercomparison of ground-based NOy measurement techniques. *Journal of Geophysical Research*. **103**, D17 22261-22280.

Wolfe, G.M., Thornton, J.A., Yatavelli, R.L.N., McKay, M., Goldstein, A.H., LaFranchi, B., Min, K.E. and Cohen, R.C. (2009) Eddy covariance fluxes of acyl peroxy nitrates (PAN, PPN and MPAN) above a Ponderosa pine forest. *Atmospheric Chemistry and Physics*. **9**, 615-634.

Wooldridge, P.J., Perring, A.E., Bertram, T.H., Flocke, F.M., Roberts, J.M., Singh, H.B., Huey, L.G., Thornton, J.A.,Wolfe, G.M., Murphy, J.G., Fry, J.L., Rollins, A.W., LaFranchi, B.W. and Cohen, R.C. (2010) Total Peroxy Nitrates (6PNs) in the atmosphere: The Thermal Dissociation-Laser Induced Fluorescence
(TD-LIF) technique and comparisons to speciated PAN measurements. *Atmospheric Measurement Techniques*. **3**, 593-607.

Zhang, K., O'Donnell, D., Kazil, J., Stier, P., Kinne, S., Lohmann, U., Ferrachat, S., Croft, B., Quaas, J., Wan, H., Rast, S. and Feichter, J. (2012) The global aerosol-climate model ECHAMHAM, version 2: Sensitivity to improvements in process representations. *Atmospheric Chemistry and Physicas Discussions*. **12**, 7545-7615.